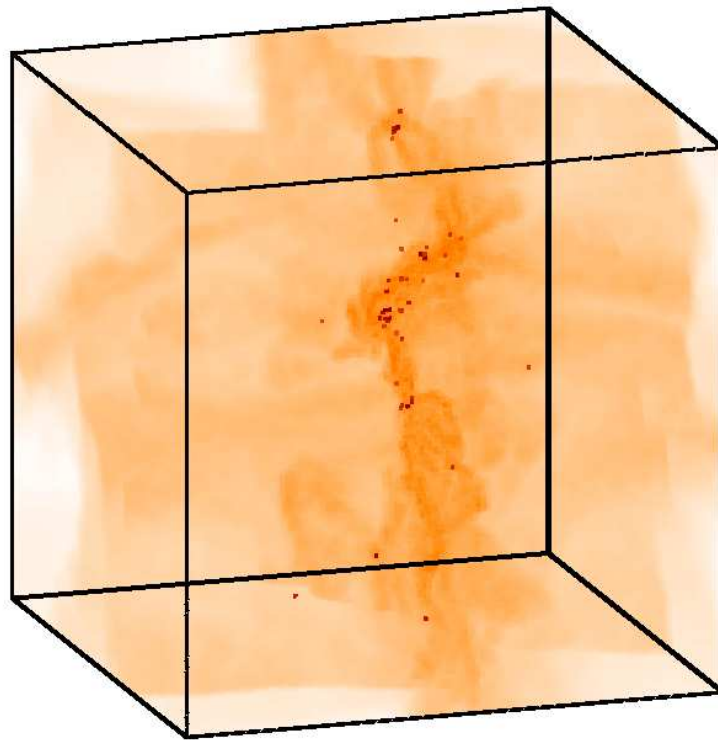


The Relation between Interstellar Turbulence and Star Formation



Ralf Klessen

The Relation between Interstellar Turbulence and Star Formation

Habilitationsschrift

zur Erlangung
der *venia legendi*
für das Fach Astronomie
an der Universität Potsdam

vorgelegt von
Ralf S. Klessen
aus Landau a. d. Isar
(im März 2003)

Deutsche Zusammenfassung:

Eine der zentralen Fragestellungen der modernen Astrophysik ist es, unser Verständnis für die Bildung von Sternen und Sternhaufen in unserer Milchstraße zu erweitern und zu vertiefen. Sterne entstehen in interstellaren Wolken aus molekularem Wasserstoffgas. In den vergangenen zwanzig bis dreißig Jahren ging man davon aus, daß der Prozeß der Sternentstehung vor allem durch das Wechselspiel von gravitativer Anziehung und magnetischer Abstoßung bestimmt ist. Neuere Erkenntnisse, sowohl von Seiten der Beobachtung als auch der Theorie, deuten darauf hin, daß nicht Magnetfelder, sondern Überschallturbulenz die Bildung von Sternen in galaktischen Molekülwolken bestimmt.

Diese Arbeit faßt diese neuen Überlegungen zusammen, erweitert sie und formuliert eine *neue Theorie der Sternentstehung* die auf dem komplexen Wechselspiel von Eigengravitation des Wolken-gases und der darin beobachteten Überschallturbulenz basiert. Die kinetische Energie des turbulenten Geschwindigkeitsfeldes ist typischerweise ausreichend, um interstellare Gaswolken auf großen Skalen gegen gravitative Kontraktion zu stabilisieren. Auf kleinen Skalen jedoch führt diese Turbulenz zu starken Dichtefluktuationen, wobei einige davon die lokale kritische Masse und Dichte für gravitativen Kollaps überschreiten können. Diese Regionen schockkomprimierten Gases sind es nun, aus denen sich die Sterne der Milchstraße bilden. Die Effizienz und die Zeitskala der Sternentstehung hängt somit unmittelbar von den Eigenschaften der Turbulenz in interstellaren Gaswolken ab. Sterne bilden sich langsam und in Isolation, wenn der Widerstand des turbulenten Geschwindigkeitsfeldes gegen gravitativen Kollaps sehr stark ist. Überwiegt hingegen der Einfluß der Eigengravitation, dann bilden sich Sterne in dichten Gruppen oder Haufen sehr rasch und mit großer Effizienz.

Die Vorhersagen dieser Theorie werden sowohl auf Skalen einzelner Sternentstehungsgebiete als auch auf Skalen der Scheibe unserer Milchstraße als ganzes untersucht. Es zu erwarten, daß protostellare Kerne, d.h. die direkten Vorläufer von Sternen oder Doppelsternsystemen, eine hochgradig dynamische Zeitentwicklung aufweisen, und keineswegs quasi-statische Objekte sind, wie es in der Theorie der magnetisch moderierten Sternentstehung vorausgesetzt wird. So muß etwa die Massenwachstumsrate junger Sterne starken zeitlichen Schwankungen unterworfen sein, was wiederum wichtige Konsequenzen für die statistische Verteilung der resultierenden Sternmassen hat. Auch auf galaktischen Skalen scheint die Wechselwirkung von Turbulenz und Gravitation maßgeblich. Der Prozeß wird hier allerdings noch zusätzlich moduliert durch chemische Prozesse, die die Heizung und Kühlung des Gases bestimmen, und durch die differenzielle Rotation der galaktischen Scheibe. Als wichtigster Mechanismus zur Erzeugung der interstellaren Turbulenz läßt sich die Überlagerung vieler Supernova-Explosionen identifizieren, die das Sterben massiver Sterne begleiten und große Mengen an Energie und Impuls freisetzen. Insgesamt unterstützen die Beobachtungsbefunde auf allen Skalen das Bild der turbulenten, dynamischen Sternentstehung, so wie es in dieser Arbeit gezeichnet wird.

Summary:

Understanding the formation of stars in galaxies is central to much of modern astrophysics. For several decades it has been thought that the star formation process is primarily controlled by the interplay between gravity and magnetostatic support, modulated by neutral-ion drift. Recently, however, both observational and numerical work has begun to suggest that supersonic interstellar turbulence rather than magnetic fields controls star formation.

This review begins with a historical overview of the successes and problems of both the classical dynamical theory of star formation, and the standard theory of magnetostatic support from both observational and theoretical perspectives. We then present the outline of a new paradigm of star formation based on the interplay between supersonic turbulence and self-gravity. Supersonic turbulence can provide support against gravitational collapse on global scales, while at the same time it produces localized density enhancements that allow for collapse on small scales. The efficiency and timescale of stellar birth in Galactic gas clouds strongly depend on the properties of the interstellar turbulent velocity field, with slow, inefficient, isolated star formation being a hallmark of turbulent support, and fast, efficient, clustered star formation occurring in its absence.

After discussing in detail various theoretical aspects of supersonic turbulence in compressible self-gravitating gaseous media relevant for star forming interstellar clouds, we explore the consequences of the new theory for both local star formation and galactic scale star formation. The theory predicts that individual star-forming cores are likely not quasi-static objects, but dynamically evolving. Accretion onto these objects will vary with time and depend on the properties of the surrounding turbulent flow. This has important consequences for the resulting stellar mass function. Star formation on scales of galaxies as a whole is expected to be controlled by the balance between gravity and turbulence, just like star formation on scales of individual interstellar gas clouds, but may be modulated by additional effects like cooling and differential rotation. The dominant mechanism for driving interstellar turbulence in star-forming regions of galactic disks appears to be supernovae explosions. In the outer disk of our Milky Way or in low-surface brightness galaxies the coupling of rotation to the gas through magnetic fields or gravity may become important.

The scientific content of this *habilitation thesis* is based on the following refereed publications. The corresponding sections of the *thesis* are indicated in parentheses:

- Heitsch, F., M.-M. Mac Low, and **R. S. Klessen**, 2001, *The Astrophysical Journal*, **547**, 280 – 291: “Gravitational Collapse in Turbulent Molecular Clouds. II. Magnetohydrodynamical Turbulence” (parts of §§2.1 – 2.6)
- **Klessen, R. S.**, 2003, *Reviews in Modern Astronomy* 16, in press (Ludwig Biermann Lecture, astro-ph/0301381, 33 pages): “Star Formation from Interstellar Clouds” (parts of §1, §§2.3 – 2.6, parts of §6)
- **Klessen, R. S.**, 2001, *The Astrophysical Journal*, **556**, 837 – 846: “The Formation of Stellar Clusters: Mass Spectra from Turbulent Fragmentation” (§4.4, §4.7)
- **Klessen, R. S.**, 2001, *The Astrophysical Journal*, **550**, L77 – L80: “The Formation of Stellar Clusters: Time Varying Protostellar Accretion Rates” (§4.4, §4.5)
- **Klessen, R. S.**, 2000, *The Astrophysical Journal*, **535**, 869 – 886: “One-Point Probability Distribution Functions of Supersonic, Turbulent Flows in Self-Gravitating Media” (§3.2)
- **Klessen, R. S.**, and A. Burkert, 2000, *The Astrophysical Journal Supplement Series*, **128**, 287 – 319: “The Formation of Stellar Clusters: Gaussian Cloud Conditions I” (parts of §§4.1 – 4.4)
- **Klessen, R. S.**, and A. Burkert, 2001, *The Astrophysical Journal*, **549**, 386 – 401: “The Formation of Stellar Clusters: Gaussian Initial Conditions II” (parts of §§4.1 – 4.4)
- **Klessen, R. S.**, and D. N. C. Lin, 2003, *Physical Review E*, in press: “Diffusion in Supersonic, Turbulent, Compressible Flows” (§3.1)
- **Klessen, R. S.**, F. Heitsch, and M.-M. Mac Low, 2000, *The Astrophysical Journal*, **535**, 887 – 906: “Gravitational Collapse in Turbulent Molecular Clouds: I. Gasdynamical Turbulence” (parts of §§2.1 – 2.6, §3.3)
- Mac Low, M.-M., and **R. S. Klessen**, 2003, *Reviews of Modern Physics*, submitted (astro-ph/0301093, 86 pages): “The Control of Star Formation by Supersonic Turbulence” (parts of §§1, 2, 4 – 6)
- Mac Low, M.-M., **R. S. Klessen**, A. Burkert, M. D. Smith, 1998, *Physical Review Letters*, **80**, 2754 – 2757: “Kinetic Energy Decay Rates of Supersonic and Super-Alfvénic Turbulence in Star-Forming Clouds” (§2.5.1)
- Ossenkopf, V., **R. S. Klessen**, and F. Heitsch, 2001, *Astronomy & Astrophysics*, **379**, 1005 – 1016: “On the Structure of Turbulent Self-Gravitating Molecular Clouds” (§3.4)
- Wuchterl, G., and **R. S. Klessen**, 2001, *The Astrophysical Journal*, **560**, L185 – L188: “The First Million Years of the Sun” (§4.5)

- 6.44 *Nicht 'wie' die Welt ist, ist das Mystische, sondern 'daß' sie ist.*
6.52 *Wir fühlen, daß selbst, wenn alle 'möglichen' wissenschaftlichen Fragen beantwortet sind, unsere Lebensprobleme noch gar nicht berührt sind. Freilich bleibt dann eben keine Frage mehr; und eben dies ist die Antwort.*

(Ludwig Wittgenstein, Logisch-Philosophische Abhandlung)

meiner Familie gewidmet

CONTENTS

1	INTRODUCTION	1
1.1	Overview	1
1.2	Turbulence	3
1.3	Outline	5
2	TOWARDS A NEW PARADIGM	7
2.1	Classical Dynamical Theory	9
2.2	Problems with Classical Theory	13
2.3	Standard Theory of Isolated Star Formation	14
2.4	Problems with Standard Theory	19
2.4.1	Singular Isothermal Spheres	19
2.4.2	Observations of Clouds and Cores	21
2.4.3	Observations of Protostars and Young Stars	25
2.5	Beyond the Standard Theory	27
2.5.1	Maintenance of Supersonic Motions	28
2.5.2	Turbulence in Self-Gravitating Gas	29
2.5.3	A Numerical Approach	30
2.5.4	Global Collapse	30
2.5.5	Local Collapse in Globally Stable Regions	31
2.5.6	Effects of Magnetic Fields	34
2.5.7	Promotion and Prevention of Local Collapse	35
2.5.8	The Timescales of Star Formation	36
2.5.9	Scales of Interstellar Turbulence	37
2.5.10	Efficiency of Star Formation	39
2.5.11	Termination of Local Star Formation	39
2.6	Outline of a New Theory of Star Formation	40

3	PROPERTIES OF SUPERSONIC TURBULENCE	43
3.1	Transport Properties	43
3.1.1	Introduction	43
3.1.2	A Statistical Description of Turbulent Diffusion	44
3.1.3	Numerical Method	45
3.1.4	Flow Properties	47
3.1.5	Transport Properties in an Absolute Reference Frame	48
3.1.6	Transport Properties in Flow Coordinates	49
3.1.7	A Mixing Length Description	50
3.1.8	Summary	53
3.2	One-Point Probability Distribution Function	54
3.2.1	Introduction	54
3.2.2	PDF's and Their Interpretation	55
3.2.3	PDF's from Gaussian Velocity Fluctuations	57
3.2.4	Analysis of Decaying Supersonic Turbulence without Self-Gravity	60
3.2.5	Analysis of Decaying Turbulence with Self-Gravity	63
3.2.6	Analysis of Driven Turbulence with Self-Gravity	68
3.2.7	Summary	70
3.3	Fourier Analysis	72
3.3.1	Fourier Spectra as Function of Driving Wavelength	73
3.3.2	Fourier Spectra During Collapse	73
3.3.3	Summary	74
3.4	Δ -Variance	76
3.4.1	Introduction	76
3.4.2	Turbulence Models	76
3.4.3	Density Structure	78
3.4.4	Velocity Structure	83
3.4.5	Comparison with Observations	84
3.4.6	Summary	87

4	LOCAL STAR FORMATION	89
4.1	Molecular Clouds	89
4.1.1	Composition of Molecular Clouds	89
4.1.2	Density and Velocity Structure of Molecular Clouds	89
4.1.3	Support of Molecular Clouds	93
4.1.4	Scaling Relations for Molecular Clouds	94
4.2	Star Formation in Molecular Clouds	95
4.3	Properties of Protostellar Cores	97
4.4	Dynamical Interactions in Clusters	102
4.5	Accretion Rates	104
4.6	Protostellar Evolutionary Tracks	106
4.6.1	Dynamical PMS Calculations	108
4.6.2	Formation of a $1 M_{\odot}$ -Star	109
4.6.3	Implications	111
4.7	Initial Mass Function	112
4.7.1	The Observed IMF	112
4.7.2	Models of the IMF	114
4.7.3	Mass Spectra from Turbulent Fragmentation	115
5	GALACTIC SCALE STAR FORMATION	117
5.1	When is Star Formation Efficient?	117
5.1.1	Overview	117
5.1.2	Gravitational Instabilities in Galactic Disks	118
5.1.3	Thermal Instability	121
5.2	Formation and Lifetime of Molecular Clouds	122
5.3	Driving Mechanisms	126
5.3.1	Magnetorotational Instabilities	126
5.3.2	Gravitational Instabilities	127
5.3.3	Protostellar Outflows	127
5.3.4	Massive Stars	128
5.4	Applications	130
5.4.1	Low Surface Brightness Galaxies	130
5.4.2	Galactic Disks	131
5.4.3	Globular Clusters	131
5.4.4	Galactic Nuclei	132
5.4.5	Primordial Dwarfs	132
5.4.6	Starburst Galaxies	132

6 CONCLUSIONS	135
6.1 Summary	135
6.2 Future Research Problems	137
BIBLIOGRAPHY	139
THANKS...	153

Chapter 1

INTRODUCTION

1.1 Overview

Stars are important. They are the primary source of radiation, with competition only from the 3K black body radiation of the cosmic microwave background and from accretion processes onto black holes in active galactic nuclei, which themselves are likely to have formed from stars. And stars have produced the bulk of all chemical elements heavier than H and He that made up the primordial gas. The Earth itself consists primarily of these heavier elements, called metals in astronomical terminology. These metals are made by nuclear fusion processes in the interior of stars, with the heaviest elements originating from the passage of the final supernova shockwave through the most massive stars. To reach the chemical abundances observed today in our solar system, the material had to go through many cycles of stellar birth and death. In a literal sense, we are star dust.

Stars are also our primary source of astronomical information and, hence, are essential for our understanding of the universe and the physical processes that govern its evolution. At optical wavelengths almost all natural light we observe in the sky originates from stars. During day this is more than obvious, but it is also true at night. The Moon, the second brightest object in the sky, reflects light from our Sun, as do the planets, while virtually every other extraterrestrial source of visible light is a star or collection of stars. Throughout the millenia, these objects have been the observational targets of traditional astronomy, and define the celestial landscape, the constellations. When we look at a dark night sky, we can also

note dark patches of obscuration along the band of the Milky Way. These are clouds of dust and gas that block the light from stars further away.

Since about a century ago we know that these clouds are associated with the birth of stars. The advent of new observational instruments and techniques gave access to astronomical information at wavelengths far shorter and longer than visible light. It is now possible to observe astronomical objects at wavelengths ranging from high-energy γ -rays down to radio frequencies. Especially useful for studying these dark clouds are radio and sub-mm wavelengths, at which they are transparent. Observations now show that *all* star formation occurring in the Milky Way is associated with these dark clouds of molecular hydrogen and dust.

Stars are common. The mass of the Galactic disk plus bulge is about $6 \times 10^{10} M_{\odot}$ (e.g. Dehnen & Binney 1998), where $1 M_{\odot} = 2 \times 10^{33} \text{ g}$ is the mass of our Sun. Thus, there are of order 10^{12} stars in the Milky Way, assuming standard values for the stellar mass spectrum (e.g. Kroupa 2002). Stars are constantly forming. Roughly 10% of the disk mass of the Milky Way is in the form of gas, which is forming stars at a rate of about $1 M_{\odot} \text{ yr}^{-1}$. Although stars dominate the baryonic mass in the Galaxy, it is dark matter that determines the overall mass budget, invisible material that indicates its presence only via its contribution to the gravitational potential. The dark matter halo of our Galaxy is about 10 times more massive than gas and stars together. At larger scales this imbalance is even more pronounced. Stars are estimated to make up only 0.4% of the total mass of the Universe (Lanzetta, Yahil, &

Fernandez-Soto 1996), and about 17% of the total baryonic mass (Walker *et al.* 1991).

Mass is the most important parameter determining the evolution of individual stars. Massive stars with high pressures at their centers have strong nuclear fusion there, making them short-lived but very luminous, while low-mass stars are long-lived but extremely faint. For example, a star with $5 M_{\odot}$ lives only for 2.5×10^7 yr, while a star with $0.2 M_{\odot}$ survives for 1.2×10^{13} yr, that is longer than the current age of the universe. For comparison the Sun with an age of 4.5×10^9 yr has reached approximately half of its life span. The mass luminosity relation is quite steep with roughly $L \propto M^{3.2}$ (Kippenhahn & Weigert 1990). During its short life the $5 M_{\odot}$ star will then emit a luminosity of $1.5 \times 10^4 L_{\odot}$, while the brightness of the $0.2 M_{\odot}$ star is only $\sim 10^{-3} L_{\odot}$. For reference, the luminosity of the Sun is $1 L_{\odot} = 3.85 \times 10^{33} \text{ erg s}^{-1}$.

The light from star-forming external galaxies in the visible and blue wavebands is dominated by young, massive stars. This is the reason why we observe beautiful spiral patterns in many disk galaxies, like NGC 4622 shown in Figure 1.1, as spiral density waves lead to gas compression and subsequent star formation at the wave locations. As optical emission from external galaxies is dominated by massive stars, and these massive stars are always young, they do not have sufficient time to disperse in the galactic disk, but still trace the characteristics of the instability that triggered their formation. Hence, understanding dynamical properties of galaxies requires an understanding of how, where, and under which conditions stars form.

In a simple approach, galaxies can be seen as gravitational potential wells containing gas that has been able to radiatively cool in less than the current age of the universe. In the absence of any hindrance, the gas would then collapse gravitationally to form stars on a free-fall time (Jeans 1902)

$$\tau_{\text{ff}} = \left(\frac{3\pi}{32G\rho} \right)^{1/2} = 150 \text{ Myr} \left(\frac{n}{0.1 \text{ cm}^{-3}} \right)^{-1/2}, \quad (1.1)$$

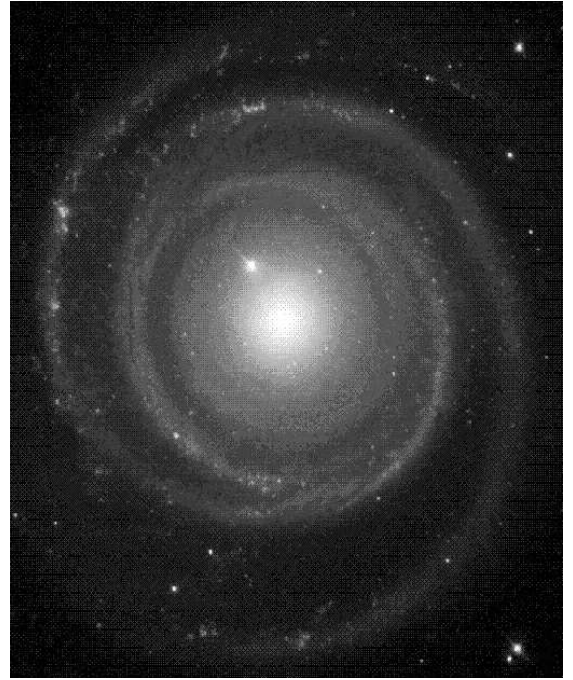


Figure 1.1: Optical image of the spiral galaxy NGC 4622 observed with the Hubble Space Telescope. (Courtesy of NASA and The Hubble Heritage Team — STScI/AURA)

where n is the number density of gas molecules scaled to typical Galactic values. Interstellar gas consists of one part He for every ten parts H. Then $\rho = \mu n$ is the mass density with $\mu = 2.11 \times 10^{-24} \text{ g}$, and G is the gravitational constant. The free-fall time τ_{ff} is very short compared to the age of the Milky Way, which is about 10^{10} yr. However, there is still gas left in the Galaxy and stars continue to form from this gas that presumably has already been cool for many billions years. What physical processes regulate the rate at which gas turns into stars, or differently speaking, what prevented that Galactic gas from forming stars at high rate immediately after it first cooled?

Observations of the star formation history of the universe demonstrate that stars did indeed form more vigorously in the past than today (e.g. Lilly *et al.* 1996, Madau *et al.* 1996, Baldry *et al.* 2002, Lanzetta *et al.* 2002), with as much as 80% of star formation being complete by redshift $z = 1$, more than 6 Gyr before the present. What mechanisms allowed rapid star formation in the past, but reduce its rate today?

The clouds in which stars form are dense enough, and well enough protected from dissociating UV radiation by self-shielding and dust scattering in their surface layers for hydrogen to be mostly in molecular form in their interior. The density and velocity structure of these molecular clouds is extremely complex and follows hierarchical scaling relations that appear to be determined by supersonic turbulent motions (e.g. Blitz & Williams 1999). Molecular clouds are large, and their masses exceed the threshold for gravitational collapse by far when taking only thermal pressure into account. Just like galaxies as a whole, naively speaking, they should be contracting rapidly and form stars at very high rate. This is generally not observed. The star formation efficiency of molecular clouds in the solar neighborhood is estimated to be of order of a few percent (e.g. Elmegreen 1991, McKee 1999).

For many years it was thought that support by magnetic pressure against gravitational collapse offered the best explanation for the slow rate of star formation. In this theory, developed by Shu (1977; and see Shu, Adams, & Lizano 1987), Mouschovias (1976; and see Mouschovias 1991b,c), Nakano (1976), and others, interstellar magnetic fields prevent the collapse of gas clumps with insufficient mass to flux ratio, leaving dense cores in magnetohydrostatic equilibrium. The magnetic field couples only to electrically charged ions in the gas, though, so neutral atoms can only be supported by the field if they collide frequently with ions. The diffuse interstellar medium (ISM) with number densities n of order unity remains ionized highly enough so that neutral-ion collisional coupling is very efficient (as we discuss below in Section 2.3). In dense cores, where $n > 10^5 \text{ cm}^{-3}$, ionization fractions drop below parts per million. Neutral-ion collisions no longer couple the neutrals tightly to the magnetic field, so the neutrals can diffuse through the field in a process known in astrophysics as ambipolar diffusion. (The same term is used by plasma physicists to describe ion-electron diffusion.) This ambipolar diffusion allows gravitational collapse to proceed in the face of magnetostatic support, but on a timescale as

much as an order of magnitude longer than the free-fall time, drawing out the star formation process.

We review a body of work that suggests that magnetohydrostatic support modulated by ambipolar diffusion fails to explain the star formation rate, and indeed appears inconsistent with observations of star-forming regions. Instead, this work suggests that support by supersonic turbulence is both sufficient to explain star formation rates, and more consistent with observations. In this picture, most gravitational collapse is prevented by turbulent motions, and any gravitational collapse that does occur does so quickly, with no passage through hydrostatic states.

1.2 Turbulence

At this point, we should briefly discuss the concept of turbulence, and the differences between supersonic, compressible (and magnetized) turbulence, and the more commonly studied incompressible turbulence. We mean by turbulence, in the end, nothing more than the gas flow resulting from random motions at many scales. We furthermore will use in our discussion only the very general properties and scaling relations of turbulent flows, focusing mainly on effects of compressibility. Some additional theoretical aspects of supersonic turbulent self-gravitating flows relevant for star-forming interstellar gas clouds are introduced in Section 3, however, for a more detailed and fundamental discussion of the complex statistical characteristics of turbulence, we refer the reader to the book by Lesieur (1991).

Most studies of turbulence treat incompressible turbulence, characteristic of most terrestrial applications. Root-mean-square (rms) velocities are subsonic, and density remains almost constant. Dissipation of energy occurs entirely on the scales of the smallest vortices, where the dynamical scale ℓ is shorter than the length on which viscosity acts ℓ_{visc} . Kolmogorov (1941a) described a heuristic theory based on dimensional analysis that captures the basic behavior of incompressible turbulence surprisingly well, although

subsequent work has refined the details substantially. He assumed turbulence driven on a large scale L , forming eddies at that scale. These eddies interact to form slightly smaller eddies, transferring some of their energy to the smaller scale. The smaller eddies in turn form even smaller ones, until energy has cascaded all the way down to the dissipation scale ℓ_{visc} .

In order to maintain a steady state, equal amounts of energy must be transferred from each scale in the cascade to the next, and eventually dissipated, at a rate

$$\dot{E} = \eta v^3 / L, \quad (1.2)$$

where η is a constant determined empirically. This leads to a power-law distribution of kinetic energy $E \propto v^2 \propto k^{-10/3}$, where $k = 2\pi/\ell$ is the wavenumber, and density does not enter because of the assumption of incompressibility. Most of the energy remains near the driving scale, while energy drops off steeply below ℓ_{visc} . Because of the local nature of the cascade in wavenumber space, the viscosity only determines the behavior of the energy distribution at the bottom of the cascade below ℓ_{visc} , while the driving only determines the behavior near the top of the cascade at and above L . The region in between is known as the inertial range, in which energy transfers from one scale to the next without influence from driving or viscosity. The behavior of the flow in the inertial range can be studied regardless of the actual scale at which L and ℓ_{visc} lie, so long as they are well separated. The behavior of higher order structure functions $S_p(\vec{r}) = \langle \{v(\vec{x}) - v(\vec{x} + \vec{r})\}^p \rangle$ in incompressible turbulence has been successfully modeled by She & Leveque (1994) by assuming that dissipation occurs in the filamentary centers of vortex tubes.

Gas flows in the ISM vary from this idealized picture in a number of important ways. Most significantly, they are highly compressible, with Mach numbers \mathcal{M} ranging from order unity in the warm, diffuse ISM, up to as high as 50 in cold, dense molecular clouds. Furthermore, the equation of state of the gas is very soft due to radiative cooling, so that pressure $P \propto \rho^\gamma$ with the polytropic index falling in the range $0.4 < \gamma <$

1.2 (e.g. Spaans & Silk 2000, Ballesteros-Paredes, Vázquez-Semadeni, & Scalo 1999b, Scalo *et al.* 1998). Supersonic flows in highly compressible gas create strong density perturbations. Early attempts to understand turbulence in the ISM (von Weizsäcker 1943, 1951, Chandrasekhar 1949) were based on insights drawn from incompressible turbulence. Although the importance of compressibility was already understood, how to incorporate it into the theory remained unclear. Furthermore, compressible turbulence is only one physical process that may cause the strong density inhomogeneities observed in the ISM. Others are thermal phase transitions (Field, Goldsmith, & Habing 1969, McKee & Ostriker 1977, Wolfire *et al.* 1995) or gravitational collapse (e.g. Wada & Norman 1999).

In supersonic turbulence, shock waves offer additional possibilities for dissipation. Shock waves can transfer energy between widely separated scales, removing the local nature of the turbulent cascade typical of incompressible turbulence. The spectrum may shift only slightly, however, as the Fourier transform of a step function representative of a perfect shock wave is k^{-2} , so the associated energy spectrum should be close to $\rho v^2 \propto k^{-4}$, as was indeed found by Porter & Woodward (1992) and Porter, Pouquet, & Woodward (1992, 1994). However, even in hypersonic turbulence, the shock waves do not dissipate all the energy, as rotational motions continue to contain a substantial fraction of the kinetic energy, which is then dissipated in small vortices. Boldyrev (2002) has proposed a theory of structure function scaling based on the work of She & Leveque (1994) using the assumption that dissipation in supersonic turbulence primarily occurs in sheet-like shocks, rather than linear filaments. First comparisons to numerical models show good agreement with this model (Boldyrev, Nordlund, & Padoan 2002a), and it has been extended to the density structure functions by Boldyrev, Nordlund, & Padoan (2002b).

The driving of interstellar turbulence is neither uniform nor homogeneous. Controversy still reigns over the most important energy sources at different scales, as described in Section 5.3, but

it appears likely that isolated and correlated supernovae dominate. However, it is not yet understood at what scales expanding, interacting blast waves contribute to turbulence. Analytic estimates have been made based on the radii of the blast waves at late times (Norman & Ferrara 1996), but never confirmed with numerical models (much less experiment). Indeed, the thickness of the blast waves may be more important

Finally, the interstellar gas is magnetized. Although magnetic field strengths are difficult to measure, with Zeeman line splitting being the best quantitative method, it appears that fields within an order of magnitude of equipartition with thermal pressure and turbulent motions are pervasive in the diffuse ISM, most likely maintained by a dynamo driven by the motions of the interstellar gas. A model for the distribution of energy and the scaling behavior of strongly magnetized, incompressible turbulence based on the interaction of shear Alfvén waves is given by Goldreich & Sridhar (1995, 1997) and Ng & Bhattacharjee (1996). The scaling properties of the structure functions of such turbulence was derived from the work of She & Leveque (1994) by Müller & Biskamp (2000; also see Biskamp & Müller 2000) by assuming that dissipation occurs in current sheets. A theory of very weakly compressible turbulence has been derived by using the Mach number $\mathcal{M} \ll 1$ as a perturbation parameter (Lithwick & Goldreich 2001), but no further progress has been made towards analytic models of strongly compressible magnetohydrodynamic (MHD) turbulence with $\mathcal{M} \gg 1$. See also Cho & Lazarian (2003), Cho *et al.* (2002).

With the above in mind, we propose that stellar birth is regulated by interstellar turbulence and its interplay with gravity. Turbulence, even if strong enough to counterbalance gravity on global scales, will usually provoke local collapse on small scales. Supersonic turbulence establishes a complex network of interacting shocks, where converging flows generate regions of high density. This density enhancement can be sufficient for gravitational instability. Collapse sets in. However, the random flow that creates local density enhancements also may disperse them again.

For local collapse to actually result in the formation of stars, collapse must be sufficiently fast for the region to ‘decouple’ from the flow, i.e. it must be shorter than the typical time interval between two successive shock passages. The shorter this interval, the less likely a contracting region is to survive. Hence, the efficiency of star formation depends strongly on the properties of the underlying turbulent velocity field, on its lengthscale and strength relative to gravitational attraction. This principle holds for star formation throughout all scales considered in this review, ranging from small local star forming regions in the solar neighborhood up to galaxies as a whole. For example, we predict in star burst galaxies self-gravity to completely overwhelm any turbulent support, whereas in the other extreme, in low surface brightness galaxies we argue that turbulence is strong enough to essentially quench any noticeable star formation activity.

1.3 Outline

To lay out this new picture of star formation in more detail, in Section 2 we first critically discuss the historical development of star formation theory, and then argue that star formation is controlled by the interplay between gravity and supersonic turbulence. We begin this section by describing the classical dynamic theory, and then move on to what has been until recently the standard theory, where the star formation process is controlled by magnetic fields. After describing the theoretical and observational problems that both approaches have, we present work that leads us to an outline of the new theory of star formation. Then we introduce some further properties of supersonic turbulence in self-gravitating gaseous media relevant to star-forming interstellar gas clouds in Section 3. We consider the transport properties of supersonic turbulence, discuss energy spectra in Fourier space, and quantify the structural evolution of gravitational collapse in turbulent flows by means of one-point probability distribution functions of density and velocity and by calculating the Δ -variance. In Section 4 we then apply the new theory of turbulent

star formation, first to local star forming regions in the Milky Way in. We discuss the properties of molecular clouds, stellar clusters, and protostellar cores (the direct progenitors of individual stars), and we investigate the implications of the new theory on protostellar mass accretion, and on the subsequent distribution of stellar masses. In Section 5, we discuss the control of star formation by supersonic turbulence on galactic scales. We ask when is star formation efficient, and how are molecular clouds formed and destroyed. We review the possible mechanisms that generate and maintain supersonic turbulence in the interstellar medium, and come to the conclusion that supernova explosions accompanying the death of massive stars are the most likely agents. Then we apply the theory to various types of galaxies, ranging from low surface brightness galaxies to massive star bursts. Finally, in Section 6 we summarize, and describe unsolved problems open for future research.

Chapter 2

TOWARDS A NEW PARADIGM

Stars form from gravitational contraction of molecular cloud material. A crude estimate of the stability of such a system against gravitational collapse can be made by simply considering its energy balance. To become unstable gravitational attraction must outweigh the combined action of all dispersive or resistive forces. In the most simplistic case, the absolute value of the potential energy of a system in virial equilibrium is exactly twice the total kinetic energy, $E_{\text{pot}} + 2E_{\text{kin}} = 0$. If $E_{\text{pot}} + 2E_{\text{kin}} < 0$ the system collapses, while for $E_{\text{pot}} + 2E_{\text{kin}} > 0$ it expands. This estimate can easily be extended by including surface terms and additional physical forces. In particular taking magnetic field effects into account may become important for describing interstellar clouds (Chandrasekhar, 1953; see also McKee *et al.*, 1993, for a more recent discussion). In the presence of turbulence the total kinetic energy not only includes the internal energy but also the contribution from turbulent gas motions. Simple energy considerations can in general already provide qualitative insight into the dynamical behavior of a system (Bonazzola *et al.*, 1987).

A thorough investigation, however, requires a linear stability analysis. For the case of a non-magnetic, isothermal, infinite, homogeneous, self-gravitating medium at rest (i.e. without turbulent motions) Jeans (1902) derived a relation between the oscillation frequency ω and the wavenumber k of small perturbations,

$$\omega^2 - c_s^2 k^2 + 4\pi G \rho_0 = 0, \quad (2.1)$$

where c_s is the isothermal sound speed, G the gravitational constant, and ρ_0 the initial mass density. The derivation neglects viscous effects

and assumes that the linearized version of the Poisson equation describes only the relation between the perturbed potential and the perturbed density (neglecting the potential of the homogeneous solution, the so-called 'Jeans swindle', see e.g. Binney and Tremaine, 1997). The third term in Equation (2.1) is responsible for the existence of decaying and growing modes, as pure sound waves stem from the dispersion relation $\omega^2 - c_s^2 k^2 = 0$. Perturbations are unstable against gravitational contraction if their wavenumber is below a critical value, the Jeans wavenumber k_J , i.e. if

$$k^2 < k_J^2 \equiv \frac{4\pi G \rho_0}{c_s^2}, \quad (2.2)$$

or equivalently if the wavelength of the perturbation exceeds a critical size given by $\lambda_J \equiv 2\pi k_J^{-1}$. Assuming the perturbation is spherical with diameter λ_J , this directly translates into a mass limit

$$M_J \equiv \frac{4\pi}{3} \rho_0 \left(\frac{\lambda_J}{2}\right)^3 = \frac{\pi}{6} \left(\frac{\pi}{G}\right)^{3/2} \rho_0^{-1/2} c_s^3. \quad (2.3)$$

All perturbations exceeding the Jeans mass M_J will collapse under their own weight. For isothermal gas $c_s^2 \propto T$ and subsequently $M_J \propto \rho_0^{-1/2} T^{3/2}$. The critical mass M_J decreases when the density ρ_0 grows or when the temperature T sinks.

The Jeans instability has a simple physical interpretation in terms of the energy budget. The energy density of a sound wave is positive. However, its gravitational energy is negative, because the enhanced attraction in the compressed regions outweighs the reduced attraction in the dilated regions. The instability sets in at the

wavelength λ_J where the net energy density becomes negative. The perturbation will grow allowing the energy to decrease even further. For a fundamental derivation of this instability from the canonical ensemble in statistical physics see de Vega and Sánchez (2001). In isothermal gas, there is no mechanism that prevents complete collapse. In reality, however, during the collapse of molecular gas clumps, the opacity increases and at densities of $n(\text{H}_2) \approx 10^{10} \text{ cm}^{-3}$ the equation of state becomes adiabatic. Then collapse proceeds slower. Finally at very high central densities ($\rho \approx 1 \text{ g cm}^{-3}$) fusion processes set in. This energy source leads to a new equilibrium (e.g. Tohline 1982): a new star is born.

Attempts to include the effect of turbulent motions into the star formation process were already being made in the middle of the 20th century by von Weizsäcker (1943, 1951) based on Heisenberg's (1948a,b) concept of turbulence. He also considered the production of interstellar clouds from the shocks and density fluctuations in compressible turbulence. A more quantitative theory was proposed by Chandrasekhar (1951a,b), who investigated the effect of microturbulence in the subsonic regime. In this approach the scales of interest, e.g. for gravitational collapse, greatly exceed the outer scale of turbulence. If turbulence is isotropic (and more or less incompressible), it simply contributes to the pressure on large scales, and Chandrasekhar derived a dispersion relation similar to Equation (2.1) by introducing an effective sound speed

$$c_{s,\text{eff}}^2 = c_s^2 + 1/3 \langle v^2 \rangle, \quad (2.4)$$

where $\langle v^2 \rangle$ is the rms velocity dispersion due to turbulent motions.

In reality, however, the outer scales of turbulence typically exceed or are at least comparable to the size of the system (e.g. Ossenkopf and Mac Low, 2001), and the assumption of microturbulence is invalid. In a more recent analysis, Bonazzola *et al.* (1987) therefore suggested a wavelength-dependent effective sound speed $c_{s,\text{eff}}^2(k) = c_s^2 + 1/3 v^2(k)$ for Equation (2.1). In this description, the stability of the system depends not only on the total amount of energy, but

also on the wavelength distribution of the energy, since $v^2(k)$ depends on the turbulent power spectrum. A similar approach was also adopted by Vázquez-Semadeni and Gazol (1995), who added Larson's (1981) empirical scaling relations to the analysis.

A most elaborate investigation of the stability of turbulent, self-gravitating gas was undertaken by Bonazzola *et al.* (1992), who used renormalization group theory to derive a dispersion relation with a generalized, wavenumber-dependent, effective sound speed and an effective kinetic viscosity that together account for turbulence at all wavelengths shorter than the one in question. According to their analysis, turbulence with a power spectrum steeper than $P(k) \propto 1/k^3$ can support a region against collapse at large scales, and below the thermal Jeans scale, but not in between. On the other hand, they claim that turbulence with a shallower slope, as is expected for incompressible turbulence (Kolmogorov 1941a,b), Burgers turbulence (Lesieur 1997), or shock dominated flows (Passot, Pouquet & Woodward 1988), cannot support clouds against collapse at scales larger than the thermal Jeans wavelength.

Analytic attempts to characterize turbulence have a fundamental limitation, so far they are all restricted to incompressible flows. However, molecular cloud observations clearly show extremely non-uniform structure. It may even be possible to describe the equilibrium state as an inherently inhomogeneous thermodynamic critical point (de Vega, Sánchez and Combes, 1996a,b; de Vega and Sánchez, 1999). This may render all applications of incompressible turbulence to the theory of star formation meaningless. In fact, it is the main goal of this review to introduce and stress the importance of compressional effects in supersonic turbulence for determining the outcome of star formation.

In order to do that, we need to recapitulate the development of our understanding of the star formation process over the last few decades. We begin with the classical dynamical theory (Section 2.1) and describe the problems that it encounters in its original form (Section 2.2). In particular the timescale problem lead astrophysicists

think about the influence of magnetic fields. This line of reasoning resulted in the construction of the paradigm of magnetically mediated star formation, which we discuss in Section 2.3. However, it became clear that this so called “standard theory” has a variety of very serious shortcomings (Section 2.5). They lead us to rejuvenate the earlier dynamical concepts of star formation and to reconsider them in the modern framework of compressible supersonic turbulence (Section 2.6). Consequently, we propose in Section 2.6 a new paradigm of dynamical turbulent star formation.

2.1 Classical Dynamical Theory

The classical dynamical theory focuses on the interplay between self-gravity on the one side and pressure gradients on the other. Turbulence can be taken into account, but only on microscopic scales significantly smaller than the collapse scales. In this microturbulent regime random gas motions yield an isotropic pressure which can be absorbed into the equations of motion by defining an effective sound speed as in Equation (2.4). The dynamical behavior of the system remains unchanged, and we will not distinguish between effective and thermal sound speed c_s in this and the following two sections.

Because of the importance of gravitational instability for stellar birth, Jeans’ (1902) pioneering work has triggered numerous attempts to derive solutions to the collapse problem, rigorous analytical as well as numerical ones. Particularly noteworthy are the studies by Bonnor (1956) and Ebert (1957) who independently of each other derived analytical solutions for the equilibrium structure of spherical density perturbations in self-gravitating isothermal ideal gases and a criterion for gravitational collapse (see Lombardi and Bertin, 2001, for a recent analysis; and studies by Schmitz, 1983, 1984, 1986, 1988, and Schmitz & Ebert, 1986, 1987, for the treatment of generalized polytropic equations-of-state and/or rotation). It has been shown recently that this may be a good description for the density distribution in quiescent molecular cloud cores just be-

fore they begin to collapse and form stars (Bacman *et al.* 2000, Alves, Lada, and Lada 2001). The first numerical calculations of protostellar collapse became possible in the late 1960’s (e.g. Bodenheimer & Sweigart, 1968; Larson, 1969; Penston, 1969a,b) and showed that gravitational contraction proceeds in a highly nonhomologous manner, contrary to what has previously been assumed (Hayashi 1966). This is illustrated in Figure 2.1, which shows the radial density distribution of a protostellar core at various stages of the isothermal collapse phase. The gas sphere initially follows a Bonnor-Ebert critical density profile but carries a four times larger mass than allowed by the equilibrium conditions. Therefore it is gravitationally unstable and begins to collapse. As the inner part has no pressure gradient it contracts in free fall. As matter falls inwards, the density in the interior grows and decreases in the outer parts. This builds up pressure gradients in the outer parts, where contraction becomes significantly retarded from free fall. In the interior, however, the collapse remains approximately free falling. This means it actually speeds up, because the free-fall timescale τ_{ff} scales with density as $\tau_{\text{ff}} \propto \rho^{-1/2}$. Changes in the density structure occur in a smaller and smaller region near the center and on shorter and shorter timescale, while practically nothing happens in the outer parts. As a result the overall matter distribution becomes strongly centrally peaked with time, and approaches $\rho \propto r^{-2}$. This the well known density profile of isothermal spheres. The establishment of a central singularity corresponds to the formation of the protostar which grows in mass by accreting the remaining envelope until the reservoir of gas is exhausted.

In reality, however, the isothermal collapse phase ends when the central density reaches densities of $n(\text{H}_2) \approx 10^{10} \text{ cm}^{-3}$. Then gas becomes optically thick and the heat generated by the collapse is no longer radiated away freely. The central region begins to heat up and contraction comes to a first halt. But as the temperature reaches $T \approx 2000 \text{ K}$ molecular hydrogen begins to dissociate. The core becomes unstable again and collapse sets in anew. Most of the released gravitational

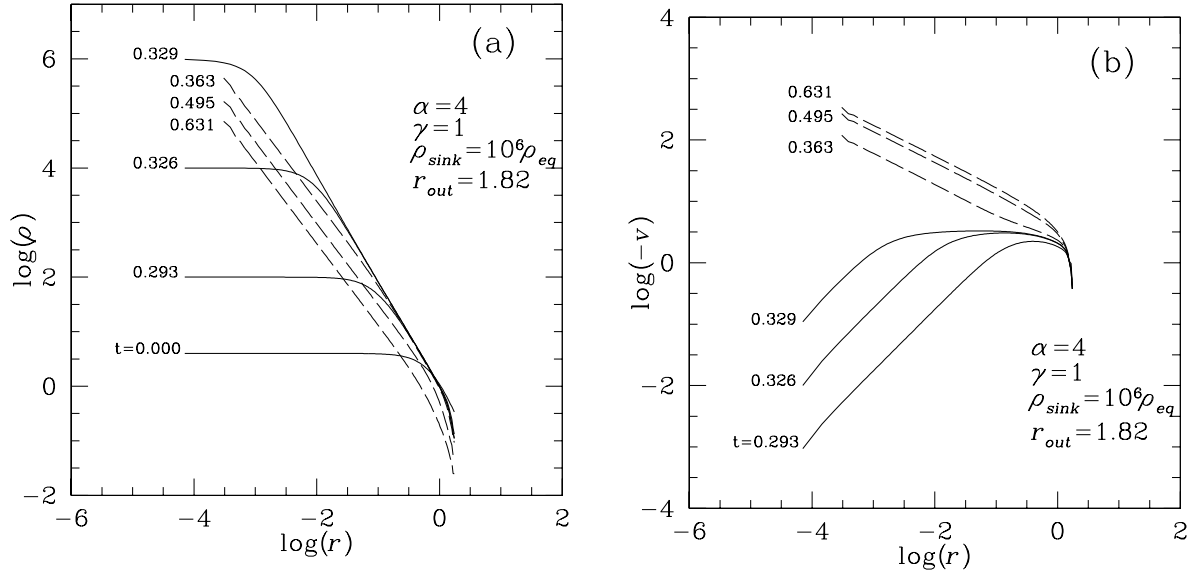


Figure 2.1: Radial density profile (a) and infall velocity profile (b) depicted at various stages of dynamical collapse. All quantities are given in normalized units. The initial configuration at $t = 0$ corresponds to a critical isothermal ($\gamma = 1$) Bonnor-Ebert sphere with outer radius $r_{\text{out}} = 1.82$. It carries $\alpha = 4$ times more mass than allowed by hydrostatic equilibrium, and therefore begins to contract. The numbers on the left denote the evolutionary time and illustrate the ‘runaway’ nature of collapse. Since the relevant collapse timescale, the free-fall time τ_{ff} , scales with density as $\tau_{\text{ff}} \propto \rho^{-1/2}$ central collapse speeds up as ρ increases. When density contrast reaches a value of 10^6 a “sink” cell is created in the center, which subsequently accretes all incoming matter. This time roughly corresponds to the formation of the central protostar, and allows for following its subsequent accretion behavior. The profiles before the formation of the central point mass indicated by solid lines, and for later times by dashed lines. The figure is from Ogino *et al.* (1999).

energy goes into the dissociation of H_2 -molecules so that the temperature rises only slowly. This situation is similar to the first isothermal collapse phase. When all molecules in the core are dissociated, the temperature rises sharply and pressure gradients again become able to halt the collapse. The second hydrostatic core has formed. This is the first occurrence of the protostar which subsequently grows in mass by the accretion of the still infalling material from the outer parts of the original cloud fragment. As this matter is still in free fall, most of the luminosity of the protostar at that stage is generated in a strongly supersonic accretion shock. Consistent dynamical calculations of all phases of protostellar collapse are presented by Masunaga, Miyama, & Inutsuka (1998), Masunaga & Inutsuka (2000a,b), Wuchterl & Klessen (2001), and Wuchterl & Tscharnuter (2002).

It was Larson (1969) who realized that the dynamical evolution in the initial isothermal collapse phase can be described by an analytical

Table 2.1: Properties of the Larson-Penston solution of isothermal collapse.

	before core formation ($t < 0$)	after core formation ($t > 0$)
density profile	$\rho \propto (r^2 + r_0^2)^{-1}$ ($r_0 \rightarrow 0$ as $t \rightarrow 0_-$)	$\rho \propto r^{-3/2}$, $r \rightarrow 0$ $\rho \propto r^{-2}$, $r \rightarrow \infty$
velocity profile	$v \propto r/t$ as $t \rightarrow 0_-$ $v \approx -3.3 c_s$ as $r \rightarrow \infty$	$v \propto r^{-1/2}$, $r \rightarrow 0$ $v \approx -3.3 c_s$ as $r \rightarrow \infty$
accretion rate		$\dot{M} = 47 c_s^3 / G$

similarity solution. This was independently discovered also by Penston (1969b), and later extended by Hunter (1977) into the regime after the protostar has formed. This so called Larson-

Penston solution describes the isothermal collapse of homogeneous ideal gas spheres initially at rest. Its properties are summarized in Table 2.1. Two predictions are most relevant for the astrophysical context. The first is the occurrence of supersonic infall velocities that extend over the entire protostellar cloud. Before the formation of the central protostar the infall velocity tends towards ~ 3.3 times the sound speed c_s , and afterwards approaches free fall collapse in the center with $v \propto r^{-1/2}$ while still maintaining $v \approx 3.3c_s$ in the outer envelope for some time (Hunter 1977). Second, the Larson-Penston solution predicts protostellar accretion rates which are constant and of order $\dot{M} \approx 30c_s^3/G$. It is important to note that the dynamical models conceptually allow for time-varying protostellar mass accretion rates, if the gradient of the density profile of a collapsing cloud core varies with radius. Most relevant in the astrophysical context, if the core has a flat inner region and decreasing density outwards (as it is observed in low-mass cores, see Section 2.4), then \dot{M} has a high initial peak, when the flat core gets accreted, and later declines as the lower-density outer-envelope material is falling in (e.g. Ogino *et al.* 1999). For the collapse of a Plummer-type sphere with specifications such as to fit the protostellar core L1544, the time evolution of \dot{M} is illustrated in Figure 2.2 (see Whitworth & Ward-Thompson 2001). Plummer-type spheres have flat inner density profile followed by an outer power-law decline, and thus similar basic properties as the Larson-Penston spheres in mid collapse. The dynamical properties of the Larson-Penston solution set it clearly apart from the inside-out collapse model (Shu 1977) derived for magnetically mediated star formation (Section 2.3). One-dimensional numerical simulations of the dynamical collapse of homogeneous isothermal spheres typically demonstrate global convergence to the Larson-Penston solution, but also show that certain deviations occur, e.g. in the time evolution \dot{M} , due to pressure effects (Bodenheimer & Sweigart 1968; Larson 1969, Hunter 1977; Foster & Chevalier 1993; Tomisaka 1996b; Basu 1997; Hanawa & Nakayama, 1997; Ogino *et al.* 1999).

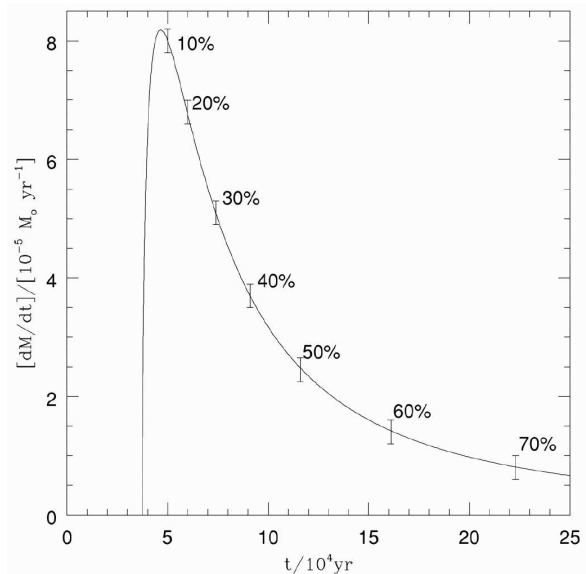


Figure 2.2: Time evolution of the protostellar accretion rate for the collapse of a gas clump with Plummer-type density distribution similar to observed protostellar cores. For details see Whitworth & Ward-Thompson (2001)

With the rapid advances in computer technology, both two-dimensional and three-dimensional computations became possible. Some of the first two dimensional calculations are reported by Larson (1972), Tscharnuter (1975), Black & Bodenheimer (1976), Fricke, Moellenhoff, & Tscharnuter (1976), Nakazawa, Hayashi, & Takahara (1976), Bodenheimer & Tscharnuter (1979), Boss (1980a), and Norman, Wilson, & Barton (1980). Two-dimensional dynamical modeling has the advantage to be fast compared to three-dimensional simulations, and therefore allows for including a larger number of physical processes while reaching higher spatial resolution. The obvious disadvantage is that only axisymmetric perturbations can be studied. Initial attempts to study collapse in three dimensions are reported by Cook & Harlow (1978), Bodenheimer & Boss (1979), Boss (1980b), Rozyczka *et al.* (1980), or Tohline (1980). Since these early studies, numerical simulations of the collapse of isolated isothermal objects have been extended, for example, to include highly oblate cores (Boss, 1996) or elongated filamentary cloud cores (e.g. Bastien *et al.* 1991; Inutsuka & Miyama, 1997), differential rotation (Boss & Myhill, 1995), and differ-

ent density distributions for the initial spherical cloud configuration with or without bar-like perturbations (Burkert & Bodenheimer 1993; Klapp, Sigalotti, & de Felice 1993; Burkert & Bodenheimer 1996; Bate & Burkert 1997; Burkert, Bate, & Bodenheimer 1997; Truelove *et al.* 1997, 1978; Tsuribe & Inutsuka 1999a; Klein 1999; Boss *et al.* 2000). The inclusion of magnetic fields into the treatment will be discussed in Section 2.4.

Whereas spherical collapse models can only treat the formation of single stars, the two- and three-dimensional calculations show that the formation of binary and higher-order multiple stellar systems can well be described in terms of the classical dynamical theory and is a likely outcome of protostellar collapse and molecular cloud fragmentation (for a comprehensive overview see Bodenheimer *et al.* 2000). Observationally, the fraction of binary and multiple stars relative to single stars is about 50% for the field star population in the solar neighborhood. This has been determined for all known F7-G9 dwarf stars within 22 pc from the Sun by Duquennoy & Mayor (1991) and for M dwarfs out to similar distances by Fischer & Marcy (1992; also Leinert *et al.* 1997). The binary fraction for pre-main sequence stars appears to be at least equally high (see e.g. Table 1 in Mathieu *et al.* 2000). These findings put strong constraints on the theory of star formation, as *any* reasonable model needs to explain the observed high number of binary and multiple stellar systems. It has long been suggested that sub-fragmentation and multiple star formation is a natural outcome of isothermal collapse (Hoyle 1954), however, stability analyses show that the growth time of small perturbations in the isothermal phase is typically small compared to the collapse timescale itself (e.g. Silk & Suto 1988; Hanawa & Nakayama 1997). Hence, in order to form multiple stellar systems, either perturbations to the collapsing core must be external and strong, or subfragmentation occurs at later non-isothermal phase of collapse after a protostellar disk has formed. This disk may become gravitationally unstable if the surface density exceeds a critical value given by the epicyclic frequency and the sound speed (Safranov, 1960; Toomre

1964) and fragment into multiple objects (as summarized by Bodenheimer *et al.* 2000). This naturally leads to two distinct modes of multiple star formation.

Contracting gas clumps with strong external perturbation occur naturally in turbulent molecular clouds or when stars form in clusters. While collapsing to form or feed protostars, clumps may loose or gain matter from interaction with the ambient turbulent flow (Klessen *et al.* 2000). In a dense cluster environment, collapsing clumps may merge to form larger clumps containing multiple protostellar cores, which subsequently compete with each other for accretion from the common gas environment (Murray & Lin, 1996; Bonnell *et al.* 1997, Klessen & Burkert, 2000, 2001). Strong external perturbations and capture through clump merger leads to *wide* binaries or multiple stellar systems. Stellar aggregates with more than two stars are dynamically unstable, hence, some protostars may become ejected again from the gas rich environment they accrete from. This not only terminates their mass growth, but leaves the remaining stars behind more strongly bound. These dynamical effects may transform the original wide binaries into close binaries (see also Kroupa 1995a,b,c). Binary stars that form through disk fragmentation are close binaries right from the beginning, as typical sizes of protostellar disks are of order of a few 100 AU¹.

The formation of clusters of stars (as opposed to binary or small multiple stellar systems) is easily accounted for in the classical dynamical theory by simply considering larger and more massive molecular cloud regions. The proto-cluster cloud will fragment and build up a cluster of stars if it has highly inhomogeneous density structure similar to the observed clouds (Keto, Lattanzio, & Monaghan 1991; Inutsuka & Miyama 1997, Klessen & Burkert 2000, 2001) or, equivalently, if it is subject to strong external perturbations, e.g. from cloud-cloud collisions (Whithworth *et al.* 1995; Turner *et al.* 1995), or is highly turbulent (see Section 2.5 and Section 2.6).

¹One astronomical unit is the mean radius of Earth's orbit around the Sun, 1 AU = 1.5×10^{13} cm.

2.2 Problems with Classical Theory

The classical theory of gravitational collapse balanced by pressure and microturbulence did not take into account the conservation of angular momentum and magnetic flux during collapse. It became clear from observations of polarized starlight (Hiltner 1949, 1951) that substantial magnetic fields thread the interstellar medium (Chandrasekhar & Fermi 1953a), forcing the magnetic flux problem to be addressed, but also raising the possibility that the solution to the angular momentum problem might be found in the action of magnetic fields. The typical strength of the magnetic field in the diffuse ISM was not known to an order of magnitude, though, with estimates ranging as high as 30 μG from polarization (Chandrasekhar & Fermi 1953a) and synchrotron emission (e.g. Davies & Shuter 1963). Lower values from Zeeman measurements of HI (Troland & Heiles 1986) and from measurements of pulsar rotation and dispersion measures (Rand & Kulkarni 1989, Rand & Lyne 1994) comparable to the modern value of around 3 μG only gradually became accepted over the next two decades.

The presence of a field, especially one as strong as was then considered possible, formed a major problem for the classical theory of star formation. To see why, let us consider the behavior of a field in an isothermal region of gravitational collapse (Mestel & Spitzer 1956, Spitzer 1968). If we neglect all surface terms except thermal pressure P_0 (a questionable assumption as shown by Ballesteros-Paredes *et al.* 1999a, but the usual one at the time), and assume that the field, with magnitude B is uniform within a region of average density ρ and effective spherical radius R , we can write the virial equation as

$$4\pi R^3 P_0 = 3 \frac{M k_B T}{\mu} - \frac{1}{R} \left(\frac{3}{5} G M^2 - \frac{1}{3} R^4 B^2 \right), \quad (2.5)$$

where $M = 4/3\pi R^3 \rho$ is the mass of the region, k_B is Boltzmann's constant, T is the temperature of the region, and μ is the mean mass per particle. So long as the ionization is sufficiently high for the field to be frozen to the matter, the flux

through the cloud $\Phi = \pi R^2 B$ must remain constant. Therefore, the opposition to collapse due to magnetic energy given by the last term on the right hand side of equation (2.5) will remain constant during collapse. If it is insufficient to prevent collapse at the beginning, it remains insufficient as the field is compressed.

If we write the radius R in terms of the mass and density of the region, we can rewrite the two terms in parentheses on the right hand side of equation (2.5) to show that gravitational attraction can only overwhelm magnetic repulsion if

$$M > M_{\text{cr}} \equiv \frac{5^{3/2}}{48\pi^2} \frac{B^3}{G^{3/2} \rho^2} = (4 \times 10^6 M_{\odot}) \left(\frac{n}{1 \text{ cm}^{-3}} \right)^2 \left(\frac{B}{3 \mu\text{G}} \right)^3, \quad (2.6)$$

where the numerical constant is correct for a uniform sphere, and the number density n is computed with mean mass per particle $\mu = 2.11 \times 10^{-24} \text{ g cm}^{-3}$. Mouschovias & Spitzer (1976) noted that the critical mass can also be written in terms of a critical mass-to-flux ratio

$$\left(\frac{M}{\Phi} \right)_{\text{cr}} = \frac{\zeta}{3\pi} \left(\frac{5}{G} \right)^{1/2} = 490 \text{ g G}^{-1} \text{ cm}^{-2}, \quad (2.7)$$

where the constant $\zeta = 0.53$ for uniform spheres (or flattened systems, as shown by Strittmatter 1966) is used in the final equality. (Assuming a constant mass-to-flux ratio in a region results in $\zeta = 0.3$ [Nakano & Nakamura 1978]). For a typical interstellar field of 3 μG , the critical surface density for collapse is $7M_{\odot} \text{ pc}^{-2}$, corresponding to a number density of 230 cm^{-2} in a layer of thickness 1 pc. A cloud is termed *subcritical* if it is magnetostatically stable and *supercritical* if it is not.

The very large value for the magnetic critical mass in the diffuse ISM given by equation 2.6 forms a crucial objection to the classical theory of star formation. Even if such a large mass could be assembled, how could it fragment into objects with stellar masses of 0.01–100 M_{\odot} , when the critical mass should remain invariant under uniform spherical gravitational collapse?

Two further objections to the classical theory were also prominent. First was the embarrassingly high rate of star formation predicted by a model governed by gravitational instability, in which objects should collapse on roughly the free-fall timescale, Equation (1.1), orders of magnitude shorter than the ages of typical galaxies.

Second was the gap between the angular momentum contained in a parcel of gas participating in rotation in a galactic disk and the much smaller angular momentum contained in any star rotating slower than breakup (Spitzer 1968). The disk of the Milky Way rotates with angular velocity $\Omega \simeq 10^{-15} \text{ s}^{-1}$. A uniformly collapsing cloud with initial radius R_0 formed from material with density $\rho_0 = 2 \times 10^{-24} \text{ g cm}^{-3}$ rotating with the disk will find its angular velocity increasing as $(R_0/R)^2$, or as $(\rho/\rho_0)^{2/3}$. By the time it reaches a typical stellar density of $\rho = 1 \text{ g cm}^{-3}$, its angular velocity has increased by a factor of 6×10^{15} , giving a rotation period of well under a second. The centrifugal force $\Omega^2 R$ exceeds the gravitational force by eight orders of magnitude for solar parameters. A detailed discussion including a demonstration that binary formation does not solve this problem can be found in Mouschovias (1991b).

The observational discovery of bipolar outflows from young stars (Snell, Loren & Plambeck 1980) was a surprise that was unanticipated by the classical model of star formation. It has become clear that the driving of these outflows is one part of the solution of the angular momentum problem, and that magnetic fields transfer the angular momentum from infalling to outflowing gas (e.g. Königl & Pudritz 2001).

Finally, mm-wave observations of emission lines from dense molecular gas revealed a further puzzle: extremely superthermal linewidths indicating that the gas was moving randomly at hypersonic velocities. (Zuckerman & Palmer 1974). Such motions in unmagnetized gas generate shocks that would dissipate the energy of the motions within a crossing time because of shock formation (e.g. Field 1978). Attempts were made using clump models of turbulence to

show that the decay time might be longer (Scalo & Pumphrey 1982, Elmegreen 1985). In hindsight, isolated spherical clumps turn out not to be a good model for turbulence however, so these models failed to accurately predict its behavior (Mac Low *et al.* 1998).

2.3 Standard Theory of Isolated Star Formation

The problems outlined in the preceding subsection were addressed in what we will call the “standard theory” of star formation that has formed the base of most work in the field for the past two decades. Mestel & Spitzer (1956) first noted that the problem of magnetic support against fragmentation could be resolved if mass could move across field lines, and proposed that this could occur in mostly neutral gas through the process of ion-neutral drift, usually known as ambipolar diffusion in the astrophysical community.² The other problems outlined then appeared solvable by the presence of strong magnetic fields, as we now describe.

Ambipolar diffusion can solve the question of how magnetically supported gas can fragment if it allows neutral gas to gravitationally condense across field lines. The local density can then increase without also increasing the magnetic field, thus decreasing the critical mass for gravitational collapse M_c given by Equation (2.6). This can also be interpreted as increasing the local mass-to-flux ratio, approaching the critical value given by Equation (2.7).

The timescale τ_{AD} on which this occurs can be derived by considering the relative drift velocity of neutrals and ions $\vec{v}_D = \vec{v}_i - \vec{v}_n$ under the influence of the magnetic field \vec{B} (Spitzer 1968). So long as the ionization fraction is small and we do not care about instabilities (e.g. Wardle 1990), the inertia and pressure of the ions may be neglected. The ion momentum equation then reduces in the

²In plasma physics, the term ambipolar diffusion is applied to ions and electrons held together electrostatically rather than magnetically while drifting together out of neutral gas.

steady-state to a balance between Lorentz forces and ion-neutral drag,

$$\frac{1}{4\pi}(\nabla \times \vec{B}) \times \vec{B} = \alpha \rho_i \rho_n (\vec{v}_i - \vec{v}_n), \quad (2.8)$$

where the coupling coefficient $\alpha = \langle \sigma v \rangle / (m_i + m_n)$, with m_i and m_n the mean mass per particle for the ions and neutrals, and ρ_i and ρ_n the ion and neutral densities. Typical values in molecular clouds are $m_i = 10 m_H$, $m_n = (7/3)m_H$, and $\alpha = 9.2 \times 10^{13}$. This is roughly independent of the mean velocity, as the cross-section σ scales linearly with velocity in the regime of interest (Osterbrock 1961, Draine 1980). To estimate the typical timescale, consider drift occurring across a cylindrical region of radius R , with a typical bend in the field also of order R so the Lorentz force can be estimated as roughly $B^2/4\pi R$. Then the ambipolar diffusion timescale can be derived by solving for v_D in Equation (2.8) to be

$$\begin{aligned} \tau_{AD} = \frac{R}{v_D} &= \left(\frac{4\pi\alpha\rho_i\rho_n R}{(\nabla \times \vec{B}) \times \vec{B}} \right) \approx \\ &= \frac{4\pi\alpha\rho_i\rho_n R^2}{B^2} = (25 \text{ Myr}) \left(\frac{B}{3 \mu\text{G}} \right)^{-2} \\ &\times \left(\frac{n_n}{10^2 \text{ cm}^{-3}} \right)^2 \left(\frac{R}{1 \text{ pc}} \right)^2 \left(\frac{x}{10^{-6}} \right), \end{aligned} \quad (2.9)$$

For ambipolar diffusion to solve the magnetic flux problem on an astrophysically relevant timescale, the ionization fraction x must be extremely small. With the direct observation of dense molecular gas (Palmer & Zuckerman 1967, Zuckerman & Palmer 1974) more than a decade after the original proposal by Mestel & Spitzer (1956), such low ionization fractions came to seem plausible. Nakano (1976, 1979) and Elmegreen (1979) computed the detailed ionization balance of molecular clouds for reasonable cosmic ray ionization rates, showing that at densities greater than 10^4 cm^{-3} , the ionization fraction was roughly

$$x \simeq (5 \times 10^{-8}) \left(\frac{n}{10^5 \text{ cm}^{-3}} \right)^{1/2} \quad (2.10)$$

(Elmegreen 1979), becoming constant at densities higher than 10^7 cm^{-3} or so. Below densities of

10^4 cm^{-3} , the ionization is controlled by the external UV radiation field, and the gas is tightly coupled to the magnetic field.

With typical molecular cloud parameters τ_{AD} is of order 10^7 yr (Equation 2.9). The ambipolar diffusion timescale τ_{AD} is thus about 10 – 20 times longer than the corresponding dynamical timescale τ_{ff} of the system (e.g. McKee *et al.* 1993). The delay induced by waiting for ambipolar diffusion to occur has the not incidental benefit of explaining why star formation is not occurring in a free-fall time, i.e. at rates far higher than observed in normal galaxies. On the other hand, the timescale is short enough to apparently explain why magnetic fields in the standard model do not completely shut off any star formation at all by fully preventing the collapse and fragmentation of molecular clouds. Altogether the ambipolar diffusion timescale appeared to be consistent with molecular cloud lifetimes, which in the 1980's were thought to be about 30-100 Myr (Solomon *et al.* 1987, Blitz & Shu 1980; see however Ballesteros-Paredes *et al.* 1999, and Elmegreen 2000, who argue for much shorter cloud lifetimes).

These considerations lead scientists to investigate star formation models that are based on magnetic diffusion as dominant physical process rather than rely on simple hydrodynamical collapse. In particular Shu (1977) proposed the self-similar collapse of initially quasi-static singular isothermal spheres as the most likely description of the star formation process. He assumed that ambipolar diffusion in a magnetically subcritical isothermal cloud core would lead to the build-up of a quasi-static $1/r^2$ -density structure which contracts on timescales of order of τ_{AD} . This evolutionary phase is denoted quasi-static because $\tau_{AD} \gg \tau_{ff}$. Ambipolar diffusion is supposed to eventually lead to the formation of a singularity in central density, at that stage the system becomes unstable and undergoes inside-out collapse. During collapse the model assumes that magnetic fields are no longer dynamically important and they are subsequently ignored in the original formulation of the theory. A rarefaction wave moves outward with the speed of sound

Table 2.2: Properties of the Shu solution of isothermal collapse.

	before core formation ($t < 0$)	after core formation ($t > 0$)
density profile	$\rho \propto r^{-2}, \forall r$ <i>sing. isothermal sphere</i>	$\rho \propto r^{-3/2},$ $\forall r \leq c_s t$ $\rho \propto r^{-2},$ $\forall r > c_s t$
velocity profile	$v \equiv 0, \forall r$	$v \propto r^{-1/2},$ $\forall r \leq c_s t$ $v \equiv 0, \forall r > c_s t$
accretion rate		$\dot{M} = 0.975 c_s^3 / G$ (<i>const.</i>)

with the cloud material behind the wave free-falling onto the core and matter ahead still being at rest. The Shu (1977) model predicts constant mass accretion onto the central protostar at a rate $\dot{M} = 0.975 c_s^3 / G$. This is significantly below the values derived for Larson-Penston collapse. In the latter case the entire system is collapsing dynamically and delivers mass to the center very efficiently, in the former case inward mass transport is comparatively inefficient as the cloud envelope remains at rest until reached by the rarefaction wave. The density structure of the inside-out collapse, however, is essentially indistinguishable from the predictions of dynamical collapse. To observationally differentiate between the two models one needs to obtain kinematical data and determine magnitude and spatial extent of infall motions with high accuracy. The basic predictions of inside-out collapse are summarized in Table 2.2. As singular isothermal spheres per definition carry infinite mass, the growth of the central protostar is thought to come to a halt when feedback processes (like bipolar outflows, stellar winds, etc.) become important and terminate further infall.

The overall picture of magnetic mediation and collapse of the singular isothermal sphere has become known as the so called ‘standard theory’ of star formation (as best summarized in the review by Shu *et al.* 1987). The process of stellar birth

can be subdivided into four stages: as visualized in Figure 2.3: (a) The *prestellar phase* describes the evolution of molecular cloud cores before the formation of a central protostar. Subcritical clumps contract slowly due to leakage of magnetic support by ambipolar diffusion, those cores form single stars. Supercritical cores evolve rapidly and may fragment to form multiple stellar systems. (b) Once the central density has reached a singular state, i.e. the protostar has formed, the system goes into inside-out collapse and feeds the protostar at constant rate $\dot{M} = 0.975 c_s^3 / G$. In this evolutionary phase the central protostar and its disk are deeply embedded in the protostellar envelope of dust and gas. The mass of the envelope M_{env} largely exceeds the combined mass M_* of star and disk. The main contribution to the total luminosity is accretion, and the system is best observable at sub-mm and infra-red wavelengths. In the astronomical classification scheme it is called ‘class 0’ object. (c) At later times, powerful protostellar outflows develop which clear out the envelope along the rotational axis. This is the ‘class I’ stage at which the system is observable in infra-red and optical wavebands and for which $M_{\text{env}} \ll M_*$. The central protostar is directly visible when looking along the outflow direction. (d) During the ‘class II’ phase, the outflow eventually removes the envelope completely. This terminates further mass accretion and the protostar enters the classical pre-main sequence contraction phase. It still is surrounded by a very low-mass disk of gas and dust which adds infrared ‘excess’ to the spectral energy distribution of the system (which is already dominated by the stellar Planck spectrum at visible wavelength, see e.g. Beckwith 1999). This is the stage during which planets are believed to form (e.g. Lissauer 1993, Ruden 1999). Protostellar systems at that stage are commonly called T Tauri stars (Bertout 1989). As time evolves further the disk becomes more and more depleted until only a tenuous dusty debris disk remains that is long-lived and lasts (i.e. continuously reforms) into and throughout the stellar main-sequence phase (Zuckermann 2001).

Largely within the framework of the ‘stan-

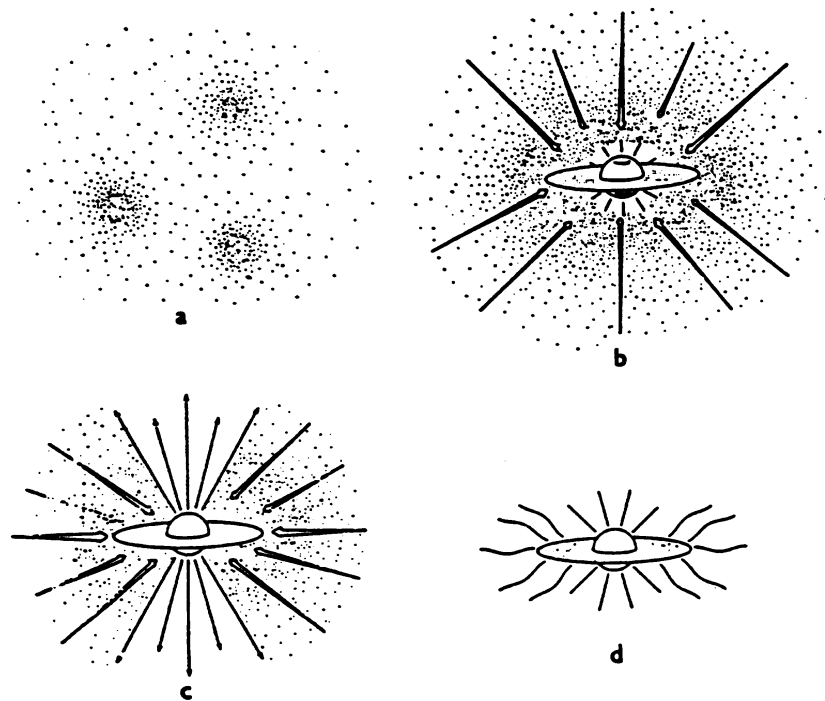


Figure 2.3: The main stages of star formation. (a) *Prestellar phase*. Protostellar cores form within molecular clouds in areas where self-gravity overwhelms non-thermal support mechanisms (i.e. magnetic flux loss via ambipolar diffusion in the ‘standard scenario’, or localized decay of supersonic turbulence in the new paradigm). (b) *Class 0 phase*. A protostellar object surrounded by an accretion disk has formed and grows in mass at the center of the infalling cloud. The object is visible in sub-mm and infra-red wavelength only because the central star is deeply embedded and its visible light is completely obscured by the massive cloud envelope. (c) *Class I phase*. Stellar winds and radiation break out along the rotational axis of the system, create a bipolar outflow and dissolve the envelope. The object becomes observable in the optical. (d) *Class II phase*. The envelope has become almost fully accreted or has been removed by stellar feedback processes and infall terminates. The young star and its (proto) planetary disk is fully revealed. This picture is still valid when star formation is controlled by supersonic turbulence. — Adopted from Shu *et al.* (1987).

dard theory’, numerous (analytical) extensions to the simplistic original inside-out collapse model have been proposed. The stability of isothermal gas clouds with rotation for example has been investigated by Schmitz (1983, 1984, 1986), Tereby, Shu, & Cassen (1984), Schmitz & Ebert (1986, 1987), Inutsuka & Miyama (1992), Nakamura, Hanawa, & Nakano (1995), and Tsuribe & Inutsuka (1999b). The effects of magnetic fields on the equilibrium structure of clouds and later during the collapse phase (where they have been neglected in the original inside-out scenario) are considered by Schmitz (1987), Baureis, Ebert, & Schmitz (1989), Tomisaka, Ikeuchi, & Nakamura (1988a,b, 1989a,b, 1990), Tomisaka (1991, 1995, 1996a,b), Galli & Shu (1993a,b), Li & Shu (1996, 1997), Galli *et al.* (1999, 2001), and Shu *et al.* (2000). The proposed picture is that ambipolar diffusion

of initially subcritical protostellar cores that are threaded by uniform magnetic fields will lead to the build-up of disk-like structures with constant mass-to-flux ratio. These disks are called ‘isopedic’. The mass-to-flux ratio increases steadily with time. As it exceeds the maximum value consistent with magnetostatic equilibrium the entire core becomes supercritical and begins to collapse from the inside out with the mass-to-flux ratio assumed to remain approximately constant. It can be shown (Shu & Li 1997), that for isopedic disks the forces due to magnetic tension are just a scaled version of the disks self-gravity with opposite sign (i.e. obstructing gravitational collapse), and that the magnetic pressure scales as the gas pressure (although the proportionality factor in general is spatially varying except in special cases). These findings allow to apply

many results derived for unmagnetized disks to the magnetized regime with only little modification to the equations. One application of this result is that for isopedic disks the derived mass accretion rate is just a scaled version of the original Shu (1977) rate, i.e. $\dot{M} \approx (1 + H_0) c_s^3 / G$, with the dimensionless parameter H_0 depending on the effective mass-to-flux ratio. Note, however, that the basic assumption of constant mass-to-flux ratio during the collapse phase appears inconsistent with detailed numerical calculations of ambipolar diffusion processes (see Section 2.4.1). In these computations the mass-to-flux ratio in the central region increases more rapidly than in the outer parts of the cloud. This leads to a separation into a dynamically collapsing inner core with $(M/\Phi)_n > 1$, and an outer envelope with $(M/\Phi)_n < 1$ that is still held up by the magnetic field. The parameter $(M/\Phi)_n$ is the dimensionless mass-to-flux ratio normalized to the critical value as given in Equation (2.7). The isopedic description may therefore only be valid in the central region with $(M/\Phi)_n > 1$.

Note also that the ‘standard theory’ introduces a somehow artificial dichotomy to the star formation process, in the sense that low-mass stars are thought to form from low-mass magnetically subcritical cores, whereas high-mass stars (or entire stellar clusters) form from magnetically supercritical cloud cores (e.g. Lizano & Shu 1989). This distinction became necessary as it became clear that the formation of very massive stars or stellar clusters cannot be regulated by magnetic fields and ambipolar diffusion processes (see Section 2.4.3). We will argue in the next section that this probably is true for low-mass stars also, and therefore that star formation is *not* regulated by magnetic mediation on *any* scale, but instead is mediated by interstellar turbulence (Section 2.6). The new theory constitutes a unifying scheme for both low-mass *and* high-mass star formation, thus removing the undesired artificial dichotomy introduced by the ‘standard theory’.

Finally let us remark, that the presence of strong magnetic fields was suggested as a way to explain the universally observed (Zuckerman & Palmer 1974) presence of hypersonic random mo-

tions in molecular clouds by Arons & Max (1975). They noted that linear Alfvén waves have no dissipation associated with them, as they are purely transverse. In a cloud with Alfvén speed $v_A = B/(4\pi\rho)^{1/2}$ much greater than the sound speed c_s , such Alfvén waves could produce the observed motions without necessarily forming strong shocks. This was generally, though incorrectly, interpreted to mean that these waves could therefore survive from the formation of the cloud, explaining the observations without reference to further energy input into the cloud. The actual work acknowledged that ambipolar diffusion would still dissipate these waves (Kulsrud & Pearce 1969, Zweibel & Josafatsson 1983) at a rate substantial enough to require energy input from a driving source to maintain the observed motions.

Strong magnetic fields furthermore provided a mechanism to reduce the angular momentum in collapsing molecular clouds through magnetic braking. Initially this was treated assuming that clouds were rigid rotating spheres (Ebert, von Hoerner, & Temesváry 1960), but was accurately calculated by Mouschovias & Paleologou (1979, 1980) for both perpendicular and parallel cases. They showed that the criterion for braking to be effective was essentially that the outgoing helical Alfvén waves from the rotating cloud had to couple to a mass of gas equal to the mass in the cloud. Mouschovias & Paleologou (1980) show that this leads to a characteristic deceleration time for a parallel rotator of density ρ and thickness H embedded in a medium of density ρ_0 and Alfvén velocity $v_A = B/(4\pi\rho_0)^{1/2}$ of

$$\tau_{\parallel} = (\rho/\rho_0)(H/2v_A), \quad (2.11)$$

and a characteristic time for a perpendicular rotator with radius R ,

$$\tau_{\perp} = \frac{1}{2} \left[\left(1 + \frac{\rho}{\rho_0} \right)^{1/2} - 1 \right] \frac{R}{v_A}. \quad (2.12)$$

For typical molecular cloud parameters, these times can be less than the free-fall time, leading to efficient transfer of angular momentum away from collapsing cores. This may help to resolve the so called angular momentum problem in star formation (e.g. Bodenheimer 1995)

which describes the puzzle that single stars have considerably smaller specific angular momenta j compared to the observed molecular cloud cores they supposedly form from. The angular momentum problem occurs essentially on all scales, as values of j in molecular cloud cores again are smaller than in the average molecular cloud material which they condense out of, and on the largest scales molecular cloud complexes as a whole seem again to have smaller specific angular momenta than the global interstellar medium in differentially rotating galactic disks.

2.4 Problems with Standard Theory

During the 1980's the theory of magnetically mediated star formation discussed in the previous section was widely advocated and generally accepted as the standard theory of low-mass star formation, almost completely replacing the earlier dynamical models. However, despite its success and intellectual beauty, the picture of magnetically mediated star formation suffers from a series of severe shortcomings. It may not actually bear much relevance for the astrophysical problem of how stars form and grow in mass – although for its simplicity and elegance it clearly is a pedagogically important model of the star formation process. The prediction that low-mass stars, and hence the vast majority of all stars, form from molecular cloud cores that closely resemble quasi-static, singular, isothermal spheres which built up via ambipolar diffusion processes from magnetically supported gas on timescales of several tens of the free-fall timescale deserves criticism from several sides – for theoretical as well as for observational reasons. This became obvious in the 1990's with improved numerical simulations and the advent of powerful new observational techniques, especially in the sub-mm and infrared wavelength regime. Critical summaries are given by Whitworth *et al.* (1996) and Nakano (1998). Note also that the theory traditionally was applied to the formation of low-mass stars, it was never seriously held accountable for describing the birth of very high-mass stars and

stellar clusters (Shu *et al.* 1987). This led to speculations about two distinct modes of star formation, low-mass stars forming from magnetically supported cloud cores and high-mass stars forming from magnetically supercritical cloud material. We shall discuss in Sections 2.5 and 2.6 that replacing magnetic fields as the pivotal physical mechanism of the theory and introducing instead interstellar turbulence as the central mediating agent of star formation naturally leads to a unified scheme for all mass and length scales and removes this disturbing dichotomy.

Before we introduce the new dynamical theory of star formation based on interstellar turbulence, we need to analyze in detail the properties and shortcomings of the theory we seek to replace. The following therefore is a list of critical remarks and summarizes the inconsistencies of models of magnetically mediated star formation. We begin with the *theoretical* considerations that make the inside-out collapse of quasistatic singular isothermal spheres a very unlikely description of stellar birth, which constitutes the essence of the 'standard theory'. We then discuss the *observational* inconsistencies of the theory.

2.4.1 Singular Isothermal Spheres

The collapse of singular isothermal spheres is the astrophysically most unlikely and unstable member of a large family of self-similar solutions to the 1-dimensional collapse problem. Ever since the seminal studies by Bonnor (1956) and Ebert (1957) and by Larson (1969) and Penston (1969a) much attention in the star formation community has been focused on finding astrophysically relevant analytic asymptotic solutions to the 1-dimensional collapse problem. The standard solution was derived by Shu (1977) considering the evolution of initially singular isothermal spheres as they leave equilibrium. His findings subsequently were extended by Hunter (1977, 1986), and Whitworth & Summers (1985) demonstrated that all solutions to the isothermal collapse problem are members of a two-parameter family with the Larson-Penston-type solutions (collapse of spheres with uniform central density) and the

Shu-type solutions (expansion-wave collapse of singular spheres) populating extreme ends of parameter space. The problem set has been extended to include a polytropic equation of state (Suto & Silk 1988), shocks (Tsai and Hsu 1995), and/or cylinder and disk-like geometries (Inutsuka and Miyama 1992; Nakamura, Hanawa, & Nakano 1995). In addition, mathematical generalization using a Lagrangian formulation has been proposed by Hendriksen (1989, see also Hendriksen, André, and Bontemps 1997).

Of all proposed initial configurations for protostellar collapse, quasi-static, singular, isothermal spheres seem to be the most difficult to realize in nature. Stable equilibria for self-gravitating spherical isothermal gas clouds embedded in an external medium of given pressure are only possible up to a density contrast of $\rho_c/\rho_s \approx 14$ between the cloud center and surface. Clouds that are more centrally concentrated than that critical value can only find unstable equilibrium states. Hence, all evolutionary paths that could yield a central singularity lead through instability, and collapse is likely to set in long before a $1/r^2$ density profile is established at small radii r (Whitworth *et al.* 1996; also Silk & Suto 1988, and Hanawa & Nakayama 1997). External perturbations tend to break spherical symmetry in the innermost region and degrade the overall density profile at small radii. It will become less strongly peaked. The resulting behavior in the central region then more closely resembles the Larson-Penston description of collapse. Similar behavior is found if outward propagating shocks are considered (Tsai and Hsu 1995). As a consequence, the existence of physical processes that are able to produce singular isothermal equilibrium spheres in nature is highly questionable. Furthermore, the original proposal of ambipolar diffusion processes in magnetostatically supported gas does not yield the desired result either.

Ambipolar diffusion in initially magnetically supported gas clouds results in dynamical Larson-Penston-type collapse of the central region where magnetic support is lost, while the outer part is still hold up primarily by the field (and develops a $1/r^2$ density profile). Mass is

fed to the center not due to an outward moving expansion wave, but due to ambipolar diffusion in the outer envelope. The proposal that singular isothermal spheres may form through ambipolar diffusion processes in magnetically subcritical cores has been extensively studied by Mouschovias and collaborators in a series of numerical simulations with ever increasing accuracy and astrophysical detail (Mouschovias 1991, Mouschovias & Morton 1991, 1992a,b, Fiedler & Mouschovias 1992, 1993, Morton *et al.* 1994, Ciolek & Mouschovias 1993, 1994, 1995, 1996, 1998, Basu and Mouschovias 1994, 1995a,b, Desch & Mouschovias 2001; see however also Nakano 1979, 1982, 1983, Lizano & Shu 1989, or Safier *et al.* 1997). The numerical results indicate that the decoupling between matter and magnetic fields occurs over several orders of magnitude in density becoming important at densities $n(\text{H}_2) > 10^{10} \text{ cm}^{-3}$ (i.e. there is no single critical density below which matter is fully coupled to the field and above which it is not), and that ambipolar diffusion indeed is the dominant physical decoupling process (e.g. Desch & Mouschovias 2001). As a consequence of ambipolar diffusion, initially subcritical protostellar gas clumps separate into a central nucleus, which becomes both thermally and magnetically supercritical, and an extended envelope that is still held up by static magnetic fields. The central region goes into rapid collapse sweeping up much of its residual magnetic flux with it. The dynamical behavior of this core more closely resembles the Larson-Penston description of collapse than the Shu solution (Basu 1997). The low-density envelope contains most of the mass, roughly has a $1/r^2$ density profile, and contracts only slowly. It feeds matter into the central collapse region on the ambipolar diffusion timescale.

Star formation from singular isothermal spheres is biased against binary formation. The collapse of rotating singular isothermal spheres very likely will result in the formation of single stars, as the central protostellar object forms very early and rapidly increases in mass with respect to a simultaneously forming and growing rotationally supported protostellar disk (e.g. Tsuribe & Inut-

suka 1999a,b). By contrast, the collapse of cloud cores with flat inner density profiles will deliver a much smaller fraction of mass directly into the central protostar within a free-fall time. More matter will go first into a rotationally supported disk-like structure. These disks tend to be more massive with respect to the central protostar in a Larson-Penston-type collapse scenario compared to collapsing singular isothermal spheres, and they are more likely to become unstable against sub-fragmentation resulting in the formation of binary or higher-order stellar systems (see the review by Bodenheimer *et al.* 2000). Since the majority of stars seems to form as part of binary or higher-order system (e.g. Mathieu *et al.* 2000), star formation in nature appears incompatible with collapse from strongly centrally peaked initial conditions (Whitworth *et al.* 1996).

2.4.2 Observations of Clouds and Cores

Before we consider the observational evidence against the ‘standard theory’ of magnetically mediated star formation, let us recapitulate its basic predictions as introduced in Section 2.3. The theory predicts (a) constant accretion rates and (b) infall motions that are confined to regions that have been passed by a rarefaction wave that moves outwards with the speed of sound, while the parts of a core that lie further out are assumed to remain static. The theory furthermore (c) relies on the presence of magnetic field strong enough to hold up the protostellar gas from collapsing, i.e. it predicts that protostellar cores should be magnetically subcritical during the largest fraction of their lifetime. In the following we demonstrate *all* these predictions are contradicted by observations.

Magnetic Support

Most (if not all) protostellar cores with magnetic field measurements are supercritical. When the theory was promoted in the late 1970’s and 1980’s accurate measurements of magnetic field strength in molecular clouds and cloud cores did not exist or were highly uncertain. Consequently, magnetic fields in molecular cloud were

essentially *assumed* to have the desired properties necessary for the theory to work and to circumvent the observational problems associated with the classical dynamical theory (Section 2.2). In particular the field was thought to have a strong fluctuating component associated with magnetohydrodynamic waves that give rise to the super-thermal linewidths ubiquitously observed in molecular cloud material and non-thermal support against self-gravity. Even today, accurate determinations of magnetic field strengths in molecular cloud cores are rare. Most field estimates rely on measuring the Zeeman splitting in molecular lines, typically OH, which is very difficult and observationally challenging (e.g. Heiles 1993). Hence, the number of clouds in which the Zeeman effect has been detected above the 3σ significance level at present is less than 20, whereas the number of non-detections or upper limits is considerably larger. For a compilation of field strengths in low-mass cores see Crutcher (1999), or more recent work by Bourke *et al.* (2001). Results from studying masers around high-mass stars are excluded in these analyses as in that environment the gas density and velocity dispersion are very uncertain, and the presence of the high-mass star is likely to significantly alter the local density and magnetic field structure with respect to the initial cloud properties at the onset of star formation.

In his critical review of the ‘standard theory’ of star formation Nakano (1998) pointed out that *no* convincingly magnetically subcritical core had been found up to that time. Similar conclusions still hold today, *all* magnetic field measurements are consistent with protostellar cores typically being magnetically supercritical or at most marginally critical. This is indicated in Figure 2.4, which plots the observed line-of-sight magnetic field B_{los} against the column density $N(\text{H}_2)$ determined from CO measurements. In particular when including non-detections and upper limits into the analysis, the general conclusion is that magnetic fields are too weak to prevent or considerably postpone the gravitational collapse of protostellar cores. The basic assumption of the ‘standard theory’ of magnetically mediated star

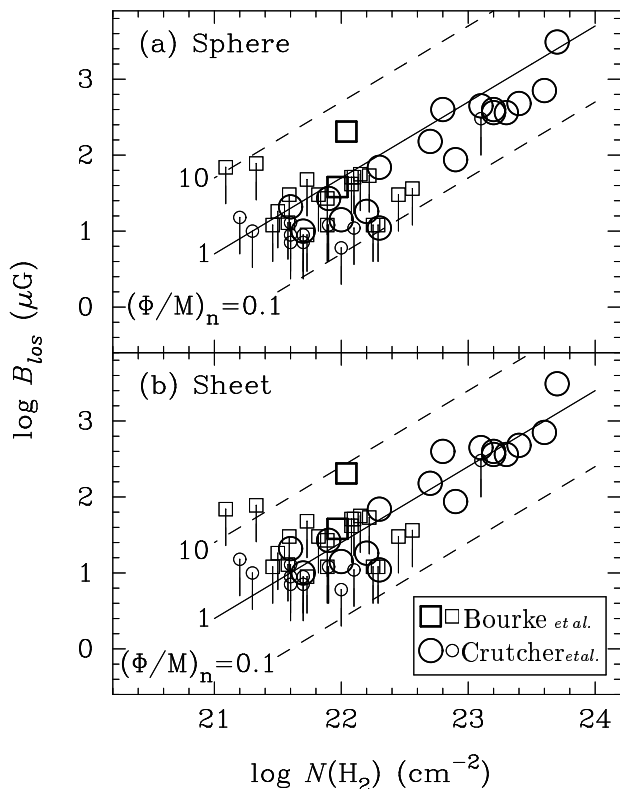


Figure 2.4: Line-of-sight magnetic field strength B_{los} versus column density $N(\text{H}_2)$ for various molecular cloud cores. Squares indicated values determined by Bourke *et al.* (2001) and circles denote observations summarized by Crutcher (1990), Sarma *et al.* (2000), and Crutcher & Troland (2000). The large symbols represent clear detections of the Zeeman effect, whereas the small denote 3σ upper limits to the field strength. The lines drawn for the upper limits illustrate the shift from the 3σ to the 1σ level of detection. To guide your eye, lines of constant flux-to-mass ratio $(\Phi/M)_n$ are indicated normalized to the critical value, i.e. to the inverse of equation (2.7). The observed line-of-sight component B_{los} of the field is being (statistically) deprojected to obtain the absolute value of the field B . The upper panel (a) hereby assumes spherical core geometry, while the flux-to-mass ratios in the lower panel (b) are computed for sheetlike structures. Values $(\Phi/M)_n < 1$ indicate magnetic field strengths insufficient of supporting against gravitational contraction, i.e. cores are magnetically supercritical. On the other hand, $(\Phi/M)_n > 1$ indicates magnetic support as required by the ‘standard theory’. Note that almost all cores are magnetically supercritical. This is evident when assuming spherical symmetry, but also in the case of sheetlike protostellar cores the average ratio is $\langle(\Phi/M)_n\rangle \approx 0.4$ when considering the 1σ upper limits. This is significantly lower than the critical value. (From Bourke *et al.* 2001.)

formation therefore seems in contradiction to the observational facts. Partial reconciliation, however, between the theory and the observations may be achieved when taking the extreme ge-

ometrical assumption that all protostellar cores are highly flattened, i.e. essentially sheetlike objects (Shu *et al.* 1999). Only then, flux-to-mass ratios can be derived that come close to the critical value of equilibrium between magnetic pressure and gravity, but even for sheetlike ‘cores’ the average flux-to-mass ratio lies by a factor of 2 to 3 below the critical value when taking all measurements into account including the upper limits at the 1σ level (Bourke *et al.* 2001). In addition, highly flattened morphologies appears to be inconsistent with the observed density structure of protostellar cores. They typically appear as ‘roundish’ objects (like the dark globule B68 which almost perfectly resembles a Bonnor-Ebert sphere, see Alves *et al.* 2001) and more likely are moderately prolate (with axis ratios of about 2:1) than highly oblate (with axis ratios $\sim 6:1$) when statistically deprojected (Myers *et al.* 1991, Ryden 1996; however, some authors prefer the oblate interpretation, see Li & Shu 1996, Jones, Basu, & Dubinski 2001). Altogether the observational evidence suggests that stars form from magnetically supercritical cloud core rather than from magnetically supported structures.

Molecular clouds as a whole are magnetically highly supercritical and therefore subject to dynamical collapse. It is generally believed that molecular clouds and giant molecular cloud complexes as a whole are dynamical objects that are magnetically supercritical and bound by self-gravity, rather than being magnetically subcritical and prevented from expansion by external pressure or large-scale galactic magnetic fields. This follows from a careful analysis of the virial balance equations (McKee 1989, McKee *et al.* 1993, Williams *et al.* 2000). This analysis can be extended to the substructure within molecular clouds, to clumps and protostellar cores. Bertoldi & McKee (1992) already argued that very massive clumps that form stellar clusters need to be magnetically supercritical.

This conclusion was extended to low-mass cloud cores by Nakano (1998) on the basis of the following argument: Clumps and cores in molecular clouds are generally observed as regions of significantly larger column density compared to

the cloud as a whole (e.g. Benson and Myers 1989, Tatematsu *et al.* 1993). If a protostellar core were magnetically subcritical it needs to be confined by the mean cloud pressure or mean magnetic field in the cloud, otherwise it would quickly expand and disappear. Calculations of the collapse of strongly subcritical cores such as those by Ciolek & Mouschovias (1994) fix the magnetic field at the outer boundaries, artificially confining the cloud. Under the assumption of virial equilibrium, typical values for the mean pressure and mean magnetic field in molecular clouds demand column densities in cores that are comparable to those in the ambient molecular cloud material. This contradicts the observed large column density enhancements in cloud cores, and is additional evidence that also low-mass cores are magnetically supercritical and collapsing.

Infall Motions

Protostellar infall motions are detected on scales larger and with velocities greater than predicted by the ‘standard theory’. One of the basic assumptions of the standard theory is the existence of a long-lasting quasi-static phase in protostellar evolution. Before the formation of the central young stellar object (YSO), molecular cloud cores are held up by strong magnetic fields and evolve slowly as matter filters through the field lines by ambipolar diffusion on timescales exceeding the free-fall time by a factor of ten or more. Once the central singularity is established, the system undergoes collapse from the inside out, set in motion by an expansion wave that moves outwards with the speed of sound. Gas inside the expansion wave approaches free-fall and feeds the central protostar at a constant accretion rate, while gas further out remains at rest. Therefore the theory predicts that prestellar cores (i.e. cloud cores without central YSO, see e.g. André *et al.* 2000 for a discussion) should show no signatures of infall motions, and that protostellar cores at later stages of the evolution should exhibit collapse motions confined to their central regions. This can be tested by mapping molecular cloud cores at the same time in optically thick as well as thin lines. Inward motions can in principle be inferred

from the asymmetry of optically thick lines, however the signal is convolved with signatures of rotation and possible outflows (when looking at protostellar cores that already contain embedded YSO’s). The optically thin line is needed to determine the zero point of the velocity frame (see e.g. Myers *et al.* 1996).

One of the best studied examples is the ‘starless’ core L1544 which exhibits infall asymmetries (implying velocities up to 0.1 km s^{-1}) that are too extended ($\sim 0.1 \text{ pc}$) to be consistent with inside-out collapse (Tafalla *et al.* 1998, Williams *et al.* 1999). Similar conclusions can be derived for a variety of other sources (see the review of Myers, Evans, & Ohashi 2000; or the extended survey for infall motions in prestellar cores by Lee, Myers, and Tafalla 1999, 2001). Typical contraction velocities in the prestellar phase are between 0.05 and 0.1 km s^{-1} , corresponding to mass infall rates ranging from a few 10^{-6} to a few $10^{-5} M_{\odot} \text{ yr}^{-1}$. The sizes of the infalling regions (e.g. as measured in CS) typically exceed the sizes of the corresponding cores as measured in high-density tracers like N_2H^+ by a factor of 2–3. Even the dark globule B335, which was considered “a theorists dream” (Myers *et al.* 2000) and which was thought to match ‘standard theory’ very well (Zhou *et al.* 1993) is also consistent with Larson-Penston collapse (e.g. Masunaga and Inutsuka 2001) when using improved radiation transfer techniques but relying on single dish data only. The core however exhibits considerable sub-structure and complexity (clumps, outflows, etc.) when observed with high spatial and spectral resolution using interferometry (Wilner *et al.* 2001). This raises questions about the applicability of *any* 1D isothermal collapse model to objects where high resolution data are available.

Extended inward motions are a common feature in prestellar cores, and appear a necessary ingredient for the formation of stars as predicted by dynamical theories (Sections 2.1 and 2.6).

Density Profiles

Prestellar cores have flat inner density profiles. The basis of the Shu (1977) model is the singu-

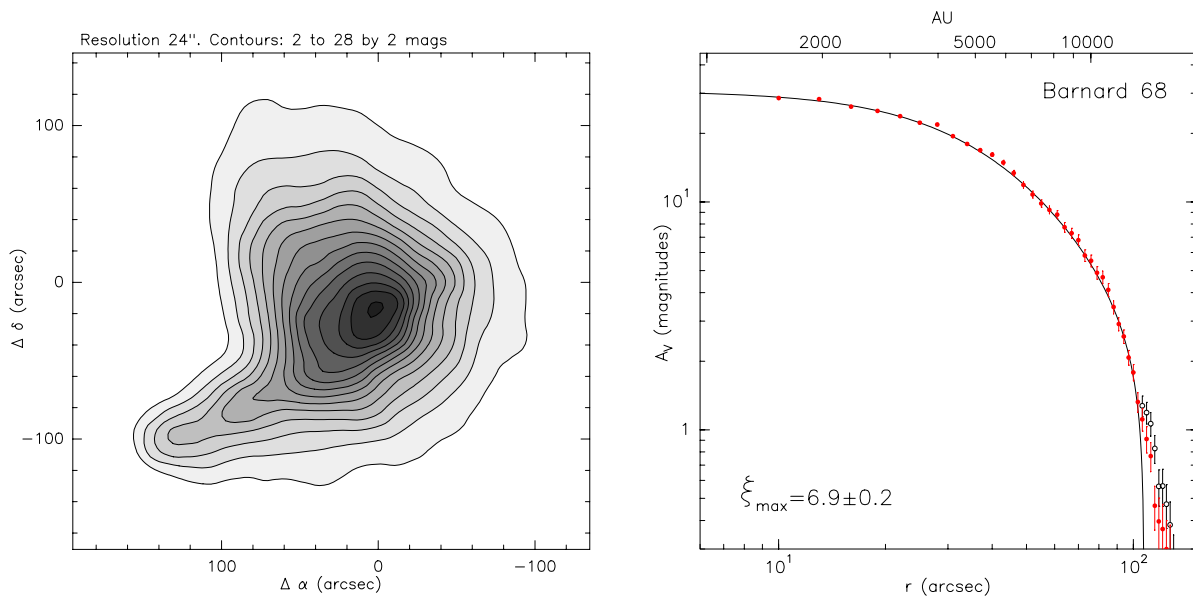


Figure 2.6: Optical extinction map (left image) and resulting azimuthally averaged radial surface density profile (right image) of the dark globule B68 (from Alves *et al.* 2001). The resolution of the map is $24''$ and the contour levels indicate steps of two magnitudes of extinction. The density profile is remarkably well fitted by a marginally supercritical Bonnor-Ebert sphere with concentration parameter $\xi_{\max} \approx 6.9$ (where the critical value is $\xi_{\max} = 6.5$). Filled red symbols give the observed radial profile and corresponding errors when the elongated tail at the lower left is dismissed, open symbols denote the result from the complete map. Spherical symmetry is an excellent approximation for the inner parts of B68, noticeable deviations occur at the surface layers at the 10%-level of the central density. Data are from Alves *et al.* (2001).

lar isothermal sphere, i.e. the theory assumes radial density profiles $\rho \propto 1/r^2$ at all radii r as starting conditions of protostellar collapse. The advent of a new generation of infrared detectors and powerful receivers in the radio and sub-mm waveband in the late 1990's made it possible to directly test this hypothesis and determine the radial (column) density profile of prestellar cores with high sensitivity and resolution (e.g. Ward-Thompson *et al.* 1994, André *et al.* 1996, Motte, André, and Neri 1998, Ward-Thompson *et al.* 1999, Bacmann *et al.* 2001, Motte and André 2001). These studies show that starless cores typically have flat inner density profiles out to radii of a few 10^{-2} pc followed by a radial decline of roughly $\rho \propto 1/r^2$ and possibly a sharp outer edge at radii 0.05 – 0.3 pc (see the review of André *et al.* 2000). This is illustrated in Figure 2.5 which shows the observed column density of the starless core L1689B derived from combining mid-infrared absorption maps with 1.3 mm dust continuum emission maps (Bacmann *et al.* 2001). The density structure in the prestellar

phase appears consistent with pressure-bounded Bonnor-Ebert spheres (Bonnor 1956, Ebert 1955) with sufficient density contrast to imply instability against gravitational collapse. This impression is strengthened further by recent findings from multi-wavelength stellar extinction studies of dark globules. For example, the density distribution of the dark globule B68 is in nearly perfect agreement with being a marginally supercritical Bonnor-Ebert sphere, as illustrated in Figure 2.6 (Alves, Lada, & Lada 2001). Altogether high-resolution mapping of prestellar cores provides the most direct evidence against singular isothermal spheres as initial conditions of protostellar collapse.

Chemical Ages

The chemical age of substructure in molecular cloud is much smaller than the ambipolar diffusion time. This poses a timescale argument against magnetically regulated star formation, and comes from the investigation of the chemical status of density fluctuations in molecular

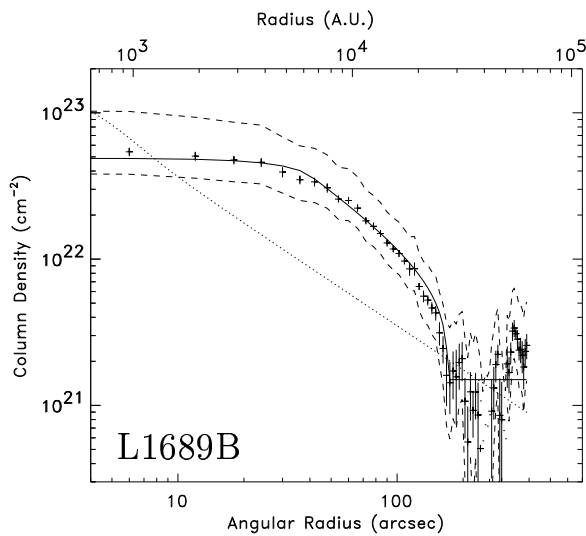


Figure 2.5: Radial column density profile of the prestellar core L1689B derived from combined infrared absorption and 1.3 mm continuum emission maps. Crosses show the observed values with the corresponding statistical errors, while the total uncertainties in the method are indicated by the dashed lines. For comparison, the solid line denotes the best-fitting Bonnor-Ebert sphere and the dotted line the column density profile of an singular isothermal sphere. The observed profile is well reproduced by an unstable Bonnor-Ebert sphere with a density contrast of ~ 50 , see Bacmann *et al.* 2000 for a further details.

clouds. The comparison of multi-molecule observations of cloud cores with time-dependent chemical models indicates typical ages of about 10^5 years (e.g. Bergin & Langer 1997, Pratap *et al.* 1997, Aikawa *et al.* 2001; or see the reviews by van Dishoeck *et al.* 1993, van Dishoeck & Black 1998, and Langer *et al.* 2000). This is significantly shorter than the timescale required for ambipolar diffusion to become important as required in the standard model. The inferred chemical ages of molecular cloud cores appear only compatible with supersonic, and super-Alfvénic turbulence as being the main agent that determines molecular cloud structure and regulates the star formation process (see Sections 2.5 and 2.6).

2.4.3 Observations of Protostars and Young Stars

Accretion Rates

Protostellar accretion rates decline with time. As an immediate consequence of the assumed sin-

gular $1/r^2$ initial density profile, the Shu (1977) model predicts constant protostellar accretion rates $\dot{M}_* = 0.975c_s^3/G$, with sound speed c_s and gravitational constant G . As matter falls onto the central protostar it goes through a shock and releases energy that is radiated away giving rise to a luminosity $L_{\text{acc}} \approx GM_*\dot{M}_*/R_*$ (Shu *et al.* 1987, 1993). The fact that most of the matter first falls onto a protostellar disk, where it gets transported inwards on a viscous timescale before it is able to accrete onto the star does not alter the expected overall luminosity by much (see e.g. Hartmann 1998).

During the early phases of protostellar collapse, i.e. as long as the mass M_{env} of the infalling envelope exceed the mass M_* of the central protostar, the accretion luminosity L_{acc} by far exceeds the intrinsic luminosity L_* of the young star. Hence the observed bolometric luminosity L_{bol} of the object is a direct measure of the accretion rate as long as reasonable estimates of M_* and R_* can be obtained. Determinations of bolometric temperature T_{bol} and luminosity L_{bol} therefore should provide a fair estimate of the evolutionary stage of a protostellar core (e.g. Chen *et al.* 1995, Myers *et al.* 1998). Scenarios in which the accretion rate decreases with time and increases with total mass of the collapsing cloud fragment yield qualitatively better agreement with the observations than do models with constant accretion rate (André *et al.* 2000, see however Jayawardhana, Hartmann, & Calvet 2001, for an alternative interpretation based on environmental conditions). A comparison of observational data with theoretical models where \dot{M}_* decreases exponentially with time is shown in Figure 2.7.

A closely related method to estimate the accretion rate \dot{M}_* is by determining protostellar outflow strengths (Bontemps *et al.* 1996). It is known that most embedded young protostars are associated with powerful molecular outflows (Richer *et al.* 2000) and that the outflow activity decreases towards later evolutionary stages. For protostars at the end of their main accretion phase there exists a clear correlation between the outflow momentum flux F_{CO} and the bolometric luminosity L_{bol} (e.g. Cabrit & Bertout 1992). Furthermore,

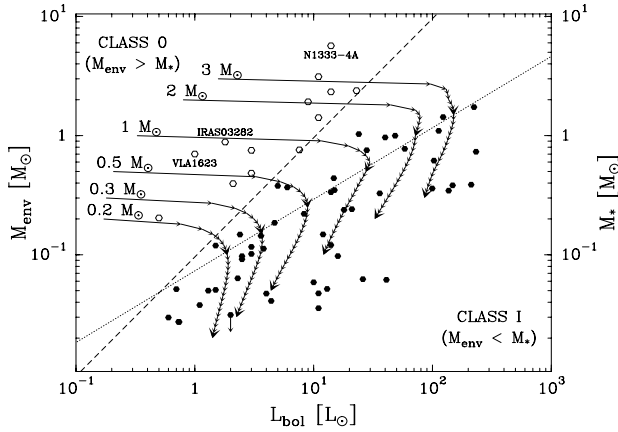


Figure 2.7: $M_{\text{env}} - L_{\text{bol}}$ diagram for a sample of protostellar cores in the main accretion phase from André & Montmerle (1994) and Saraceno *et al.* (1996). Open circles indicate objects for which the envelope mass exceeds the mass of the central protostar ($M_{\text{env}} > M_{\star}$) and filled circles denote the later evolutionary stage where $M_{\text{env}} < M_{\star}$. Overlaid are evolutionary tracks that assume bound initial configuration of finite mass and that have $L_{\text{bol}} = GM_{\star}\dot{M}_{\star}/R_{\star} + L_{\star}$ with L_{\star} from Stahler (1988) and with both, M_{env} and $\dot{M}_{\star} = M_{\text{env}}/\tau$ ($\tau \approx 10^5$ yr), declining exponentially with time (Bontemps *et al.* 1996, also Myers *et al.* 1998). Exponentially declining \dot{M}_{\star} show better agreement with the data than do constant accretion rates. Small arrows are plotted on the tracks every 10^4 yr, and large arrows when 50% and 90% of the total mass is accreted onto the central YSO. The dashed and dotted lines indicate the transition from $M_{\text{env}} > M_{\star}$ to $M_{\text{env}} < M_{\star}$ using two different relations, $M_{\star} \propto L_{\text{bol}}$ and $M_{\star} \propto L_{\text{bol}}^{0.6}$, respectively, indicating the range proposed in the literature (e.g. André & Montmerle 1994, or Bontemps *et al.* 1996). The latter relation is suggested by the accretion scenario adopted in the tracks. The figure is adapted from André *et al.* (2000).

F_{CO} is well correlated with M_{env} for all protostellar cloud cores (Bontemps *et al.* 1996, Hoherheijde *et al.* 1998, Henning and Launhardt 1998). This result is independent of the $F_{\text{CO}} - L_{\text{bol}}$ relation and most likely results from a progressive decrease of outflow power with time during the main accretion phase. With the linear correlation between outflow mass loss and protostellar accretion rate (Hartigan *et al.* 1995) these observations therefore suggest stellar accretion rates \dot{M}_{\star} that decrease with time. This is illustrated in Figure 2.8 which compares the observed values of the normalized outflow flux and the normalized envelope mass for a sample of ~ 40 protostellar cores with a simplified dynamical collapse model

with decreasing accretion rate \dot{M}_{\star} (Hendriksen *et al.* 1997). The model describes the data relatively well, as opposed to models of constant \dot{M}_{\star} .

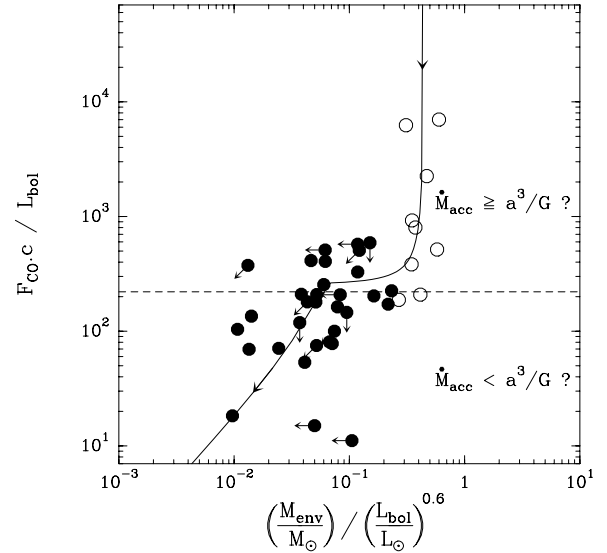


Figure 2.8: Outflow momentum flux F_{CO} plotted against envelope mass M_{env} normalized to the bolometric luminosity L_{bol} using the relations $M_{\text{env}} \propto L_{\text{bol}}^{0.6}$ and $F_{\text{CO}c} \propto L_{\text{bol}}$. Protostellar cores with $M_{\text{env}} > M_{\star}$ are indicated by open circles, and $M_{\text{env}} < M_{\star}$ by filled circles (data from Bontemps *et al.* 1996). $F_{\text{CO}c}/L_{\text{bol}}$ is an empirical tracer for the accretion rate, and the speed of light c is invoked in order to obtain a dimensionless quantity. $M_{\text{env}}/L_{\text{bol}}^{0.6}$ is an evolutionary indicator that decreases with time. The abscissa therefore corresponds to a time axis with early times at the right and late evolutionary stages at the left. Overlaid on the data is a evolutionary model that assumes a flat inner density profile (for details see Hendriksen *et al.* 1997, where the figure was published originally).

Embedded Objects

The fraction of protostellar cores with embedded protostellar objects is very high. Further indication that the standard theory may need to be modified comes from estimates of the time spent by protostellar cores during various stages of their evolution. For a sample of protostars, the relative numbers of objects in distinct evolutionary phases roughly correspond to the relative time spent in each phase. Beichman *et al.* (1986) used the ratio of numbers of starless cores to the numbers of cores with embedded objects detected with the *Infrared Astronomical Satellite* (IRAS) and estimated that the duration of

the prestellar phase is about equal to the time needed for a young stellar object to completely accrete the protostellar envelope it is embedded in. As the standard model assumes cloud cores in the prestellar phase evolve on ambipolar diffusion timescales, which are an order of magnitude longer than the dynamical timescales of the later accretion phase, one would expect a significantly larger number of starless cores than cores with embedded protostars. Millimeter continuum mapping of pre-stellar cores gives similar results (Ward-Thompson *et al.* 1994, 1999), leading André *et al.* (2000) to argue that the timespan of cores to increase their central density $n(\text{H}_2)$ from $\sim 10^4$ to $\sim 10^5 \text{ cm}^{-3}$ is about the same as to go from $n(\text{H}_2) \approx 10^5 \text{ cm}^{-3}$ to the formation of the central protostar. This clearly disagrees with standard ambipolar diffusion models (e.g. Ciolek & Mouschovias 1994) which predict a six times longer duration. Ciolek & Basu (2000) were indeed able to accurately model infall in L1544 using an ambipolar diffusion model, but they did so by using initial conditions that were already almost supercritical, so that very little ambipolar diffusion had to occur before dynamical collapse would set in. Ciolek & Basu (2001) quantify the central density required to match the observations, and conclude that observed pre-stellar cores are either already supercritical or just about to be. Altogether these considerations suggest that already in the prestellar phase the timescales of core contraction are determined by fast dynamical processes rather than by slow ambipolar diffusion.

Stellar Ages

Stellar age spreads in young clusters are small. If the contraction time of individual cloud cores in the prestellar phase is determined by ambipolar diffusion rather than by dynamical collapse (or turbulent dissipation, see Sections 2.5 and 2.6), then the age spread in a stellar population (say in a young cluster) should considerably exceed the relevant dynamical timescales. Within a star-forming region high-density protostellar cores will evolve and form a central YSO faster than their low-density counterparts, and the age

distribution is roughly determined by the evolution time of the lowest-density condensation. Note, that ambipolar diffusion time τ_{AD} and free-fall time τ_{ff} both are inversely proportional to square root of the density, $\tau_{\text{AD}} \propto \tau_{\text{ff}} \propto \rho^{-1/2}$, and that $\tau_{\text{AD}} \approx 10\tau_{\text{ff}}$ under typical conditions (e.g. McKee *et al.* 1993).

However, the age spread in star clusters is very short. For example in the Orion Trapezium cluster it is less than 10^6 years (Prosser *et al.* 1994, Hillenbrand 1997, Hillenbrand & Hartmann 1998), and the same holds for L1641 (Hodapp & Deane 1993). The age spread is comparable to the dynamical time in these clusters. Similar conclusions can be obtained for Taurus (Hartmann 2001), NGC 1333 (Bally *et al.* 1996, Lada *et al.* 1996), NGC 6531 (Forbes 1996), and a variety of other clusters (see Elmegreen *et al.* 2000 for a review, also Palla & Stahler 1999, Hartmann 2001). There is a relation between the duration of star formation and the size of the star forming region. Larger regions form stars for a longer timespan. This correlation is comparable to the linewidth-size relation, or the crossing time-size relation, respectively, found for molecular gas, and suggests that typical star formation times correspond to about 2 to 3 turbulent crossing times in that region (Efremov & Elmegreen 1998). This is very fast compared to the ambipolar diffusion timescale, which is about 10 crossing times in a uniform medium with cosmic ray ionization (Shu *et al.* 1987) and is even longer if stellar UV sources contribute to the ionization (Myers & Khersonsky 1995) or if the cloud is very clumpy (Elmegreen & Combes 1992). Magnetic fields, therefore, cannot regulate star formation on scales of stellar clusters.

2.5 Beyond the Standard Theory

New understanding of the behavior of turbulence has suggested that it may be more important than previously thought in the support of molecular clouds against gravitational collapse.

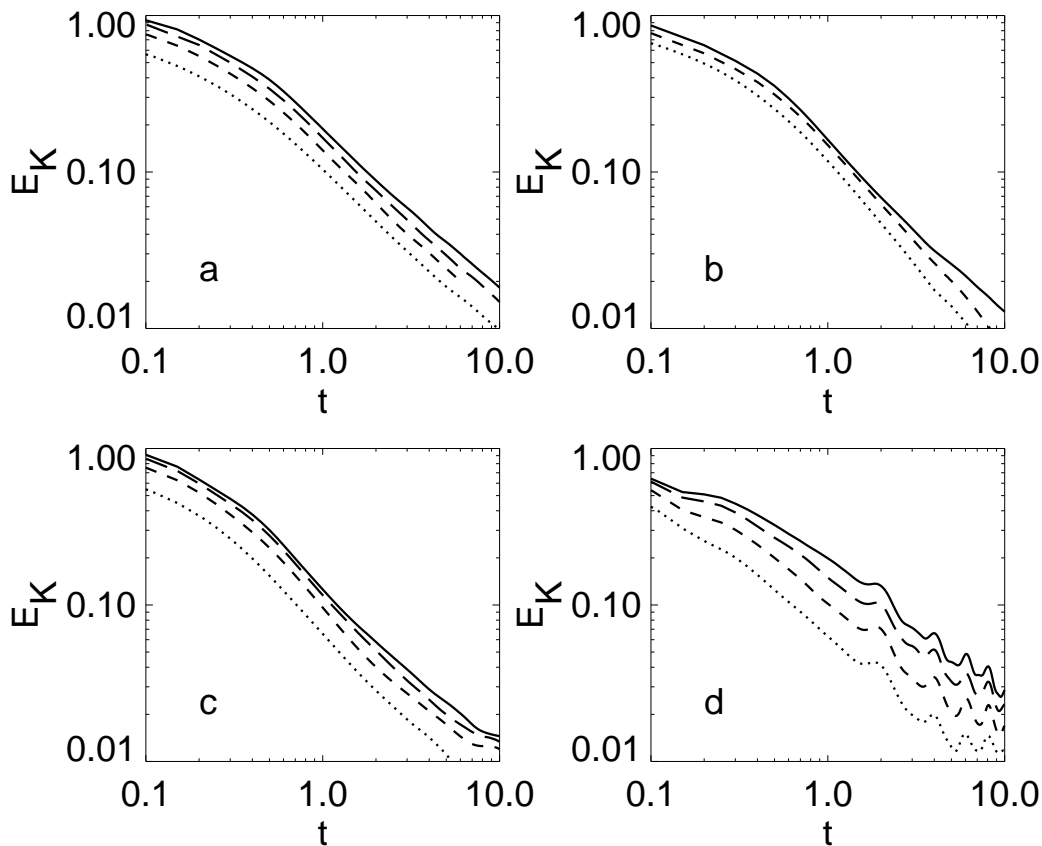


Figure 2.9: Three-dimensional resolution studies of the decay of supersonic turbulence for initial Mach number $M = 5$, isothermal models. ZEUS models have 32^3 (dotted), 64^3 (short dashed), 128^3 (long dashed), or 256^3 (solid) zones, while the SPH models have 7000 (dotted), 50,000 (short dashed), or 350,000 (solid) particles. Panels show *a*) hydro runs with ZEUS, *b*) hydro runs with SPH, *c*) $A = 5$ MHD runs with ZEUS, and *d*) $A = 1$ MHD runs with ZEUS (From Mac Low *et al.* (1998)).

Indeed, it may take many of the roles traditionally assigned to magnetic fields in the standard model.

2.5.1 Maintenance of Supersonic Motions

We first consider the question of how to maintain the observed supersonic motions. As described above, magnetohydrodynamic waves were generally thought to provide the means to prevent the dissipation of interstellar turbulence. However, numerical models have now shown that they probably do not. One-dimensional simulations of decaying, compressible, isothermal, magnetized turbulence by Gammie & Ostriker (1996) showed quick decay of kinetic energy K in the absence of driving, but found that the quantitative decay rate depended strongly on initial

and boundary conditions because of the low dimensionality. Mac Low *et al.* (1998), Stone, Ostriker & Gammie (1998), and Padoan & Nordlund (1999) measured the decay rate in direct numerical simulations in three dimensions, using a number of different numerical methods. They uniformly found rather faster decay, with Mac Low *et al.* (1998) characterizing it as $E_{\text{kin}} \propto t^{-\eta}$, with $0.85 < \eta < 1.1$. A resolution and algorithm study is shown in Figure 2.9. Magnetic fields with strengths ranging up to equipartition with the turbulent motions (ratio of thermal to magnetic pressures as low as $\beta = 0.025$) do indeed reduce η to the lower end of this range, but not below that, while unmagnetized supersonic turbulence shows values of $\eta \simeq 1$ –1.1.

Stone *et al.* (1998) and Mac Low (1999) showed that supersonic turbulence decays in less than a

free-fall time under molecular cloud conditions, regardless of whether it is magnetized or unmagnetized. The hydrodynamical result agrees with the high-resolution, transsonic, decaying models of Porter & Woodward (1992, 1994). Mac Low (1999) showed that the formal dissipation time $\tau_d = K/\dot{K}$ scaled in units of the free fall time t_{ff} is

$$\tau_d/\tau_{\text{ff}} = \frac{1}{4\pi\xi} \left(\frac{32}{3}\right)^{1/2} \frac{\kappa}{\mathcal{M}_{\text{rms}}} \simeq 3.9 \frac{\kappa}{\mathcal{M}_{\text{rms}}}, \quad (2.13)$$

where $\xi = 0.21/\pi$ is the energy-dissipation coefficient, $\mathcal{M}_{\text{rms}} = v_{\text{rms}}/c_s$ is the rms Mach number of the turbulence, and κ is the ratio of the driving wavelength to the Jeans wavelength λ_J . In molecular clouds, \mathcal{M}_{rms} is typically observed to be of order 10 or higher. If the ratio $\kappa < 1$, as is probably required to maintain gravitational support (Léorat *et al.* 1990), then even strongly magnetized turbulence will decay long before the cloud collapses and not markedly retard the collapse.

Either observed supersonic motions must be continually driven, or molecular clouds must be less than a single free-fall time old. As we discuss in Section 5.2, the observational evidence does suggest that clouds are a few free-fall times old, on average, though perhaps not more than two or three, so there is likely some continuing energy input into the clouds.

2.5.2 Turbulence in Self-Gravitating Gas

This leads to the question of what effects supersonic turbulence will have on self-gravitating clouds. Can turbulence alone delay gravitational collapse beyond a free-fall time? In Section 1 and Section 2.1, we summarized analytic approaches to this question, and pointed out that they were all based on the assumption that the turbulent flow is close to incompressible. Analytic attempts to statistically characterize highly compressible turbulence such as that we actually see in molecular clouds have usually been based on heuristic models (Elmegreen 1993), although recently they have been able to start making some progress in recovering the velocity structure (Boldyrev 2002, Boldyrev, Nordlund, & Padoan 2002).

Numerical models of highly compressible, self-gravitating turbulence have shown the importance of density fluctuations generated by the turbulence to understanding support against gravity. Early models were done by Bonazzola *et al.* (1987), who used low resolution (32×32 collocation points) calculations with a two-dimensional spectral code to support their analytical results. The hydrodynamical studies by Passot *et al.* (1988), Léorat, Passot & Pouquet (1990), Vázquez-Semadeni, Passot, & Pouquet (1995) and Ballesteros-Paredes, Vázquez-Semadeni & Scalo (1999), were also restricted to two dimensions, and were focused on the interstellar medium at kiloparsec scales rather than molecular clouds, although they were performed with far higher resolution (up to 800×800 points). Magnetic fields were introduced in these models by Passot, Vázquez-Semadeni, & Pouquet (1995), and extended to three dimensions with self-gravity (though at only 64^3 resolution) by Vázquez-Semadeni, Passot, & Pouquet (1996). One-dimensional computations focused on molecular clouds, including both MHD and self-gravity, were presented by Gammie & Ostriker (1996) and Balsara, Crutcher & Pouquet (1999). Ostriker, Gammie, & Stone (1999) extended their work to 2.5 dimensions more recently.

These early models at low resolution, low dimension, or both, suggested several important conclusions. First, gravitational collapse, even in the presence of magnetic fields, does not generate sufficient turbulence to markedly slow continuing collapse. Second, turbulent support against gravitational collapse may act at some scales, but not others. More recent three-dimensional, high-resolution computations by Klessen *et al.* (1998, 2000) Klessen (2000), Klessen & Burkert (2000, 2001), and Heitsch *et al.* (2001a) have now confirmed both of these results. In the following subsections, we give a brief description of the numerical methods used, give more details on these results, and draw consequences for the theory of star formation.

2.5.3 A Numerical Approach

Klessen *et al.* (2000) and Heitsch *et al.* (2001a) used two different numerical methods: ZEUS-3D (Stone & Norman 1992ab, Hawley & Stone 1995), an Eulerian MHD code; and an implementation of smoothed particle hydrodynamics (SPH; Benz 1990, Monaghan 1992), a Lagrangian hydrodynamics method using particles as an unstructured grid, while Klessen *et al.* (1998), Klessen (2000), and Klessen & Burkert (2000, 2001) used only SPH computations. Both codes were used to examine the gravitational stability of three-dimensional hydrodynamical turbulence at high resolution. The use of both Lagrangian and Eulerian methods to solve the equations of self-gravitating hydrodynamics in three dimensions (3D) allowed them to attempt to bracket reality by taking advantage of the strengths of each approach. This also gave them some protection against interpreting numerical artifacts as physical effects.

SPH can resolve very high density contrasts because it increases the particle concentration, and thus the effective spatial resolution, in regions of high density, making it well suited for computing collapse problems. By the same token, though, it resolves low-density regions poorly. Shock structures tend to be broadened by the averaging kernel in the absence of adaptive techniques. The correct numerical treatment of gravitational collapse requires the resolution of the local Jeans mass at every stage of the collapse (Bate & Burkert 1997). In the current code, once an object with density beyond the resolution limit of the code has formed in the center of a collapsing gas clump it is replaced by a ‘sink’ particle (Bate, Bonnell, & Price 1995). Adequately replacing high-density cores and keeping track of their further evolution in a consistent way prevents the time step from becoming prohibitively small. This allows modeling of the collapse of a large number of cores until the overall gas reservoir becomes exhausted.

ZEUS-3D, conversely, gives equal resolution in all regions, and allows good resolution shocks everywhere, as well as allowing the inclusion of

magnetic fields (see Section 2.5.6). On the other hand, collapsing regions cannot be followed to scales less than one or two grid zones. The numerical resolution required to follow gravitational collapse must be considered. For a grid-based simulation, the criterion given by Truelove *et al.* (1997) holds. Equivalent to the SPH resolution criterion, the mass contained across two or three grid zones has to be rather smaller than the local Jeans mass throughout the computation.

The computations presented here are done on periodic cubes, with an isothermal equation of state, using up to 256^3 zones (with one model at 512^3 zones) or 80^3 SPH particles. To generate turbulent flows Gaussian velocity fluctuations are introduced with power only in a narrow interval $k - 1 \leq |\vec{k}| \leq k$, where $k = L/\lambda_d$ counts the number of driving wavelengths λ_d in the box (Mac Low *et al.* 1998). This offers a simple approximation to driving by mechanisms that act on that scale. To drive the turbulence, this fixed pattern is normalized to maintain constant kinetic energy input rate $\dot{E}_{\text{in}} = \Delta E/\Delta t$ (Mac Low 1999). Self-gravity is turned on only after a state of dynamical equilibrium has been reached. In Table 2.3 we summarize the numerical models used in the subsequent analysis and give a list of their basic properties.

2.5.4 Global Collapse

First we examine the question of whether gravitational collapse can generate enough turbulence to prevent further collapse. Hydrodynamical SPH models initialized at rest with Gaussian density perturbations show fast collapse, with the first collapsed objects forming in a single free-fall time (Klessen, Burkert, & Bate 1998; Klessen & Burkert 2000, 2001). Models set up with a freely decaying turbulent velocity field behaved similarly (Klessen 2000). Further accretion of gas onto collapsed objects then occurs over the next free-fall time, defining the predicted spread of stellar ages in a freely-collapsing system. The turbulence generated by the collapse (or virialization) does not prevent further collapse as suggested by many people (e.g. Elmegreen 1993). Such a mechanism only works for thermal pressure support in

Name	Method	Resolution	k_{drv}	\dot{E}_{in}	$E_{\text{kin}}^{\text{eq}}$	$\langle M_{\text{J}} \rangle_{\text{turb}}$	$t_{5\%}$
$\mathcal{A}1$	SPH	200 000	1 – 2	0.1	0.15	0.6	0.5
$\mathcal{A}2$	SPH	200 000	3 – 4	0.2	0.15	0.6	0.7
$\mathcal{A}3$	SPH	200 000	7 – 8	0.4	0.15	0.6	2.2
$\mathcal{B}1$	SPH	50 000	1 – 2	0.5	0.5	3.2	0.5
$\mathcal{B}1h$	SPH	200 000	1 – 2	0.5	0.5	3.2	0.4
$\mathcal{B}2$	SPH	50 000	3 – 4	1.0	0.5	3.2	1.5
$\mathcal{B}2h$	SPH	200 000	3 – 4	1.0	0.5	3.2	1.4
$\mathcal{B}3$	SPH	50 000	7 – 8	2.4	0.5	3.2	6.0
$\mathcal{B}4$	SPH	50 000	15 – 16	5.0	0.5	3.2	8.0
$\mathcal{B}5$	SPH	50 000	[39 – 40]	[5.9]	[0.3]	[1.7]	—
$\mathcal{C}2$	SPH	50 000	3 – 4	7.5	2.0	18.2	6.0
$\mathcal{D}1$	ZEUS	128^3	1 – 2	0.4	0.5	3.2	0.4
$\mathcal{D}2$	ZEUS	128^3	3 – 4	0.8	0.5	3.2	1.2
$\mathcal{D}3$	ZEUS	128^3	7 – 8	1.6	0.5	3.2	2.4
$\mathcal{D}1h$	ZEUS	256^3	1 – 2	0.4	0.5	3.2	0.4
$\mathcal{D}2h$	ZEUS	256^3	3 – 4	0.8	0.5	3.2	1.2
$\mathcal{D}3h$	ZEUS	256^3	7 – 8	1.6	0.5	3.2	3.1

Table 2.3: Overview of the models. The columns give model name, numerical method, resolution, driving wave lengths k , energy input rate \dot{E}_{in} , equilibrium value of kinetic energy without self-gravity $E_{\text{kin}}^{\text{eq}}$, turbulent Jeans mass $\langle M_{\text{J}} \rangle_{\text{turb}}$, and the time required to reach a core mass fraction $M_* = 5\%$. The resolution is given for SPH as particle number and for ZEUS as number of grid cells. Dashes in the last column indicate that no sign of local collapse was observed within $20\tau_{\text{ff}}$, while stars indicate that the numerical resolution was insufficient for unambiguous identification of collapsed cores. The total mass in the system is $M = 1$. Model $\mathcal{B}5$ focuses on a subvolume with mass $M = 0.25$ and decreased sound speed $c_s = 0.05$. When scaled up to the standard cube this corresponds to the *effective* values given in square brackets. Adapted from Klessen *et al.* (2000).

systems such as galaxy cluster halos when dissipation is ineffective, while the dissipation for turbulence is quite effective (Equation 2.13).

Models of freely collapsing, magnetized gas remain to be done, but models of self-gravitating, decaying, magnetized turbulence by Balsara, Ward-Thompson, & Crutcher (2001) using an MHD code incorporating a Riemann solver suggest that the presence of magnetic fields is unlikely to markedly extend collapse timescales. They further show that accretion down filaments aligned with magnetic field lines onto cores occurs readily. This allows high mass-to-flux ratios to be maintained even at small scales, which is necessary for supercritical collapse to continue after fragmentation occurs.

2.5.5 Local Collapse in Globally Stable Regions

Second, we examine whether continuously driven turbulence can support against gravitational collapse. The models of driven, self-gravitating turbulence by Klessen *et al.* (2000) and Heitsch *et al.* (2001a) described above (Section 2.5.3) show that *local* collapse occurs even when the turbulent velocity field carries enough energy to counterbalance gravitational contraction on global scales. This confirms the results of two-dimensional (2D) and low-resolution (64^3) 3D computations with and without magnetic fields by Vázquez-Semadeni *et al.* (1996). An example of local collapse in a globally supported cloud is given in Figure 2.10. A hallmark of global turbulent support is isolated, inefficient, local collapse.

Local collapse in a globally stabilized cloud is

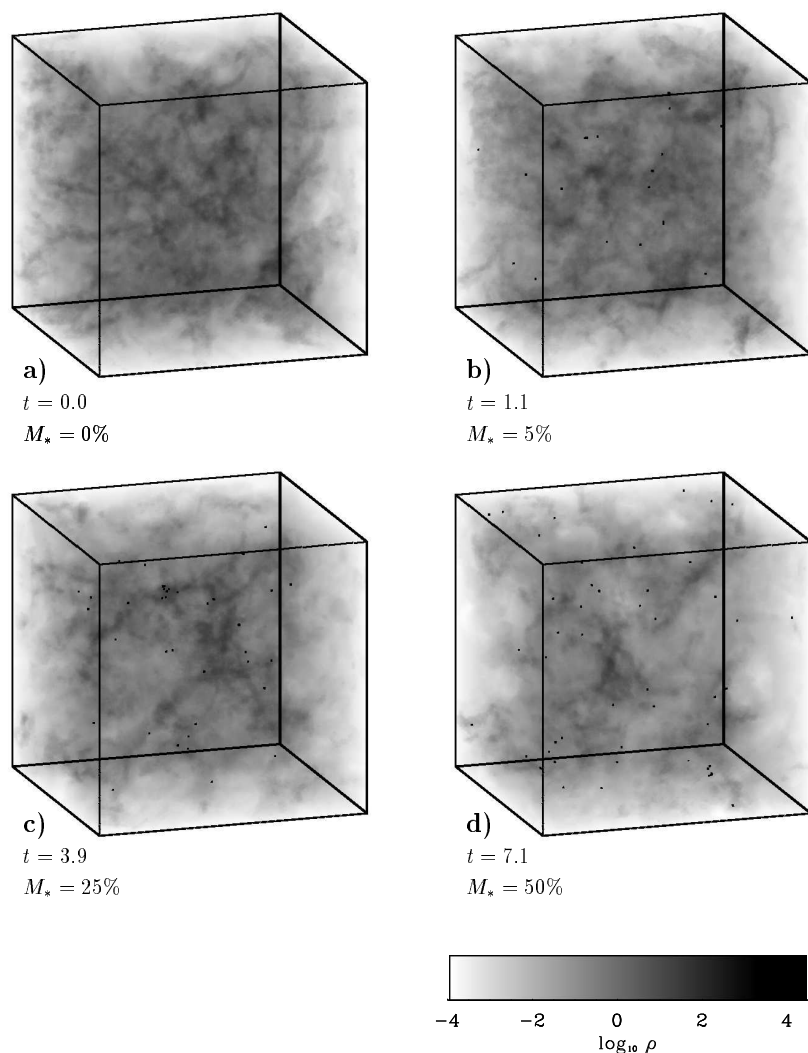


Figure 2.10: Density cubes for model *B2h* from Klessen *et al.* (2000), which is driven in the at intermediate wavelength, shown (a) at the time when gravity is turned on, (b) when the first collapsed cores are formed and have accreted $M_* = 5\%$ of the mass, (c) when the mass in dense cores is $M_* = 25\%$, and (d) when $M_* = 50\%$. Time is measured in units of the global system free-fall time scale τ_{ff} , dark dots indicate the location of the collapsed cores.

not predicted by any of the analytic models (as discussed in Klessen *et al.* 2000). The resolution to this apparent paradox lies in the requirement that any substantial turbulent support must come from supersonic flows, as otherwise pressure support would be at least equally important. Supersonic flows compress the gas in shocks; in isothermal gas with density ρ the postshock gas has density $\rho' = \mathcal{M}^2 \rho$, where \mathcal{M} is the Mach number of the shock. The turbulent Jeans length $\lambda_J \propto \rho'^{-1/2}$ in these density enhancements, so it drops by a factor of \mathcal{M} in isothermal shocks.

Klessen *et al.* (2000) demonstrated that turbulent

support can completely prevent collapse only when it can support not just the average density, but also these high-density shocked regions, as shown in Figure 2.11. (This basic point was appreciated by Elmegreen [1993] and Vázquez-Semadeni *et al.* [1995].) Two criteria must be fulfilled: the rms velocity must be sufficiently high for the turbulent Jeans criterion to be met in these regions, and the driving wavelength $\lambda_d < \lambda_J(\rho')$. If these two criteria are not fulfilled, the high-density regions collapse, although the surrounding flow remains turbulently supported. The efficiency of collapse depends on the properties of the supporting turbulence. Sufficiently strong

driving on short enough scales can prevent local collapse for arbitrarily long periods of time, but such strong driving may be rather difficult to arrange in a real molecular cloud. If we assume that stellar driving sources have an effective wavelength close to their separation, then the condition that driving acts on scales smaller than the Jeans wavelength in ‘typical’ shock generated gas clumps requires the presence of an extraordinarily large number of stars evenly distributed throughout the cloud, with typical separation 0.1 pc in Taurus, or only 350 AU in Orion. This is not observed. Very small driving scales seem to be at odds with the observed large-scale velocity fields at least in some molecular clouds (e.g. Ossenkopf & Mac Low 2002).

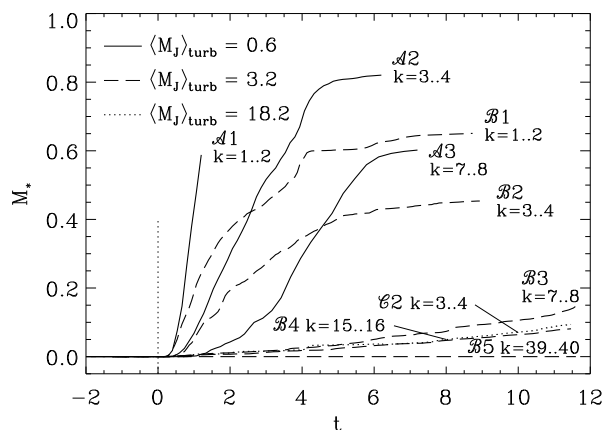


Figure 2.11: Fraction M_* of mass accreted in dense cores as function of time for different models of self-gravitating supersonic turbulence. The models differ by driving strength and driving wavenumber, as indicated in the figure. The mass in the box is initially unity, so the solid curves are formally unsupported, while the others are formally supported. The figure shows how the efficiency of local collapse depends on the scale and strength of turbulent driving. Time is measured in units of the global system free-fall time scale τ_{ff} . Only a model driven strongly at scales smaller than the Jeans wavelength λ_J in shock-compressed regions shows no collapse at all. (From Klessen *et al.* 2000.)

The first collapsed cores form in small groups randomly dispersed throughout the volume. Their velocities directly reflect the turbulent velocity field of the gas from which they formed and continue to accrete. However, as more and more mass accumulates in protostars, their mutual gravitational interaction becomes increas-

ingly important, beginning to determine the dynamical state of the system. It behaves more and more like a collisional N -body system, where close encounters occur frequently (see Section 4.4).

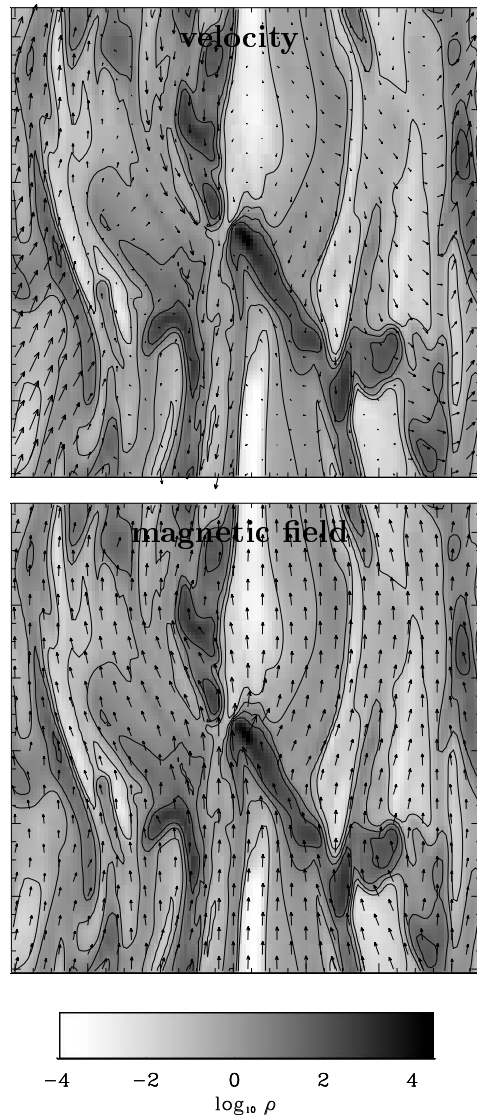


Figure 2.12: Two dimensional slice through a cube of magnetostatically supported large-scale driven, self-gravitating turbulence from Heitsch *et al.* (2001a). The upper panel shows the velocity field vectors and the lower panel the magnetic field vectors. The initial magnetic field is along the z -direction, i.e. vertically oriented in all plots presented. The field is strong enough in this case not only to prevent the cloud from collapsing perpendicular to the field lines, but even suppress the turbulent motions in the cloud. The turbulence only scarcely affects the mean field. The picture is taken at $t = 5.5\tau_{\text{ff}}$. (From Heitsch *et al.* 2001a.)

2.5.6 Effects of Magnetic Fields

So far, we have concentrated on the effects of purely hydrodynamic turbulence. How does the picture discussed here change if we consider the presence of magnetic fields? Magnetic fields have been suggested to support molecular clouds well enough to prevent gravitationally unstable regions from collapsing (McKee 1999), either magnetostatically or dynamically through MHD waves.

Assuming ideal MHD, a self-gravitating cloud of mass M permeated by a uniform flux Φ is stable unless the mass-to-flux ratio exceeds the value given by equation (2.7). Without any other mechanism of support, such as turbulence acting along the field lines, a magnetostatically supported cloud collapses to a sheet which is then supported against further collapse. Fiege & Pudritz (1999) found an equilibrium configuration of helical field that could support a filament, rather than a sheet, from fragmenting and collapsing, but realizing this configuration in highly turbulent molecular clouds appears difficult.

Investigation of support by MHD waves concentrates mostly on the effect of Alfvén waves, as they (1) are not as subject to damping as magnetosonic waves and (2) can exert a force *along* the mean field, as shown by Dewar (1970) and Shu *et al.* (1987). This is because Alfvén waves are *transverse* waves, so they cause perturbations $\delta\vec{B}$ perpendicular to the mean magnetic field \vec{B} . McKee & Zweibel (1994) argue that Alfvén waves can even lead to an isotropic pressure, assuming that the waves are neither damped nor driven. However, in order to support a region against self-gravity, the waves would have to propagate outwardly, because inwardly propagating waves would only further compress the cloud. Thus, this mechanism requires a negative radial gradient in wave sources in the cloud (Shu *et al.* 1987).

It can be demonstrated (e.g. Heitsch *et al.* 2001a) that supersonic turbulence does not cause a magnetostatically supported region to collapse, and vice versa, that in the absence of magnetostatic support, MHD waves cannot completely prevent collapse, although they can retard it to some

degree. The case of a subcritical region with $M < M_{cr}$ is illustrated in Figure 2.12. Indeed, sheets form, though always perpendicular to the field lines. This is because the turbulent driving can shift the sheets along the field lines without changing the mass-to-flux ratio. The sheets do not collapse further, because the shock waves cannot sweep gas across field lines and the entire region is initially supported magnetostatically.

A supercritical cloud with $M > M_{cr}$ could only be stabilized by MHD wave pressure. This is insufficient to completely prevent gravitational collapse, as shown in Figure 2.13. Collapse occurs in all models of unmagnetized and magnetized turbulence regardless of the numerical resolution and magnetic field strength as long as the system is magnetically supercritical. This is shown quantitatively in Figure 2.14. Increasing the resolution makes itself felt in different ways in hydrodynamical and MHD models. In the hydrodynamical case, higher resolution results in thinner shocks and thus higher peak densities. These higher density peaks form cores with deeper potential wells that accrete more mass and are more stable against disruption. Higher resolution in the MHD models, on the other hand, better resolves short-wavelength MHD waves, which apparently can delay collapse, but not prevent it. This result extends to models with 512^3 zones (Heitsch *et al.* 2001b, Li *et al.* 2001).

The delay of local collapse seen in our magnetized simulations is caused mainly by weakly magnetized turbulence acting to decrease density enhancements due to shock interactions. Although a simple additional pressure term will model this effect for small field strength, this approximation cannot be used to follow the subsequent collapse of the cores, as done by Boss (2000, 2002), as it entirely neglects the effects of magnetic tension on angular momentum. As a result, magnetic braking of rotating cores (Section 2.3) is neglected, allowing binary formation to proceed where it would otherwise not occur.

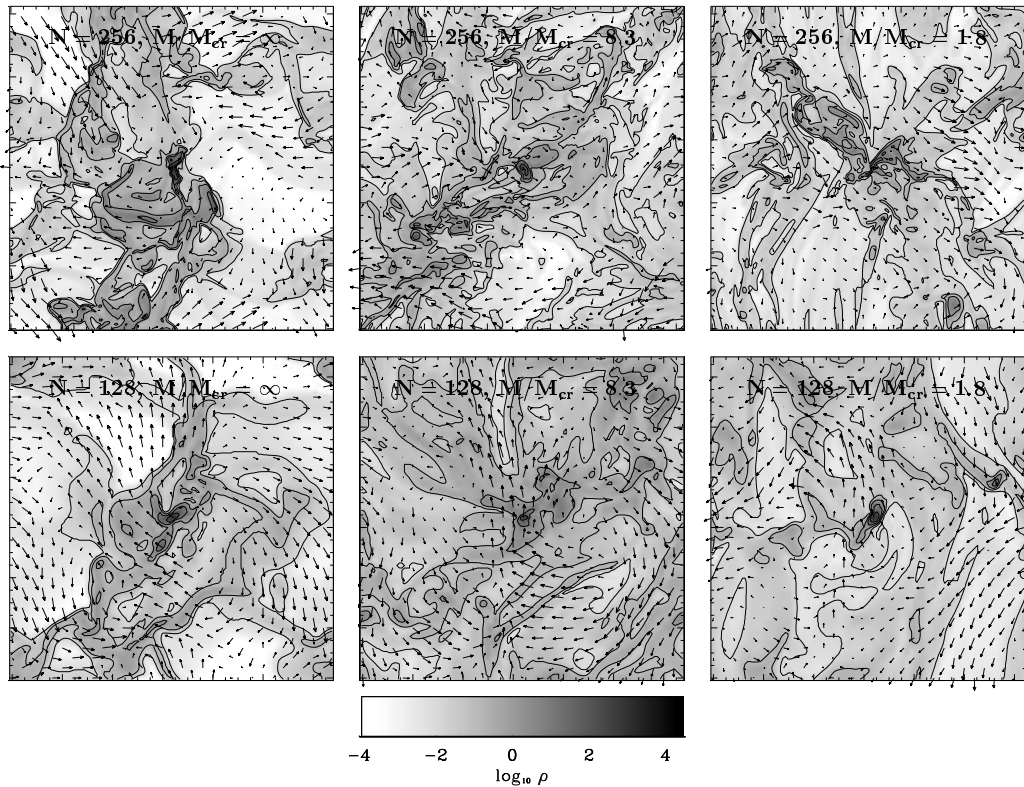


Figure 2.13: Two-dimensional slices of 256^3 models from Heitsch *et al.* (2001a) driven at large scales with wavenumbers $k = 1 - 2$ hard enough that the mass in the box represents only $1/15 \langle M_J \rangle_{\text{turb}}$, and with initially vertical magnetic fields strong enough to give critical mass fractions as shown. The slices are taken at the location of the zone with the highest density at the time when 10% of the total mass has been accreted onto dense cores. The plot is centered on this zone. Arrows denote velocities in the plane. The length of the largest arrows corresponds to a velocity of $v \sim 20c_s$. The density greyscale is given in the colorbar. As fields become stronger, they influence the flow more, producing anisotropic structure. (From Heitsch *et al.* 2001b.)

2.5.7 Promotion and Prevention of Local Collapse

Highly compressible turbulence both promotes and prevents collapse. Its net effect is to inhibit collapse globally, while perhaps promoting it locally. This can be seen by examining the dependence of the Jeans mass $M_J \propto \rho^{-1/2} c_s^3$, Equation (2.3), on the rms turbulent velocity v_{rms} . If we follow the classical picture that treats turbulence as an additional pressure, then we define $c_{s,\text{eff}}^2 = c_s^2 + v_{\text{rms}}^2/3$. However, compressible turbulence in an isothermal medium causes local density enhancements that increase the density by $\mathcal{M}^2 \propto v_{\text{rms}}^2$. Combining these two effects, we find that

$$M_J \propto v_{\text{rms}}^2 \quad (2.14)$$

for $v_{\text{rms}} \gg c_s$, so that ultimately turbulence does inhibit collapse. However, there is a broad intermediate region, especially for long wavelength driving, where local collapse occurs despite global support.

The total mass and lifetime of a fluctuation determine whether it will actually collapse. Roughly speaking, the lifetime of a clump is determined by the interval between two successive passing shocks: the first creates it, while the second one, if strong enough, may disrupt the clump again (Klein, McKee & Colella 1994, Mac Low *et al.* 1994). If the timeinterval between two shocks is sufficiently long, however, a Jeans unstable clump can contract to high densities to effectively decouple from the ambient gas flow and becomes able to survive the encounter with further shock

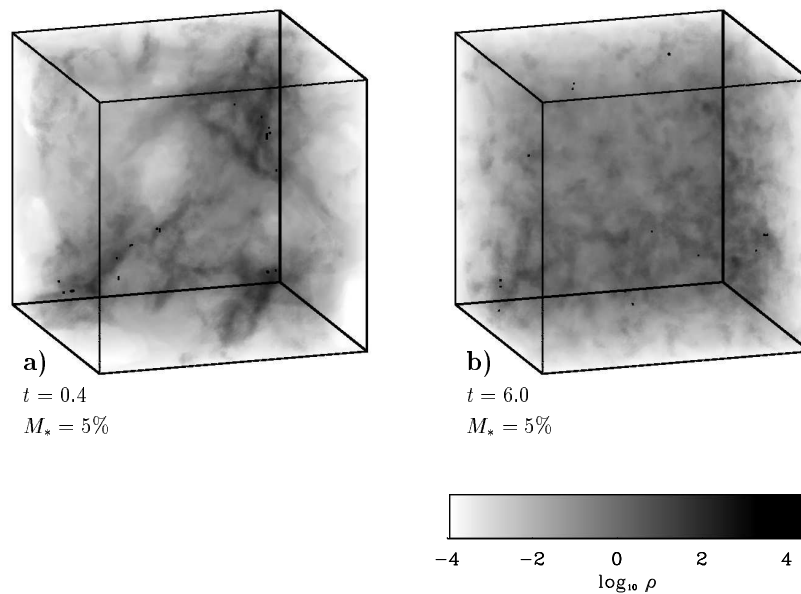


Figure 2.15: Density cubes for (a) a model of large-scale driven turbulence ($B1h$) and (b) a model of small-scale driven turbulence ($B3$) at dynamical stages where the core mass fraction is $M_* = 5\%$. Compare with Figure 2.10b. Together they show the influence of different driving wavelengths for otherwise identical physical parameters. Larger-scale driving results in collapsed cores in more organized structure, while smaller-scale driving results in more randomly distributed cores. Note the different times at which $M_* = 5\%$ is reached. (From Klessen *et al.* 2000.)

fronts (e.g. Krebs & Hillebrandt 1983). Then it continues to accrete from the surrounding gas, forming a dense core. The weaker the passing shocks, and the greater the separation between them, the more likely that collapse will occur. Therefore, weak driving and long driving wavelengths enhance collapse. The influence of the driving wavelength is enhanced because individual shocks sweep up more mass when the typical wavelength is longer, so density enhancements resulting from the interaction of shocked layers have larger masses, and so are more likely to exceed their local Jeans limit. Turbulent driving mechanisms that act on large scales produce large coherent structures (filaments of compressed gas with embedded dense cores) on relatively short timescales compared to small-scale driving even if the total kinetic energy in the system is the same (Figure 2.15, can be directly compared with Figure 2.10b).

A more detailed understanding of how local collapse proceeds comes from examining the full time history of accretion for different models (Figure 2.11). The cessation of strong accretion onto cores occurs long before all gas has been ac-

creted, with the mass fraction at which this occurs depending on the properties of the turbulence. This is because the time that dense cores spend in shock-compressed, high-density regions decreases with increasing driving wave number and increasing driving strength. In the case of long wavelength driving, cores form coherently in high-density regions associated with one or two large shock fronts that can accumulate a considerable fraction of the total mass of the system, while in the case of short wavelength driving, the network of shocks is tightly knit, and cores form in smaller clumps and remain in them for shorter times.

2.5.8 The Timescales of Star Formation

Turbulent control of star formation predicts that stellar clusters form predominantly in regions that are insufficiently supported by turbulence or where only large-scale driving is active. In the absence of driving, molecular cloud turbulence decays more quickly than the free-fall timescale τ_{ff} (Equation 2.13), so dense stellar clusters will form on the free-fall time scale. Even in the presence

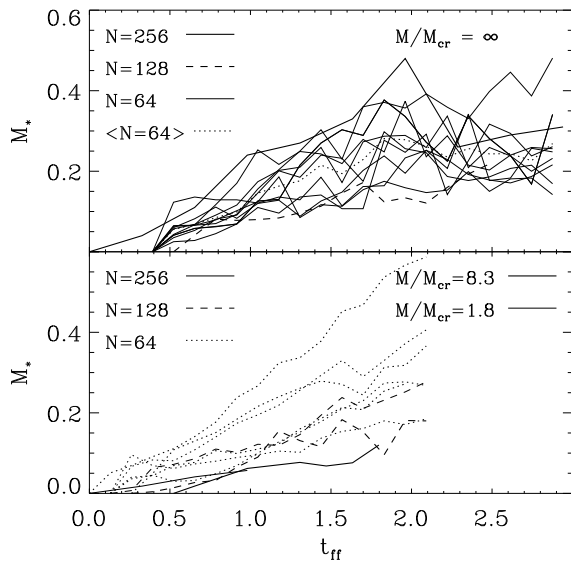


Figure 2.14: *Upper panel:* Core-mass accretion rates for 10 different low-resolution models ($N = 64^3$ cells) of purely hydrodynamic turbulence with equal parameter set but different realizations of the turbulent velocity field. The thick line shows a “mean accretion rate”, calculated from averaging over the sample. For comparison, higher-resolution runs with identical parameters but $N = 128^3$ and $N = 256^3$ are shown as well. The latter one can be regarded as an envelope for the low resolution models. *Lower panel:* Mass accretion rates for various models with different magnetic field strength and resolution. Common to all models is the occurrence of local collapse and star formation regardless of the detailed choice of parameters, as long as the system is magnetostatically supercritically. (For further details see Heitsch *et al.* 2001a.)

of support from large-scale driving, substantial collapse still occurs within a few free-fall times (Figures 2.11 and 2.16a). If the dense cores followed in these models continue to collapse on a short timescale to build up stellar objects in their centers, then this directly implies the star formation time. Therefore the age distribution will be roughly τ_{ff} for stellar clusters that form coherently with high star formation efficiency. When scaled to low densities, say $n(\text{H}_2) \approx 10^2 \text{ cm}^{-3}$ and $T \approx 10 \text{ K}$, the global free-fall timescale in the models is $\tau_{\text{ff}} = 3.3 \times 10^6$ years. If star forming clouds such as Taurus indeed have ages of order τ_{ff} , as suggested by Ballesteros-Paredes *et al.* (1999), then the long star formation timescale computed here is quite consistent with the very low star formation efficiencies seen in Taurus (e.g. Leisawitz *et al.* 1989, Palla & Stahler 2000, Hart-

mann 2001), as the cloud simply has not had time to form many stars. In the case of high-density regions, $n(\text{H}_2) \approx 10^5 \text{ cm}^{-3}$ and $T \approx 10 \text{ K}$, the dynamical evolution proceeds much faster and the corresponding free-fall timescale drops to $\tau_{\text{ff}} = 10^5$ years. These values are indeed supported by observational data such as the formation time of the Orion Trapezium cluster. It is inferred to stem from gas of density $n(\text{H}_2) \lesssim 10^5 \text{ cm}^{-3}$, and is estimated to be less than 10^6 years old (Hillenbrand & Hartmann 1998). The age spread in the models increases with increasing driving wave number k and increasing $\langle M_{\text{J}} \rangle_{\text{turb}}$, as shown in Figure 2.16. Long periods of core formation for globally supported clouds appear consistent with the low efficiencies of star-formation in regions of isolated star formation, such as Taurus, even if they are rather young objects with ages of order τ_{ff} .

2.5.9 Scales of Interstellar Turbulence

Turbulence only has self-similar properties on scales between the driving and dissipation scales. What are these scales for interstellar turbulence? In a purely hydrodynamic system the dissipation scale is the scale where molecular viscosity becomes important. In interstellar clouds the situation may be different. Zweibel & Josafatsson (1983) showed that ambipolar diffusion (ion-neutral drift) is the most important dissipation mechanism in typical molecular clouds with very low ionization fractions $x = \rho_i/\rho_n$, where ρ_i is the density of ions, ρ_n is the density of neutrals, and the total density $\rho = \rho_i + \rho_n$. An ambipolar diffusion strength can be defined as

$$\lambda_{\text{AD}} = v_{\text{A}}^2/\nu_{\text{ni}}, \quad (2.15)$$

where $v_{\text{A}}^2 = B^2/4\pi\rho_n$ approximates the effective Alfvén speed for the coupled neutrals and ions if $\rho_n \gg \rho_i$, and $\nu_{\text{ni}} = \gamma\rho_i$ is the rate at which each neutral is hit by ions. The coupling constant depends on the cross-section for ion-neutral interaction, and for typical molecular cloud conditions has a value of $\gamma \approx 9.2 \times 10^{13} \text{ cm}^3 \text{ s}^{-1} \text{ g}^{-1}$ (e.g. Smith & Mac Low 1997). Zweibel & Brandenburg (1997) define an ambipolar diffusion Reynolds number as

$$R_{\text{AD}} = \tilde{L}\tilde{V}/\lambda_{\text{AD}} = \mathcal{M}_{\text{A}}\tilde{L}\nu_{\text{ni}}/v_{\text{A}}, \quad (2.16)$$

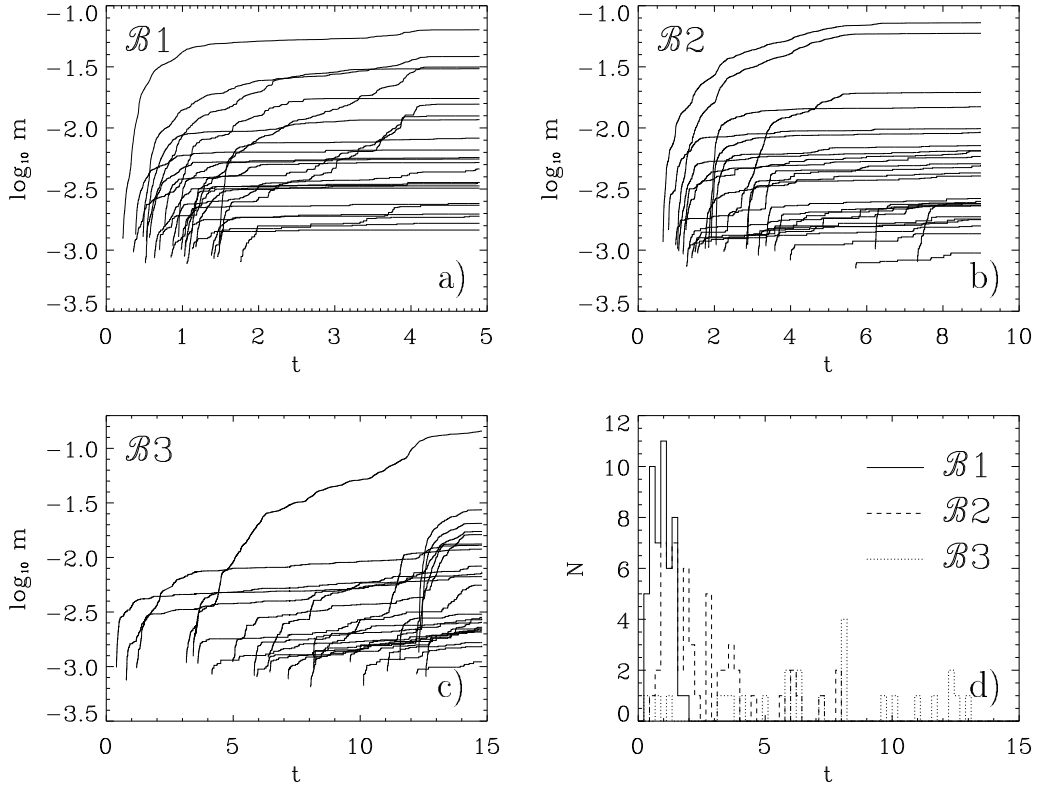


Figure 2.16: Masses of individual protostars as function of time in SPH models (a) $B1$ driven at large scales with $k = 1 - 2$ driving, (b) $B2$ with $k = 3 - 4$ driving, i.e. at intermediate scales, and (c) $B3$ with $k = 7 - 8$ small-scale driving. The curves represent the formation and accretion histories of individual protostars. For the sake of clarity, only every other core is shown in (a) and (b), whereas in (c) the evolution of every single core is plotted. Time is given in units of the global free-fall time τ_{ff} . Note the different time scale in each plot. In the depicted time interval models $B1$ and $B2$ reach a core mass fraction $M_* = 70\%$, and both form roughly 50 cores. Model $B3$ reaches $M_* = 35\%$ and forms only 25 cores. Figure (d) compares the distributions of formation times. The age spread increases with decreasing driving scale showing that clustered core formation should lead to a coeval stellar population, whereas a distributed stellar population should exhibit considerable age spread. (From Klessen *et al.* 2000.)

which must fall below unity for ambipolar diffusion to be important (also see Balsara 1996), where \tilde{L} and \tilde{V} are the characteristic length and velocity scales, and $\mathcal{M}_A = \tilde{V}/v_A$ is the characteristic Alfvén Mach number. In our situation we again can take the rms velocity as typical value for \tilde{V} . By setting $R_{\text{AD}} = 1$, we can derive a critical lengthscale below which ambipolar diffusion is important

$$\tilde{L}_{\text{cr}} = \frac{v_A}{\mathcal{M}_A v_{\text{ni}}} \approx (0.041 \text{ pc}) \left(\frac{B}{10 \mu\text{G}} \right) \mathcal{M}_A^{-1} \times \left(\frac{x}{10^{-6}} \right)^{-1} \left(\frac{n_n}{10^3 \text{ cm}^{-3}} \right)^{-3/2}, \quad (2.17)$$

with the magnetic field strength B , the ionization fraction x , the neutral number density n_n , and where we have taken $\rho_n = \mu n_n$, with $\mu = 2.36 m_{\text{H}}$. This is consistent with typical

sizes of protostellar cores (e.g. Bacmann *et al.* 2000), if we assume that ionization and magnetic field both depend on the density of the region and follow the empirical laws $n_i = 3 \times 10^{-3} \text{ cm}^{-3} (n_n/10^5 \text{ cm}^{-3})^{1/2}$ (e.g. Mouschovias 1991b) and $B \approx 30 \mu\text{G} (n_n/10^3 \text{ cm}^{-3})^{1/2}$ (e.g. Crutcher 1999). Balsara (1996) notes that there are wave families that can survive below L_{cr} that resemble hydrodynamical sound waves. This means that this scale may determine where the magnetic field becomes uniform, but not necessarily where the hydrodynamical turbulent cascade cuts off.

On large scales, a maximum upper limit to the turbulent cascade in the Milky Way is given by the extent and thickness of the Galactic disk. If indeed molecular clouds are created at least in part

by converging large-scale flows generated by the collective influence of recurring supernovae explosions in the gaseous disk of our Galaxy, as we argue in Section 5.3, then the extent of the Galactic disk is indeed the true upper scale of turbulence in the Milky Way. For individual molecular clouds this means that turbulent energy is fed in at scales well above the size of the cloud itself.

The initial compression that assembles the cloud may generate the bulk of a cloud's turbulent energy content (see Section 5.2). If the surrounding flow is not strong enough to continue to drive the cloud, the turbulence will quickly dissipate, resulting in collapse and active star formation. If the same compressional motions that created the cloud in the first place can also act as a continuing source of kinetic energy, they may be strong enough to again destroy the cloud after several crossing times (e.g. Hartmann *et al.* 2001). Either way, the result is short cloud life times, as argued by Ballesteros-Paredes *et al.* (1999) and Elmegreen (2000). This picture of molecular cloud turbulence being driven by large-scale, external sources is supported by the observation that density and velocity structure shows power-law scaling extending up to the largest scales observed in all clouds that have been analyzed (Ossenkopf & Mac Low 2002).

2.5.10 Efficiency of Star Formation

The *global* star formation efficiency in normal molecular clouds is usually estimated to be of the order of a few per cent. Their life times may be on the order of a few crossing times, i.e. a few 10^6 years (e.g. Ballesteros-Paredes *et al.* 1999, Fukui *et al.* 1999, Elmegreen 2000). In this case nearly all models of interstellar turbulence discussed below are consistent with the observed overall efficiencies. If molecular clouds survive for several tens of their free-fall time τ_{ff} (i.e. a few 10^7 years as proposed by Blitz & Shu 1980), turbulence models are more strongly constrained. However, even in this case models with parameters reasonable for Galactic molecular clouds can maintain global efficiencies below $M_* = 5\%$ for $10 \tau_{\text{ff}}$ (Klessen *et al.* 2000). Furthermore, it needs to be noted

that the *local* star formation efficiency in molecular clouds can reach very high values. For example, the Trapezium star cluster in Orion is likely to have formed with an efficiency of about 50% (Hillenbrand & Hartmann 1998).

2.5.11 Termination of Local Star Formation

It remains quite unclear what terminates stellar birth on scales of individual star forming regions, and even whether these processes are the primary factor determining the overall efficiency of star formation in a molecular cloud. Three main possibilities exist. First, feedback from the stars themselves in the form of ionizing radiation and stellar outflows may heat and stir surrounding gas up sufficiently to prevent further collapse and accretion. Second, accretion might peter out either when all the high density, gravitationally unstable gas in the region has been accreted in individual stars, or after a more dynamical period of competitive accretion, leaving any remaining gas to be dispersed by the background turbulent flow. Third, background flows may sweep through, destroying the cloud, perhaps in the same way that it was created. Most likely the astrophysical truth lies in some combination of all three possibilities.

If a stellar cluster formed in a molecular cloud contains OB stars, then the radiation field and stellar wind from these high-mass stars strongly influence the surrounding cloud material. The UV flux ionizes gas out beyond the local star forming region. Ionization heats the gas, raising its Jeans mass, and possibly preventing further protostellar mass growth or new star formation. The termination of accretion by stellar feedback has been suggested at least since the calculations of ionization by Oort & Spitzer (1955). Whitworth (1979) and Yorke *et al.* (1989) computed the destructive effects of individual blister HII regions on molecular clouds, while in series of papers, Franco *et al.* (1994), Rodriguez-Gaspar *et al.* (1995), and Diaz-Miller *et al.* (1998) concluded that indeed the ionization from massive stars may limit the overall star forming capacity

of molecular clouds to about 5%. Matzner (2002) analytically modeled the effects of ionization on molecular clouds, concluding as well that turbulence driven by HII regions could support and eventually destroy molecular clouds. The key question facing these models is whether HII region expansion couples efficiently to clumpy, inhomogeneous molecular clouds, a question probably best addressed with numerical simulations.

Bipolar outflows are a different manifestation of protostellar feedback, and may also strongly modify the properties of star forming regions (Norman & Silk 1980, Lada & Gautier 1982, Adams & Fatuzzo 1996). Recently Matzner & McKee (2000) modeled the ability of bipolar outflows to terminate low-mass star formation, finding that they can limit star formation efficiencies to 30–50%, although they are ineffective in more massive regions. How important these processes are compared to simple exhaustion of available reservoirs of dense gas (Klessen *et al.* 2000, Vázquez-Semadeni *et al.* 2003) remains an important question.

The models relying on exhaustion of the reservoir of dense gas argue that only dense gas will actually collapse, and that only a small fraction of the total available gas reaches sufficiently high densities, due to cooling (Schaye 2002), gravitational collapse and turbulent triggering (Elmegreen 2002), or both (Wada, Meurer, & Norman 2002). This of course pushes the question of local star formation efficiency up to larger scales, which may indeed be the correct place to ask it.

Other models focus on competitive accretion in local star formation, showing that the distribution of masses in a single group or cluster can be well explained by assuming that star formation is fairly efficient in the dense core, but that stars that randomly start out slightly heavier tend to fall towards the center of the core and accrete disproportionately more gas (Bonnell *et al.* 1997; 2001a). These models have recently been called into question by the observation that the stars in lower density young groups in Serpens simply have not had the time to engage in competitive accretion, but still have a normal IMF (Olmí & Testi 2002).

Finally, star formation in dense clouds created by turbulent flows may be terminated by the same flows that created them. Ballesteros-Paredes *et al.* (1999) suggested that the coordination of star formation over large molecular clouds, and the lack of post-T Tauri stars with ages greater than about 10 Myr tightly associated with those clouds, could be explained by their formation in a larger-scale turbulent flow. Hartmann *et al.* (2001) make the detailed argument that these flows may disrupt the clouds after a relatively short time, limiting their star formation efficiency that way. Below, in Section 5.3 we will argue that field supernovae are the most likely driver for this background turbulence, at least in the star-forming regions of galaxies.

2.6 Outline of a New Theory of Star Formation

The support of star-forming clouds by supersonic turbulence can explain many of the same observations successfully explained by the standard theory, while also addressing the inconsistencies between observation and the standard theory described in the previous section. The key point that is new in our argument is that supersonic turbulence produces strong density fluctuations in the interstellar gas (Padoan & Nordlund 1999), sweeping gas up from large regions into dense sheets and filaments (Vázquez-Semadeni, Passot, & Pouquet 1996, Klessen *et al.* 2000), even in the presence of magnetic fields (Passot, Vázquez-Semadeni, & Pouquet 1995, Heitsch *et al.* 2001a,b). Supersonic turbulence decays quickly (Mac Low *et al.* 1998, Stone *et al.* 1998, Mac Low 1999), but so long as it is maintained by input of energy from some driver (Section 5.3), it can support regions against gravitational collapse.

Such support comes at a cost, however. The very turbulent flows that support the region produce density enhancements in which the Jeans mass determining gravitational collapse drops as $M_J \propto \rho^{-1/2}$, (Equation 2.3), and the magnetic critical mass above which magnetic fields can no

longer support against that collapse drops even faster, as $M_{\text{cr}} \propto \rho^{-2}$ in Equation (2.6). For local collapse to actually result in the formation of stars, Jeans-unstable, shock-generated, density fluctuations must collapse to sufficiently high densities on time scales shorter than the typical time interval between two successive shock passages. Only then can they decouple from the ambient flow and survive subsequent shock interactions. The shorter the time between shock passages, the less likely these fluctuations are to survive. Hence, the timescale and efficiency of protostellar core formation depend strongly on the wavelength and strength of the driving source (Section 2.5), and the accretion histories of individual protostars are strongly time varying (Section 4.5). Global support by supersonic turbulence thus tends to produce local collapse and low rate star formation (Klessen *et al.* 2000, Heitsch *et al.* 2001a,b), exactly as seen in low-mass star formation regions characteristic of the disks of spiral galaxies. Conversely, lack of turbulent support results in regions that collapse freely. In hydrodynamic simulations (Wada & Norman 1999, Klessen & Burkert 2000), freely collapsing gas forms a web of density enhancements in which star formation can proceed efficiently, as seen in regions of massive star formation and starbursts.

The regulation of the star formation rate then occurs not just at the scale of individual star-forming cores through ambipolar diffusion balancing magnetostatic support, but rather at all scales (Elmegreen 2002), via the dynamical processes that determine whether regions of gas become unstable to prompt gravitational collapse. Efficient star formation occurs in collapsing regions; apparent inefficiency occurs when a region is turbulently supported and only small subregions get compressed sufficiently to collapse. The star formation rate is determined by the balance between turbulent support and local density, and is a continuous function of the strength of turbulent support for any given region. Fast and efficient star formation is the natural behavior of gas lacking sufficient turbulent support for its local density.

Regions that are gravitationally unstable in this picture collapse quickly, on the free-fall time scale. They never pass through a quasi-equilibrium state as envisioned by the standard model. Large-scale density enhancements such as molecular clouds could be caused either by gravitational collapse, or by ram pressure from turbulence (Ballesteros-Paredes *et al.* 1999). If collapse does not succeed, the same large-scale turbulence that formed molecular clouds can destroy them again (Section 5.2).

Chapter 3

SOME FURTHER PROPERTIES OF SUPERSONIC TURBULENCE

In the current review we argue that it is the subtle interplay between self-gravity and supersonic turbulence in interstellar gas clouds that determines where, when, and with which overall efficiency stars will form. We claim that stars form in shock-generated molecular cloud clumps where density and mass exceed the threshold for gravitational collapse to set in. In the previous Section we therefore have concentrated on discussing the effects of compressibility. However, turbulence is a highly complex physical phenomenon with further statistical properties that are relevant for the star formation process. We begin this Section by studying the transport properties of supersonic turbulence which is important for understanding element mixing in interstellar gas clouds and the distribution of stellar chemical abundances (Section 3.1). We also investigate of the one-point probability distribution functions (PDF) of density and velocity in turbulent compressible flows (Section 3.2). Then, we analyze the Fourier spectrum of turbulent velocity fields (3.3) and use the Δ -variance to quantify the statistical properties of the density distribution on star-forming clouds (Section 3.4).

3.1 Transport Properties

3.1.1 Introduction

Laboratory and terrestrial gases and liquids are usually well described by incompressible flows. In contrast, the dynamical behavior of typical astrophysical gases, are characterized by poorly un-

derstood highly compressible supersonic turbulent motion. For example, the large observed linewidths in large molecular clouds show direct evidence for the presence of chaotically oriented velocity fields with magnitudes in excess of the sound speed. This random motion carries enough kinetic energy to counterbalance and sometimes overcompensate the effects of self-gravity of these clouds (Section 4.1). The intricate interplay between supersonic turbulence and self-gravity determines the overall dynamical evolution of these clouds and their observable features such as their density structure, the star formation rate within them, and their lifetimes. Thus, it is importance for the description of many astrophysical systems to understand in detail the momentum and heat transfer properties of compressible turbulent gases.

Some important clues on the nature and efficiency of mixing associated with the clouds' supersonic turbulence can be constrained by the observed metallicity distribution of the stars formed within them. In the Pleiades cluster, stars which emerged from the same molecular cloud have nearly identical metal abundance (Wilden *et al.* 2002). This astronomical context therefore imposes a strong motivation for a general analysis of the transport and mixing processes in compressible supersonically turbulent media.

Analytical and numerical studies of diffusion processes are typically restricted to certain families of statistical processes, like random walk (Metzler & Klafter 2000) or remapping models or certain Hamiltonian systems (Isichenko 1992).

The direct numerical modeling of turbulent physical flows mostly concentrates on incompressible media (Domolevo & Sainsaulieu 1997; Moser *et al.* 1999; Ossia & Lesieur 2001), but some studies have been extended into the weakly compressible regime (Coleman *et al.* 1995; Huang *et al.* 1995; Porter *et al.* 1992; Porter *et al.* 1999). Although highly compressible supersonic turbulent flows have been studied in several specific astrophysical contexts (see Vázquez-Semadeni *et al.* 2000 for a review)¹, the diffusion properties of such flows have not been investigated in detail.

It is the goal of this Section to analyze transport phenomena in supersonic compressible turbulent flows and to demonstrate that – analogous to the incompressible case – a simple mixing length description can be found even for strongly supersonic and highly compressible turbulence. We first briefly recapitulate in Section 3.1.2 the Taylor formalism for describing the efficiency of turbulent diffusion in subsonic flows. In Section 3.1.3 we describe the numerical method which we use to integrate the Navier-Stokes equation. In Section 3.1.4 we report the diffusion coefficient obtained in our numerical models, and in Section 3.1.7 we introduce an extension of the well known mixing length approach to diffusion into the supersonic compressible regime. Finally, in Section 3.1.8 we summarize our results.

3.1.2 A Statistical Description of Turbulent Diffusion

Transport properties in fluids and gases can be characterized by studying the time evolution of the second central moment of some representative fluid-elements' displacement in the medium,

$$\xi_{\vec{r}}^2(t - t') = \langle [\vec{r}_i(t) - \vec{r}_i(t')]^2 \rangle_i, \quad (3.1)$$

¹See also Ballesteros-Paredes & Mac Low (2002), Ballesteros-Paredes *et al.* (1999b), Balsara & Pouquet (1999), Balsara *et al.* (2001), Boldyrev *et al.* (2002a), Gomez *et al.* (2001), Heitsch *et al.* (2001a,b), Klessen *et al.* (2000), Klessen (2001a,b), Mac Low (1999), Mac Low *et al.* (1998, 2001), Ostriker *et al.* (1999, 2001), Padoan & Nordlund (1999), Padoan *et al.* (2000), Passot *et al.* (1995), Passot & Vázquez-Semadeni (1998), Porter & Woodward (2000), Smith *et al.* (2000), Stone *et al.* (1998), Sytine *et al.* (2000), or Vázquez-Semadeni *et al.* (1995)

where the average $\langle \cdot \rangle_i$ is taken over an ensemble of passively advected tracer particles i (e.g. dye in a fluid, or smoke in air) that are placed in the medium at a time t' at positions $\vec{r}_i(t')$; or where the average is taken over the fluid molecules themselves (or equivalently, over sufficiently small and distinguishable fluid elements). The dispersion in one spatial direction, say along the x -coordinate, is $\xi_x^2(t - t') = \langle [x_i(t) - x_i(t')]^2 \rangle_i$. For isotropic turbulence it follows that $\xi_x^2 = \xi_y^2 = \xi_z^2 = 1/3 \xi_{\vec{r}}^2$. For fully-developed stationary turbulence, the initial time t' can be chosen at random and for simplicity is set to zero in what follows.

The quantity $\xi_{\vec{r}}(t)$ can be associated with the diffusion coefficient D as derived for the classical diffusion equation,

$$\frac{\partial n}{\partial t} = D \vec{\nabla}^2 n, \quad (3.2)$$

where $n(\vec{r}_i, t)$ is the probability distribution function (PDF) for finding a particle i at position $\vec{r}_i(t)$ at time t when it initially was at a location $\vec{r}_i(0)$. This holds if the particle position is a random variable with a Gaussian distribution (Batchelor 1949). In the classical sense, $n(\vec{r}, t)$ may correspond to the contaminant density in the medium. Equation (3.2) holds for normal diffusion processes and for time scales larger than the typical particles' correlation time scale τ .

In general, however, the Lagrangian diffusion coefficient is time dependent and can be defined as

$$D(t) = \frac{d\xi_{\vec{r}}^2(t)}{dt} = 2 \langle \vec{r}_i(t) \cdot \vec{v}_i(t) \rangle_i, \quad (3.3)$$

where $\vec{v}_i(t) = d\vec{r}_i(t)/dt$ is the Lagrangian velocity of the particle. The diffusion coefficient along one spatial direction, say along the x -coordinate, follows accordingly as $D_x = d\xi_x^2(t)/dt = 2 \langle x_i(t) v_{x,i}(t) \rangle_i$. Equation (3.3) holds for homogeneous turbulence with zero mean velocity. From $\vec{r}_i(t) = \vec{r}_i(0) + \int_0^t \vec{v}_i(t') dt'$ it follows that

$$\begin{aligned} D(t) &= 2 \left\langle \left[\vec{r}_i(0) + \int_0^t \vec{v}_i(t') dt' \right] \cdot \vec{v}_i(t) \right\rangle_i \\ &= 2 \int_0^t \langle \vec{v}_i(t') \cdot \vec{v}_i(t) \rangle_i dt'. \end{aligned} \quad (3.4)$$

The above expression allows us to related $D(t)$ to the trace of the Lagrangian velocity autocorrelation tensor $\text{tr } \mathcal{C}(t - t') = \langle \vec{v}_i(t') \cdot \vec{v}_i(t) \rangle_i$ as

$$D(t) = 2 \int_0^t \text{tr } \mathcal{C}(t - t') dt' = 2 \int_0^t \text{tr } \mathcal{C}(t') dt' , \quad (3.5)$$

a result which was already derived by Taylor (1921). This formulation has the advantage that it is fully general and that it allows us to study anomalous diffusion processes. Note, that strictly speaking any transport process with $\xi_{\vec{r}}(t)$ not growing linearly in time is called anomalous diffusion. This is always the case for time intervals shorter than the correlation time τ , but sometimes anomalous diffusion can also occur for $t \gg \tau$. If $\xi_{\vec{r}}(t) \propto t^\alpha$ and if $\alpha < 1$ transport processes are called *subdiffusive*, if $\alpha > 1$ they are called *superdiffusive* (Lesieur 1997; Isichenko 1992; Castiglione *et al.* 1999; Lillo & Mantegna 2000). Studying transport processes directly in terms of the particle displacement, i.e. Equation (3.1), is useful when attempting to find simple approximations to the diffusion coefficient $D(t)$ for example in a mixing length approach.

3.1.3 Numerical Method

In order to utilize the above formalism, we carry out a series of numerical simulation of supersonic turbulent flows. A variety of numerical schemes can be used to describe the time evolution of gases and fluids. By far the most widely used and thoroughly-studied class of methods is based on the finite difference representations of the equations of hydrodynamics (e.g. Potter 1977). In the most simple implementation, the fluid properties are calculated on equidistant spatially fixed grid points in a Cartesian coordinate system. Finite difference schemes have well defined mathematical convergence properties, and can be generalized to very complex, time varying, non-equidistant meshes with arbitrary geometrical properties. However, it is very difficult to obtain a Lagrangian description, which is essential when dealing with compressible supersonic turbulence with a high degree of vorticity. Methods that do not rely on any kind of mesh representation at all are therefore highly desirable.

For the current investigation we use smoothed particle hydrodynamics (SPH), which is a fully Lagrangian, particle-based method to solve the equations of hydrodynamics. The fluid is represented by an ensemble of particles, where flow properties and thermodynamic observables are obtained as local averages from a kernel smoothing procedure (typically based on cubic spline functions) (Benz 1990; Monaghan 1992). Each particle i is characterized by mass m_i , velocity \vec{v}_i and position \vec{r}_i and carries in addition density ρ_i , internal energy ϵ_i or temperature T_i , and pressure p_i . The SPH method is commonly used in the astrophysics community because it can resolve large density contrasts simply by increasing the particle concentration in regions where it is needed. This versatility is important for handling compressible turbulent flows where density fluctuations will occur at random places and random times. The same scheme that allows for high spatial resolution in high-density regions, however, delivers only limited spatial resolution in low-density regions. There, the number density of SPH particles is small and thus the volume necessary to obtain a meaningful local average tends to be large. Furthermore, SPH requires the introduction of a von Neumann Richtmyer artificial viscosity to prevent interparticle penetration, shock fronts are thus smeared out over two to three local smoothing lengths. Altogether, the performance and convergence properties of the method are well understood and tested against analytic models and other numerical schemes, for example in the context of turbulent supersonic astrophysical flows (Mac Low *et al.* 1998; Klessen & Burkert 2000, 2001; Klessen *et al.* 2000), and its intrinsic diffusivity is sufficiently low to allow for the current investigation of turbulent diffusion phenomena (Lombardi *et al.* 1999).

To simplify the analysis we assume the medium is infinite and isotropic on large scales, and consider a cubic volume which is subject to periodic boundary conditions. The medium is described as an ideal gas with an isothermal equation of state, i.e. pressure p relates to the density ρ as $p = c_s^2 \rho$ with c_s being the speed of sound. Throughout this paper we adopt normalized units, where

Table 3.1: Model properties

(1) model	(2) k	(3) \mathcal{M}	(4) t_{cross}	(5) $\bar{\sigma}_x$	(6) $\bar{\sigma}_y$	(7) $\bar{\sigma}_z$	(8) $D_x(\infty)$	(9) $D_y(\infty)$	(10) $D_z(\infty)$	(11) $2\bar{\sigma}_x/k$	(12) $2\bar{\sigma}_y/k$	(13) $2\bar{\sigma}_z/k$
0ℓ	1.2	0.6	35.3	0.030	0.028	0.027	0.027	0.021	0.019	0.030 – 0.060	0.028 – 0.057	0.027 – 0.054
$0i$	3.4	0.5	39.1	0.026	0.026	0.025	0.010	0.010	0.009	0.013 – 0.017	0.013 – 0.017	0.013 – 0.017
$0s$	7..8	0.4	46.2	0.021	0.022	0.022	0.005	0.005	0.005	0.005 – 0.006	0.005 – 0.006	0.005 – 0.006
1ℓ	1.2	1.9	10.4	0.106	0.084	0.098	0.140	0.069	0.111	0.106 – 0.213	0.084 – 0.167	0.098 – 0.196
$1i$	3.4	1.9	10.6	0.097	0.096	0.092	0.042	0.047	0.038	0.048 – 0.065	0.048 – 0.064	0.046 – 0.061
$1s$	7..8	1.7	11.5	0.086	0.089	0.087	0.025	0.026	0.024	0.021 – 0.024	0.022 – 0.025	0.022 – 0.025
2ℓ	1.2	3.1	6.5	0.173	0.129	0.158	0.223	0.103	0.169	0.173 – 0.346	0.129 – 0.257	0.158 – 0.315
$2i$	3.4	3.1	6.4	0.167	0.155	0.151	0.084	0.071	0.063	0.083 – 0.111	0.077 – 0.103	0.075 – 0.100
$2s$	7..8	3.2	6.3	0.154	0.163	0.157	0.044	0.054	0.047	0.038 – 0.044	0.041 – 0.046	0.039 – 0.045
3ℓ	1.2	5.2	3.8	0.301	0.252	0.227	0.314	0.245	0.169	0.301 – 0.603	0.252 – 0.505	0.227 – 0.454
$3i$	3.4	5.8	3.5	0.261	0.287	0.316	0.131	0.189	0.233	0.130 – 0.174	0.143 – 0.191	0.158 – 0.211
$3s$	7..8	5.8	3.4	0.297	0.288	0.289	0.106	0.092	0.091	0.074 – 0.085	0.072 – 0.082	0.072 – 0.083
4ℓ	1.2	8.2	2.4	0.467	0.318	0.444	0.693	0.241	0.558	0.467 – 0.933	0.318 – 0.635	0.444 – 0.887
$4i$	3.4	9.7	2.1	0.451	0.478	0.520	0.248	0.323	0.349	0.225 – 0.301	0.239 – 0.319	0.260 – 0.347
$4s$	7..8	10.4	1.9	0.532	0.513	0.519	0.194	0.167	0.170	0.133 – 0.152	0.128 – 0.147	0.130 – 0.148

1. *column*: Model identifier, with the letters ℓ , i , and s standing for large-scale, intermediate-wavelength, and short-wavelength turbulence, respectively.

2. *column*: Driving wavelength interval.

3. *column*: Mean Mach number, defined as ratio between the time-averaged one-dimensional velocity dispersion $\bar{\sigma}_v = 3^{-1/2}(\bar{\sigma}_x^2 + \bar{\sigma}_y^2 + \bar{\sigma}_z^2)^{1/2}$ and the isothermal sound speed c_s , $\mathcal{M} = \bar{\sigma}_v/c_s$. The values for the different velocity components x , y , and z may differ considerably, especially for large-wavelength turbulence. Please recall from Section 3.1.3 that the speed of sound is $c_s = 0.05$, and thus the sound crossing time $t_{\text{sound}} = 20$.

4. *column*: Average shock crossing time through the computational volume.

5. to 7. *column*: Time averaged velocity dispersion along the three principal axes x , y , and z , e.g. for the x -component $\bar{\sigma}_x^2 = \int_0^t \langle (v_{x,i}(t') - \langle v_{x,i}(t') \rangle_i)^2 \rangle_i dt' / t$.

8. to 10. *column*: Mean-motion corrected diffusion coefficients along the three principal axes computed from Equation (3.3) for time intervals $t \gg \tau$.

11. to 13. *column*: Predicted values of the mean motion corrected diffusion coefficients D'_x , D'_y , and D'_z from extending mixing length theory into the supersonic regime (Section 3.1.7).

all physical constants (like the gas constant), total mass M , mean density $\langle \rho \rangle$, and the linear size L of the cube all are set to unity. The speed of sound is $c_s = 0.05$, hence, the sound crossing time through the cube follows as $t_{\text{sound}} = 20$. In all models discussed here, the fluid is represented by an ensemble of 205 379 SPH particles which gives sufficient resolution for the purpose of the current analysis.

Supersonic turbulence is known to decay rapidly (Mac Low *et al.* 1998; Stone *et al.* 1998; Padoan & Nordlund 1999; Biskamp & Müller 2000; Müller & Biskamp 2000). Stationary turbulence in the interstellar medium therefore requires a continuous energy input. To generate and maintain the turbulent flow we introduce random Gaussian forcing fields in a narrow range of wavenumbers such that the total kinetic energy contained in the system remains approximately constant. We generate the forcing field for each direction

separately and simply add up the three contributions. Thus, we excite both, solenoidal as well as compressible modes at the same time. The typical ratio between the solenoidal and compressible energy component is between 2:1 and 3:1 in the resulting turbulent flow (see e.g. Figure 8 in Klessen *et al.* 2000). We keep the forcing field fixed in space, but adjust its amplitude in order to maintain a constant energy input rate into the system compensating for the energy loss due to dissipation (for further details on the method see Mac Low 1999 or Klessen *et al.* 2000). This non-local driving scheme allows us to exactly control the (spatial) scale which carries the peak of the turbulent kinetic energy. It is this property that motivated our choice of random Gaussian fields as driving source. In reality the forcing of turbulence in the interstellar medium is likely to be a multi-scale phenomenon with appreciable contributions from differential rotation (i.e. shear)

in the Galactic disk and energy input from supernovae explosions ending the lives of massive stars. Comparable to the values observed in interstellar gas, we study flows with Mach numbers in the range 0.5 to 10, where we define the Mach number from the *one-dimensional* rms velocity dispersion σ_v as $\mathcal{M} = \sigma_v/c_s$. For each value of the Mach number we consider three different cases, one case where turbulence is driven on large scales only (i.e. with wavenumbers k in the interval $1 \leq k \leq 2$), intermediate-wavelength turbulence ($3 \leq k \leq 4$), and small-scale turbulence ($7 \leq k \leq 8$), as summarized in Table 3.1. Note that our models are not subject to global shear because of the adopted periodic boundary conditions. We call turbulence "large scale" when the Fourier decomposition of the velocity field is dominated by the largest scales possible for the considered volume L^3 , i.e. the system becomes isotropic and homogeneous only on scales larger than L . On scales below L it may exhibit a considerable degree of anisotropy. This is most noticeable in the case $1 \leq k \leq 2$, because wavenumber space is very poorly sampled and variance effects become significant. The system is dominated by one or two large shock fronts that cross through the medium. In the interval $7 \leq k \leq 8$ the number of Fourier modes contribution to the velocity field is large, and the system appears more isotropic and homogeneous already on distances smaller than L . This trend is clearly visible in Figure 3.1.

Similar to any other numerical calculations, the models discussed here fall short of describing real gases in comprehensive details as they cannot include all physical processes that may act on the medium. In interstellar gas clouds, transport properties and chemical mixing will not only be determined by the compressible turbulence alone, but the density and velocity structure is also influenced by magnetic fields, chemical reactions, and radiation transfer processes. Furthermore, all numerical models are resolution limited. The turbulent inertial range in our large-scale turbulence simulations spans over about 1.5 decades in wavenumber. This range is considerably less than what is observed in interstellar

gas clouds. The same limitation holds for the Reynolds numbers achieved in the models, they fall short of the values in real gas clouds by several orders of magnitude. Nevertheless, despite these obvious shortcomings, the results derived here do characterize global transport properties in interstellar gas clouds and in other supersonically turbulent compressible flows.

3.1.4 Flow Properties

Supersonic turbulence in compressible media establishes a complex network of interacting shocks. Converging shock fronts locally generate large density enhancements, diverging flows create rarefied voids of low gas density. The fluctuations in turbulent velocity fields are highly transient, as the random flow that creates local density enhancements can disperse them again. The life time of individual shock-generated clumps corresponds to the time interval for two successive shocks to pass through the same location in space, which in turn depends on the length scale of turbulence and on the Mach number of the flow.

The velocity field of turbulence that is driven at large wavelengths is found to be dominated by large-scale shocks which are very efficient in sweeping up material, thus creating massive coherent density structures. The shock passing time is rather long, and shock-generated clumps can travel quite some distance before begin disrupted. On the contrary, when energy is inserted mainly on small scales, the network of interacting shocks is very tightly knit. Clumps have low masses and the time interval between two shock fronts passing through the same location is small, hence, swept-up gas cannot travel far before being dispersed again.

The density and velocity structure of three models with large-, intermediate-, and small-wavelength turbulence is visualized in Figure 3.1. It shows cuts through the centers of the simulated volume. As turbulence is stationary, all times are equivalent, and the snapshot in the upper panel is taken at some arbitrary time. The lower panel

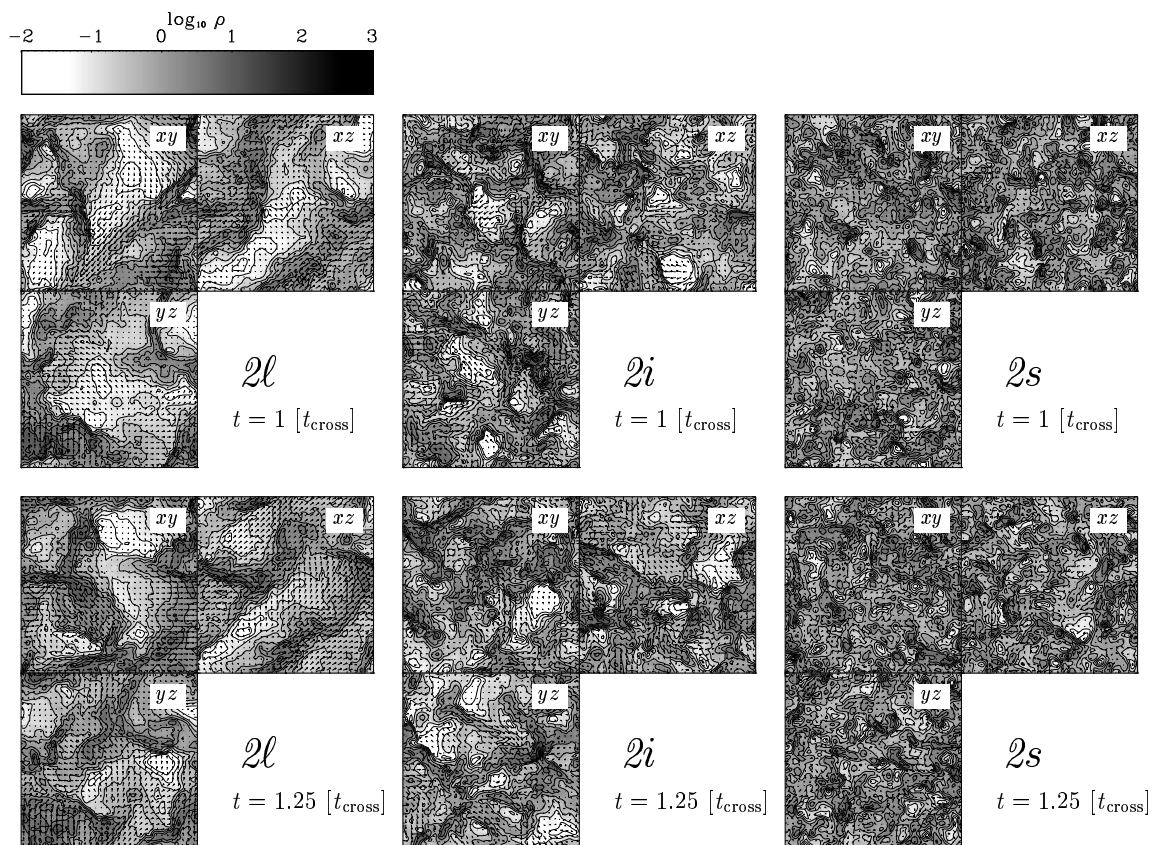


Figure 3.1: Density and velocity structure of models $2l$, $2i$, and $2s$ (from left to right). The panels show cuts through the center of the computational volume normal to the three principal axes of the system, after one shock crossing time $t_{\text{cross}} = L/\sigma_v \approx 6.5$ and $1/4 t_{\text{cross}}$ later. Density is scaled logarithmically as indicated in the greyscale key at the upper left side. The maximum density is ~ 100 , while the mean density is one in the normalized units used. Vectors indicate the velocity field in the plane. The rms Mach number is $\mathcal{M} \approx 3.1$. Large-scale turbulence ($2l$) is dominated by large coherent density and velocity gradients leading a large degree of anisotropy, whereas small-scale turbulence ($2s$) exhibits noticeable structure only on small scales with the overall density structure being relatively homogeneous and isotropic. (From Klessen & Lin 2003)

depicts the system some time interval later corresponding to $1/4$ shock crossing time through the cube. One clearly notices markable differences in the density and velocity field between the three models.

3.1.5 Transport Properties in an Absolute Reference Frame

In order to drive supersonic turbulence and to maintain a given rms Mach number in the flow, we use a random Gaussian velocity field with zero mean to ‘agitate’ the fluid elements at each timestep. However, despite the fact that the driving scheme has zero mean, the system is likely to

experience a net acceleration and develop an appreciable drift velocity, because of the compressibility of the medium. This evolutionary trend is well illustrated in Figure 3.2 which plots the time evolution of the three components of the mean velocity for models $2l$, $2i$, and $2s$, with rms Mach numbers $\mathcal{M} \approx 3.1$, where turbulence is driven on (a) large (i.e. with small wavenumbers $1 \leq k \leq 2$), (b) intermediate ($3 \leq k \leq 4$), and (c) small scales (with $7 \leq k \leq 8$). The net acceleration is most pronounced when turbulent energy is inserted on the global scales, as in this case larger and more coherent velocity gradients can build up across the volume compared to small-scale turbulence.

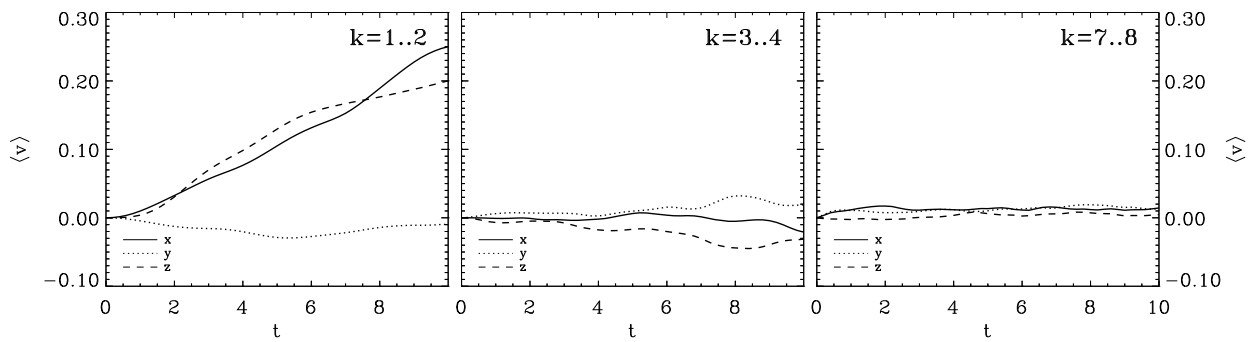


Figure 3.2: Time evolution of the mean flow velocity $\langle \bar{v}_i(t) \rangle_i$ in models 2ℓ , $2i$, and $2s$. Time t and velocity v are given in normalized units. (From Klessen & Lin 2003)

The tendency for the zero-mean Gaussian driving mechanisms to induce significant center-of-mass drift velocities in highly compressible media can be understood as follows. Suppose the gas is perturbed by one single mode in form of a sine wave. If the medium is homogeneous and incompressible, equal amounts of mass would be accelerated in the forward as well as in the backward direction. But, if the medium is inhomogeneous, there would be an imbalance between the two directions and the result would be a net acceleration of the system. If the density distribution remains fixed, this acceleration would be compensated by an equal amount of deceleration after half a period, and the center of mass would simply oscillate. However, if the system is highly compressible and the driving field is a superposition of plane waves, the density distribution would change continuously (and randomly). Any net acceleration at one instance in time would not be completely compensated after some finite time interval later. This will only occur for $t \rightarrow \infty$ assuming ergodicity of the flow. Subsequently, the system is expected to develop a net flow velocity in some random direction for $t < \infty$. This effect is most clearly noticeable for long-wavelength turbulence, where density and velocity structure is dominated by the coherent large-scale structure. But the effect is small for turbulence that is excited on small scales, because in this limit, there is a large number of accelerated ‘cells’ which in turn compensate for another’s acceleration.

The property that the compressible turbulent flows are likely to pick up average drift velocities, even when driven by Gaussian fields with

zero mean, has implications for the transport coefficients. Figure 3.3 shows the time evolution of the absolute (Eulerian) diffusion coefficients D_x , D_y , and D_z in each spatial direction computed from Equation (3.1). Note that for stationary turbulence, only time differences are relevant and one is free to choose the initial time. In order to improve the statistical significance of the analysis, we obtain $D(t)$ and $\xi_r^2(t)$ by further averaging over all time intervals t that ‘fit into’ the full timespan of the simulation.

Due to the (continuous) net acceleration experienced by the system, the quantity $\xi_r^2(t)$ grows faster than linearly with time, even for intervals much larger than the correlation time τ , i.e. for $\tau \ll t < \infty$. The system resides in a superdiffusive regime, where $D(t)$ does not saturate. Instead, $D(t)$ grows continuously with time, which is most evident in model 2ℓ of large-scale turbulence. The ever increasing drift velocity $\langle \bar{v}_i(t) \rangle_i$ causes strong velocity correlations leading continuous growth of the velocity autocorrelation tensor $\int_0^t \text{tr } \mathcal{C}(t') dt'$. This net motion, however, can be corrected for, allowing us to study the dispersion of particles in a reference frame that moves along with the average flow velocity of the system.

3.1.6 Transport Properties in Flow Coordinates

In order to gain further insight into the transport properties of compressible supersonic turbulent flows, we study the time evolution of the relative

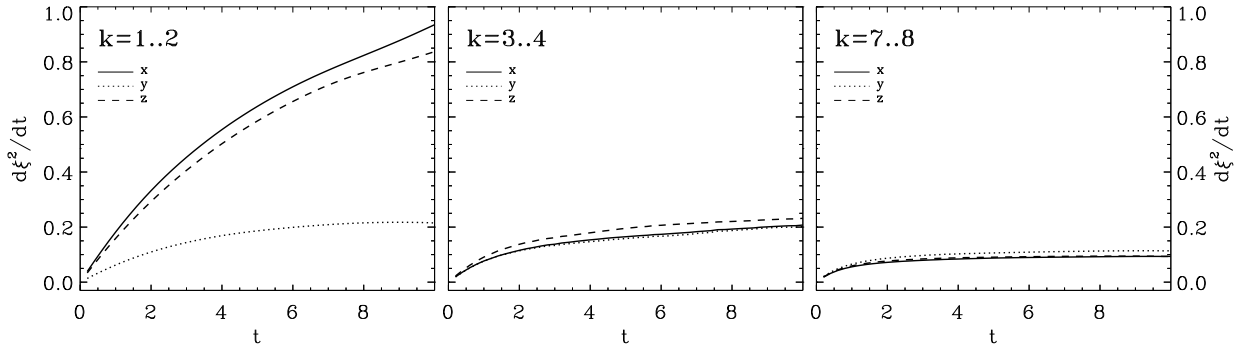


Figure 3.3: Time evolution of the diffusion coefficient $D(t) = d\langle[\vec{r}_i(t) - \vec{r}_i(0)]^2\rangle_i/dt$ for models 2*l*, 2*i*, and 2*s* computed in an absolute reference frame. All units are normalized as described in Section 3.1.3. (From Klessen & Lin 2003)

(Lagrangian) diffusion coefficient. In this prescription,

$$D'(t) = \frac{d\xi_{\vec{r}}^2(t)}{dt} \quad (3.6)$$

is obtained relative to a frame of reference which comoves with the mean motion of the system $\langle\vec{v}_i(t)\rangle_i$ on the trajectory $\langle\vec{r}_i(t)\rangle_i = \int_0^t \langle\vec{v}_i(t')\rangle_i dt'$. Then, $\xi_{\vec{r}}^2(t-t') = \langle[(\vec{r}_i(t) - \langle\vec{r}_i(t)\rangle_i) - (\vec{r}_i(t') - \langle\vec{r}_i(t')\rangle_i)]^2\rangle_i$ (see Equation 3.1).

In Figure 3.4, we show the evolution of $D'(t)$ for each coordinate direction for the complete suite of models. The rms Mach numbers range from about 0.5 to 10, each considered for three cases where turbulence is driven on large, intermediate, and small scales, respectively. The plots are rescaled such that the time-averaged one-dimensional rms velocity dispersion $\bar{\sigma}_v$ is normalized to unity (for each direction separately). We also rescale the time t with respect to the average shock crossing time scale through the computational volume, $t_{\text{cross}} = L/\bar{\sigma}_v$. Recall that $L = 1$, and note that $\bar{\sigma}_v$ usually differs between the three spatial directions because of the variance effects, especially in models of large-scale turbulence.

In Figure 3.4, we demonstrate that the magnitude of $D'(t)$ saturates for large time intervals $t > \tau$ in all directions. In a reference frame that follows the mean motion of the flow, diffusion in compressible supersonically turbulent media indeed behaves in a normal manner. For small time intervals $t < \tau$, however, the system still exhibits an anomalous diffusion even with the mean-motion correction. In this regime $D'(t)$ grows roughly linearly with time. For $t > \tau$ the diffusion coefficient $D'(t)$ reaches an asymptotic limit. This

result holds for the entire range of Mach numbers studied and for turbulence that is maintained by energy input on very different spatial scales.

From Figure 3.4, we find that diffusion in compressible supersonic turbulent flows follows a universal law. It can be obtained by using the rms Mach number (together with the sound speed c_s) as characterizing parameter for rescaling the velocity dispersion σ_v , and the rms shock crossing time scale through the volume $t_{\text{cross}} = L/(\mathcal{M}c_s)$ for rescaling the time. The normalized diffusion coefficient $D'(t)$ exhibits a universal slope of two at times $t < \tau$ (i.e. in the superdiffusive regime), and approaches a constant value that depends only on the length scale but not on the strength (i.e. the resulting Mach number) of the mechanism that drives the turbulence. Even for highly compressible supersonic turbulent flows it is possible to find simple scaling relations to characterize the transport properties — analogous to the mixing length description of diffusive processes in incompressible subsonic turbulent flows.

3.1.7 A Mixing Length Description

Incompressible turbulence is often described in terms of a hierarchy of turbulent eddies, where each eddy contains multiple eddies of smaller size on the lower levels of the hierarchy, while itself being part of turbulent eddy at larger scales (Richardson 1922; Kolmogorov 1941; Obukhov 1941). At each level of the hierarchy, an eddy is characterized by a typical lengthscale $\tilde{\ell}$ and a typical velocity \tilde{v} . The typical lifetime of an eddy is its ‘turn-over’ time $\tau = \tilde{\ell}/\tilde{v}$. This mixing length

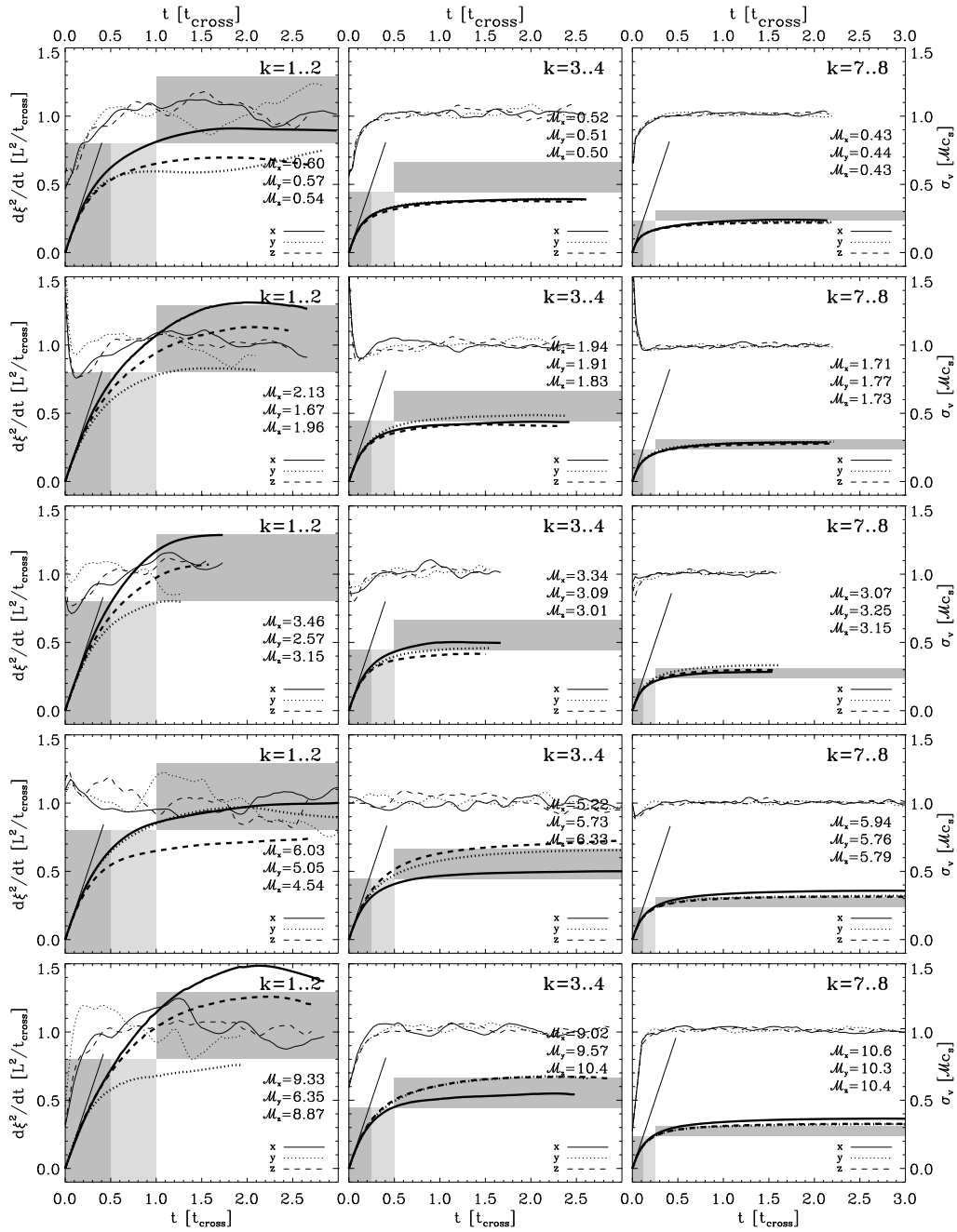


Figure 3.4: Time evolution of the diffusion coefficient $D'(t) = d\xi_i^2/dt$ computed in a reference frame that follows the average flow velocity (*thick line*, axis scaling on the left ordinate), i.e. is centered on $\langle \bar{v}_i(t) \rangle_i = \int_0^t \langle \bar{v}_i(t') \rangle_i dt'$. Velocity dispersions along the three major axes x , y , and z are each normalized to unity using the time-averaged one-dimensional Mach number \mathcal{M} (as indicated in each plot) together with the given value of the sound speed c_s (*thin lines*, axis scaling on the right ordinate). Times are rescaled to the rms shock crossing time through the simulated cube $t_{\text{cross}} = L/\sigma_v = L/(Mc_s)$. Details for each model are given in Table 3.1. The horizontal gray shaded area indicates the mixing length prediction for $t \rightarrow \infty$, and the vertical gray and light gray shaded areas show a time interval of $\tau = L/(kMc_s)$ and 2τ , respectively. For $t \ll \tau$ diffusion should be anomalous and coherent, with $D'(t)$ growing linearly with time. The expected behavior from mixing length theory in this regime is indicated by the straight line originating at $t = 0$. It indeed gives a good fit. Note that all models driven on large scales ($1 \leq k \leq 2$) exhibit a considerable degree of anisotropy, manifested by different rms Mach numbers \mathcal{M} along the three principal axes and different values $D'(t)$. For the models with intermediate-scale and small-scale driving anisotropy effects are increasingly less important. (From Klessen & Lin 2003)

prescription is an attempt to characterize the flow properties in terms of the typical scales $\tilde{\ell}$ and \tilde{v} . For example, this classical picture defines an effective ‘eddy’ viscosity $\mu = \rho\tilde{\ell}\tilde{v}$, where ρ is the density. The mixing length $\tilde{\ell}$ is interpreted to be the turbulent analogue of the mean free path of molecules in the kinetic theory of gases, with \tilde{v} being the characteristic velocity of the turbulent fluctuation.

In such a model, the velocities of gas molecules within an eddy are strongly correlated within a time interval $t < \tau$. They all follow the eddy rotation; the diffusion process is coherent. However, for $t \gg \tau$ the velocities of gas molecules become uncorrelated, as the eddy has long been destroyed and dispersed. Hence, the velocity autocorrelation function vanishes for large time intervals, $\mathcal{C}(t) \rightarrow 0$ for $t \rightarrow \infty$. Diffusion becomes incoherent as in Brownian motion or the random walk. The diffusion coefficient in the mixing length approach simply is $D(t) \approx 2\tilde{v}^2 t$ in the regime $t < \tau$, which follows from replacing $\vec{r}(t)$ by $\tilde{v}t$ and $\vec{v}(t)$ by \tilde{v} in Equation (3.3). As the largest correlation length is the eddy size, $\vec{r}(t)$ is substituted by $\tilde{\ell} = \tilde{v}\tau$ for times $t \gg \tau$, and the classical mixing length theory yields $D(t) \approx 2\tilde{\ell}\tilde{v} = 2\tilde{v}^2\tau = \text{constant}$.

Compressible, supersonic, turbulent flows rapidly build up a network of interacting shocks with highly transient density and velocity structure. Density fluctuations are generated by locally converging flows, and their lifetimes are determined by the time τ between two successive shock passages. This time interval is determined by the typical shock velocity, which is roughly the rms velocity of the flow, i.e. the Mach number times the sound speed, $\sigma_v = \mathcal{M}c_s$. It also depends on the length scale at which energy is inserted into the system to maintain the turbulence, which in our case is L/k with k being the driving wavenumber and L being the size of the considered region (recall that in our models L is unity). This length scale is also the typical traveling distance before two shocks interact with each other. As basic ingredients for a supersonic compressible mixing length

description we can thus identify:

$$\text{shock travel length : } \tilde{\ell} \approx L/k, \quad (3.7)$$

$$\text{rms velocity : } \tilde{v} \approx \sigma_v = \mathcal{M}c_s. \quad (3.8)$$

The Lagrangian velocity correlation time scale, τ , is analogous to the time interval during which shock-generated density fluctuation remains unperturbed and moves coherently before it is being dispersed by the interaction with a new shock front. This time interval is equivalent to the time scale a shock travels along its ‘mean free path’ $\tilde{\ell}$ with an rms velocity \tilde{v} . This crossing time is $\tau = \tilde{\ell}\tilde{v} \approx \sigma_v L/k$. For $t < \tau$ gas molecules can travel coherently within individual shock generated density fluctuations, and the diffusion coefficient in the mixing length prescription follows as

$$D'(t) \approx 2\tilde{v}^2 t \approx 2\sigma_v^2 t. \quad (3.9)$$

$D'(t)$ grows linearly with time with slope $2\sigma_v^2$. For large times, $t \gg \tau$, $D'(t)$ approaches a constant value,

$$D'(t) \approx 2\tilde{v}^2\tau \approx 2\sigma_v L/k. \quad (3.10)$$

This mixing length approach (Equations 3.9 and 3.10) suggests a unique scaling dependence of the diffusion coefficients in supersonic compressible flows on the *Mach number* \mathcal{M} and on the *length scale* $\tilde{\ell}$ of the most energy containing modes *with respect to the total size* L of the system considered.

We can use \mathcal{M} (together with the given value of the sound speed) to normalize the rms velocity: $\sigma_v = \mathcal{M}c_s \mapsto \sigma'_v = 1$. And we can also rescale the time with respect to the rms shock crossing time scale through the total volume, which is $t_{\text{cross}} = L/\sigma_v = L/(\mathcal{M}c_s) = t_{\text{sound}}/\mathcal{M}$ with $t_{\text{sound}} = L/c_s$ being the sound crossing time, so that $t \mapsto t' = t/t_{\text{cross}}$. From this normalization procedure, we get $D'(t) \mapsto D''(t') = D'(t) \mathcal{M}c_s L$ and obtain the following universal profile for the diffusion coefficient,

$$D''(t') = 2t' \quad \text{for } t' \ll 1/k \quad (3.11)$$

$$D''(t') = 2/k \quad \text{for } t' \gg 1/k. \quad (3.12)$$

Note that this result holds for each velocity component separately, as the results in Figure 3.4

indicate. In this case σ_v stands for σ_x , σ_y , or σ_z in Equations (3.9) and (3.10), and it holds for the total diffusion coefficient, when using $\sigma_v = (\sigma_x^2 + \sigma_y^2 + \sigma_z^2)^{1/2}$ instead.

The validity of the mixing length approximation is quantified in Figure 3.5 which plots the mixing length predictions against the values obtained from the numerical models. For large-scale and intermediate scale turbulence, the mixing length approach gives very satisfying results, only for small-scale turbulence it underestimates the diffusion strength. This disparity probably has to do with the numerical resolution of the code, in the sense that driving wavenumbers of $k \approx 8$ come close to the dissipation scale of the method and hence the inertial range of turbulence is limited (Klessen *et al.* 2000). That limitation leads to an effective driving for the turbulent motion on somewhat larger scales than $1/8$. Consequently, it leads to a stronger diffusion, i.e. somewhat larger diffusion coefficients than those predicted by Equations (3.11) and (3.12). The same numerical effects also account for the slightly shallower slope of $D'(t)$ for $t \ll \tau$ for models $7 \leq k \leq 8$.

Figures 3.4 and 3.5 indicate that the classical mixing length theory can be extended from incompressible (subsonic) turbulence into the regime of supersonic turbulence of highly compressible media. In this case, driving length $\tilde{\ell}$ and rms velocity dispersion $\sigma_v = \mathcal{M}c_s$ act as characteristic length and velocity scales in the mixing length approach. Note, that this only applies to mean-motion corrected transport. In general (i.e. in an absolute reference frame), supersonic turbulence in compressible media leads to superdiffusion as visualized in Figure 3.3.

3.1.8 Summary

Supersonic turbulence in compressible media establishes a complex network of interacting shocks. Converging shock fronts locally generate large density enhancements, diverging flows create voids of low gas density. The fluctuations in turbulent velocity fields are highly transient, as the random flow that creates local density enhancements can disperse them again.

Due to compressibility, supersonically turbulent flows will usually develop noticeable drift velocities, especially when turbulence is driven on large scales, even when it is excited with Gaussian fields with zero mean. This tendency has consequences for the transport properties in an absolute reference frame. The flow exhibits super-diffusive behavior (see also Balk 2001). However, when the diffusion process is analyzed in a comoving coordinate system, i.e. when the induced bulk motion is being corrected, the system exhibits normal behavior. The diffusion coefficient $D(t)$ saturates for large time intervals, $t \rightarrow \infty$.

By extending classical mixing length theory into the supersonic regime we propose a simple description for the diffusion coefficient based on the rms velocity \tilde{v} of the flow and the typical shock travel distance $\tilde{\ell}$,

$$\begin{aligned} D'(t) &= 2\tilde{v}^2 t \quad \text{for } t \ll \tilde{\ell}/\tilde{v}, \\ D'(t) &= 2\tilde{v}\tilde{\ell} \quad \text{for } t \gg \tilde{\ell}/\tilde{v}. \end{aligned}$$

This functional form may be used in those numerical models where knowledge of the mixing properties of turbulent supersonic flows is required, but where these flows cannot be adequately resolved. This is the case, for example, in astrophysical simulations of galaxy formation and evolution, where the chemical enrichment of the interstellar gas and the distribution and spreading of heavy elements produced from massive stars throughout galactic disks needs to be treated without being able to follow the turbulent motion of interstellar gas on small enough scales relevant to star formation (Rana 1991; Bertschinger 1998). Our results furthermore are directly relevant for understanding the properties of individual star-forming interstellar gas clouds within the disk of our Milky Way. These are dominated by supersonic turbulent motions which can provide support against gravitational collapse on global scales, while at the same time produce localized density enhancements that allow for collapse, and thus stellar birth, on small scales. The efficiency and timescale of star formation in galactic gas clouds depend on the in-

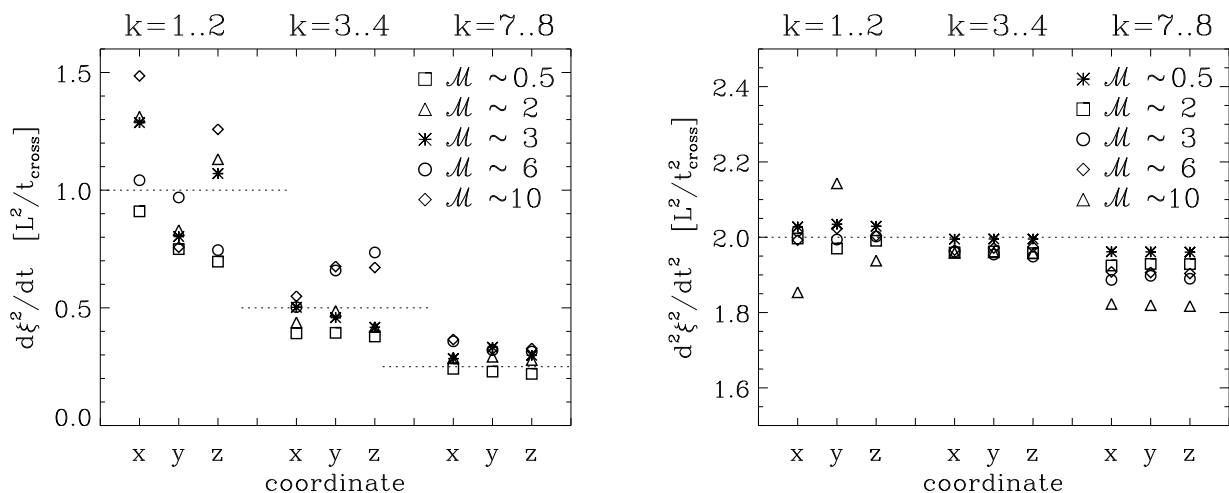


Figure 3.5: Comparison between mixing length predictions and numerical models. At the left we plot the normalized, mean-motion corrected diffusion coefficient $D''(t')$ for $t \rightarrow \infty$, and at the right its slope $dD''(t')/dt'$ for $t' \ll 1/k$. For each suite of models, large-scale, intermediate-scale, and small-scale turbulence, respectively (as indicated by the forcing wavenumber k at the top of each plot), we separately show the three velocity components (as indicated at the bottom). The different Mach numbers in each model suite are denoted by different symbols (as identified at the right-hand side of each plot). The dotted lines give the corresponding prediction of the mixing-length theory, $D''(t') = 2/k$ and $dD''(t')/dt' = 2$, respectively, where we take k to be the maximum wavenumber of the forcing scheme indicated at the top of each plot. (From Klessen & Lin 2003)

tricate interplay between their internal gravitational attraction and their turbulent energy content. The same is true for the statistical properties of the resulting star clusters. For example, the element abundances in young stellar clusters are found to be very homogeneous (Wilden *et al.* 2002), implying that the gas out of which these stars formed must have been chemically well mixed initially. On the basis of the results discussed here, this observation can be used to constrain astrophysical models of interstellar turbulence in star-forming regions. Understanding transport processes and element mixing in supersonic turbulent flows thus is a prerequisite for gaining deeper insight into the star formation phenomenon in our Galaxy.

3.2 One-Point Probability Distribution Function

3.2.1 Introduction

Correlation and distribution functions of dynamical variables are frequently deployed for characterizing the kinematical properties of turbulent molecular clouds. Besides using 2-point

statistics (e.g. Scalo 1984, Kleiner & Dickman 1987, Kitamura *et al.* 1993, Miesch & Bally 1994, LaRosa, Shore & Magnani 1999), many studies have hereby concentrated on 1-point statistics, namely on analyzing the probability distribution function (PDF) of the (column) density and of dynamical observables, e.g. of the centroid velocities of molecular lines and their increments. The density PDF has been used to characterize numerical simulations of the interstellar medium by Vázquez-Semadeni (1994), Padoan, Nordlund, & Jones (1997), Passot, & Vázquez-Semadeni (1998) and Scalo *et al.* (1998). Velocity PDF's for several star-forming molecular clouds have been determined by Miesch & Scalo (1995) and Miesch, Scalo & Bally (1998). Lis *et al.* (1996, 1998) analyzed snapshots of a numerical simulation of mildly supersonic, decaying turbulence (without self-gravity) by Porter *et al.* (1994) and applied the method to observations of the ρ -Ophiuchus cloud. Altogether, the observed PDF's exhibit strong non-Gaussian features, they are often nearly exponential with possible evidence for power-law tails in the outer parts. This disagrees with the nearly Gaussian behavior typically found in experimental measurements and

numerical models of incompressible turbulence. The observed centroid velocity *increment* PDF's are more strongly peaked and show stronger deviations from Gaussianity than numerical models of incompressible turbulence predict. Furthermore, the spatial distribution of the largest centroid velocity differences (determining the tail of the distribution) appears 'spotty' across the face of the clouds; there is no convincing evidence for filamentary structure. Miesch *et al.* (1998) conclude that turbulence in molecular clouds involves physical processes that are not adequately described by incompressible turbulence or mildly supersonic decay simulations (see also Mac Low & Ossenkopf 2000).

Based on Klessen (2000), we extend in this Section previous determinations of PDF's from numerical models into a regime more applicable for interstellar turbulence by (1) by calculating fully supersonic flows, (2) by including self-gravity, and (3) by incorporating a (simple analytic) description of turbulent energy input. To do this, we use numerical models introduced and discussed in Section 2.5.3, and compare with existing molecular cloud observations in the literature. The PDF's for the density, for the line centroid velocity and for their increments are derived as function of time and evolutionary state of the turbulent model.

3.2.2 PDF's and Their Interpretation

Turbulence and PDF's

The Kolmogorov (1941) approach to incompressible turbulence is a purely phenomenological one and assumes the existence of a stationary turbulent cascade. Energy is injected into the system at large scales and cascades down in a self-similar way. At the smallest scales it gets converted into heat by molecular viscosity. The flow at large scales is essentially inviscid, hence for small wave numbers the equation of motion is dominated by the advection term. If the stationary state of fully developed turbulence results from random external forcing then one naïvely expects the velocity distribution in the fluid to

be Gaussian on time scales larger than the correlation time of the forcing, irrespectively of the statistics of the forcing term which follows from the central limit theorem. However, the situation is more complex (e.g. Frisch 1995, Lesieur 1997). One of the most striking (and least understood) features of turbulence is its intermittent spatial and temporal behavior. The structures that arise in a turbulent flow manifest themselves as high peaks at random places and at random times. This is reflected in the PDF's of dynamical variables or passively advected scalars. They are sensitive measures of deviations from Gaussian statistics. Rare strong fluctuations are responsible for extended tails, whereas the much larger regions of low intensity contribute to the peak of the PDF near zero (for an analytical approach see e.g. Forster, Nelson & Stephens 1977, Falkovich & Lebedev 1997, Chertkov, Kolokolov & Vergassola 1997, Balkovsky *et al.* 1997, Balkovsky & Falkovich 1998). For incompressible turbulence the theory predicts velocity PDF's which are mainly Gaussian with only minor enhancement at the far ends of the tails. The distribution of velocity *differences* (between locations in the system separated by a given shift vector $\Delta\vec{r}$) is expected to deviate considerably from being normal and is likely to resemble an exponential. This finding is supported by a variety of experimental and numerical determinations (e.g. Kida & Murakami 1989, Vincent & Meneguzzi 1991, Jayesh & Warhaft 1991, She 1991, She, Jackson & Orszag 1991, Cao, Chen, & She 1996, Vainshtein 1997, Lamballais, Lesieur, & Métais 1997, Machiels & Deville 1998). Compressible turbulence has remained to be too complex for a satisfying mathematical analysis.

PDF's of Observable Quantities

It is not clear how to relate the analytical work on incompressible turbulence to molecular clouds. In addition to the fact that interstellar turbulence is highly supersonic and self-gravitating, there are also observational limitations. Unlike the analytical approach or numerical simulations, molecular cloud observations allow access only to dimensionally reduced information. Velocity

measurements are possible only along the line-of-sight, and the spatial structure of a cloud is only seen in projection onto the plane of the sky, i.e. as variations of the column density. Although some methods can yield information about the 3-dimensional spatial structure of the cloud (see Stutzki & Güsten 1990, Williams, De Geus, & Blitz 1994), the result is always model dependent and equivocal (see also Ballesteros-Paredes, Vázquez-Semadeni, & Scalo 1999).

A common way of obtaining knowledge about the velocity structure of molecular clouds is to study individual line profiles at a large number of various positions across the cloud. In the optical thin case line shapes are in fact histograms of the radial velocities of gas sampled along the telescope beam. Falgarone & Phillips (1990) and Falgarone *et al.* (1994) showed that line profiles constructed from high-sensitivity CO maps exhibit non-Gaussian wings and attributed this to turbulent intermittency (see also Falgarone *et al.* 1998 on results from the IRAM-key project). Dubinski, Narayan, & Phillips (1995) demonstrated that non-Gaussian line profiles can be produced from *any* Gaussian random velocity field if variance effects become important (which is always the case for very steep or truncated power spectra). They concluded that non-Gaussian line profiles do not provide clear evidence for intermittency.

Another method of inferring properties of the velocity distribution in molecular clouds is to analyze the PDF of line centroid velocities obtained from a large number of individual measurements scanning the entire projected surface area of a cloud (Miesch & Scalo 1995, Lis *et al.* 1998, Miesch *et al.* 1998). Each line profile (i.e. the PDF along the line-of-sight) is collapsed into one single number, the centroid velocity, and then sampled *perpendicular* to the line-of-sight. Hence, the two functions differ in the direction of the sampling and in the quantity that is considered. A related statistical measure is the PDF of centroid velocity increments, it samples the velocity differences between the centroids for line measurements which are offset by a given separation. The observational advantage of using centroid and increment PDF's is, that the line measurements can typi-

cally be taken with lower sensitivity as only the centroid has to be determined instead of the detailed line shape. These measures are also less dependent on large-scale systematic motions of the cloud and they are less effected by line broadening due to the possible presence of warm dilute gas. However, to allow for a meaningful analysis of the PDF's especially in the tails, the number of measurements needs to be very large and should not be less than about 1000. In order to sample the entire volume of interstellar clouds, the molecular lines used to obtain the PDF's are optically thin. We follow this approach in the present investigation and use a mass-weighted velocity sampling along the line-of-sight to determine the line centroid. This zero-opacity approximation does not require any explicit treatment of the radiation transfer process.

The observed PDF's are obtained from *averaged* quantities (from column densities or line centroids). To relate these observational measures to quantities relevant for turbulence theory, i.e. to the full 3-dimensional PDF, numerical simulations are necessary as only they allow unlimited access to all variables in phase space. A first attempt to do this was presented by Lis *et al.* (1996, 1998) who analyzed a simulation of mildly supersonic decaying hydrodynamic turbulence by Porter *et al.* (1994). Since their model did neither include self-gravity nor consider flows at high Mach number or mechanisms to replenish turbulence, the applicability to the interstellar medium remained limited. This fact prompts the current investigation which extends the previous ones by calculating *highly supersonic flows*, and by including *self-gravity* and a *turbulent driving scheme*. The current study does not consider magnetic fields. Their influence on the PDF's needs to be addressed separately. However, the overall importance of magnetic fields and MHD waves on the dynamical structure of molecular clouds may not be large. The energy associated with the observed fields is of the order of the (turbulent) kinetic energy content of molecular clouds (Crutcher 1999). Magnetic fields cannot prevent the decay of turbulence (e.g. Mac Low *et al.* 1998) which implies the presence of exter-

nal driving mechanisms. These energy sources replenish the turbulent cascade and may excite MHD waves explaining the inferred equipartition between turbulent and magnetic energies.

Statistical Definitions

The one-point probability distribution function $f(x)$ of a variable x is defined such that $f(x)dx$ measures the probability for the variable to be found in the interval $[x, x + dx]$. The *density PDF* (ρ -PDF) discussed in this paper is obtained from the local density associated with each SPH particle. It is basically the normalized histogram summed over all particles in the simulation, i.e. a mass-weighted sampling procedure is applied. The *line-of-sight velocity centroid PDF* (v -PDF) is more complicated to compute. The face of the simulated cube is divided into 64^2 equal-sized cells. For each cell, the line profile is computed by sampling the normal (line-of-sight) velocity component of all gas particles that are projected into that cell. The line centroid is determined as the abscissa value of the peak of the distribution. This procedure corresponds to the formation of optically thin lines in molecular clouds, where all molecules within a certain column through the clouds contribute equally to the shape and intensity of the line. To reduce the sampling uncertainties, this procedure is repeated with the location of the cells shifted by half a cell size in each direction. Altogether about 20 000 lines contribute to the PDF. This is procedure is repeated for line-of-sights along all three system axes to identify projection effects. The *line centroid increment PDF* (Δv -PDF) is obtained in a similar fashion. However, the sampled quantity is now the velocity *difference* between line centroids obtained at two distinct locations separated across the face of the cloud by a fixed shift vector $\Delta\vec{r}$. The Δv -PDF for a spatial lag Δr is obtained as azimuthal average, i.e. as superposition of all individual PDF's with shift vectors of length Δr .

Also statistical moments of the distribution can be used to quantify the spread and shape of PDF's. For the current analysis we use the first four moments. Mean value μ and standard deviation σ (the 1. and 2. moments) quantify the lo-

cation and the width of the PDF and are given in units of the measured quantity. The third and fourth moments, skewness θ and kurtosis κ , are dimensionless quantities characterizing the shape of the distribution. The skewness θ describes the degree of asymmetry of a distribution around its mean. The kurtosis κ measures the relative peakedness or flatness of the distribution. We use a definition where $\kappa = 3$ corresponds to a normal distribution. Smaller values indicate existence of a flat peak compared to a Gaussian, larger values point towards a stronger peak or equivalently towards the existence of prominent tails in the distribution. A pure exponential results in $\kappa = 6$. Gaussian random fields are statistically fully determined by their mean value and the 2-point correlation function, i.e. by their first two moments, μ and σ . All higher moments can be derived from those. The 2-point correlation function is equivalent to the power spectrum in Fourier space (e.g. Bronstein & Semendjajew 1979).

Besides using moments there are other possibilities of characterizing a distribution. Van den Marel & Franx (1993) and Dubinski *et al.* (1995) applied Gauss-Hermite expansion series to quantify non-normal contributions in line profiles. A more general approach has been suggested by Vio *et al.* (1994), who discuss alternatives to the histogram representation of PDF's. However, as astrophysical data sets typically *are* histograms of various types and as histograms are the most commonly used method to describe PDF's, this approach is also adopted here.

3.2.3 PDF's from Gaussian Velocity Fluctuations

Variance effects in poorly sampled Gaussian velocity fields can lead to considerable *non-normal* contributions to the v - and Δv -PDF's. If a random process is the result of sequence of independent events (or variables), then in the limit of large numbers, its distribution function will be a Gaussian around some mean value. However, only the properties of a large *ensemble* of Gaussian fields

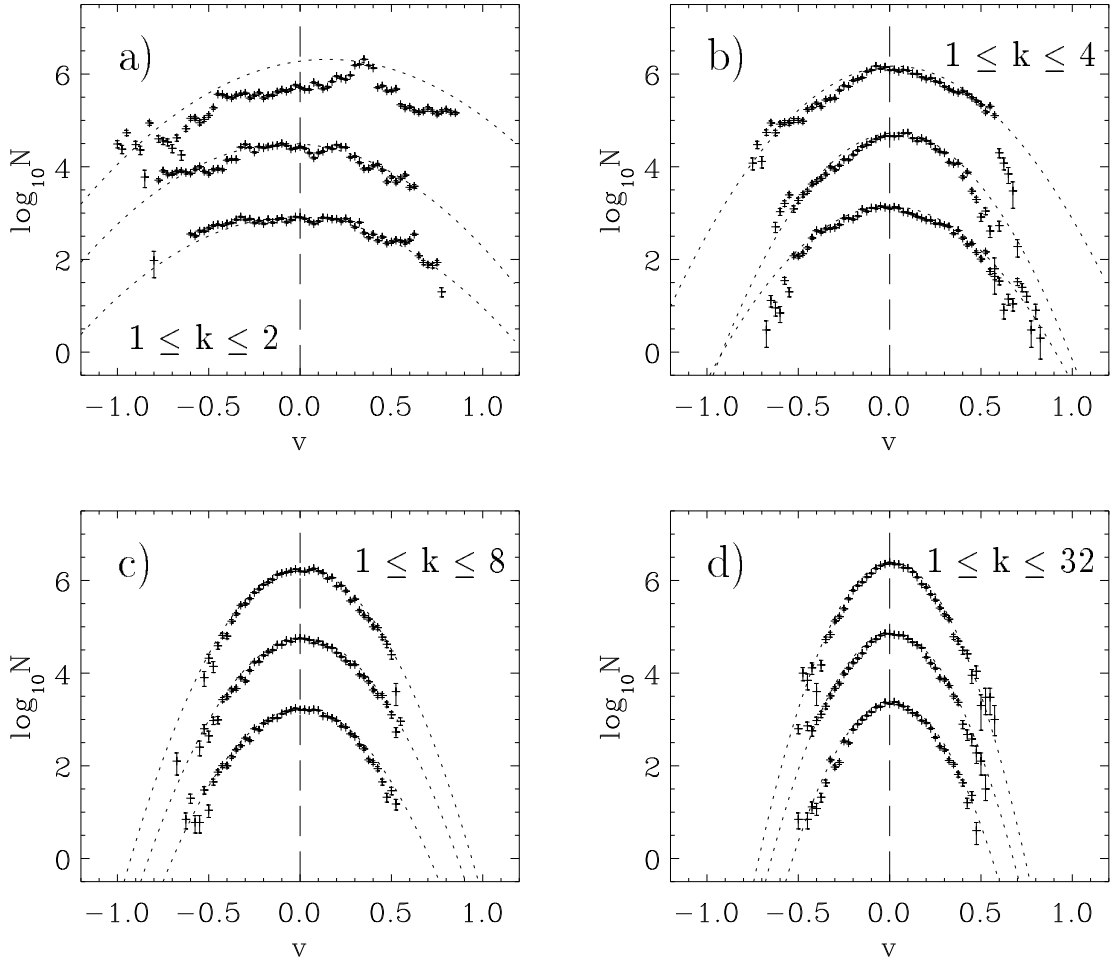


Figure 3.6: PDF's of line centroids for a homogeneous gaseous medium with Gaussian velocity field. The power spectrum is $P(k) = \text{const.}$ with wave numbers in the intervals (a) $1 \leq k \leq 2$, (b) $1 \leq k \leq 4$, (c) $1 \leq k \leq 8$, to (d) $1 \leq k \leq 32$. All other modes are suppressed. Each figure plots PDF's of the x -, y -, and z -component of the velocity offset by $\Delta \log_{10} N = 1.5$ (lowest, middle, and upper distribution, respectively). The length of the error bars is determined by the square root of the numbers of entries per velocity bin. The Gaussian fit from the first two moments is shown with dotted lines. (From Klessen 2000)

are determined in a statistical sense. Individual realizations may exhibit considerable deviations from the mean. The effect is strongest when only few (spatial) modes contribute to the field or, almost equivalently, when the power spectrum falls off very steeply. In this case, most kinetic energy is in large-scale motions.

This is visualized in Figure 3.6, it shows v -PDF's for homogeneous gas (sampled by 64^3 SPH particles placed on a regular grid) with Gaussian velocity fields with power spectra $P(k) = \text{const.}$ which are truncated at different wave numbers k_{max} ranging from (a) $k_{\text{max}} = 2$ to (d) $k_{\text{max}} = 32$.

Each realization is scaled such that the rms velocity dispersion is $\sigma_v = 0.5$. The figure displays the PDF's for the x -, y -, and z -component of the velocity. The PDF's of the strongly truncated spectrum (Figure 3.6a) do not at all resemble normal distributions. The Gaussian statistics of the field is very badly sampled with only very few modes. Note that the PDF's of the same field may vary considerably for different velocity *components*, i.e. for different *projections*. With the inclusion of larger number of Fourier modes this situation improves, and in Figure 3.6d the PDF's of all projections sample the expected Gaussian distribution very well.

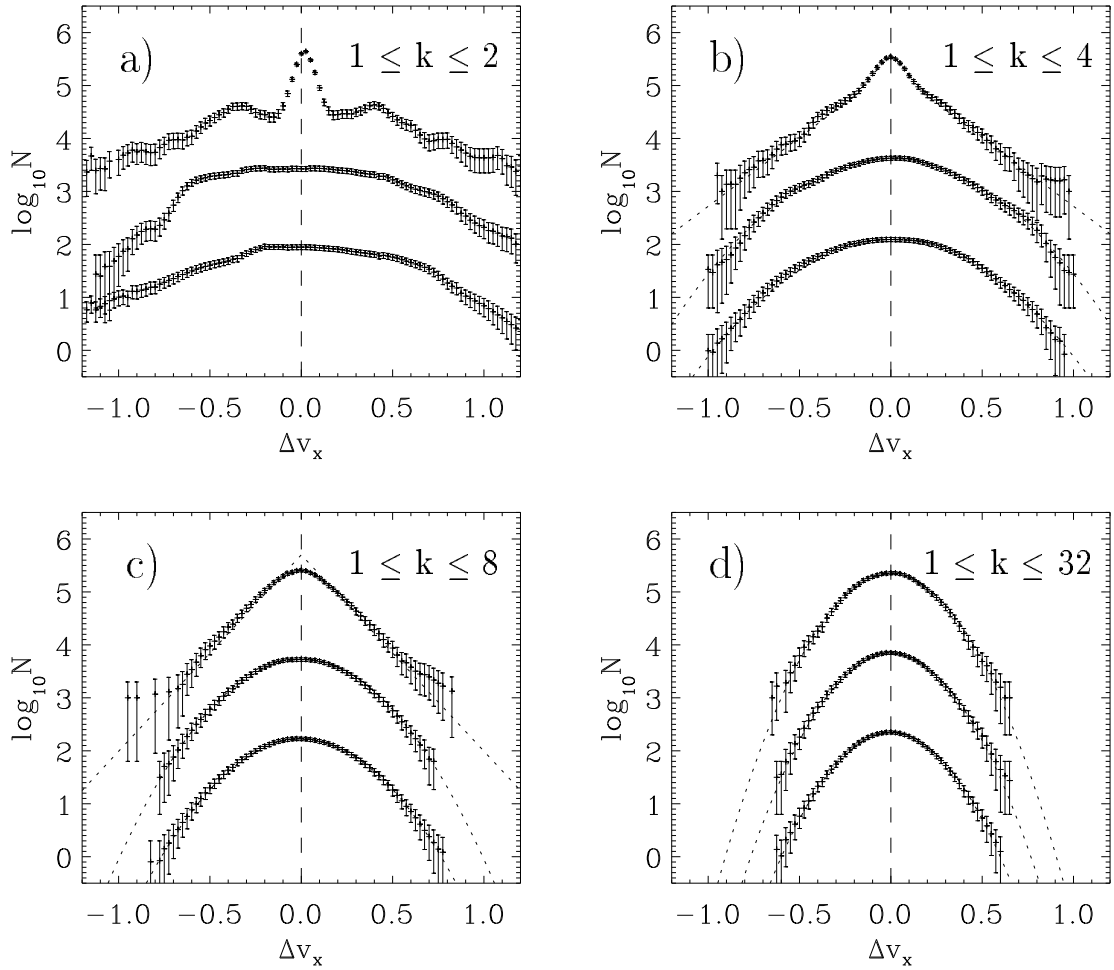


Figure 3.7: PDF's of line centroid increments for the same systems as in Figure 3.6: (a) $1 \leq k \leq 2$, (b) $1 \leq k \leq 4$, (c) $1 \leq k \leq 8$, to (d) $1 \leq k \leq 32$. Each plot shows the distribution of centroid velocity differences between locations separated by the distance Δr — upper curve: $\Delta r = 1/32$, middle curve: $\Delta r = 10/32$, and lower curve: $\Delta r = 30/32$. Only the velocity component for the line-of-sight parallel to the x -axis is considered. Again, the dotted lines represent the best fit Gaussian, except for the upper curve in (b) and (c) where the best exponential fit is shown. (From Klessen 2000)

A similar conclusion can be derived for Δv -PDF. This measure is even more sensitive to deviations from Gaussian statistics. Figure 3.7 plots the Δv -PDF's for the same sequence of velocity fields. For brevity, only the line-of-sight component parallel to the x -axis is considered. Furthermore, from the sequence of possible Δv -PDF's (defined by the spatial lag Δr) only three are shown, at small ($\Delta r = 1/32$, upper curve), medium ($\Delta r = 10/32$, middle curve), and large spatial lags ($\Delta r = 30/32$, lower curve). Sampling the Gaussian field with only two modes (Figure 3.7a) is again insufficient to yield increment PDF's of normal shape. The velocity field is very smooth, and the line centroid velocity difference between

neighboring cells is very small. Hence, for $\Delta r = 1/32$ the PDF is dominated by a distinct central peak at $\Delta v = 0$. The tails of the distribution are quite irregularly shaped. The situation becomes 'better' when sampling increasing distances, as regions of the fluid separated by larger Δr are less strongly correlated in velocity. For $\Delta r = 10/32$ and $\Delta r = 30/32$ the PDF's follow the Gaussian distribution more closely although irregularities in the shapes are still present. In Figures 3.7b and c the Δv -PDF's for medium to large lags are very well fit by Gaussians. Deviations occur only at small Δr , the PDF's are exponential (and the distribution for $k_{\max} = 4$ is still a bit cuspy). Finally, Figure 3.7d shows the three Δv -PDF's for the case

where all available spatial modes contribute to the velocity field ($1 \leq k \leq 32$). The PDF's follow a Gaussian for all spatial lags.

This behavior is also seen in the variation of the moments of the distribution as function of the spatial lag Δr . Applied to the above sequence of Gaussian velocity fields, Figure 3.8 displays the dispersion σ and the kurtosis κ of the distribution. The corresponding models are indicated at the right hand side of each plot. The width of the distribution, as indicated by the dispersion σ (Figure 3.8a), typically grows with increasing Δr , reflecting the relative peakedness of the distribution at small lags. For example, the distribution (a) yields a slope of 0.3 in the range $-0.6 \leq \log_{10} \Delta r \leq -0.4$, and (b) leads to a value of 0.2 in relatively large interval $-1.5 \leq \log_{10} \Delta r \leq -0.5$. The effect disappears for the better sampled fields. Typical values for that slope in observed molecular clouds are -0.3 to -0.5 (Miesch *et al.* 1998).² A direct measure of the peakedness of the distribution is its fourth moment, the kurtosis κ (Figure 3.8b). At small lags Δr , clearly the PDF's of model (a) are more strongly peaked than exponential ($\kappa = 6$). Comparing the entire sequence reveals again the tendency of the PDF's to become Gaussian at decreasing Δr with increasing number of modes considered in the construction of the velocity field.

Taking all together, it is advisable to consider conclusions about interstellar turbulence derived from solely analyzing one-point probability distribution functions from molecular clouds with caution. Similar to what has been shown by Dubinski *et al.* (1995) for molecular line profiles, deviations from the regular Gaussian shape found in v - and Δv -PDF's need not be the signpost of

²Note, that Miesch *et al.* (1998) are plotting the function σ^2 versus the spatial lag Δr . For a comparison with the present study, their numbers have to be divided by a factor of two. Furthermore, they use a relatively narrow range of Δr -values to compute the slope of the function; larger intervals would on average tend to decrease these values (see their Figure 14). In addition, Miesch *et al.* (1998) applied spatial filtering to remove large-scale velocity gradients in the clouds. These would lead to steeper slopes. The fact that in the present study the functions σ and κ level out for large spatial lags Δr is a consequence of the periodic boundary conditions which do not allow for large-scale gradients.

turbulent intermittency. Gaussian velocity fields which are dominated by only a small number of modes (either because the power spectrum falls off steeply towards larger wave numbers, or because small wave length distortions are cut away completely) will lead to very similar distortions. In addition, the properties of the PDF may vary considerably between different projections. The same velocity field may lead to smooth and Gaussian PDF's for one velocity component, whereas another projection may result in strong non-Gaussian wings (see also Figure 3.13).

3.2.4 Analysis of Decaying Supersonic Turbulence without Self-Gravity

In this section the PDF's of freely decaying initially highly supersonic turbulence without self-gravity are discussed. They are calculated from an SPH simulation with 350 000 particles (Mac Low *et al.* 1998, model G). Initially the system is homogeneous with a Gaussian velocity distribution with $P(k) = \text{const.}$ in the interval $1 \leq k \leq 8$. The rms Mach number of the flow is $\mathcal{M} = 5$.

After the onset of the hydrodynamic evolution the flow quickly becomes fully turbulent resulting in rapid dissipation of kinetic energy. The energy decay is found to follow a power law $t^{-\eta}$ with exponent $\eta = 1.1 \pm 0.004$. The overall evolution can be subdivided into several phases. The first phase is very short and is defined by the transition of the initially Gaussian velocity field into fully developed supersonic turbulence. It is determined by the formation of the first shocks which begin to interact with each other and build up a complex network of intersecting shock fronts. Energy gets transferred from large to small scales and the turbulent cascade builds up. The second phase is given by the subsequent self-similar evolution of the network of shocks. Even though individual features are transient, the overall properties of this network change only slowly. In this phase of highly supersonic turbulence the loss of kinetic energy is dominated by dissipation in shocked regions. In the transsonic regime, i.e. the transition from highly

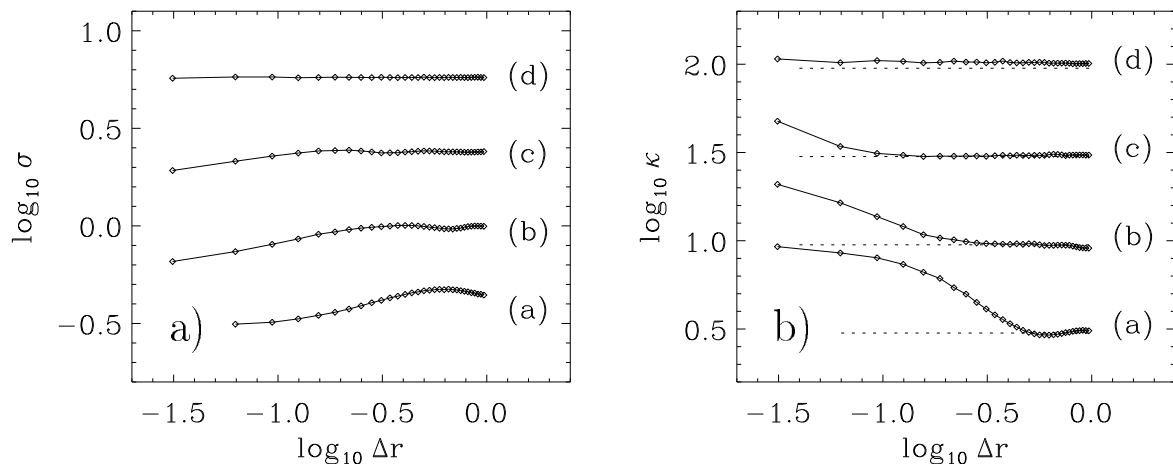


Figure 3.8: (a) The second, dispersion σ , and (b) the fourth moment, kurtosis κ , of the distribution of velocity increments displayed in Figure 3.7 as function of spatial lag Δr . The letters on the right-hand side indicate the corresponding time with (a) $t = 0$, (b) $t = 0.5$, and so forth. Each plot is offset by $\Delta \log_{10} \sigma = 0.5$ and $\Delta \log_{10} \kappa = 0.5$, and in (b) the horizontal dotted line indicates the value for a Gaussian $\kappa = 3$ ($\log_{10} \kappa = 0.48$). (From Klessen 2000)

supersonic to fully subsonic flow, energy dissipation in vortices generated by shock interactions becomes more and more important. Only the strongest shocks remain in this phase. Surprisingly, the energy decay law does not change during this transition. It continues to follow a power law with exponent $\eta \approx 1$. In the subsonic phase the flow closely resembles incompressible turbulence. Its properties are similar to those reported from numerous experiments and simulations (e.g. Porter *et al.* 1994, Lesieur 1997, Boratav *et al.* 1997). The simulation is stopped at $t = 20.0$ when the flow has decayed to a rms Mach number of $\mathcal{M} = 0.3$. Since the energy loss rate follows a power law, the duration of each successive phase grows.

This sequence of evolutionary stages is seen in the PDF's of the system. One noticeable effect is the decreasing width of the distribution functions as time progresses. As the kinetic energy decays the available range of velocities shrinks. This not only leads to 'smaller' v - and Δv -PDF's, but also to a smaller ρ -PDF since compressible motions lose influence and the system becomes more homogeneous. This is indicated in Figure 3.9, it displays (a) the ρ -PDF and (b) v -PDF at the following stages of the dynamical evolution (from top to bottom): Shortly after the start, at $t = 0.2$ when the first shocks occur, then at $t = 0.6$ when the

network of interacting shocks is established and supersonic turbulence is fully developed, during the transonic transition at $t = 3.5$, and finally at $t = 20.0$ when the flow has progressed into the subsonic regime. The rms Mach numbers at these stages are $\mathcal{M} = 5.0$, $\mathcal{M} = 2.5$, $\mathcal{M} = 1.0$, and $\mathcal{M} = 0.3$, respectively. The density PDF always closely follows a log-normal distribution, i.e. it is Gaussian in the *logarithm* of the density. Also the distribution of line centroids at the four different evolutionary stages of the system is best described by a Gaussian with only minor deviations at the far ends of the velocity spectrum.

For the same points in time, Figure 3.10 shows the Δv -PDF's for x -component of the velocity. The displayed spatial lags are selected in analogy to Figure 3.7. Note the different velocity scaling in each plot reflecting the decay of turbulent energy as the system evolves in time. Throughout the entire sequence, spatial lags larger than about 10% of the system size always lead to Δv -PDF's very close to Gaussian shape (the middle and lower curves). Considerable deviations occur only at small spatial lags (the upper curves). For those, the increment PDF's exhibit exponential wings during all stages of the evolution. When scaling the PDF's to the same width, the distribution in the subsonic regime (d) appears to be more strongly peaked than during the supersonic or

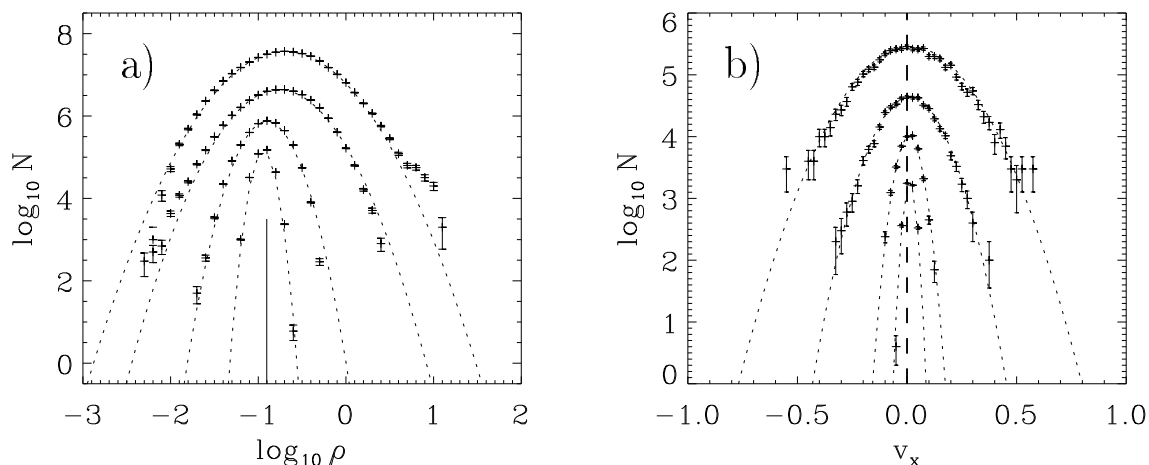


Figure 3.9: PDF's of (a) density and of (b) centroid velocities for the line-of-sight being parallel to the x -axis of the system. The PDF's are obtained at four different phases of the dynamical evolution of the system (see the main text), at $t = 0.2$ (upper curves), at $t = 0.6$ (second curve from the top), at $t = 3.5$ (third curve), and at $t = 20.0$ (lowest curve). These times correspond to Mach numbers $\mathcal{M} = 5.0$, $\mathcal{M} = 2.5$, $\mathcal{M} = 1.0$, and $\mathcal{M} = 0.3$, respectively. For each distribution, the best-fit Gaussian is indicated using dotted lines. (From Klessen 2000)

transsonic phase (a – c). There, the central parts of the PDF's are still reasonably well described by the Gaussian obtained from the first two moments, whereas in (d) the peak is considerably narrower, or vice versa, the tails of the distribution are more pronounced.

These results can be compared with the findings by Lis *et al.* (1998). They report increment PDF's for three snapshots of a high-resolution hydrodynamic simulation of decaying mildly super-sonic turbulence performed by Porter *et al.* (1994). They analyze the system at three different times corresponding to rms Mach numbers of $\mathcal{M} \approx 0.96$, $\mathcal{M} \approx 0.88$, and $\mathcal{M} \approx 0.52$. Their first two data sets thus trace the transition from supersonic to subsonic flow and are comparable to phase (c) of the current model; their last data set corresponds to phase (d). In the transsonic regime both studies agree: Lis *et al.* (1998) report enhanced tails in the increment PDF's for the smallest spatial lags which they considered and near Gaussian distributions for larger lags (however, the largest separation they study is about 6% of the linear extent of the system). In the subsonic regime, Lis *et al.* (1998) find near Gaussian PDF's for very small spatial lags ($< 1\%$), but extended wings in the PDF's for lags of 3% and 6% of the system size. They associate this with the 'disappearance' of large-scale structure. Indeed, their

Figure 7 exhibits a high degree of fluctuations on small scales which they argue become averaged away when considering small spatial lags in the Δv -PDF. Comparing the PDF with spatial lags of 3% (upper curves in Figure 3.10, compared to the PDF's labeled with $\Delta = 15$ in Lis *et al.* 1998) both studies come to the same result. At these scales the Δv -PDF's tend to exhibit more pronounced wings in the subsonic regime as in the supersonic regime. The SPH calculations reported here do not allow for a meaningful construction of δv -PDF's for $\Delta r < 3\%$. The Gaussian behavior of PDF's for very small spatial lags reported by Lis *et al.* (1998) therefore cannot be examined. However, neither of the purely hydrodynamic simulations lead to PDF's that are in good agreement with the observations. Observed PDF's typically are much more centrally peaked at small spatial separation (see e.g. Figure 4 in Lis *et al.* 1998 and Miesch *et al.* 1998).

Figure 3.11 shows the spatial distribution of centroid velocity differences between cells separated by a vector lag of $\Delta \vec{r} = (1/32, 1/32)$ (i.e. between neighboring cells along the diagonal). Data are obtained at the same times as above. Each figure displays the array of the absolute values of the velocity increments Δv_x in linear scaling as indicated at the top. Note the decreasing velocity range reflecting the decay of turbulent energy.

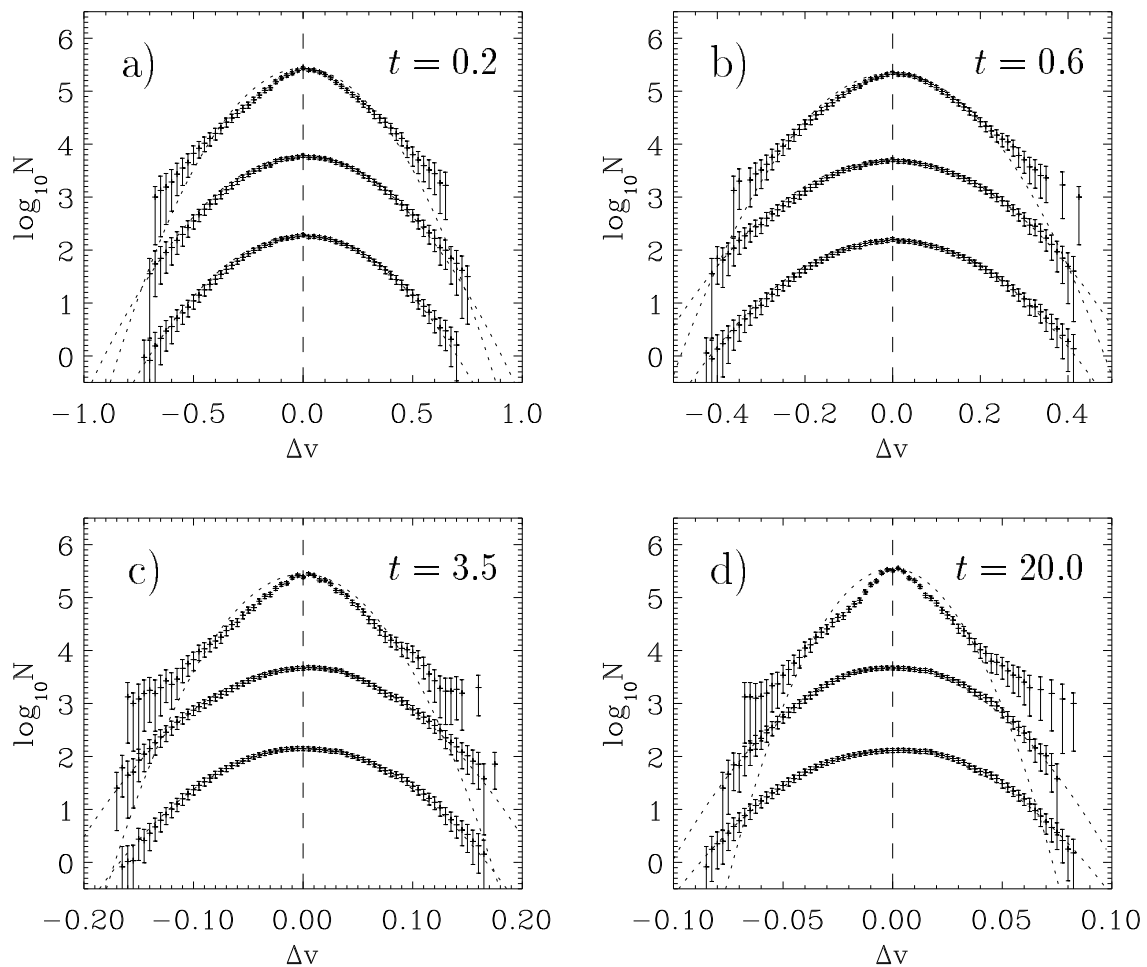


Figure 3.10: PDF's of the x -component of the centroid velocity increments for three spatial lags: upper curve $-\Delta r = 1/32$, middle curve $-\Delta r = 10/32$, and lower curve $-\Delta r = 30/32$. As in Figure 3.9, the PDF's are obtained at (a) $t = 0.2$, (b) $t = 0.6$, (c) $t = 3.5$, and (d) $t = 20.0$. The Gaussian fits are again indicated by dotted lines. (From Klessen 2000)

The distribution of Δv_x appears random, there is no clear indication for coherent structures. This corresponds to most observations. Miesch *et al.* (1998) find for their sample of molecular clouds that high-amplitude velocity differences for very small spatial lags typically are well distributed resulting in a 'spotty' appearance. Note, however, that using azimuthal averaging Lis *et al.* 1998 report the finding of filamentary structures for the ρ -Ophiuchus cloud. Altogether, filamentary structure is difficult to define and a mathematical thorough analysis is seldomly performed (for an astrophysical approach see Adams & Wise-man 1994, for a discussion of the filamentary vortex structure in incompressible turbulence consult Frisch 1995 or Lesieur 1997). The visual inspection of maps is often misleading and influenced by the parameters used to display the im-

age. Larger velocity bins for instance tend to produce a more 'filamentary' structure than very fine sampling of the velocity structure. Further uncertainty may be introduced by the fact that molecular clouds are only seen in one projection as the signatures of the dynamical state of the system can strongly depend on the viewing angle.

3.2.5 Analysis of Decaying Turbulence with Self-Gravity

In this section, we concentrate on the properties of decaying, initially supersonic turbulence in a self-gravitating medium. We analyze an SPH simulation with 205379 particles which is initially homogeneous and its velocity field is generated with $P(k) = \text{const.}$ using modes with wave numbers $1 \leq k \leq 8$. From the choice

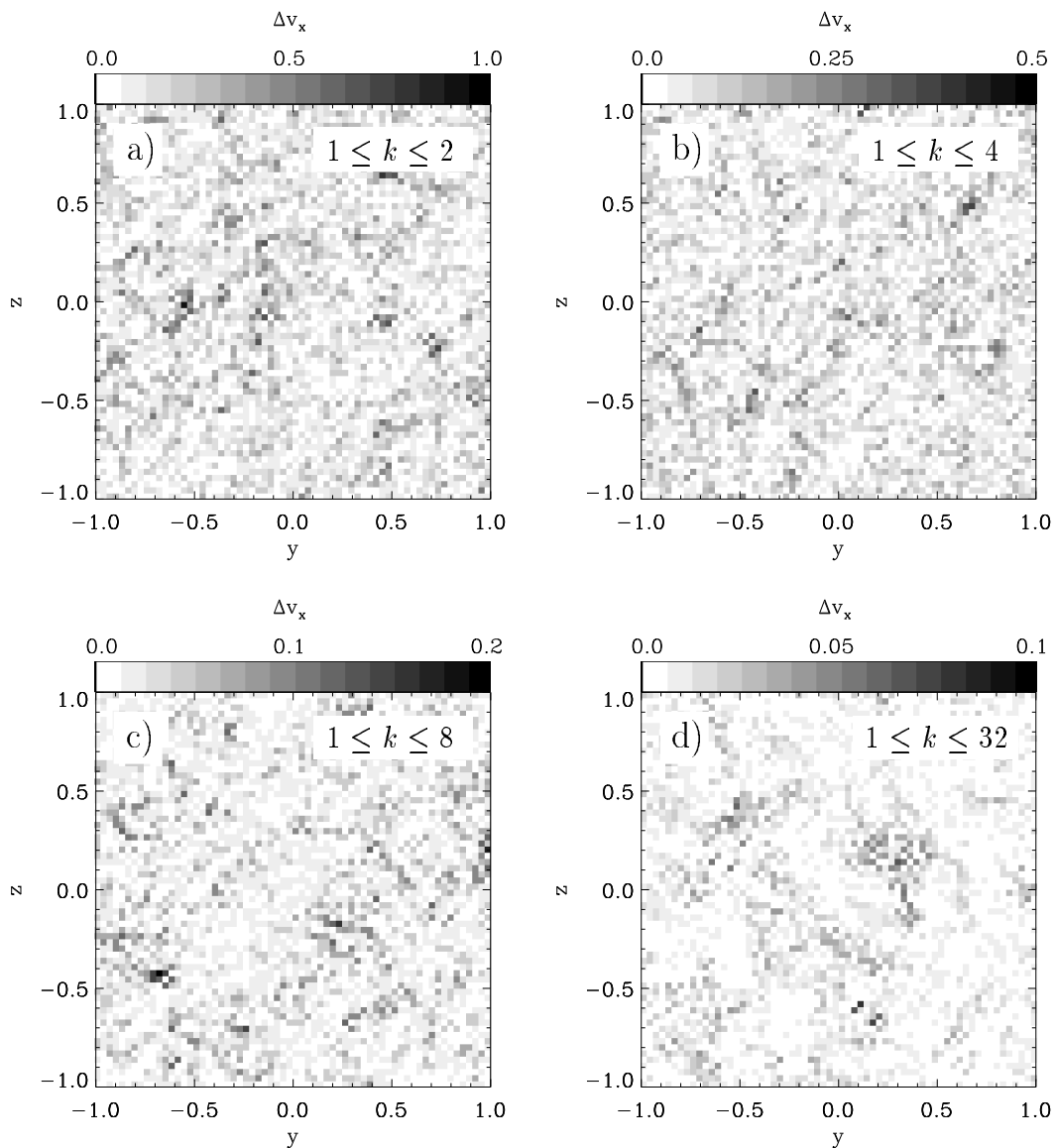


Figure 3.11: 2-dimensional distribution (in the yz -plane) of centroid increments for velocity profiles along the x -axis of the system between locations separated by a vector lag $\Delta\vec{r} = (1/32, 1/32)$. Analog to the previous figures, the data are displayed for times (a) $t = 0.2$, (b) $t = 0.6$, (c) $t = 3.5$, and (d) $t = 20.0$. The magnitude of the velocity increment Δv_x is indicated at the top of each plot; note the different scaling. (From Klessen 2000)

$\alpha = 0.01$ it follows that the system contains 120 *thermal* Jeans masses. The initial rms velocity dispersion is $\sigma_v = 0.5$ and with the sound speed $c_s = 0.082$ the rms Mach number follows as $\mathcal{M} = 6$. These values imply that the initial turbulent velocity field contains sufficient energy to globally *stabilize* the system against gravitational collapse. Scaled to physical units using a density $n(\text{H}_2) = 10^5 \text{ cm}^{-3}$, which is typical for massively star-forming regions (e.g. Williams *et al.* 2000), the system corresponds to a volume of $[0.32 \text{ pc}]^3$ and contains a gas mass of $200 M_\odot$. As

the simulation starts, the system quickly becomes fully turbulent and loses kinetic energy. Like in the case without self-gravity a network of intersecting shocks develops leading to density fluctuations on all scales. During the early evolution, there is enough kinetic energy to prevent global collapse and the properties of the system are similar to those of pure hydrodynamic turbulence discussed in the previous section. However, as time progresses and turbulent energy decays the effective Jeans mass decreases, and after sufficient time also large-scale collapse becomes pos-

sible. Gas clumps follow the global flow pattern towards a common center of gravity where they may merge or sub-fragment. Gradually a cluster of dense cores is built up. In the isothermal model this process continues until all available gas is accreted onto the ‘protostellar’ cluster (see the discussion in Section 2).

The PDF’s of (a) the density and of (b) the x -component of the line centroid velocities for the above six model snapshots are displayed in Figure 3.12. The corresponding time is indicated by the letters at the right side of each panel. During the dynamical evolution of the system the density distribution develops a high density tail. This is the imprint of local collapse. The densities of compact cores are indicated by solid dots (at $t = 2.0$ and $t = 2.5$). Virtually all particles in the high density tails at earlier times (at $t = 1.0$ and more so at $t = 1.5$) are accreted onto these cores. The bulk of matter roughly follows a log-normal density distribution as indicated by the dotted parabola. The v -PDF’s are nearly Gaussian as long as the dynamical state of the system is dominated by turbulence. Also the width of the PDF remains roughly constant during this phase. This implies that the decay of turbulent kinetic energy is in balance with the gain of kinetic energy due to gravitational (‘quasi-static’) contraction on large scales. The time scale for this process is determined by the energy dissipation in shocks and turbulent eddies. However, once *localized* collapse is able to set in, accelerations on small scales increase dramatically and the evolution ‘speeds up’. For times $t > 2.0$ the centroid PDF’s become wider and exhibit significant deviations from the original Gaussian shape. The properties of the PDF’s are similar to those observed in star-forming regions (Miesch & Scalo 1995, Lis *et al.* 1998, Miesch *et al.* 1998). This is expected since gravitational collapse is a necessary ingredient for forming stars.

Gravity creates *non*-isotropic density and velocity structure structures. When analyzing v - and Δv -PDF’s, their appearance and properties will strongly depend on the viewing angle. This is a serious point of caution when interpreting observational data, as molecular cloud are seen only in

one projection. As illustration, Figure 3.13 plots the centroid PDF at the time $t = 2.0$ for the line-of-sight projection along all three axes of the system. Whereas the PDF’s for the x - and the y -component of the velocity centroid are highly structured (upper and middle curve – the latter one is even double peaked), the distribution of the z -component (lowest curve) is smooth and much smaller in width, comparable to the ‘average’ PDF at *earlier* stages of the evolution. As the variations between different viewing angles or equivalently different velocity components can be very large, statements about the 3-dimensional velocity structure from only observing one projection can be misleading.

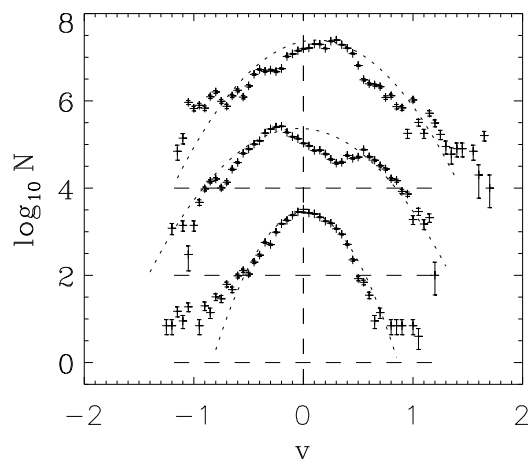


Figure 3.13: Centroid velocity PDF’s for the simulation of initially supersonic, decaying turbulence in self-gravitating gas at $t = 2.0$ for the line-of-sight being along the x -axis (upper curve – it is identical to the fifth PDF in Figure 3.12b), along the y -axis (middle), and along the z -axis of the system (bottom). Each distribution is offset by $\Delta \log_{10} N = 2.0$ with the horizontal lines indicating the base $\log_{10} N = 0.0$. The PDF’s of various projections and velocity components can differ considerably. (From Klessen 2000)

Gravity effects the Δv -PDF. Figure 3.14 displays the increment PDF’s at small, intermediate and large spatial lags, analog to Figures 3.7 and 3.10. Time ranges from (a) $t = 1.0$ to (d) $t = 2.5$. The PDF’s for $t = 0.0$ and $t = 0.5$ are not shown since at these stages supersonic turbulence dominates the dynamic of the system and the PDF’s are comparable to the ones without gravity (Figure 3.10). This still holds for $t = 1.0$. The increment PDF’s for medium to large spatial lags appear Gaussian,

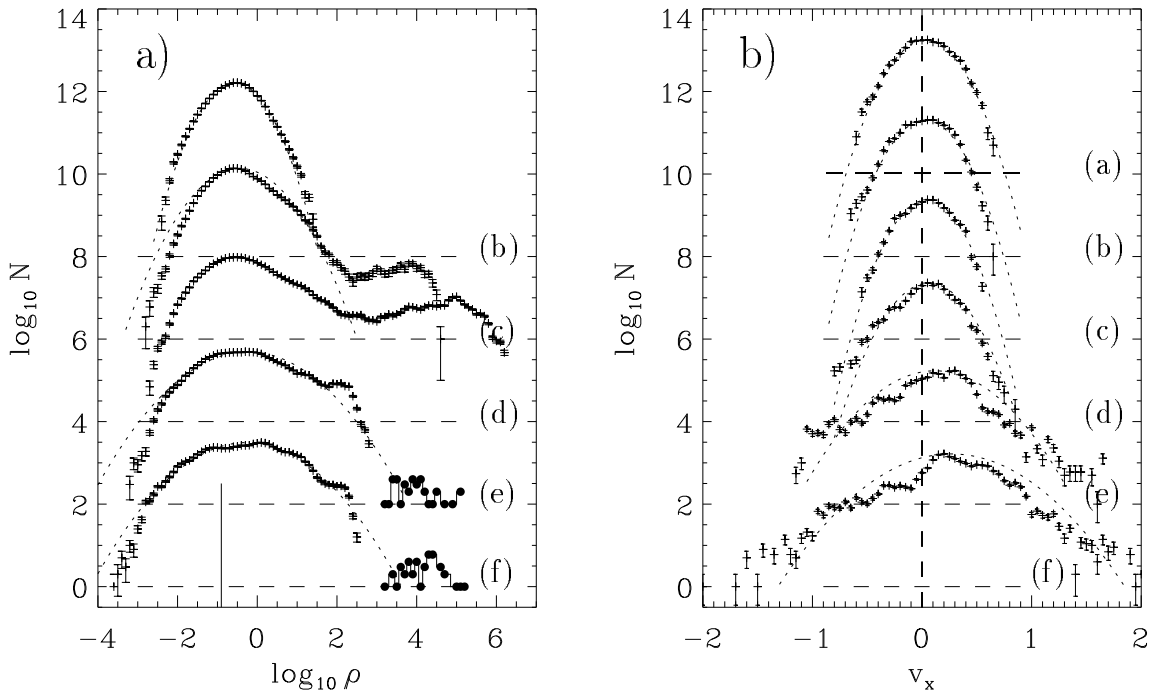


Figure 3.12: PDF's of (a) the density and (b) the x -component of line centroids for the simulation of initially supersonic, decaying turbulence in self-gravitating gas. The time sequence again is (a) $t = 0.0$, (b) $t = 0.5$, and so forth. In the left panel, the initial density is indicated by the vertical line at $\rho = 1/8$. The density contributions from collapsed cores forming in the late stages of the evolution are indicated by solid dots. The core density corresponds to a mean value computed from the core mass divided by its accretion volume. In both figures, each PDF is offset by $\Delta \log_{10} N = 2.0$ with the base $\log_{10} N = 0.0$ indicated by horizontal dashed lines. The best-fit Gaussian curves are shown as dotted lines. (From Klessen 2000)

however, the PDF for the smallest lag follows a perfect exponential all the way inwards to $\Delta v = 0$. Unlike in the case without gravity, the peak of the distribution is not 'round', i.e. is not Gaussian in the innermost parts (when scaled to the same width). *It is a sign of self-gravitating systems that the increment PDF at smallest lags is very strongly peaked and remains exponential over the entire range of measured velocity increments.* This behavior is also seen Figures 3.14b–d. At these later stages of the evolution in addition non-Gaussian behavior is also found at medium lags. This results from the existence of large-scale filaments and streaming motions. The same behavior is found for the increment PDF's from observed molecular clouds (for ρ -Ophiuchus see Lis et al 1998; for Orion, Mon R2, L1228, L1551, and HH83 see Miesch et al. 1998). In each case, the distribution for the smallest lag (one pixel size) is very strongly peaked at $\Delta v = 0$, in some cases even more than exponential. The deviations from the Gaussian shape re-

main for larger lags but are not so pronounced. The inclusion of self-gravity into models of interstellar turbulence leads to good agreement with the observed increment PDF's. However, this result may *not* be unique as in molecular clouds additional processes are likely to be present that could also lead to strong deviations from Gaussianity.

The time evolution of the statistical moments of the Δv -PDF for various spatial lags is presented in Figure 3.15. It plots (a) the dispersion σ , and (b) the kurtosis κ . At $t = 0.0$ the width σ of the PDF is approximately constant for all Δr and the kurtosis κ is close to normal value of three. Both indicate that Gaussian statistics very well describes the initial velocity field. As turbulent energy decays, gravitational collapse sets in. Because of the gravitational acceleration, the amplitudes of centroid velocity differences between separate regions in the cloud grow larger, the width σ of the Δv -PDF's increases. This becomes more im-

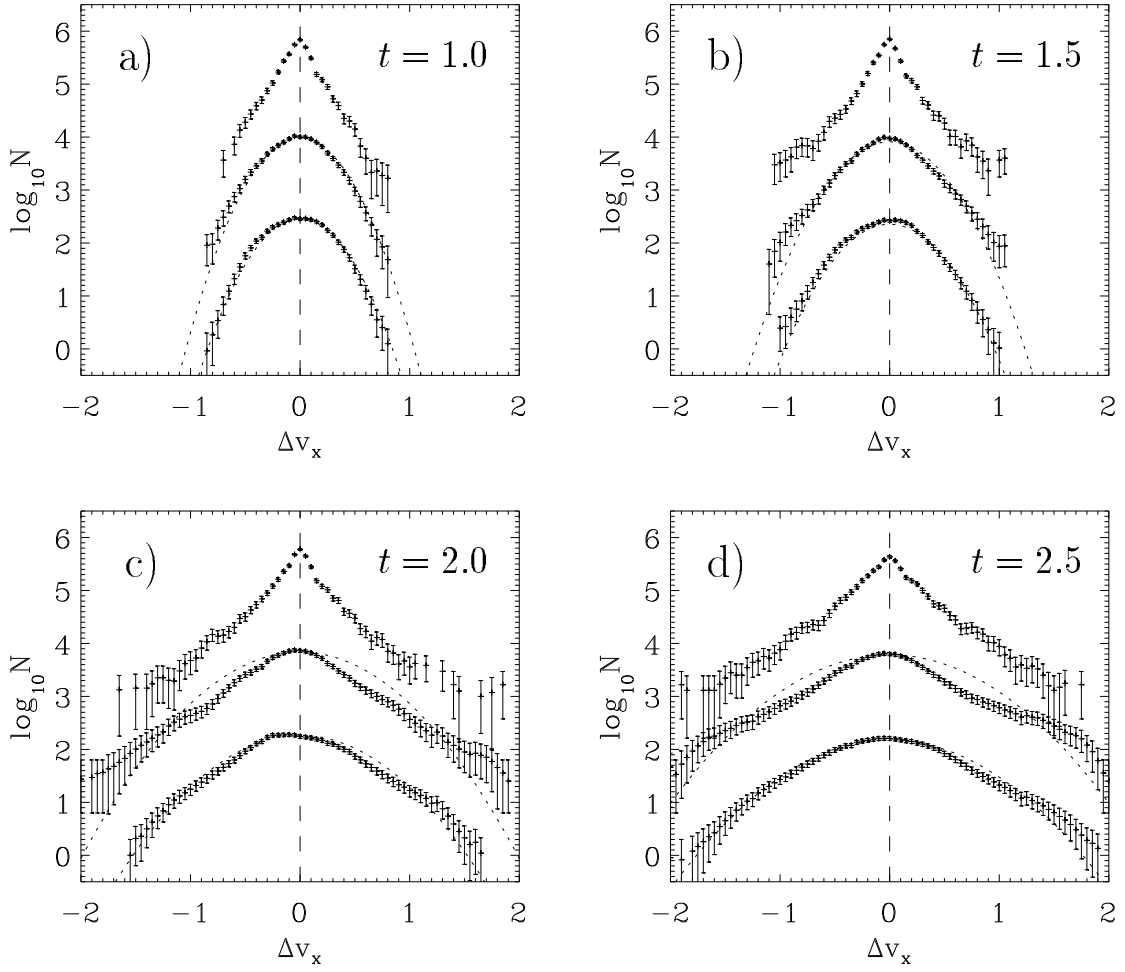


Figure 3.14: PDF's of the x -component of the centroid velocity increments for three spatial lags: upper curve $-\Delta r = 1/32$, middle curve $-\Delta r = 10/32$, and lower curve $-\Delta r = 30/32$. The functions are computed from the simulation of initially supersonic, decaying turbulence in self-gravitating gas at (a) $t = 1.0$, (b) $t = 1.5$, (c) $t = 2.0$, and (d) $t = 2.5$. Where appropriate, the Gaussian curves obtained from the first two moments of the distribution are indicated by dotted lines. During the early phases of the evolution, the flow is similar to pure hydrodynamic turbulence (the PDF's are close to the ones in Figure 3.10). As turbulent energy decays self-gravity gains influence and the late stages of the evolution are dominated by gravitational contraction. Consequently the PDF's in the sequence (a) to (d) become more and more non-Gaussian with the progression of time. This concerns the PDF's for small to intermediate lags Δr . (From Klessen 2000)

portant when sampling velocity differences on larger spatial scales, hence σ also increases with Δr . The slope is $d \log_{10} \sigma / d \log_{10} \Delta r \lesssim 0.2$. For $\log_{10} \Delta r > -0.4$ it levels out, which is a result of the adopted periodic boundary conditions. They do not allow for large-scale velocity gradients. The increasing 'peakedness' of Δv -PDF is reflected in the large values of the kurtosis κ at the later stages of the evolution. For small spatial lags the PDF's are more centrally concentrated than exponential (i.e. $\kappa > 6$), and even at large spatial separations they are still more strongly peaked than Gaussian ($\kappa > 3$). The slope at

$t = 2.5$ is $d \log_{10} \kappa / d \log_{10} \Delta r \approx -0.4$ which is indeed comparable to what is found in observed star-forming regions (Miesch *et al.* 1998).

For the above simulation of self-gravitating, decaying, supersonic turbulence, Figure 3.16 plots the 2-dimensional distribution of centroid increments for a vector lag $\Delta \vec{r} = (1/32, 1/32)$. The velocity profiles are sampled along the x -axis of the system. The magnitude of the velocity increment Δv_x is indicated at the top of each plot. The spatial distribution of velocity increments during the initial phases appears random. Later on, gravity gains influence over the flow and creates

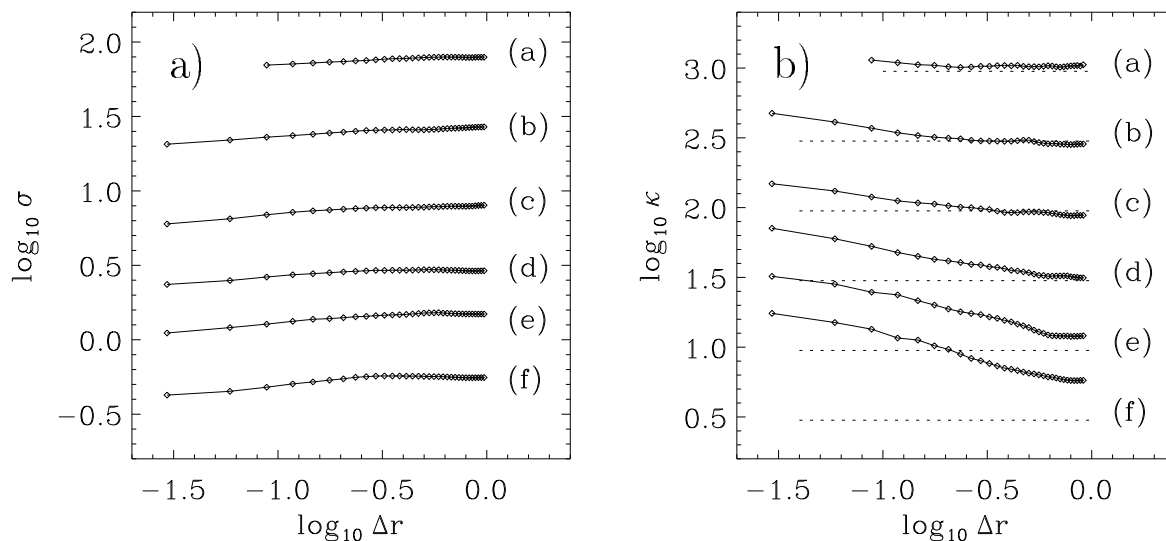


Figure 3.15: (a) The second, dispersion σ , and (b) the fourth moment, kurtosis κ , as function of spatial lag Δr for the distribution of velocity increments in the simulation of self-gravitating, decaying, supersonic turbulence. The letters on the right-hand side indicate the time at which the increment PDF's are computed ranging from $t = 0.0$ at the top down to $t = 2.5$ at the bottom (see Figure 3.12). Each PDF is offset by $\Delta \log_{10} \sigma = 0.5$ and $\Delta \log_{10} \kappa = 0.5$, respectively. (From Klessen 2000)

a network of intersecting filaments where gas streams onto and flows along towards local potential minima. At that stage, the velocity increments with the highest amplitudes tend to trace the large-scale filamentary structure. This is the sign of the anisotropic nature of gravitational collapse motions.

3.2.6 Analysis of Driven Turbulence with Self-Gravity

For the analysis of continuously driven turbulence in self-gravitating gaseous media, we take model $2Bh$ discussed in Section 2.5 (Table 2.3; for full details consult Klessen *et al.* 2000).

The PDF's of (a) the density and (b) the x -component of the line centroid velocities corresponding to the above four snapshots are displayed in Figure 3.17. As in the previous model, the bulk of gas particles that are not accreted onto cores build up an approximately log-normal ρ -PDF (indicated by the dotted lines). Also the v -PDF remains close to the Gaussian value. This is different from the case of purely decaying self-gravitating turbulence, where at some stage global collapse motions set in and lead to very

wide and distorted centroid PDF's. This is not possible in the simulation of driven turbulence, as it is stabilized on the largest scales by turbulence. Collapse occurs only locally which leaves the width of the PDF's relatively unaffected and only mildly alters their shape.

Also the Δv -PDF's show no obvious sign of evolution. For the x -component of the velocity these functions are displayed in Figure 3.18, again for three different spatial lags. The chosen times correspond (a) to the equilibrium state at $t = 0.0$, and (b) to $t = 4.8$ which is the final state of the simulation. The PDF's only marginally grow in width. At every evolutionary stage, the PDF for the smallest spatial lag is exponential, whereas the PDF's for medium and large shift vectors closely follow the Gaussian curve defined by the first two moments of the distribution (dotted lines). The functions are similar to the ones in the previous model before the large scale collapse motions set in (Figure 3.14a, b). Only overall contraction will affect Δv -PDF at medium to large lags. This behavior also follows from comparing the statistical moments. Figure 3.19 plots (a) the dispersion σ and (b) the kurtosis κ as function of the spatial lag Δr . Figures 3.15a and

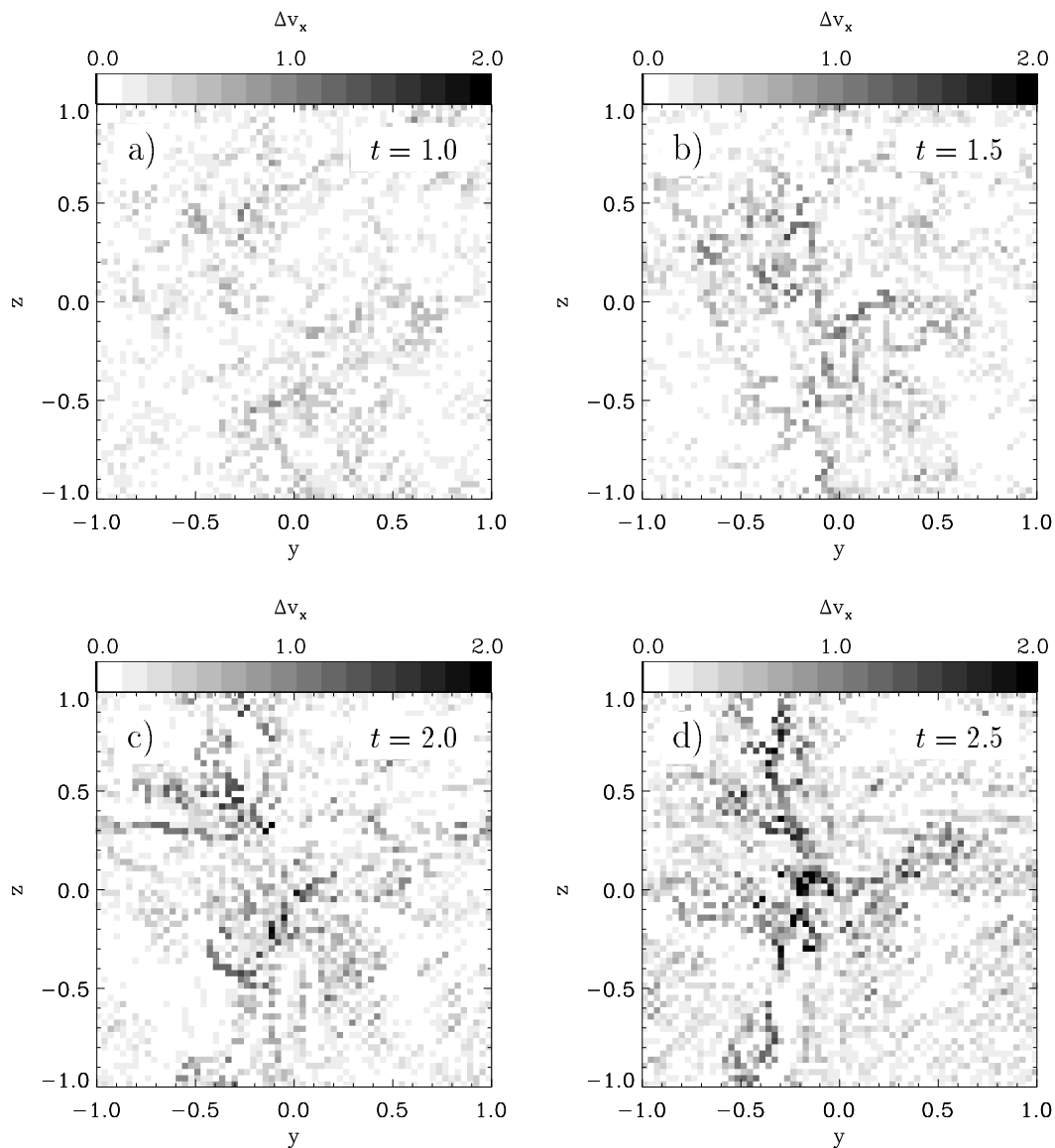


Figure 3.16: 2-dimensional distribution (in the yz -plane) of centroid increments for velocity profiles along the x -axis of the system between locations separated by a vector lag $\Delta\vec{r} = (1/32, 1/32)$ for the simulation of self-gravitating, decaying, supersonic turbulence. Analog to Figure 3.14, the data are displayed for times (a) $t = 1.0$, (b) $t = 1.5$, (c) $t = 2.0$, and (d) $t = 2.5$. The magnitude of the velocity increment Δv_x is indicated at the top of each plot. (From Klessen 2000)

3.19a are very similar, as soon as turbulence is established the width σ of the PDF increases with Δr with a slope of $d \log_{10} \sigma / d \log_{10} \Delta r \lesssim 0.2$ for small to medium lags and levels out for larger ones. However, when comparing the ‘peakedness’ of the PDF as indicated by κ (Figures 3.15b and 3.19b) the model of decaying self-gravitating turbulence yields much higher values since the PDF’s are more strongly peaked due to the presence of large-scale collapse motions.

Figure 3.20 finally shows the spatial distribu-

tion of the x -component of the line centroid increments for a vector lag $\Delta\vec{r} = (1/32, 1/31)$. Since the increment maps at different evolutionary times are statistically indistinguishable, only times (a) $t = 0.0$ and (b) $t = 4.8$ are displayed in the figure. As in the case of supersonic, purely hydrodynamic turbulence the spatial distribution of velocity increments appears random and uncorrelated.

The adopted driving mechanism prevents global collapse. The bulk properties of the sys-

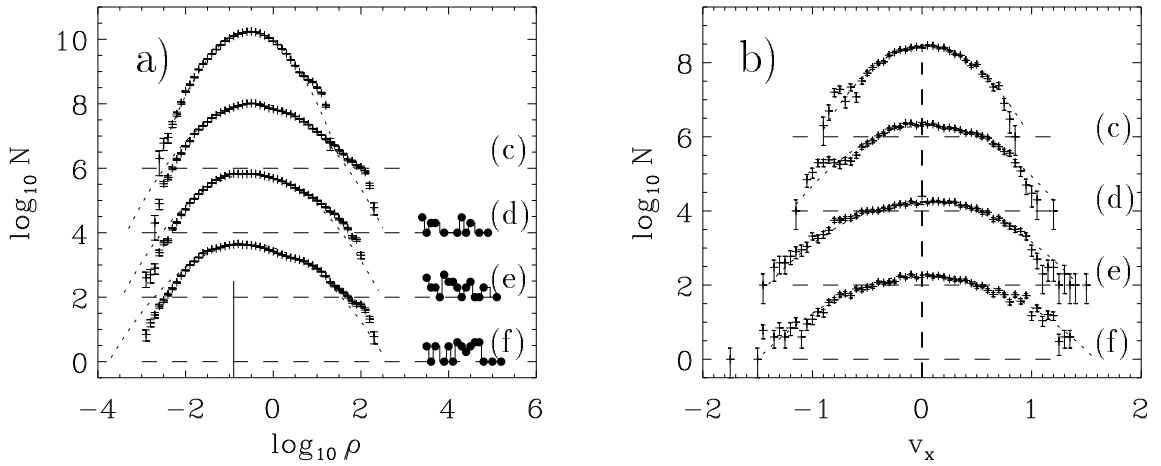


Figure 3.17: PDF's of (a) the density and (b) the x -component of line centroids for the simulation of driven turbulence in self-gravitating gas. The time sequence is the same as in the previous figures as indicated by the letters to the right. Each PDF is offset by $\Delta \log_{10} N = 2.0$ with the base $\log_{10} N = 0.0$ indicated by horizontal dashed lines. The best-fit Gaussian curves are shown as dotted lines. The density contributions in (a) coming from collapsed cores are indicated by solid dots. (From Klessen 2000)

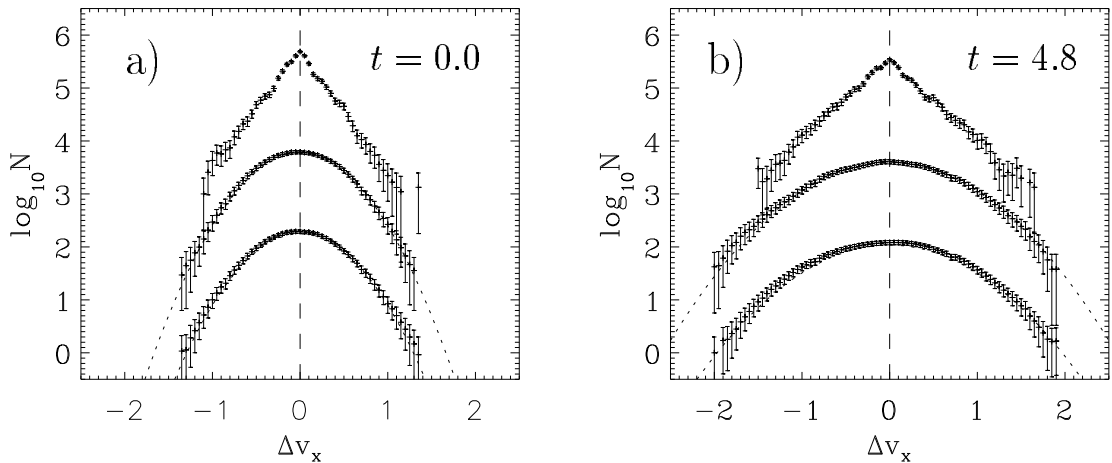


Figure 3.18: PDF's of the x -component of the centroid velocity increments for three spatial lags: upper curve $-\Delta r = 1/32$, middle curve $-\Delta r = 10/32$, and lower curve $-\Delta r = 30/32$. The functions are computed from the simulation of driven, self-gravitating, supersonic turbulence at (a) $t = 0.0$ and (b) $t = 4.8$. As in the previous models the increment PDF's for small spatial lags are approximately exponential, however, the PDF's for larger separations remain close to Gaussian throughout the evolution. (From Klessen 2000)

tem therefore resemble hydrodynamic, *non*-self-gravitating turbulence. However, local collapse motions do exist and are responsible for noticeable distortions away from the Gaussian statistics. As the non-local driving scheme adopted here introduces a bias towards Gaussian velocity fields, these distortions are not very large. There is a need to introduce other, more realistic driving agents into this analysis. These could lead to much stronger non-Gaussian signatures in the

PDF's.

3.2.7 Summary

Klessen (2000) analyzed SPH simulations of driven and decaying, supersonic, turbulent flows with and without self-gravity, thus extending previous investigations of mildly supersonic, decaying, *non*-self-gravitating turbulence (Lis *et al.* 1996, 1998) into a regime more relevant molec-

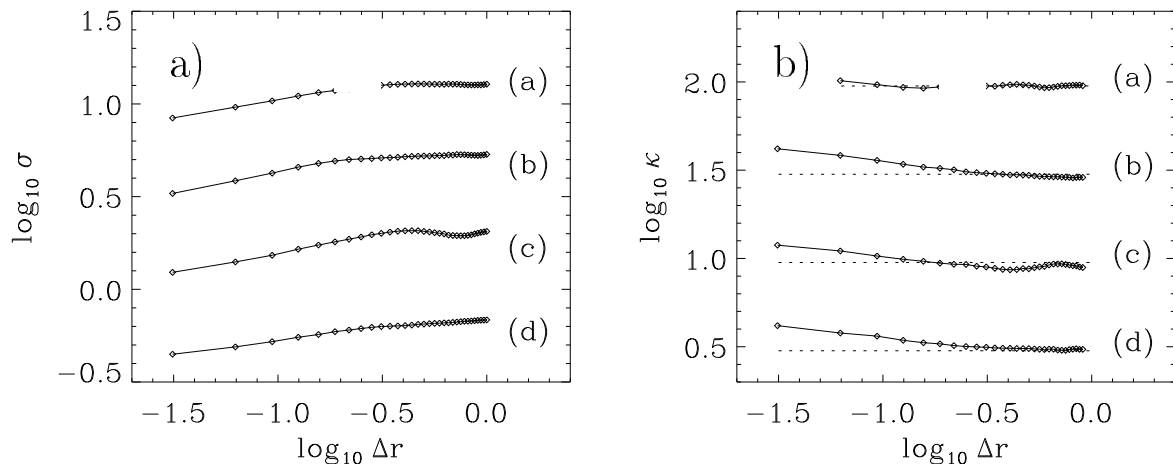


Figure 3.19: (a) The second, dispersion σ , and (b) the fourth moment, kurtosis κ , as function of spatial lag Δr for the distribution of velocity increments in the simulation of driven, self-gravitating, supersonic turbulence. The letters on the right-hand side indicate again the corresponding times. Each PDF is offset by $\Delta \log_{10} \sigma = 0.5$ and $\Delta \log_{10} \kappa = 0.5$, respectively. (From Klessen 2000)

ular clouds. The flow properties are characterized by using the probability distribution functions of the density, of the line-of-sight velocity centroids, and of their increments. Furthermore the dispersion and the kurtosis of the increment PDF's are discussed, as well as the spatial distribution of the velocity increments for the smallest spatial lags.

(1) To assess the influence of variance effects, simple Gaussian velocity fluctuations are studied. The insufficient sampling of random Gaussian ensembles leads to distorted PDF's similar to the observed ones. For line profiles this has been shown by Dubinski *et al.* (1995).

(2) Decaying, initially highly supersonic turbulence without self-gravity leads to PDF's which also exhibit deviations from Gaussianity. For the trans- and subsonic regime this has been reported by Lis *et al.* (1996, 1998). However, neglecting gravity and thus not allowing for the occurrence of collapse motions, these distortions are not very pronounced and cannot account well for the observational data (Lis *et al.* 1998, Miesch *et al.* 1998).

(3) When including gravity into the models of decaying initially supersonic turbulence, the PDF's get into better agreement with the observations. During the early dynamical evolution of the system turbulence carries enough kinetic energy to

prevent collapse on all scales. In this phase the properties of the system are similar to those of non-gravitating hydrodynamic supersonic turbulence. However, as turbulent energy decays gravitational collapse sets in. First localized and on small scales, but as the turbulent support continues to diminish collapse motions include increasingly larger spatial scales. The evolution leads to the formation of an embedded cluster of dense protostellar cores (see also Klessen & Burkert 2000). As the collapse scale grows, the ρ -, v -, and Δv -PDF's get increasingly distorted. In particular, the Δv -PDF's for small spatial lags are strongly peaked and exponential over the entire range of measured velocities. This is very similar to what is observed in molecular clouds (for ρ -Ophiuchus see Lis *et al.* 1998; for Orion, Mon R2, L1228, L1551, and HH83 see Miesch *et al.* 1998).

(4) The most realistic model for interstellar turbulence considered here includes a simple (non-local) driving scheme. It is used to stabilize the system against collapse on large scales. Again non-Gaussian PDF's are observed. Despite global stability, local collapse is possible and the system again evolves towards the formation of an embedded cluster of accreting protostellar cores. As the adopted driving scheme introduces a bias towards maintaining a Gaussian velocity distribu-

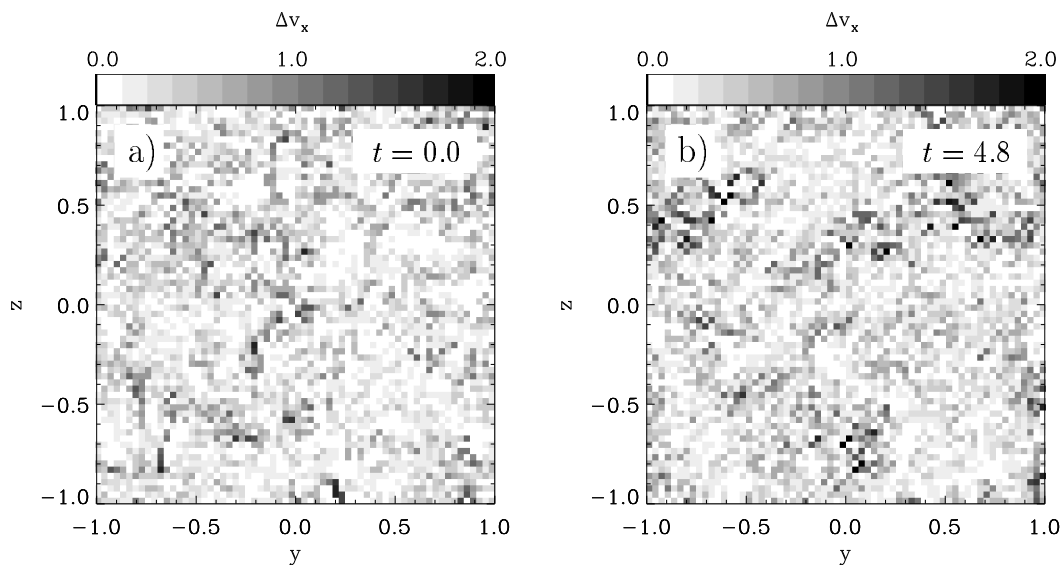


Figure 3.20: 2-dimensional distribution (in the yz -plane) of the absolute value of the x -component of centroid velocity increments between locations separated by a vector lag $\Delta\vec{r} = (1/32, 1/32)$ for the simulation of driven self-gravitating supersonic turbulence. The data are displayed at times (a) $t = 0.0$, and (b) $t = 4.8$. The scaling is indicated at the top of each figure. (From Klessen 2000)

tion, the properties of the PDF's fall in between the ones of pure hydrodynamic supersonic turbulence and the ones observed in systems where self-gravity dominates after sufficient turbulent decay. This situation may change when considering more realistic driving schemes.

(5) A point of caution: The use of v - and Δv -PDF's to unambiguously characterize interstellar turbulence and to identify possible physical driving mechanisms may be limited. *All* models considered in the current analysis lead to non-Gaussian signatures in the PDF's, differences are only gradual. In molecular clouds the number of physical processes that are expected to give rise to deviations from Gaussian statistics is large. Simple statistical sampling effects (Sec. 3.2.3) and turbulent intermittency caused by vortex motion (Lis *et al.* 1996, 1998), as well as the effect self-gravity (Sec. 3.2.5) and of shock interaction in highly supersonic flows (Mac Low & Ossenkopf 2000), *all* will lead to non-Gaussian signatures in the observed PDF's. Also stellar feedback processes, galactic shear and the presence of magnetic fields will influence the interstellar medium and create distortions in the velocity field. This needs to be studied in further detail. In addition,

the full 3-dimensional spatial and kinematical information is not accessible in molecular clouds, measured quantities are always projections along the line-of-sight. As the structure of molecular clouds is extremely complex, the properties of the PDF's may vary considerably with the viewing angle. Attempts to disentangle the different physical processes influencing interstellar turbulence therefore should not rely on analyzing velocity PDF's alone, they require additional statistical information.

3.3 Fourier Analysis

In this section we discuss the energy distribution on different spatial scales during various stages of the dynamical evolution of supersonically turbulent self-gravitating gaseous systems. We perform a Fourier analysis of the energy, computing the power spectra of kinetic and potential energies from the numerical models introduced in Section 2.5 (Table 2.3; for full details see Klessen *et al.* 2000). To allow for a direct comparison, all models are analyzed on a Cartesian grid with 128^3 cells. For the SPH models this is done using

the kernel smoothing algorithm, while the 256³-ZEUS models are simply degraded in resolution. For each cell the potential and kinetic energy content is calculated, and the kinetic energy is further decomposed into its solenoidal (rotational) and compressional parts. These quantities are then all transformed into Fourier space, to find the contribution of different dimensionless wave numbers k , or equivalently, to find the distribution of energy over different spatial scales $\lambda_k = L/k$.

3.3.1 Fourier Spectra as Function of Driving Wavelength

The energy spectrum of fully developed turbulence for small-, medium- and large-scale driving is shown in figure 3.21. It shows the SPH models (a) $\mathcal{A}1$, (b) $\mathcal{A}2$ and (c) $\mathcal{A}3$ just at the time $t = 0.0$ when gravity is turned on. In each plot the thick solid lines describe the potential energy as a function of wave number k , and the thick long-dashed lines represent the kinetic energy, which can be decomposed into its solenoidal (rotational) and compressional components. They are defined via the velocities by $\vec{\nabla} \cdot \vec{v}_{\text{sol}} = 0$ and $\vec{\nabla} \times \vec{v}_{\text{com}} = 0$, respectively.

The models $\mathcal{A}1$ and $\mathcal{A}2$, which are driven at long and intermediate wave lengths ($k = 1 - 2$ and $k = 3 - 4$), appear to exhibit an inertial range below the driving scale, i.e. between $0.5 \lesssim \log_{10} k \lesssim 1.5$. Note that, in real clouds, the dissipation scale may lie near the upper end of this wave number range as discussed in Section 4.1. In this interval the energy distribution approximately follows a power law very similar to that predicted by the Kolmogorov (1941) theory ($E_{\text{kin}} \propto k^{-5/3}$). This is understandable given that, in our models, once turbulence is fully established, the solenoidal component of the kinetic energy always dominates over the compressible one, $E_{\text{sol}} > E_{\text{com}}$. For a pure shock dominated flow ($E_{\text{com}} \gg E_{\text{sol}}$) one would expect a power spectrum with slope -2 (Passot *et al.* 1988). To guide the eye, both slopes are indicated as thin dotted lines in plots (a) to (c). For model $\mathcal{A}3$ the smaller number of available modes between the driving scale $k = 7 - 8$ and the Nyquist

frequency does not allow for an unambiguous identification of a turbulent inertial range. The permanent energy input necessary to sustain an equilibrium state of turbulence produces a signature in the energy distribution at the driving wave length. This is most clearly visible in figure 3.21c.

The system is globally stable against gravitational collapse, as indicated by the fact that for every wave number k the kinetic energy exceeds the potential energy. For comparison we plot in figure 3.21d the energy distribution of a system without turbulent support. The data are taken from Klessen *et al.* (1998) and stem from an SPH simulation with 500 000 particles containing 220 thermal Jeans masses and no turbulent velocity field, but otherwise identical physical parameters. The snapshot is taken at $t = 0.2\tau_{\text{ff}}$ after the start of the simulation. This system contracts on *all* scales and forms stars at very high rate within a few free-fall times τ_{ff} . Contrary to the case of hydrodynamic turbulence, the kinetic energy distribution is dominated by compressional modes, especially at small wave numbers. The overall energy budget is determined by the potential energy E_{pot} , which outweighs the kinetic energy E_{kin} on all spatial scales k by about an order of magnitude.

3.3.2 Fourier Spectra During Collapse

Figure 3.22 concentrates on model $\mathcal{B}2h$ with $\langle M_{\text{J}} \rangle_{\text{turb}} = 3.2$ and $k = 3 - 4$. It describes the time evolution of the energy distribution. Figure 3.22a shows the state of fully established turbulence for this model just when gravity is turned on ($t = 0.0$). In the subsequent evolution, local collapse occurs in shock-generated density enhancements where the potential energy dominates over the kinetic energy. This affects the *small* scales first, as seen in the plotted time sequence. As collapse progresses to higher and higher densities, the scale where the potential energy dominates rapidly grows. Once the mass fraction in dense cores has reached about $\sim 3\%$, the potential energy outweighs the kinetic energy on all scales. However, this should not be confused with the signature of global collapse. The

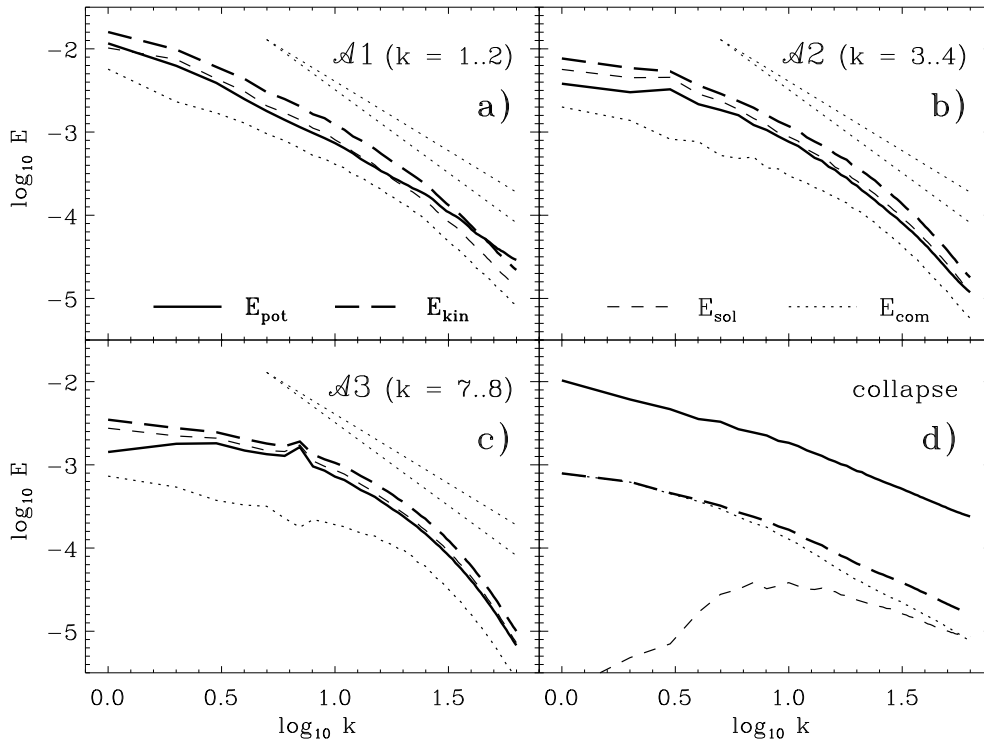


Figure 3.21: Energy as function of wave number k for models with different driving scale: (a) $\mathcal{A}1$ with $k = 1 - 2$, (b) $\mathcal{A}2$ with $k = 3 - 4$ and (c) $\mathcal{A}3$ with $k = 7 - 8$. The simulations are studied at $t = 0.0$, when the hydrodynamic turbulence is fully developed, immediately after gravity is included. The plots show potential energy E_{pot} (thick solid lines), kinetic energy E_{kin} (thick long-dashed lines), its solenoidal component E_{sol} (short-dashed lines) and its compressional component E_{com} (dotted lines). The thin dotted lines indicate the slope $-5/3$ expected from the Kolmogorov (1941) theory and the slope -2 expected for velocity discontinuities associated with shocks. For comparison, plot (d) shows a strongly self-gravitating model that completely lacks turbulent support and therefore contracts on all scales (data from Klessen *et al.* 1998). The energy spectra are computed on a 128^3 grid onto which the SPH particle distribution has been assigned using the kernel smoothing procedure. (From Klessen *et al.* 2000)

power spectrum of the potential energy is constant for all k . It is the Fourier transform of a delta function. Local collapse has produced point-like high-density cores. The overall filling factor of collapsing clumps and cores is very low, so most of the volume is dominated by essentially pure hydrodynamic turbulence. As a consequence, the velocity field on large scales is not modified much (besides a shift to higher energies). On small scales, however, the flow is strongly influenced by the presence of collapsed cores which is noticeable as a flattening of the power spectra at large wave numbers. Despite their small volume filling factor, the cores dominate the overall power spectrum. The solenoidal part of the kinetic energy always dominates over the compressional modes and also the signature of the driv-

ing source in the energy spectrum remains, visible as a ‘bump’ in the kinetic energy spectrum at $k \approx 8$.

3.3.3 Summary

In turbulent flows, it is impossible to predict from the start when and where individual cores form and how they evolve. In all models except the ones driven below the fluctuation Jeans scale, gravity eventually begins to dominate over kinetic energy. The Fourier spectra show that this first occurs on small scales. This indicates the presence of local collapse. As dense collapsed cores form, the power spectrum of the gravitational energy becomes essentially flat. The kinetic

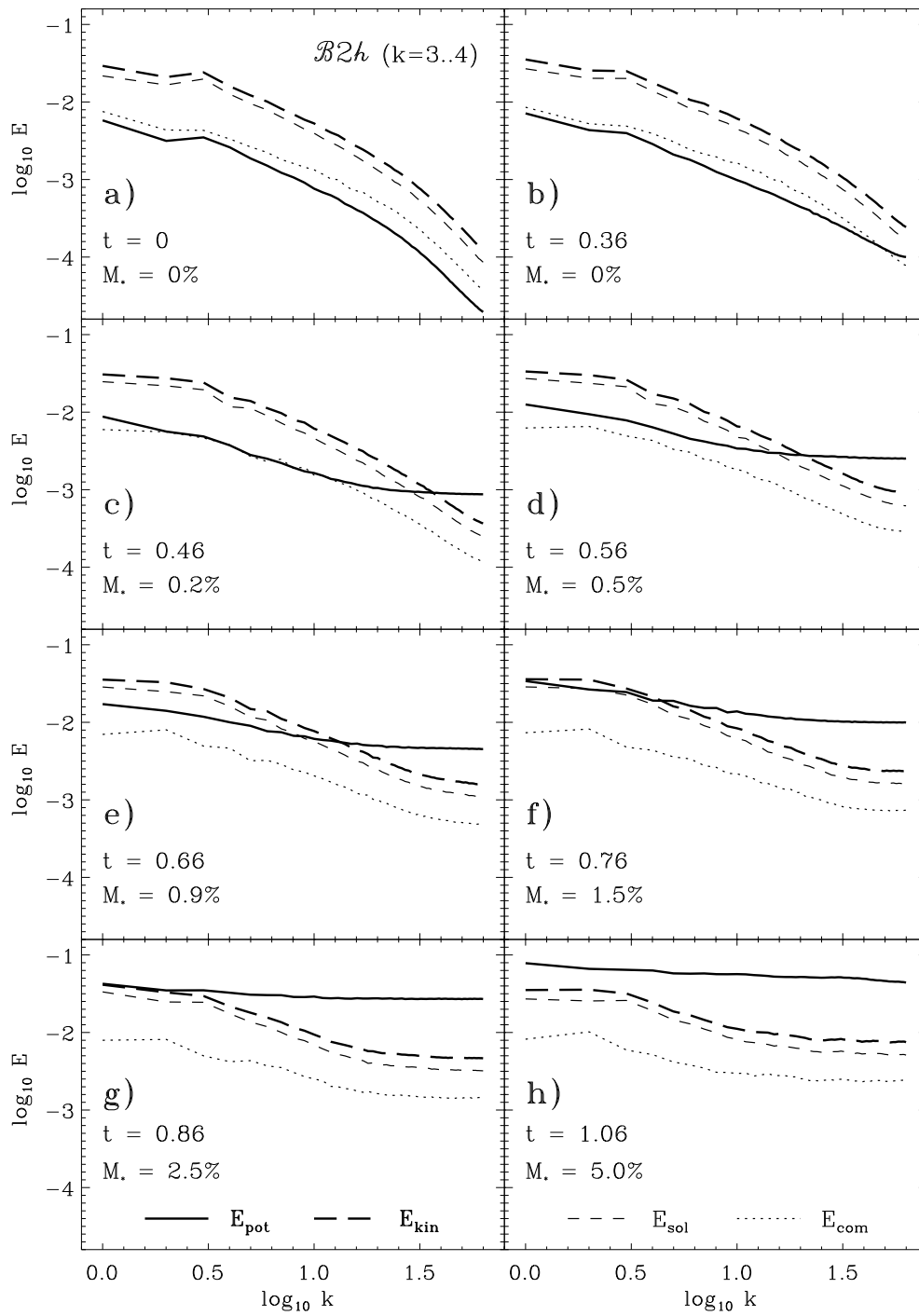


Figure 3.22: Fourier analysis of the high-resolution model $B2h$ ($\langle M_J \rangle_{\text{turb}} = 3.2$ and $k = 3 - 4$) at different stages of its dynamical evolution indicated on each plot. Notation and scaling are the same as in figure 3.21. (From Klessen *et al.* 2000)

energy, on the other hand, appears to follow at intermediate wave numbers a Kolmogorov power spectrum with slope $-5/3$, less steep than the spectrum expected for pure shock flows. The slope remains almost unaltered during the course of the evolution, indicating that a large volume fraction of the system is always well described by pure hydrodynamic turbulence. The spatial extent of collapsing regions (where infall motions dominate over the turbulent flow) is relatively small. This also explains the fact that the solenoidal component of the flow always dominates over the compressional part.

3.4 Δ -Variance

3.4.1 Introduction

In the previous two Sections we have focused on PDF's and Fourier transforms to quantify molecular cloud structure – other statistical measures are summarized in the reviews by Vázquez-Semadeni (2000) and Ossenkopf *et al.* (2000). One further technique especially sensitive to the discrimination of the relative structural variation on different spatial scales is the Δ -variance introduced by Stutzki *et al.* (1998). It provides a good separation of noise and observational artifacts from the real cloud structure and for isotropic systems its slope is directly related to the spectral index of the corresponding power spectrum. Bensch *et al.* (2001) and Mac Low & Ossenkopf (2000) have shown that it can be applied in an equivalent way both to observational data and hydrodynamic and magneto-hydrodynamic turbulence simulations allowing a direct comparison.

Their investigations, however, neglect the influence of gravitational collapse on the structure formation so that their conclusions may be limited when applied to star-forming regions. It is essential to include the effects of self-gravity for the analysis of star-forming regions. It was the aim of an investigation by Ossenkopf, Klessen, & Heitsch (2001) to close this gap and investigate the interaction between turbulence and self-gravity. We follow their line of reasoning and apply the Δ -variance to characterize the structure

in numerical models of driven and decaying self-gravitating supersonic (magneto-)hydrodynamic turbulence and compare the results to observed regions of star formation.

3.4.2 Turbulence Models

The large observed linewidths in molecular clouds imply the presence of supersonic velocity fields that carry enough energy to counterbalance gravity on global scales (Section 4.1). As turbulent energy dissipates rapidly, i.e. roughly on the free-fall time scale (Section 2.5), either interstellar turbulence is continuously replenished in order to prevent or considerably postpone global collapse, or alternatively, molecular clouds evolve rapidly and never reach dynamical equilibrium between kinetic energy and self-gravity (Ballesteros-Paredes *et al.* 1999a, Elmegreen 2000b).

We select a set of numerical models mostly from preexisting studies that spans a large range of the parameter space relevant for Galactic molecular clouds. We analyze the time evolution of their density and velocity structure as gravitational collapse progresses. Altogether, we include eight models summarized in Table 3.2. They differ in the scale on which turbulent driving occurs, the persistence of this driving, the inclusion of magnetic fields, and the numerical algorithm used to solve the hydrodynamic or magnetohydrodynamic equations. The models are calculated using the particle-based SPH method and the grid-based ZEUS code as introduced in Section 2.5.3 (for full details see Ossenkopf *et al.* 2001).

In the present analysis we neglect feedback effects from the produced young stellar objects (like bipolar outflows, stellar winds, or ionizing radiation from new-born O or B stars). Thus our results will hold only for early stages of star-forming systems.

To test the influence of magnetic fields we consider the driven turbulence model which carries most energy on large scales and add magnetic fields to the ZEUS simulations. By comparing the resulting model M01 with the hydrodynamic

Table 3.2: Properties of the considered turbulence models together with the resulting time scales

model	description	k_d^a	numerical method	further reference ^b	$\tau_{5\%}^c$	$f_{\tau_{\text{ff}}}^d$
S01	driven HD turbulence	1...2	SPH	$\mathcal{B}1h$ in KHM	0.6	28%
Sd1	decaying HD turbulence	1...2	SPH	—	0.6	60%
S02	driven HD turbulence	7...8	SPH	—	> 5.5	0.6%
Sd2	decaying HD turbulence	7...8	SPH	—	2.0	0.0%
G	Gaussian density	—	SPH	\mathcal{I} in KB	1.3	9%
H01	driven HD turbulence	1...2	ZEUS	$\mathcal{D}1h$ in KHM	0.6	24%
H02	driven HD turbulence	7...8	ZEUS	$\mathcal{D}3h$ in KHM	4.7	0.5%
M01	driven MHD turbulence	1...2	ZEUS	$\mathcal{E}h1i$ in HMK	1.2	6%

^aWavenumber of the original driving

^bModel names in the original papers: KB – Klessen & Burkert (2000), KHM – Klessen *et al.* (2000), HMK – Heitsch *et al.* (2001)

^cTime at which 5% of the total mass is accreted onto cores in internal units where $\tau_{\text{ff}} = 1.5$.

^dMass fraction that is accreted onto cores after one global free-fall time. — Adopted from Ossenkopf *et al.* (2001).

model H01 we get a direct measure for the significance of magnetic fields for the interplay of turbulence and self-gravity in structure formation.

The magnetic field in this model is selected to be a major factor where the ratio between thermal and magnetic pressure $\beta = p_{\text{th}}/p_{\text{mag}} = 8\pi c_s^2 \rho / B^2 = 0.04$. With a turbulent Mach number of $\mathcal{M}_{\text{rms}} = 10$ we find that the turbulent velocity dispersion exceeds the Alfvén speed by a factor of 1.4 so that the structure is still essentially determined by supersonic turbulence and only modified by the magnetic field. The mass in the cloud still exceeds the critical mass for a magnetostatically stable cloud by a factor 2 (Heitsch *et al.* 2001) so that the field should not prevent gravitational collapse. Cases of sub-Alfvénic non-self-gravitating turbulence where the whole structure is dominated by the magnetic field have been discussed by Ossenkopf & Mac Low (2001).

The models presented here are computed in normalized units. Throughout this analysis we give all size values relative to the total cube size, all density values relative to the average density in the cube, and all velocities relative to the sound speed. Model G contains 220 thermal Jeans masses, whereas all other models have 120 thermal Jeans masses³. If scaled to mean densi-

ties $n(\text{H}_2) = 10^5 \text{ cm}^{-3}$, a value typical for star-forming molecular cloud regions and a temperature of 11.4 K (i.e. a sound speed $c_s = 0.2 \text{ km s}^{-1}$), the mean Jeans mass is one solar mass, $\langle M_J \rangle = 1 M_\odot$, and the size of cube G is 0.34 pc whereas all other models have a size of 0.29 pc. The global free-fall time scale, as defined by $\tau_{\text{ff}} = (3\pi/32G)^{1/2} \langle \rho \rangle^{-1/2}$ with $\langle \rho \rangle$ being the average density, is about 10^5 yr . In normalized time units it follows $\tau_{\text{ff}} = 1.5$. The simulations cover a density range from $n(\text{H}_2) \approx 100 \text{ cm}^{-3}$ in the lowest density regions to $n(\text{H}_2) \approx 10^9 \text{ cm}^{-3}$ where collapsing protostellar cores are identified and converted into “sink” particles in the SPH code.

In this density regime gas cools very efficiently and it is possible to use an effective polytropic equation-of-state in the simulations instead of solving the detailed equations of radiative transfer. The effective polytropic index is typically close to unity, $\gamma_{\text{eff}} \lesssim 1$, except for densities $10^5 \text{ cm}^{-3} < n(\text{H}_2) < 10^7 \text{ cm}^{-3}$, where somewhat smaller values of γ_{eff} are expected (Spaans & Silk 2000). For simplicity, we adopt a value of $\gamma_{\text{eff}} = 1$, i.e. an isothermal equation of state for all densities in the simulations. As the choice of

$(\pi \mathcal{R} T / G \rho)^{1/2}$, where G and \mathcal{R} are the gravitational and the gas constant. The mean Jeans mass $\langle M_J \rangle$ is determined from average density in the system $\langle \rho \rangle$. An alternative cubic definition, $M_J \equiv \rho (2\lambda_J)^3$, would yield a value roughly twice as large.

³We use the spherical definition of the Jeans mass, $M_J \equiv 4/3 \pi \rho \lambda_J^3$, with density ρ and Jeans length $\lambda_J \equiv$

γ_{eff} influences the density contrast in shock compressed gas, this idealisation may introduce some small modifications to the dynamical behavior compared to real cloud systems (see Scalo *et al.* 1998 or Ballesteros-Paredes *et al.* 1999b for further discussion).

3.4.3 Density Structure

Δ -Variance Analysis

The Δ -variance analysis was introduced by Stutzki *et al.* (1998) as an averaged wavelet transform (Zielinsky & Stutzki 1999) to measure the amount of structure present at different scales in an E -dimensional data set. The value of the Δ -variance at a certain scale is computed by convolving the E -dimensional structure with a normalized spherically symmetric down-up-down function of the considered size, and measuring the remaining variance. For two-dimensional structures, like astrophysical maps, the filter function is easily visualized as a “French hat” wavelet with a positive centre surrounded by a negative ring and equal diameters of the centre and the annulus. The analysis can be applied in the same way in arbitrary dimensions by extending the filter function to higher dimensions retaining its radial symmetry and adapting the value in the negative part to preserve normalization (Appendix B of Stutzki *et al.* 1998). The resulting Δ -variance as a function of the filter size measures the amount of structural variation on that scale.

As the convolution with the filter function corresponds to a multiplication in Fourier space, we can relate the Δ -variance to the power spectrum of the data set. If the structure is characterized by a power law power spectrum

$$P(|\vec{k}|) \propto |\vec{k}|^{-\beta} \quad (3.13)$$

the slope α of the Δ -variance as a function of lag (filter size) is related to the spectral index β of the power spectrum by $\beta = \alpha + E$ for $0 \leq \beta < E + 4$. Due to the smooth circular filter function the Δ -variance measures the spectral index in a way which is more robust with respect to edge and

gridding effects than the Fourier transform. The Δ -variance provides a clear spatial separation of different effects influencing observed structures like noise or a finite observational resolution.

Mac Low & Ossenkopf (2000) have shown that we can translate the Δ -variance of a three-dimensional isotropic structure into the Δ -variance of the maps obtained from the projections of this structure by rescaling with a factor proportional to the lag and an additional small shift. This guarantees the preservation of the power spectral index β in projection (Stutzki *et al.* 1998). As we want to compare the simulations to observational data we will always use the two-dimensional representation of the Δ -variance results also when applying the analysis directly to the three-dimensional data cubes of the simulations. To compute the Δ -variance for our models the SPH density distribution is assigned onto a Cartesian grid with 128^3 cells. The ZEUS cubes have been analyzed in full resolution at 256^3 as well as degraded to 128^3 for a one-to-one comparison with the SPH models. Higher resolution helps to extend the dynamic scale range limited by the periodic boundary conditions at the large scale end and the numerical resolution of the simulations on the small scale end, but does not change the general behavior of the resulting Δ -variance.

Collapse of a Gaussian Density Field

Before we investigate the interplay between supersonic turbulence and self-gravity, let us consider a system where the density and velocity structure is dominated by gravity on all scales and at all times. Model G describes the collapse of Gaussian density fluctuations with initial power spectrum $P(k) \propto k^{-2}$ and maximum density contrast $\delta\rho/\rho \approx 50$. The system is unstable against gravitational collapse on all scales and forms a cluster of protostellar cores within about two free-fall time scales (Klessen & Burkert 2000, 2001). The velocity structure is coupled to the density distribution via Poisson’s equation and there is no contribution from interstellar turbulence.

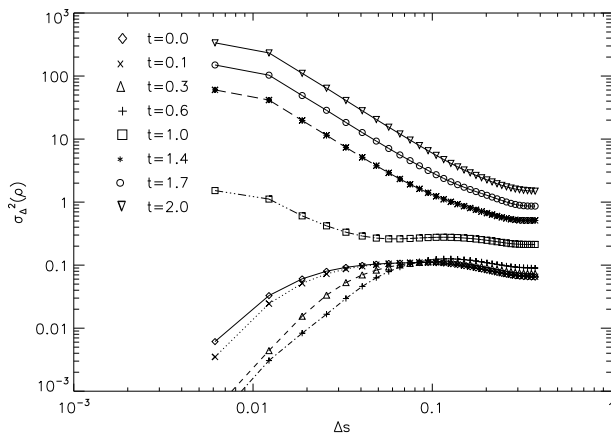


Figure 3.23: Time evolution of the strength of density fluctuations as function of their spatial scale measured with the Δ -variance for model G. The density ρ is given in units of the average density in the cube, the lag Δs in units of the cube size, and the time t in internal time units where the free-fall time $\tau_{\text{ff}} = 1.5$. (From Ossenkopf *et al.* 2001)

The time evolution of the density structure is illustrated in Figure 3.23. Initially, the Δ -variance $\sigma_{\Delta}^2(n)$ is more or less constant ($\alpha = 0$) on scales $\Delta s \gtrsim 0.02$, in agreement with the initial power spectrum $P(k) \propto k^{-2}$. The steepening below $\Delta s \approx 0.02$ is produced by the finite resolution of the SPH simulations resulting in the blurring of structures at the smallest scales.

The first changes of the variance $\sigma_{\Delta}^2(n)$ are confined to small scales. Initial fluctuations with masses below the local Jeans limit will quickly smear out by thermal pressure as the system evolves from purely Gaussian fluctuations into a hydrodynamically self-consistent state (see Appendix B in Klessen & Burkert 2000). As these fluctuations are by far more numerous than Jeans-unstable contracting ones, the Δ -variance $\sigma_{\Delta}^2(n)$ begins to decrease on small scales. However, as the central regions of massive Jeans-unstable fluctuations contract to sufficiently high densities, $\sigma_{\Delta}^2(n)$ increases again. This mainly affects the small scales as local collapse modifies the density structure on time scales of the local free-fall time. At $t = 0.7\tau_{\text{ff}}$ the first collapsed core is identified and is soon followed by others. Altogether 56 dense protostellar cores build up. As time advances larger and larger scales exhibit noticeable signs of contraction. After about

one global free-fall time collapse starts to involve all spatial modes in the system and the absolute magnitude of the density fluctuations finally grows on all scales. As the small scale structure dominates the density structure we obtain a negative slope in the Δ -variance spectrum. In the final step of the simulation roughly 30% of the mass is accumulated in dense cores and the slope is about -1.7 indicating that a small but significant contribution of large scale structure is still present, because an uncorrelated N -body system of gravitationally collapsed points would correspond to a slope of -2 equivalent to a flat power spectrum $P(k) = \text{const}$.

The flattening at $\Delta s > 0.2$ is due to periodicity. The system is *not* allowed to collapse freely, it is held up against global collapse by periodic boundaries which strongly affect the evolution of the large-scale modes. The graphs of Δ -variance are not extended beyond effective lags of about 0.4 as the largest filter that we use is half the cube size and we have to apply an average length reduction factor of $\pi/4$ on projection to two dimensions.

Interaction Between Gravity and Turbulence

To study the interplay between supersonic turbulence and self-gravity, we consider four models of interstellar turbulence which probe very disparate regions of the relevant parameter space. In models S01 and Sd1 most of the turbulent kinetic energy is carried on large scales, whereas models S02 and Sd2 involve mainly small-scale turbulent modes. In S01 and S02, turbulence is continuously driven such that at any moment the overall kinetic energy compensates the global gravitational energy. In Sd1 and Sd2, the turbulent energy is allowed to decay freely.

Figure 3.24 shows $\sigma_{\Delta}^2(n)$ for all four models as function of time. In the initial plots one can clearly see the dominance of the driving scale as discussed by Mac Low & Ossenkopf (2000). The introduction of a velocity field with a certain scale induces a pronounced peak in the density structure at a somewhat smaller scale. Thus the curves at $t = 0$ show for the large scale-driven models

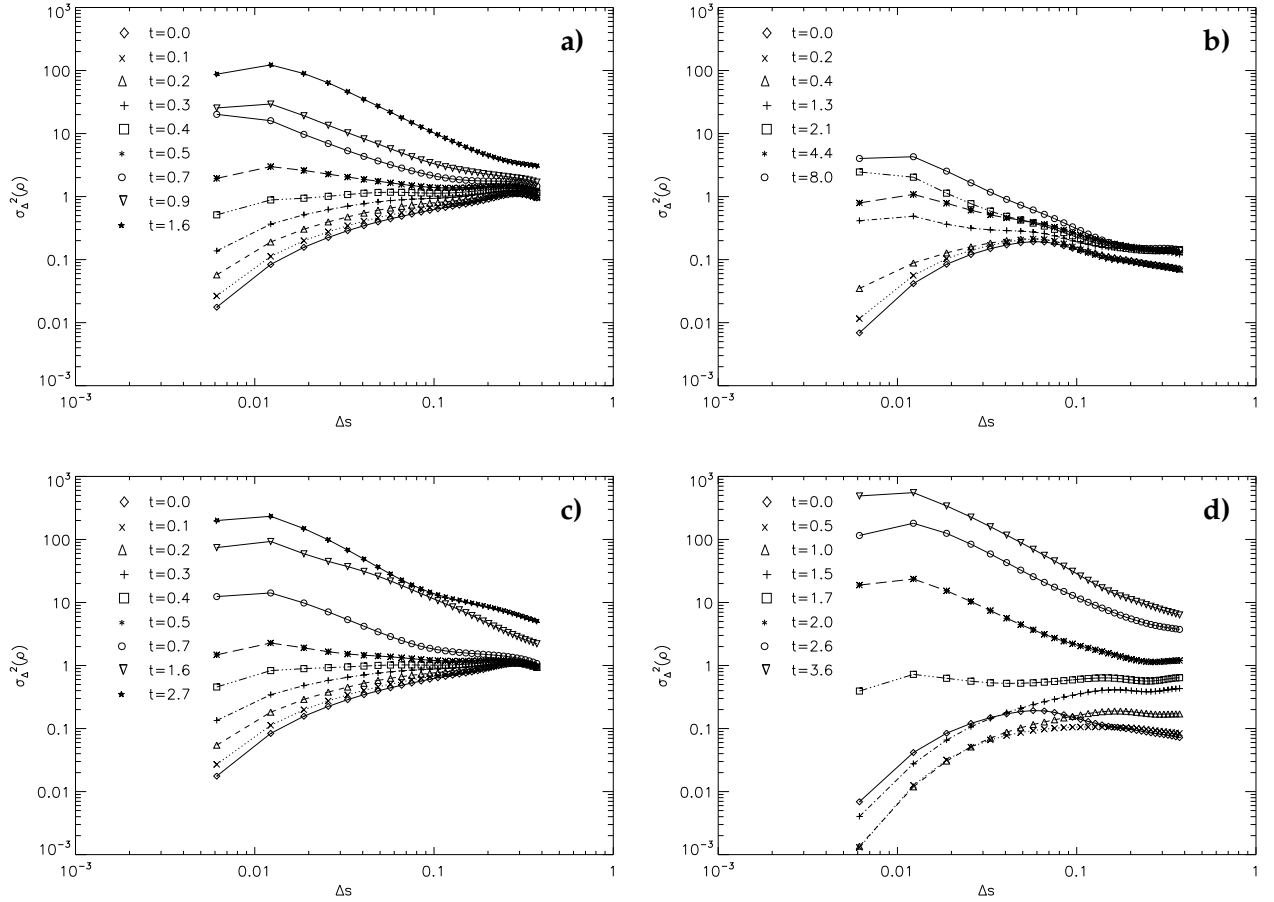


Figure 3.24: Time evolution of the size distribution of density variations as measured with the Δ -variance for the four models of (a) S01, (b) S02, (c) Sd1, and (d) Sd2. The different depicted times are indicated at the left side of each plot. (From Ossenkopf *et al.* 2001)

a power law Δ -variance from about a third of the cube size down to the numerical dissipation scale whereas in the small-scale driven model the driving feature at about 0.07 dominates the structure.

Star formation is a joint feature of all considered models. Like in the evolution of the Gaussian density field the gravitational collapse first modifies only the smallest scales, hardly changing the global behavior. As soon as local collapse occurs and the first dense protostellar cores form and grow in mass by accretion, they represent the main density fluctuations. Their power is concentrated on small scales and the Δ -variance exhibits a negative slope. The structure resulting from the collapse is very similar in the various models when we compare evolutionary stages with about the same mass fraction collapsed onto cores.

In the initially large-scale driven models a turbulent cascade covering all scales is already present from the beginning shown by the highest $\sigma_{\Delta}^2(n)$ -values at long scales. Within this cascade the number of small-scale fluctuations is small compared to models S02, Sd2, and G, and they are typically part of a larger structure so that they are only weakly dispersed in time. This leads to a monotonous growth of the Δ -variance on all scales. As larger and larger regions become gravitationally unstable the contraction comprises increasingly larger scales, and finally $\sigma_{\Delta}^2(n)$ shifts “upward” on all scales while maintaining a fixed slope. This situation is similar in *all* models with allow for large-scale collapse, i.e. it is only prevented in the small scale-driven model S02.

A different temporal behavior is visible in Sd2, the decaying turbulence which was originally

driven at small scales. Like in the collapse of the Gaussian density field we find in the first steps of the gravitational evolution a relative reduction of small-scale structure. This decrease is due to the termination of the initial small-scale driving resulting in a quick dissipation of the existing fluctuations by thermal pressure if they are not Jeans supercritical, analogously to the Gaussian collapse case. In the next steps we notice the production of structure on larger scales. The smoothing of small-scale turbulence combined with the onset of self-gravity leads to global streaming motions which produce density structures correlated on a larger scale. Large-scale structures had been initially suppressed by the non-local turbulent driving mechanism. After less than one free-fall time a kind of self-sustaining inertial cascade with a Δ -variance slope α of about 0.5 is build up like in all other decaying models and in the large scale driven model. After these initial adjustments the first protostellar cores form and we find the same dynamical behavior.

The time scale to reach a comparable collapse state and the final structure that we reach in the simulations differs between the models, mainly determined by the strength of the turbulent driving. The exponent α of the Δ -variance in the collapsed state is -1.3 in the models containing continuous driving, -1.5 in the models where the turbulence decays during the gravitational collapse, and -1.7 for the pure collapse of the Gaussian density field. This is understandable, as decreasing turbulent support leads to enhanced collapse forming stars in denser clusters. The final deviation from the uncorrelated field of protostars which has $\alpha = -2$ is thus a measurable indicator of the turbulent processes in the cloud during gravitational collapse. The local collapse produces “point-like” high-density cores with small overall filling factor whereas most of the volume is supported by hydrodynamic turbulence. In the large-scale driven model 30% of the mass and in the decaying models 60% of the total mass has turned into cores within the considered time interval. In the model continuously driven at small scales only 3% of the mass is in stable cores despite a considerably longer sim-

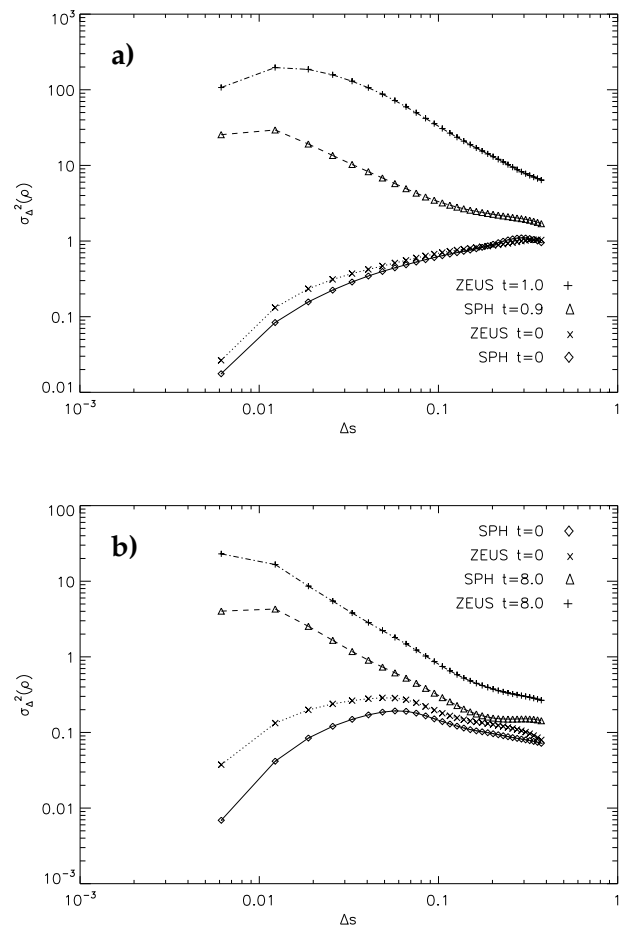


Figure 3.25: Comparison of the Δ -variance measured from the particle-based and the grid-based simulations at the beginning and at about the same timestep of the gravitationally collapsed state. Plot (a) shows the large-scale driven model, plot (b) the small scale-driven situation. (From Osenkoff *et al.* 2001)

ulation time. The small-scale driven turbulence leads to the least efficient star formation in an isolated mode, whereas the other cases result in the formation of stellar aggregates and clusters (see also Klessen *et al.* 2000, Klessen 2001).

Beside the deceleration of collapse the continuation of the initial driving has almost no influence on the resulting density structure as soon as the first stable cores have formed. It only maintains a constant level of velocity fluctuations in the main volume of the cloud which is dominated by low density gas, compared to a homogeneous reduction of these fluctuations in the purely decaying case.

Influence of the Numerical Model

Comparing the results of the particle-based SPH and the grid-based ZEUS code we can distinguish between numerical artifacts and physical results, as these two approaches practically bracket the real dynamical behavior of interstellar turbulence. In Figure 3.25 we compare the Δ -variance plots of the density structure obtained for the driven cases using either SPH or ZEUS, at the beginning of the gravitational collapse and in a step where the structure is already dominated by protostellar cores.

The scaling behavior of the density structure does not differ between both types of simulations but the absolute magnitude of the density fluctuations as seen in the total value of the Δ -variance is somewhat larger for all ZEUS models. In the first steps of the large-scale driven models both numerical approaches still agree approximately but during the evolution the scale dependent density variations become about a factor five higher in the ZEUS model than in the SPH approach. In the small scale driven models we can notice a clear difference already at the beginning of the simulations. This is consistent with the different effective resolution of the methods. Whereas the SPH code can provide a very good spatial resolution around the collapsing dense regions the general spatial resolution obtained with $2 \cdot 10^5$ particles is lower than in the ZEUS simulations on a 256^3 grid. Thus, the damping of structures at small scales due to the finite resolution of the code is slightly stronger in the SPH simulations than in the corresponding ZEUS models. One can for instance see that there is a virtual reduction of structure below 0.01 which is approximately the radius of the sink particles in the SPH code.

As the SPH resolution is explicitly density dependent it is also reduced on all larger scales in low density regions. This virtually smears out part of the structure on all scales. Consequently, the Δ -variance shows lower values on all scales than in the grid-based approach because it is not biased towards high-density regions like SPH and the observations. The effect is larger in the small-scale driven models as the same num-

ber of SPH particles has to represent more shocks than in large-scale dominated cases further reducing the effective resolution. Moreover, the resolution worsens during the collapse evolution as SPH particles “vanish” in the sink particles. Thus, the ZEUS simulations are preferential due to their higher resolution if one is interested in the absolute value of the Δ -variance whereas they provide no essential advantage for the study of the scaling behavior.

Magnetic Fields

As discussed by Mac Low & Ossenkopf (2000) magnetic fields hardly change the general scaling behavior in interstellar turbulence but create anisotropies in the velocity field and therefore aligned density structures. Since the Δ -variance cannot measure anisotropies in the density structure we do not expect to detect the influence of the magnetic field on the turbulence by the present analysis. Figure 3.26 shows the Δ -variance for the initial step and an collapsed stage in a large-scale driven hydrodynamic model and the equivalent MHD model with a strong magnetic field. The initial steps are almost identical but we find that during collapse the magnetic field effectively helps to transfer structure from larger to smaller scales. Thus we confirm the more qualitative conclusion of Heitsch *et al.* (2001) that the magnetic field slightly delays collapse by transferring part of the turbulent kinetic energy to smaller scales. The general slope of the Δ -variance is not changed but we obtain somewhat denser and smaller cores and somewhat less large-scale correlation at equivalent timesteps.

Computing the Δ -variance for maps projected either in the direction of the initial magnetic field or perpendicular to it does not show any significant difference in the density scaling behavior as mainly the shape of the collapsed regions is influenced, towards spiral-shaped structures, which is not measurable with the isotropic Δ -variance filter.

We have also tested models with a smaller magnetic field where the magnetic pressure in the order of the thermal pressure or lower. Here, we

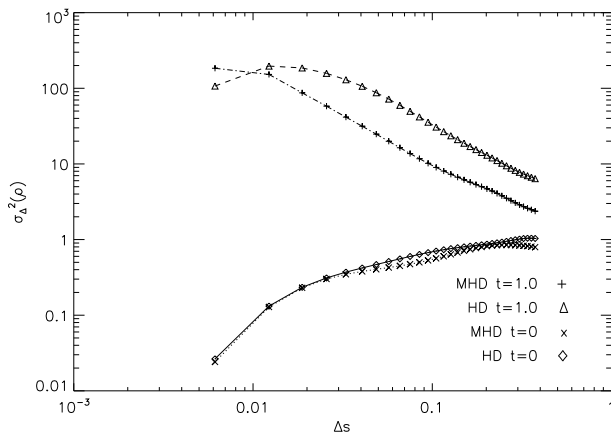


Figure 3.26: Comparison of the Δ -variance for the large-scale driven model in the hydrodynamic case or the situation with strong magnetic fields, both computed with the ZEUS code. (From Ossenkopf *et al.* 2001)

find that the field acts like an additional contribution to the overall isotropic pressure so that the collapse is somewhat delayed relative to the hydrodynamic case but the general structure does not deviate from the hydrodynamic simulations. Thus there is no need to discuss the weak-field situation here separately.

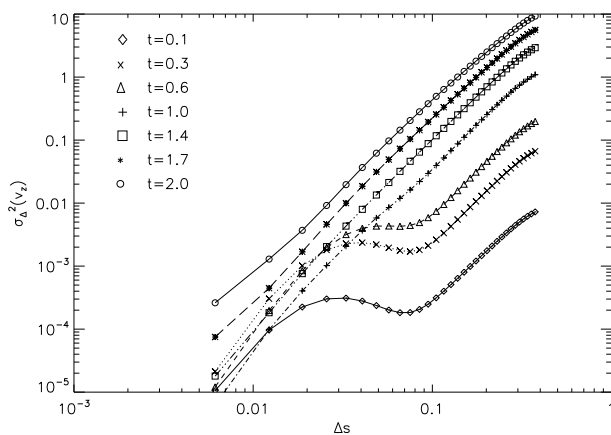


Figure 3.27: Evolution of the Δ -variance of the z -velocity in the collapse of the Gaussian density distribution (model G). The velocity v_z is given here in units of the thermal sound speed c_s . (From Ossenkopf *et al.* 2001)

3.4.4 Velocity Structure

We can apply the Δ -variance analysis in the same way to the velocity structure in the simulations (Ossenkopf & Mac Low 2001). Figure 3.27 shows

the evolution of one velocity component in the collapse of the Gaussian density fluctuations. In the first steps where we observe a relative reduction of small scale density fluctuations we find a bimodal velocity distribution with either very small or very large flows. The surplus of small-scale flows just reflects the dissipation of the initial small-scale variations by thermal pressure. When the first stable cores have formed the picture changes towards that of a typical shock-dominated medium with a slope $\alpha = 2$ (Ossenkopf & Mac Low 2001) as the result of supersonic accretion onto dense cores along the emerging filamentary structure (Klessen & Burkert 2000, 2001).

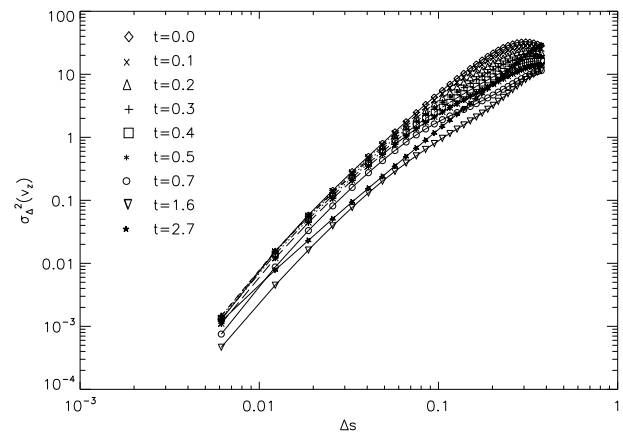


Figure 3.28: Evolution of the Δ -variance of the z -velocity component of the decaying model Sd1. (From Ossenkopf *et al.* 2001)

In all driven models we see no significant changes in the velocity structure during collapse. This is because the Δ -variance is not focused towards the dense cores where collapse motions occur, as these have only a small spatial filling factor. Instead, most of the volume is occupied by tenuous intercore gas with velocity structure that is determined by turbulent driving. The Δ -variance therefore exhibits the power-law behavior of shock dominated gas.

The same hold for decaying turbulence as well. To illustrate that point, Figure 3.28 presents the evolution of the velocity structure for model Sd1, where we drive the turbulence initially at large scales and switch off the driving during the grav-

izational collapse. The changes in the velocity structure are only minute. The Δ -variance follows the power law of shock-dominated flows throughout the entire evolution. Only the total magnitude of the velocity fluctuations decreases slightly during the initial decay of turbulence. However, after the onset of collapse, when the majority of mass is already accumulated in dense cores, the magnitude of σ_Δ increases again. The Δ -variance becomes dominated by the shock structure arising from the supersonic accretion flows onto individual cores (similar to the late stages of model G). The evolution of the small-scale decaying turbulence is not plotted separately, as we observe the same behavior. Except during the initial phase of turbulent decay where the velocity structure still peaks on small scales reflecting the smaller driving wavelength used to set up the model (see Figure 3.25d for the density structure), again after $t \approx 1.5$ when the initial turbulence is sufficiently decayed away the Δ -variance arrives at the power-law behavior of shocked gas.

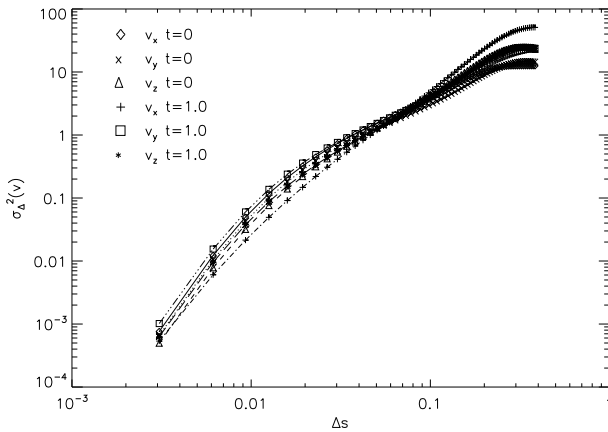


Figure 3.29: Δ -variance of all three velocity components for model the large-scale driven MHD model at the initial step and after one free-falling time. (From Ossenkopf *et al.* 2001)

In Figure 3.29 we show the three velocity components of the MHD model M01 at the same two timesteps like in the density plot in Figure 3.26. In contrast to the findings of Ossenkopf & Mac Low (2002) for sub-Alfvénic turbulence, we see no strong anisotropy of the velocity field. The velocity structure along the mean magnetic field (z -direction) is very similar to the perpendic-

ular directions throughout the dynamical evolution of the system and well within the statistical fluctuations expected for large-scale turbulence. The velocity structure is still determined by supersonic turbulence rather than by the magnetic field structure because the turbulent rms velocity dispersion exceeds the Alfvén speed in this model. The local collapse and the formation of a cluster of collapsed cores tends to make the influence of the magnetic field on the velocity structure even weaker. The magnetic field merely decelerates the gravitational collapse and changes the geometry of the collapsing regions as seen in Figure 3.26, but hardly changes the global velocity structure in this model situation.

Altogether we find that all models that are allowed to evolve freely or are driven at large scales exhibit a similar velocity scaling behavior, characteristic of shock-dominated media. This is the effect of the undisturbed turbulence evolution and the appearance of accretion shocks. Both effects lead to remarkably similar properties of the velocity Δ -variance. Any observed deviation from this large-range “Larson” behavior indicative of shock-dominated media will hint the presence of additional physical phenomena and could provide constraints on the initial conditions and the dynamical state of star-forming regions.

3.4.5 Comparison with Observations

Dust Observations

To compare the simulations of gravitational collapse with observational data of collapsed regions we have selected the observation of a star-forming cluster in Serpens by Testi & Sargent (1998) as this region represents a state of star formation that may be similar to the outcome of our simulations.

In Figure 3.30 we show the Δ -variance for the 3 mm dust continuum map of Testi & Sargent (1998). It reveals an increase of the relative amount of structure from small scales towards a peak at $7''$, an intermediate range which can be fitted by a power-law exponent $\alpha = -1.2$,

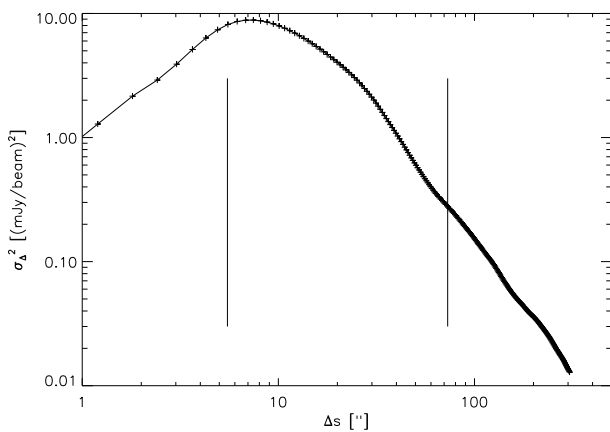


Figure 3.30: Δ -variance of the dust continuum map in Serpens taken by Testi & Sargent (1998). The two vertical lines represent the limits of the significant range as indicated with the observational data. (From Ossenkopf *et al.* 2001)

and a decay with $\alpha = -2$ indicating the complete lack of large-scale structure at lags above $40''$. The behavior at largest and smallest scales can be understood when looking at the observational base of the map. Testi & Sargent (1998) give a resolution for their interferometric observations of $5.5'' \times 4.3''$. Consequently we cannot see any structure below that size. The fact that our peak falls with $7''$ somewhat above the $5.5''$ resolution limit might indicate that the CLEAN beam used in the reduction of the interferometric data is not exactly Gaussian or slightly wider than computed. The whole map is taken with an interferometric mosaicing technique (see for details Testi & Sargent 2000) without a zero-spacing by complementary single dish observations. Thus the map cannot contain any structure on scales above the single pointing areas determined approximately by the size of the primary beam of the OVRO antennas of $73''$. This is in agreement with the lack of structure indicated by the Δ -variance slope of -2 at these scales. The two limiting sizes are indicated by vertical lines in Figure 3.30. Thus we may only discuss the range in between disregarding other information that is plotted in the interferometric map but that can eventually not be obtained from the observations.

The steepening of the Δ -variance in the intermediate size range from $\alpha = -1.2$ to $\alpha = -2$ does qualitatively agree with the behavior observed

in most collapse simulations at small scales but does not match any of them quantitatively. For a detailed comparison the dynamic scale range covered in the simulations is still insufficient due to the periodic boundary conditions constraining the large scale behavior. Hence, we can only conclude that the collapse models show the same general structure as the dust observations, indicating that they represent a realistic scenario but we cannot yet discriminate between different models using the observational data.

Molecular Line Observations

Bensch *et al.* (2001) provided a detailed Δ -variance analysis of the density structure traced by observations in different CO isotopes for several molecular clouds with different states of star formation including quiescent clouds like the Polaris Flare and clouds with violent star formation like Orion A. They found for all molecular clouds a density structure approximately characterized by a power law Δ -variance, with an exponent in the range $0.5 \leq \alpha \leq 1.3$. In the best studied cloud one smooth curve connects scales larger than 10 pc (where turbulence presumably is driven) with the dissipation scale at 0.05 pc (where ambipolar diffusion processes become important). The positive slopes indicate that the density structure seen in the CO isotopes is dominated by large-scale modes. This result is consistent with purely supersonic turbulence and appears independent of the dynamical state of the molecular cloud regions studied, i.e. regardless whether the cloud forms stars or not.

This is somewhat surprising, since we expect that the density distribution in star-forming regions is dominated by the collapsing protostellar cores on small spatial scales. The Δ -variance spectrum therefore should exhibit a *negative* slope. The molecular line results are also in obvious contradiction to the Serpens dust observations discussed above.

The explanation for the difference is hidden in the radiative transfer problem. A discussion of all major aspects of molecular line transfer in turbulent media is provided by Ossenkopf (2002).

Here, it is sufficient to concentrate on one effect – saturation at large optical depths. Molecular lines like the lower transitions of ^{13}CO , frequently used to map the density profile of molecular clouds, become typically optically thick in the cores of clouds at densities in the order of 10^5 cm^{-3} . The exact value depends on the transition, the spatial configuration, temperatures, and the geometry of the radiation field but one can always assign a typical density range to the transition from the optically thin to the optically thick regime. This leads to a saturation of the line intensities in dense clumps so that the lines do not trace their internal structure but rather see clump surfaces. Moreover, the molecules tend to freeze out in dense dark regions (Kramer *et al.* 1999) amplifying the effect that the line brightness reflects only part of the column density in dense clumps.

As we do not want to treat the full radiative transfer problem here, we give only an estimate for the influence of optical depth effects by including a saturation limit into our computations. Because the simulations are scale-free and the typical saturation density varies for different molecules and transitions there is no particular density value to be used for this limit so that we have to play with different values.

Figure 3.31 illustrates the evolution of the large-scale driven model shown in Figure 3.24a assuming now that all densities above a certain threshold are invisible so that they are equal to the value of the saturation density. In the upper plot we have chosen this limit to be the maximum density occurring in the original turbulent density distribution before gravitational collapse starts. This is 240 times the average density, i.e. a relatively large value compared to the dynamic range of molecular line observations. In the lower graph the saturation limit is reduced by a factor 10.

Although only a relatively small fraction of the material appears at densities above the limit the influence on the Δ -variance is dramatic. As the collapsing cores produce the relative enhancement of small scale structure their virtual removal by the saturation results in an almost constant Δ -variance behavior during the gravitational collapse. Even in the very conservative

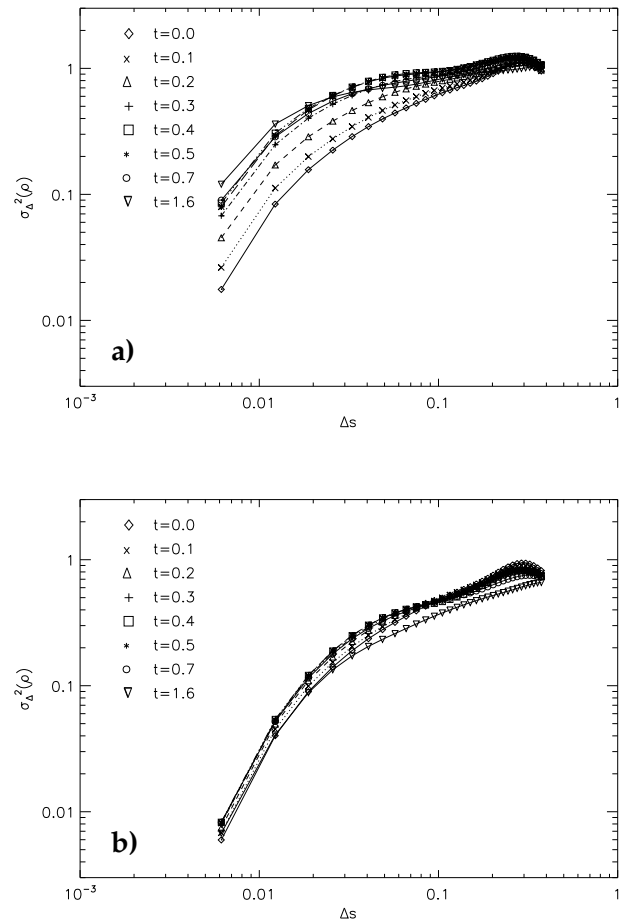


Figure 3.31: Time evolution of the Δ -variance for the large-scale driven model S01 when the density structure is assumed to saturate at densities of 240.0 (a) and 24.0 (b). (From Ossenkopf *et al.* 2001)

upper plot where we assume that all structures occurring in normal interstellar turbulence are still optically thin and only the collapsing cores become optically thick the Δ -variance stays at a positive slope during the entire evolution. In the other case where optical depth effects are assumed to be more important the Δ -variance remains at a fixed slope of 0.5 consistent with the molecular line observations of interstellar clouds.

Hence, optical depth effects can easily prevent the detection of gravitational collapse in molecular line observations, since they reproduce the Δ -variance spectrum of a turbulent molecular cloud even if collapse has lead already to the formation of protostellar cores. Even in massively star-forming clouds most molecules used for mapping trace the diffuse density structure *between*

Jeans-unstable collapsing protostellar cores. This gas is still dominated by interstellar turbulence. The density contrast in star-forming molecular cloud regions simply exceeds the density range traceable by molecular transitions. Protostellar core densities are so high that ^{13}CO at best traces the outer envelope. Therefore both, star-forming and quiescent molecular clouds, exhibit very similar molecular line maps.

It is essential to resolve large density contrasts measuring the full density structure to study the influence of self-gravity and local collapse in star-forming clouds. This can be achieved using dust continuum emission. Indeed, the 3mm continuum map of the Serpens cluster by Testi & Sargent (1998) shows a density structure that is dominated by small scales as predicted by our collapse simulations. The drawback of dust emission observations is the inherent convolution of the density structure with the unknown temperature profile. Large dust extinction maps could circumvent this problem but require long integration times at NIR wavelengths to obtain a dense sampling with background stars (Lada *et al.* 1999).

3.4.6 Summary

Contrary to what is observed for purely hydrodynamic turbulence, self-gravitating supersonic turbulence yields a density structure that contains most power on the smallest scales (i.e. in the collapsed objects) as soon as local collapse has set in. This happens in all self-gravitating turbulence models regardless of the presence or absence of magnetic fields. The Δ -variance $\sigma_{\Delta}^2(n)$ exhibits a negative slope and peaks at small scales as soon as local collapse produces dense cores. This is in contrast to the case of non-self-gravitating hydrodynamic turbulence where $\sigma_{\Delta}^2(n)$ has a positive slope and the maximum at the largest scales. Our results can therefore be used to differentiate between different stages of protostellar collapse in star-forming molecular clouds and to determine scaling properties of the underlying turbulent velocity field.

The effect of protostellar collapse, however, is not visible in molecular line maps of star-forming

clouds, as all molecules trace only a limited dynamic range of densities. The density contrast in star-forming regions is much larger. ^{12}CO and ^{13}CO observations, for example, trace only the inter-core gas distribution and at best the outer parts of individual protostellar cores. Hence, the density structure seen in these molecules is indistinguishable for star-forming and non-star-forming regions.

As resolving high density contrasts is the key for detecting the effect of star formation in the Δ -variance, we propose observations of dust continuum or of the dust extinction instead. These techniques do not have the same limitations of the dynamic range and are therefore better suited to quantitatively study the full density evolution during the star-formation process. This is confirmed by a first comparison of our models with the 3mm dust continuum map taken by Testi & Sargent (1998) in Serpens.

Chapter 4

LOCAL STAR FORMATION

All present day star formation takes place in molecular clouds (e.g. Blitz 1993, Williams, Blitz, & McKee 2000), so we must understand the dynamical evolution and fragmentation of molecular clouds to understand star formation. This section therefore begins with a brief introduction to molecular clouds properties (Section 4.1). We then show how the efficiency and time and length scales of star formation can depend on the properties of turbulence (Section 4.2), followed by a discussion of the properties of protostellar cores (Section 4.3), the immediate progenitors of individual stars. We stress the importance of the dynamical interaction between protostellar cores and their competition for mass growth in dense, deeply embedded clusters (Section 4.4). This implies strongly time-varying protostellar mass accretion rates (Section 4.5). Finally, we discuss the consequences of these probabilistic processes (turbulence and stochastic mass accretion) for the resulting stellar initial mass function (Section 4.7).

4.1 Molecular Clouds

4.1.1 Composition of Molecular Clouds

Molecular clouds are density enhancements in the interstellar gas dominated by molecular H_2 rather than the atomic H typical of the rest of the ISM, mainly because they are opaque to the UV radiation that elsewhere dissociates the molecules. In the plane of the Milky Way, interstellar gas has been extensively reprocessed

by stars, so the metallicity¹ $Z \approx Z_\odot$, the solar value, while in other galaxies with lower star formation rates, the metallicity can be as little as $10^{-3}Z_\odot$. This has important consequences for the radiation transport properties and the optical depth of the clouds. The presence of heavier elements such as carbon, nitrogen, and oxygen determines the heating and cooling processes in molecular clouds (e.g. Genzel 1991). Also important, molecules formed from these elements emit the radiation that traces the extent of molecular clouds. Radio and submillimeter telescopes mostly concentrate on the rotational transition lines of carbon, oxygen and nitrogen molecules (e.g. CO, NH_3 , or H_2O). By now, several hundred different molecules have been identified in the interstellar gas. An overview of the application of different molecules as tracers for different physical conditions can be found in the reviews by van Dishoeck *et al.* (1993), Langer *et al.* (2000), van Dishoeck & Hogerheijde (2000).

4.1.2 Density and Velocity Structure of Molecular Clouds

Emission line observations of molecular clouds reveal clumps and filaments on all scales accessible by present day telescopes. Typical parameters of different regions in molecular clouds are listed in Table 4.1, adopted from Cernicharo (1991). The mass spectrum of clumps in molecular clouds appears to be well described by a power law, indicating self-similarity: there is no natural mass

¹Metallicity is usually defined as the fraction of heavy elements relative to hydrogen. It averages over local variations in the abundance of the different elements caused by varying chemical enrichment histories.

or size scale between the lower and upper limits of the observations. The largest molecular structures considered to be single objects are giant molecular clouds (GMCs), which have masses of 10^5 to $10^6 M_\odot$, and extend over a few tens of parsecs. The smallest observed structures are protostellar cores with masses of a few solar masses or less and sizes of $\lesssim 10^{-2}$ pc, and less-dense clumps of similar size. The volume filling factor of dense clumps, even denser subclumps and so on, is of the order of 10% or less. Star formation always occurs in the densest regions within a cloud, so only a small fraction of molecular cloud matter is actually involved in building up stars, while the bulk of the material remains at lower densities.

The density structure of molecular clouds is best seen in the column density of dust, which can be observed via its thermal emission at millimeter wavelengths in dense regions (e.g. Testi & Sargent 1998, Motte, André, & Neri 1998), or via its extinction of background stars in the infrared, if a uniform screen of background stars is present (Lada *et al.* 1994, Alves, Lada, & Lada 2001). The latter method relies on the near-IR color excess to measure column densities, which ensures a much greater dynamic range than optical extinction. This method has been further developed by Cambrésy *et al.* (2002) who use an adaptive grid to extract maximum information from non-uniform background star fields. It turns out that the higher the column density in a region, the higher the variation in extinction among stars behind that region (Lada *et al.* 1994). Padoan & Nordlund (1999) demonstrated this to be consistent with a super-Alfvénic turbulent flow, while Alves *et al.* (2001) modeled it with a single cylindrical filament with density $\rho \propto r^{-2}$. Because turbulence forms many filaments, it is not clear that these two descriptions are actually contradictory (P. Padoan, 2001, private communication), although the identification of a single filament would then suggest that a minimum scale for the turbulence has been identified.

A more general technique is optically thin spectral lines. The best candidates are ^{13}CO and C^{18}O , though CO freezes out in the very densest

regions with visual extinctions above $A_V \simeq 10$ magnitudes (Alves, Lada, & Lada, 1999). Molecular line observations are therefore only sensitive to gas at relatively low densities and are limited in dynamic range to at most two decades of column density. Nevertheless, the development of sensitive radio receivers in the 1980's first made it feasible to map an entire molecular cloud region with high spatial and spectral resolution to obtain quantitative information about the overall density structure.

The hierarchy of clumps and filaments spans all observable scales (e.g. Falgarone, Puget, & Perault 1992, Falgarone & Phillips 1996, Wiesemeyer *et al.* 1997) extending down to individual protostars studied with mm-wavelength interferometry (Ward-Thompson *et al.* 1994, Langer *et al.* 1995, Gueth *et al.* 1997, Motte *et al.* 1998, Testi & Sargent 1998, Ward-Thompson, Motte, & André 1999, Bacmann *et al.* 2000, Motte *et al.* 2001). This is illustrated by Figure 4.1, which shows ^{13}CO , ^{12}CO and C^{18}O maps of a region in the Cygnus OB7 complex at three levels of successively higher resolution (from Falgarone *et al.* 1992). At each level, the molecular cloud appears clumpy and highly structured. When observed with higher resolution, each clump breaks up into a filamentary network of smaller clumps. Unresolved features exist even at the highest resolution. The ensemble of clumps identified in this survey covers a mass range from about $1 M_\odot$ up to a few $100 M_\odot$ and densities $50 \text{ cm}^{-3} < n(\text{H}_2) < 10^4 \text{ cm}^{-3}$. These values are typical for all studies of cloud clump structure, with higher densities being reached primarily in protostellar cores.

The distribution of clump masses is consistent with a power law of the form

$$\frac{dN}{dm} \propto m^\alpha, \quad (4.1)$$

with $-1.3 < \alpha < -1.9$ in molecular line studies (Carr 1987, Stutzki & Güsten 1990, Lada, Bally, & Stark 1991, Williams, de Geus, & Blitz 1994, Onishi *et al.* 1996, Kramer 1998, Heithausen *et al.* 1998). Dust continuum studies, which pick out the densest regions, find steeper values of $-1.9 < \alpha < -2.5$ (Testi & Sargent 1998,

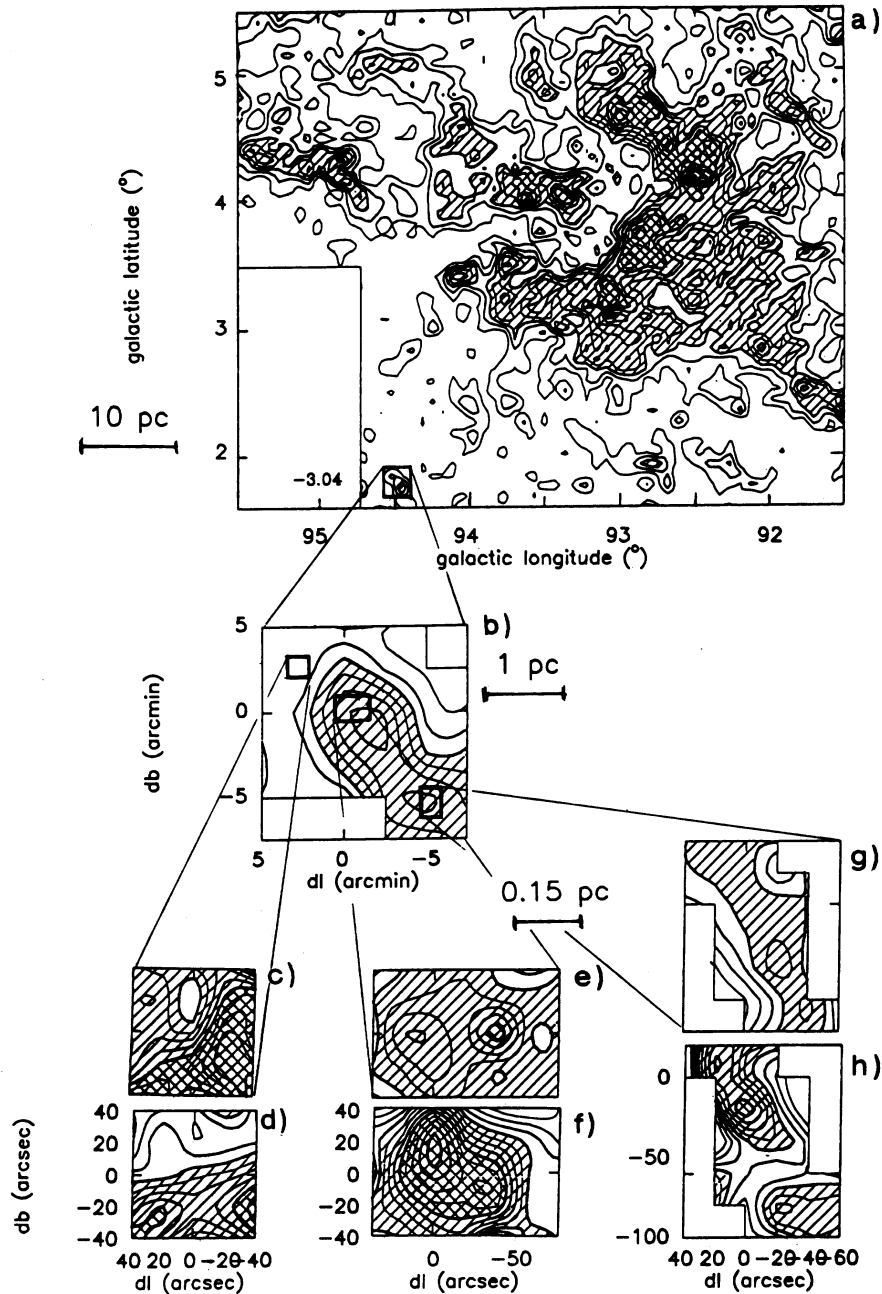


Figure 4.1: Maps of the molecular gas in the Cygnus OB7 complex. (a) Large scale map of the ^{13}CO ($J = 1 - 0$) emission. The first level and the contour spacing are 0.25 K. (b) Map of same transition line of a sub-region with higher resolution (first contour level and spacing are 0.3 K). Both maps are obtained using the Bordeaux telescope. (c) ^{12}CO ($J = 1 - 0$) and (d) ^{13}CO ($J = 1 - 0$) emission from the most transparent part of the field. (e) ^{13}CO ($J = 1 - 0$) and (f) C^{18}O ($J = 1 - 0$) emission from the most opaque field. (g) ^{13}CO ($J = 1 - 0$) and (h) C^{18}O ($J = 1 - 0$) emission from a filamentary region with medium density. The indicated linear sizes are given for a distance to Cygnus OB7 of 750 pc. (The figure is from Falgarone *et al.* 1992).

Table 4.1: Physical properties of interstellar clouds

	GIANT CULAR COMPLEX	MOLE- CLOUD	MOLECULAR CLOUD	STAR- FORMING CLUMP	PROTO- STELLAR CORE ^a
Size (pc)	10 – 60		2 – 20	0.1 – 2	$\lesssim 0.1$
Density ($n(\text{H}_2)/\text{cm}^3$)	100 – 500		$10^2 - 10^4$	$10^3 - 10^5$	$> 10^5$
Mass (M_\odot)	$10^4 - 10^6$		$10^2 - 10^4$	$10 - 10^3$	0.1 – 10
Line width (km s^{-1})	5 – 15		1 – 10	0.3 – 3	0.1 – 0.7
Temperature (K)	7 – 15		10 – 30	10 – 30	7 – 15
Examples	W51, W3, M17, Orion-Monoceros, Taurus-Auriga- Perseus complex		L1641, L1630, W33, W3A, B227, L1495, L1529		see Section 4.3

^a Protostellar cores in the "prestellar" phase, i.e. before the formation of the protostar in its interior.

Motte *et al.* 1998, see also the discussion in Osenkoff *et al.* 2001) similar to the stellar mass spectrum. The power-law mass spectrum is often interpreted as a manifestation of fractal density structure (e.g. Elmegreen & Falgarone 1996). However, the full physical meaning remains unclear. In most studies molecular cloud clumps are determined either by a Gaussian decomposition scheme (Stutzki & Güsten 1990) or by the attempt to define (and separate) clumps following density peaks (Williams *et al.* 1994). There is no one-to-one correspondence between the identified clumps in either method, however. Furthermore, molecular clouds are only seen in projection, so one only measures surface density instead of volume density. Even when velocity information is taken into account, the real three-dimensional structure of the cloud remains elusive. In particular, it can be demonstrated in models of interstellar turbulence that single clumps identified in a position-position-velocity space tend to separate into several clumps in real three-dimensional space (Ballesteros-Paredes & Mac Low 2002). This projection effect in particular may render clump mass spectra improper statistical tools for characterizing molecular cloud structure.

Other means to quantify the structural and dynamical properties of molecular clouds involve

correlations and probability distribution functions (PDF's) of dynamical variables. Two-point correlation functions have been studied by many authors, including Scalo (1984), Kleiner & Dickman (1987), Kitamura *et al.* (1993), Miesch & Bally (1994), LaRosa, Shore & Magnani (1999), and Ballesteros-Paredes, Vázquez-Semadeni, & Goodman (2002), while other studies have concentrated on analyzing the PDFs of the column density in observations, both physical and column density in computational models, and of dynamical observables such as the centroid velocities of molecular lines and their differences. The density PDF has been used to characterize numerical simulations of the interstellar medium by Vázquez-Semadeni (1994), Padoan, Nordlund, & Jones (1997), Passot, & Vázquez-Semadeni (1998), Scalo *et al.* (1998), and Klessen (2000). Velocity PDFs for several star-forming molecular clouds have been determined by Miesch & Scalo (1995) and Miesch, Scalo & Bally (1999). Lis *et al.* (1996, 1998) analyzed snapshots of a numerical simulation of mildly supersonic, decaying turbulence (without self-gravity) by Porter, Pouquet, & Woodward (1994) and applied the method to observations of the ρ -Ophiuchus cloud. Altogether, the observed PDFs exhibit strong non-Gaussian features, often being nearly exponential with possible evidence for power-law tails

in the outer parts. Further methods to quantify molecular cloud structure involve spectral correlation methods (Rosolowsky *et al.* 1999), principal component analysis (Heyer & Schloerb 1997), or pseudometric methods used to describe and rank cloud complexity (Wiseman & Adams 1994, Adams & Wiseman 1994).

A technique especially sensitive to the amount of structure on different spatial scales is wavelet analysis (e.g. Gill & Henriksen 1990; Langer, Wilson, & Anderson 1993). In particular, the Δ -variance, introduced by Stutzki *et al.* (1998), provides a good separation of noise and observational artifacts from the real cloud structure. For isotropic systems its slope is directly related to the spectral index of the corresponding Fourier power spectrum. It can be applied in an equivalent way both to observational data and hydrodynamic and MHD turbulence simulations, allowing a direct comparison, as discussed by Mac Low & Ossenkopf (2000), Bensch, Stutzki, & Ossenkopf (2001), and Ossenkopf & Mac Low (2002). They find that the structure of low-density gas in molecular clouds is dominated by large-scale modes and, equivalently, the velocity field by large-scale motions. This means that molecular cloud turbulence is likely to be driven from the outside, by sources acting external to the cloud on scales of at least several tens of parsec (Ossenkopf & Mac Low 2002). The observational findings are different, however, when focusing on high-density gas in star forming regions. In this case, the Δ -variance clearly shows that the density structure is dominated by individual protostellar cores at the smallest resolved scales (Ossenkopf, Klessen, & Heitsch 2001). This effect is best seen in dust emission maps as these are able to trace large density contrasts. Alternatively, dust extinction maps may also prove to be useful in giving high resolution and tracing large density contrasts (see e.g. Alves *et al.* 2000 for the Bok globule B68; or Padoan, Cambr esy, & Langer 2002 for the Taurus molecular cloud). Molecular line observations are only sensitive to gas at relatively low densities, so they mainly trace the gas between protostellar cores: no signs of collapse appear in Δ -variance analyses of line maps (Os-

senkopf *et al.* 2001).

4.1.3 Support of Molecular Clouds

Molecular clouds are cold (e.g. Cernicharo 1991). The kinetic temperature inferred from molecular line ratios is typically about 10 K for dark, quiescent clouds and dense cores in GMCs which are shielded from UV radiation by high column densities of dust, while it can reach 50 – 100 K in regions heated by UV radiation from high-mass stars. For example, the temperature of gas and dust behind the Trapezium cluster in Orion is about 50 K. In cold regions, the only heat source is cosmic rays, while cooling comes from emission from dust and the most abundant molecular species. The thermal structure of the gas is related to its density pattern and its chemical abundance, so it is remarkable that over a wide range of gas densities and metallicities the equilibrium temperature remains almost constant in a small range around $T \approx 10$ K (Goldsmith & Langer 1978, Goldsmith 2001). The approximation of isothermality only breaks down when the cloud becomes opaque to cooling radiation so that heat can no longer be radiated away efficiently, which occurs when the gas density $n(\text{H}_2) > 10^{10} \text{ cm}^{-3}$. The equation of state then moves from isothermal with polytropic exponent $\gamma = 1$ to adiabatic, with $\gamma \sim 7/5$ being appropriate for molecular hydrogen (see e.g. Tohline 1982 and references therein).

Because of their low temperatures, GMCs were traditionally claimed to be gravitationally bound (Kutner *et al.* 1977; Elmegreen, Lada, & Dickinson 1979; Blitz 1993; Williams *et al.* 2000). Their masses are orders of magnitude larger than the critical mass for gravitational stability M_J defined by Equation (2.3), computed from the average density and temperature. However, if only thermal pressure opposed gravitational attraction, they should be collapsing and very efficiently forming stars on a free-fall timescale, which is roughly $\tau_{\text{ff}} \approx 10^6$ years, Equation (1.1). That is not the case. Within molecular clouds low-mass gas clumps appear highly transient and pressure confined rather than being bound by self-gravity.

This is the case only for the most massive individual cores. These are the sites where star formation actually is observed (Williams, Blitz, & Stark 1995; Yonekura *et al.* 1997; Kawamura *et al.* 1998; Simon *et al.* 2001).

Molecular cloud lifetimes are estimated to lie between several 10^6 up to a few 10^7 years (see Section 5.2 for detailed discussion). With such short lifetimes, molecular clouds are likely never to reach a state of dynamical equilibrium (Ballesteros-Paredes *et al.* 1999; Elmegreen 2000). This is in contrast to the classical picture which sees molecular clouds as long-lived equilibrium structures (Blitz & Shu 1980). The overall star formation efficiency on scales of molecular clouds as a whole is low in our Galaxy, of order of 10% or smaller.

Except maybe on scales of isolated protostellar cores, the observed line widths are always wider than implied by the excitation temperature of the molecules. This is interpreted as the result of bulk motion associated with turbulence. We argue in this review that it is the interstellar turbulence that determines the lifetime and fate of molecular clouds, and that regulates their ability to collapse and form stars.

Magnetic fields have long been discussed as a stabilizing agent in molecular clouds. However, magnetic fields with average field strength of $10 \mu\text{G}$ (Verschuur 1995a,b; Troland *et al.* 1996) are not sufficient to stabilize molecular clouds as a whole. This is in particular true on scales of individual protostars where magnetic fields appear too weak to hold gravitational collapse in essentially all cases observed (see Section 2.4). Furthermore, magnetic fields are not capable of preventing turbulent velocity fields from decaying quickly (see e.g. Figure 2.9 and its discussion). It appears that the role of magnetic fields in stabilizing giant molecular clouds as a whole is less important than assumed in the standard theory (Section 2.3). The conclusion is, that molecular cloud turbulence must at least be partially driven by some energy source to have molecular clouds survive over several dynamical timescales and to explain the observed low star formation efficien-

cies on scales of molecular clouds as a whole². For a further discussion of possible driving mechanisms for interstellar turbulence see Section 5.1.

4.1.4 Scaling Relations for Molecular Clouds

Observations of molecular clouds exhibit correlations between various properties, such as clump size, velocity dispersion, density and mass. Larson (1981) first noted, using data from several different molecular cloud surveys, that the density ρ and the velocity dispersion σ appear to scale with the cloud size R as

$$\rho \propto R^\alpha \quad (4.2)$$

$$\sigma \propto R^\beta, \quad (4.3)$$

with α and β being constant scaling exponents. Many studies have been done of the scaling properties of molecular clouds. The most commonly quoted values of the exponents are $\alpha \approx -1.15 \pm 0.15$ and $\beta \approx 0.4 \pm 0.1$ (e.g. Dame *et al.* 1986, Myers & Goodman 1988, Falgarone *et al.* 1992, Fuller & Myers 1992, Wood, Myers, & Daugherty 1994, Caselli & Myers 1995). However, the validity of these scaling relations is the subject of strong controversy and significantly discrepant values have been reported by Carr (1987) and Loren (1989), for example.

The above standard values are often interpreted in terms of the virial theorem (Larson 1981, Caselli & Myers 1995). If one assumes virial equilibrium, Larson's relations (Equations 4.2 and 4.3) are not independent. For $\alpha = -1$, which implies constant column density, a value of $\beta = 0.5$ suggests equipartition between self-gravity and the turbulent velocity dispersion, that is that the ratio between kinetic and potential energy is constant with $K/|W| = \sigma^2 R / (2GM) \approx 1/2$. Note, that for

²Note that on scales of individual star forming regions the efficiency to convert molecular cloud material into stars can be very high and reach values up to 50%. Only a small fraction of molecular cloud material associated with high-density regions is involved in the star formation process. The bulk of molecular cloud matter is in 'inactive' tenous state between individual star forming regions.

any arbitrarily chosen value of the density scaling exponent α , a corresponding value of β obeying equipartition can always be found (Vázquez-Semadeni & Gazol 1995). Equipartition is usually interpreted as indicating virial equilibrium in a static object. However, Ballesteros-Paredes *et al.* (1999b) pointed out that in a dynamic, turbulent environment, the other terms of the virial equation (McKee & Zweibel 1992) can have values as large as or larger than the internal kinetic and potential energy. In particular, the changing shape of the cloud will change its moment of inertia, and turbulent flows will produce large fluxes of kinetic energy through the surface of the cloud. As a result, rough equipartition between internal kinetic and potential energy does not necessarily imply virial equilibrium.

Furthermore, Kegel (1989) and Scalo (1990) proposed that the density-size relation may be a mere artifact of the limited dynamic range in the observations, rather than reflecting a real property of interstellar clouds. In particular, in the case of molecular line data, the observations are restricted to column densities large enough that the tracer molecule is shielded against photodissociating UV radiation. Also, with limited integration times, most CO surveys tend to select objects of roughly constant column density, which automatically implies $\rho \propto R$. Surveys that use larger integration times and therefore have larger dynamic range seem to exhibit an increasingly larger scatter in density-size plots, e.g. as seen in the data of Falgarone *et al.* (1992). Results from numerical simulations, which are free from observational bias, indicate the same trend (Vázquez-Semadeni, Ballesteros-Paredes, & Rodríguez 1997). Three-dimensional simulations of supersonic turbulence (Mac Low 1999) were used by Ballesteros-Paredes & Mac Low (2002) to perform a comparison of clumps measured as density enhancements in physical space to clumps measured column density enhancements in simulated observational space (position-velocity). They found no relation between density and size in physical space, but a clear trend of $\rho \propto R$ in the simulated observations, caused simply by the tendency of clump-finding algorithms to pick out

clumps with column densities close to the local peak values.

There are two other concerns. The proportionality between line integrated CO intensity and molecular mass surface density has been reliably established only for extragalactic observations (Dickman, Snell, & Schloerb 1986). This relationship is only valid for scales larger than a few parsec, at which calibration has been possible. Also it depends on the assumption of virialization of the gas (e.g. Genzel 1991), and local thermodynamic equilibrium. Padoan *et al.* (2000) demonstrated that the assumption of local thermodynamic equilibrium can lead to underestimates of the actual column density in turbulent molecular clouds by factors of up to 7. Additionally, for clumps within molecular clouds, the structures identified in CO often do not correspond to those derived from higher-density tracers (see e.g. Langer *et al.* 1995, Bergin *et al.* 1997, Motte *et al.* 1998 for observational discussion, and Ballesteros-Paredes & Mac Low 2002 for theoretical discussion). Altogether, the existence of a unique density-size relation and its astrophysical meaning is not well established.

The velocity-size relation does not appear to be so prone to observational artifacts. However, many measurements of molecular clouds do not exhibit this correlation (e.g. Loren 1989, or Plume *et al.* 1997). If it is detected in a molecular cloud, it probably is a real property of the cloud that may be explained by a number of physical mechanisms, ranging from the standard (though incomplete) argument of virial equilibrium to the action of interstellar turbulence. In supersonic turbulent flows, however, the scaling relation is a natural consequence of the characteristic energy spectrum in an ensemble of shocks, even in the complete absence of self-gravity (Ossenkopf & Mac Low 2002, Ballesteros-Paredes & Mac Low 2002, Boldyrev, Nordlund, & Padoan 2002).

4.2 Star Formation in Molecular Clouds

All giant molecular clouds surveyed within distances less than 3 kpc form stars (Blitz 1993,

Williams *et al.* 2000), except possibly the Madalena & Thaddeus (1985) cloud (Lee, Snell, & Dickman 1996; Williams & Blitz 1998). However this cloud may have formed just recently. The star formation process in molecular clouds appears to be fast. Once the collapse of a cloud region sets in, it rapidly forms an entire cluster of stars within 10^6 years or less. This is indicated by the young stars associated with star forming regions, typically T Tauri stars with ages less than 10^6 years (e.g. Gomez *et al.* 1992, Green & Meyer 1996, Carpenter *et al.* 1997, Hartmann 2001), and by the small age spread in more evolved stellar clusters (e.g. Hillenbrand, Palla & Stahler 1999, 2001).

Star-forming molecular cloud regions in our Galaxy can vary enormously in size and mass. In small, low-density, regions stars form with low efficiency, more or less in isolation or scattered around in small groups of up to a few dozen members. Denser and more massive regions may build up stars in association and clusters of a few hundred members. This appears to be the most common mode of star formation in the solar neighborhood (Adams & Myers 2001). Examples of star formation in small groups and associations are found in the Taurus-Aurigae molecular cloud (e.g. Hartmann 2002). Young stellar groups with a few hundred members form in the Chamaeleon I dark cloud (e.g. Persi *et al.* 2000) or ρ -Ophiuchi (Bontemps *et al.* 2001). Each of these clouds is at a distance of about 130 to 160 pc from the Sun. Many nearby star forming regions have been associated with a ring-like structure in the Galactic disk called Gould's belt (Pöppel 1997), although its reality remains somewhat uncertain.

The formation of dense rich clusters with thousands of stars is rare. The closest molecular cloud region where this happens is the Orion Nebula Cluster in L1641 (Hillenbrand 1997; Hillenbrand & Hartmann 1998), which lies at a distance of ~ 450 pc. A rich cluster somewhat further away is associated with the Monoceros R2 cloud (Carpenter *et al.* 1997) at a distance of ~ 830 pc. The cluster NGC 3603 is roughly ten times more massive than the Orion Nebula Cluster. It lies in the Carina region, at about 7 kpc distance. It contains about a dozen O stars, and is the nearest

object analogous to a starburst knot (Brandl *et al.* 1999, Moffat *et al.* 2002). To find star-forming regions that capable of forming hundreds of O stars one has to look towards giant extragalactic HII-regions, the nearest of which is 30 Doradus in the Large Magellanic Cloud, a satellite galaxy of our Milky Way at a distance at 55 kpc (for an overview see the book by Chu *et al.* 1999). The giant star forming region 30 Doradus is thought to contain up to a hundred thousand young stars, including more than 400 O stars (Hunter *et al.* 1995; Walborn *et al.* 1999). Even more massive star forming regions are associated with tidal knots in interacting galaxies, as observed in the Antennae (NGC 4038/8, see e.g. Zhang, Fall, & Whitmore 2001) or as inferred for starburst galaxies at high redshift (Sanders & Mirabel 1996).

This sequence demonstrates that the star formation process spans many orders of magnitude in scale, ranging from isolated single stars ($M \approx 1 M_{\odot}$) to ultra-luminous starburst galaxies with masses of several $10^{11} M_{\odot}$ and star formation rates of 10^2 – $10^3 M_{\odot} \text{ yr}^{-1}$; for comparison the present-day rate in the Milky Way is about $1 M_{\odot} \text{ yr}^{-1}$. This enormous variety of star forming regions appears to be controlled by the competition between self-gravity and the turbulent velocity field in interstellar gas. When turbulence dominates, or at least carries sufficient energy on small scales to prevent collapse, the star formation process is inefficient and slow, and stars build up in small groups only. If turbulent gas motions are weak, or dominated by large-scale modes, stars can form in clusters with locally high efficiency, since gravity can overwhelm turbulence locally. The larger the volume where gravity dominates over turbulent kinetic energy, the larger and more massive the stellar cluster that will form. In starburst galaxies, self-gravity may overwhelm kinetic energy on scales of several kpc.

Numerical simulations of self-gravitating, turbulent clouds demonstrate that the *length scale* and *strength* of energy injection into the system determine the structure of the turbulent flow, and therefore the locations at which stars are most likely to form. Large-scale driving leads to large

coherent shock structures (e.g. figure 2.15a). Local collapse occurs predominantly in filaments and layers of shocked gas and is very efficient in converting gas into stars (Klessen *et al.* 2000). Even more so, this applies to regions of molecular gas that have become decoupled from energy input. As turbulence decays, these regions begin to contract and form dense clusters or associations of stars with very high efficiency on about a free-fall time scale (Klessen *et al.* 1998, Klessen & Burkert 2000, 2001). The same holds for insufficient support, i.e. for regions where energy input is not strong enough to completely balance gravity. They too will contract to form dense stellar clusters.

On the other hand, a more isolated mode of star formation occurs in regions that are supported by driving sources that act on *small* scales, and in an incoherent or stochastic manner. In this case, individual, shock-induced, density fluctuations form at random locations and evolve more or less independently of each other. The resulting stellar population is widely dispersed throughout the cloud and, since collapsing clumps are frequently destroyed by shock interaction, the overall star formation rate is low.

These points are illustrated in Figure 4.2., which shows the distribution of collapsed cores in several models with strong enough turbulence to formally support against collapse. Coherent, efficient local collapse occurs in model B1, where the turbulence is driven strongly at long wave lengths (compare with Figure 2.15). Incoherent, inefficient collapse occurs in model B3, on the other hand, where turbulence is driven at small scales. Individual cores form independently of each other at random locations and random times, are widely distributed throughout the entire volume, and exhibit considerable age spread. In the decaying turbulence model, once the kinetic energy level has decreased sufficiently, all spatial modes of the system contract gravitationally, including the global ones (Klessen 2000). As in the case of large-scale shock compression, stars form more or less coevally in a limited volume with high efficiency.

Despite the fact that both turbulence driven on

large scales and freely decaying turbulence lead to star formation in aggregates and clusters, Figure 4.3 suggests a possible way to distinguish between them. Decaying turbulence typically leads to the formation of a bound stellar cluster, while aggregates associated with large-scale, coherent, shock fronts often have higher velocity dispersions that result in their complete dispersal. Note, however, that at the late stages of dynamical evolution shown in Figure 4.3, our model becomes less appropriate, as feedback from newly formed stars is not included. Ionization and outflows from the stars formed first will likely retard or even prevent the accretion of the remaining gas onto protostars, possibly preventing a bound cluster from forming even in the case of freely decaying turbulence.

The control of star formation by supersonic turbulence gives rise to a continuous but articulated picture. There may not be physically distinct modes of star formation, but qualitatively different behaviors do appear over the range of possible turbulent flows. The apparent dichotomy between a clustered mode of star formation and an isolated, as discussed by Lada (1992) for L1630 and Strom, Strom, & Merrill (1993) for L1941, disappears, if a different balance between turbulent strength and gravity holds at the relevant length scales in these different clouds.

Turbulent flows tend to have hierarchical structure (e.g. She & Leveque 1994) which may explain the hierarchical distribution of stars in star forming regions shown by statistical studies of the distribution of neighboring stars in young stellar clusters (e.g. Larson 1995; Simon 1997; Bate, Clarke, & McCaughrean 1998, Nakajima *et al.* 1998; Gladwin *et al.* 1999; Klessen & Kroupa 2001). Hierarchical clustering seems to be a common feature of all star forming regions (e.g. Efremov & Elmegreen 1998). It may be a natural outcome of turbulent fragmentation.

4.3 Properties of Protostellar Cores

Protostellar cores are the direct precursors of stars. The properties of young stars are thus inti-

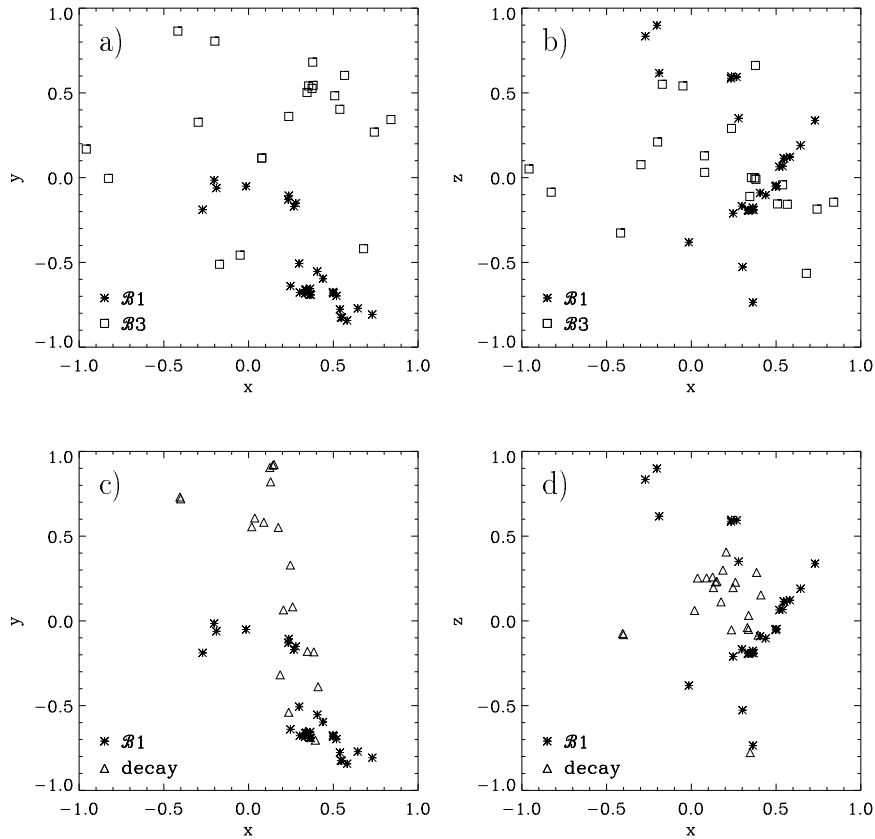


Figure 4.2: Comparison of collapsed core locations between two globally stable models with different driving wavelength projected into (a) the xy -plane and into (b) the xz -plane. $B1$ with $k = 1 - 2$ is driven at large scales, and $B3$ with $k = 7 - 8$ is driven at small ones. Plots (c) and (d) show the core locations for model $B1$ now contrasted with a simulation of decaying turbulence from Klessen (2000). The snapshots are selected such that the mass accumulated in dense cores is $M_* \lesssim 20\%$. Note the different times needed for the different models to reach this point. For model $B1$ data are taken at $t = 1.1$, for $B3$ at $t = 12.3$. The simulation of freely decaying turbulence is shown at $t = 1.1$. All times are normalized to the global free-fall time scale of the system. (From Klessen *et al.* 2000.)

mately related to the properties of their parental clumps and it is therefore important to observationally determine the characteristics of condensed cores in molecular clouds. A number of such small, dense molecular cores have been identified by low angular resolution, molecular line surveys of nearby dark clouds (e.g. Benson & Myers 1989). These cores are thought to be the sites of low-mass star formation. About half of them are associated with low-luminosity IRAS sources and CO outflows, the other half is designated as ‘starless’ or ‘prestellar’ (e.g. Beichman *et al.* 1986, André *et al.* 2000). Those may be in a evolutionary state shortly before forming stellar objects in their interior, thus they often are referred to as pre-stellar cores. One of the most

notable properties of the sampled cores are their very narrow line widths. These are very close to the line widths expected for thermal broadening alone and, as a result, many of the cores appear approximately gravitationally virialized (e.g. Myers 1983). They are thought either to be in the very early stage of gravitational collapse or have subsonic turbulence supporting the clump. A comparison of the line widths of cores with embedded protostellar objects (i.e. with associated IRAS sources) and the ‘starless’ cores reveals a substantial difference. Typically, cores with infrared sources exhibit broader lines, which suggests the presence of a considerable turbulent component not present in ‘starless’ cores. This may be caused by the central protostar feeding

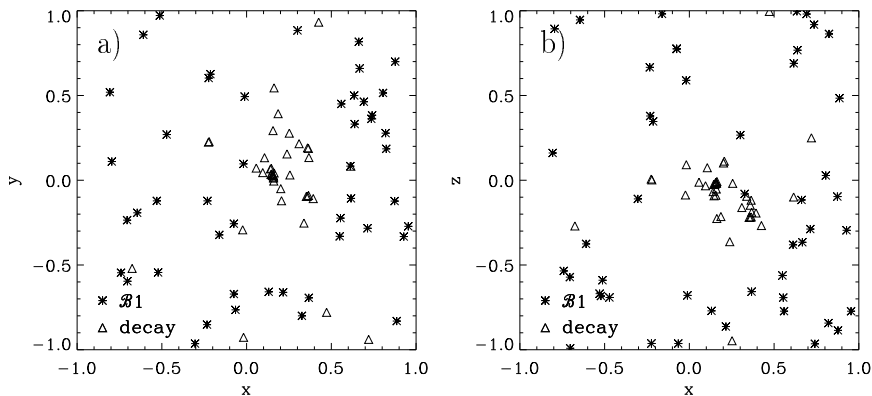


Figure 4.3: Core positions for model $\mathcal{B}1$ ($k = 1 - 2$) and the decay model when the core mass fraction is $M_* \approx 65\%$, projected into (a) the xy -plane and (b) the xz -plane (compare with Figure 4.2c & d). For $\mathcal{B}1$ the time is $t = 8.7$ and for decay model $t = 2.1$. Whereas the cluster in $\mathcal{B}1$ is completely dissolved and the stars are widely dispersed throughout the computational volume, the cluster in the decay simulation remains bound. (From Klessen *et al.* 2000.)

back energy and momentum into its surrounding envelope. Molecular outflows associated with many of the sources may be direct indication for this process. The first submillimeter continuum maps of dense pre-stellar cores were made by Ward-Thompson *et al.* (1994). By now many different star forming clouds have been surveyed (e.g. ρ -Ophiuchi: Motte *et al.* 1998, Johnstone *et al.* 2000; NGC 2068/2071: Motte *et al.* 2001; Orion: Johnstone & Bally 1999, Mitchell *et al.* 2001). The authors of this high-resolution studies found that ‘starless’ cores are larger and less centrally condensed than the cores with embedded sources. But both groups appear to have similar masses. Altogether, the ‘starless’ cores are probable the precursors of class 0 protostellar clumps and may reflect the very early stages of protostellar collapse: a gravitationally bound fragment has formed in a molecular cloud which evolves towards progressively higher degree of central condensation, but has not yet formed a hydrostatic protostar in the center (i.e. a class 0 object). The ‘starless’ cores are observed in the mass range from about $0.1 M_\odot$ to $10 M_\odot$. Typical line widths are 0.4 km s^{-1} in NH_3 and 0.6 km s^{-1} in C^{18}O for cores with embedded sources and 0.3 km s^{-1} in NH_3 and 0.5 km s^{-1} in C^{18}O for pre-stellar cores with embedded sources (e.g. Butner, Lada, & Loren 1995). For comparison, a gas temperature of 10 K corresponds to a thermal line

width of 0.16 km s^{-1} for NH_3 and 0.12 km s^{-1} for C^{18}O . High-resolution maps suggest that the radial density profiles of the pre-stellar cores on average follow a $1/r^2$ -law but are relatively steep towards their edges and flatten out near their centers (see e.g. Figure 2.5). Furthermore, their 2-dimensional shapes deviate quite considerably from spherical symmetry, as illustrated in Figure 4.4. The cores are elongated with ratios between semi-major and semi-minor axis of about 2 – 3; some even appear completely irregular.

The observed core properties can be compared with cores identified in numerical models of interstellar cloud turbulence. Like their astronomical counterparts, model clumps are generally highly distorted and triaxial. Depending on the projection angle, they often appear extremely elongated, being part of a filamentary structure which may appear as a chain of connecting, elongated individual clumps. Figure 4.5 plots a selection of model clumps from Klessen & Burkert (2000). Cores that already formed a protostellar object in their interior are plotted on the left, on the right “starless” core without central protostar are shown. Note the similarity to the appearance of observed protostellar cores (Figure 4.4). It is clearly visible that the clumps are very elongated. The ratios between the semi-major and the semi-minor axis measured at the second contour level are typically between 2:1 and 4:1. However, there

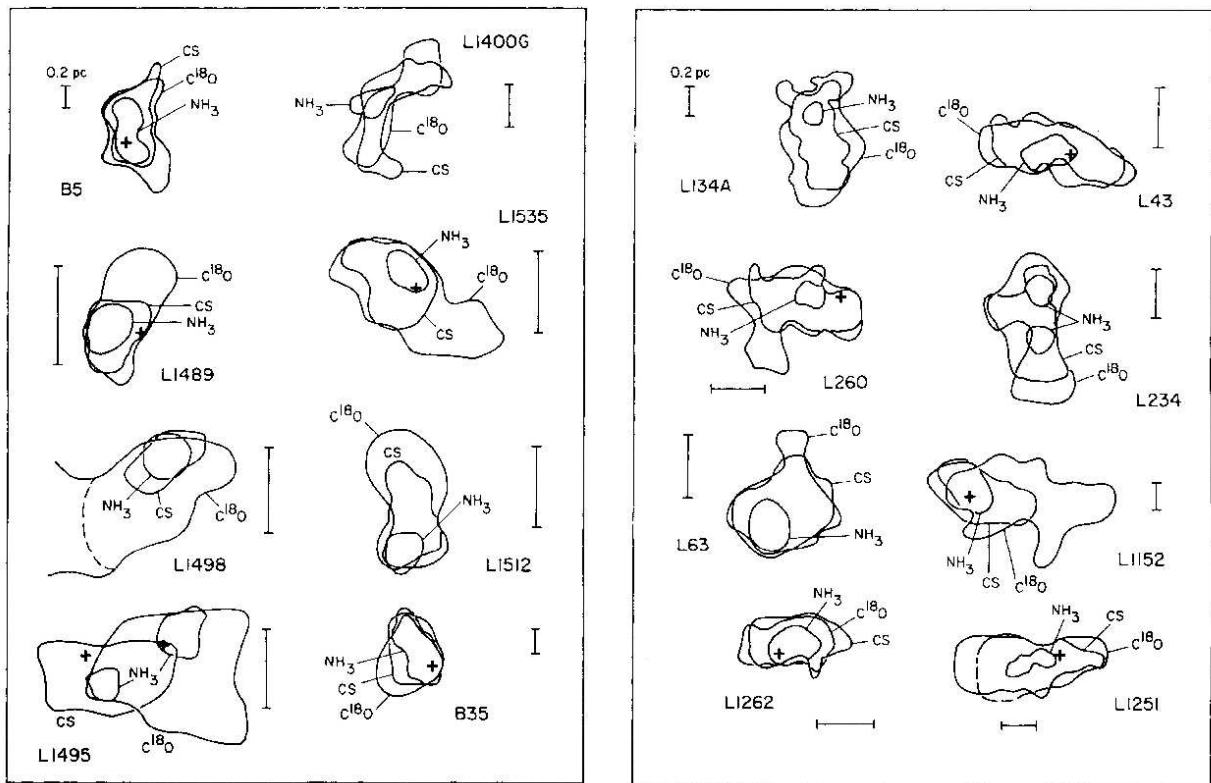


Figure 4.4: Intensity contours at half maximum of 16 dense cores in dark clouds, in the 1.3 cm $(J, k) = (1, 1)$ lines of NH_3 , in the 3.0 mm $J = 2 \rightarrow 1$ line of CS, and the 2.7 mm $J = 1 \rightarrow 0$ line of C^{18}O . A linear scale of 0.2 pc is indicated in each individual map and associated protostars are specified by a cross. The figure is from Myers *et al.* 1991.

may be significant deviations from simple triaxial shapes, see e.g. clump #4 which is located at the intersection of two filaments. This clump is distorted by infalling material along the filaments and appears 'y'-shaped when projected into the xz -plane. As a general trend, high density contour levels typically are regular and smooth, because there the gas is mostly influenced by pressure and gravitational forces. On the other hand, the lowest level samples gas that is strongly influenced by environmental effects. Hence, it appears patchy and irregular. The location of the condensed core within a clump is not necessarily identical with the center-of-mass of the clump, especially in irregularly shaped clumps.

Typically, the overall density distribution of identified clumps in our simulations follows a power law and the density increases from the outer regions inwards to the central part as $\rho(r) \propto 1/r^2$. For clumps that contain collapsed cores, this dis-

tribution continues all the way to the central protostellar object. However, for clumps that have not yet formed a collapsed core in their center, the central density distribution flattens out. This is a generic property and is illustrated in Figure 4.6, which has to be compared with radial profiles of observed cores (see Figure 2.5). The agreement is remarkable. It is a natural prediction of turbulent fragmentation that stars form from cores with initially flat inner density profile, follow by a power-law decline with moderate slope (~ -2) at intermediate radii, and which is finally truncated at some maximum radius (i.e. may be approximated by a power-law slope $\ll -2$ beyond that radius).

The surface density profiles of many observed protostellar cores are often claimed to be matched by fitting quasi-equilibrium Bonnor-Ebert spheres (Ebert 1955, Bonnor 1956). The best example is the Bok globule B68 (Alves *et al.*

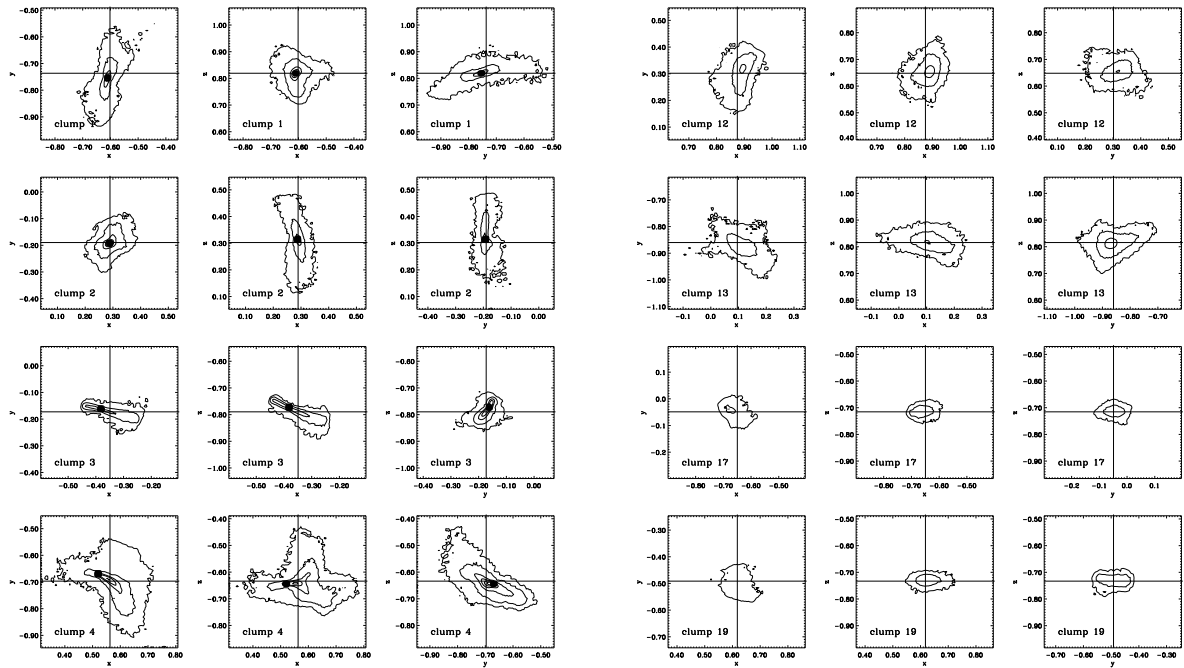


Figure 4.5: Protostellar cores from a model of clustered star formation. The left side depicts protostellar cores with collapsed central object (indicated by a black dot), the right side “starless” cores without protostar. Cores are numbered according to their peak density. Surface density contours are spaced logarithmically with two contour levels spanning one decade, $\log_{10} \Delta\rho = 0.5$. The lowest contour is a factor of $10^{0.5}$ above the mean density. (From Klessen & Burkert 2000.)

2001). Ballesteros-Paredes, Klessen, & Vázquez-Semadeni (2002) argue that turbulent fragmentation produces cores that are in $\sim 3/5$ of all cases well fit by Bonnor-Ebert profiles, of which most ($\sim 4/5$) again imply stable equilibrium conditions. However, none of the cores analyzed by Ballesteros-Paredes *et al.* (2002) are actually equilibrium configurations, but instead are dynamically evolving, because supersonic turbulence cannot create hydrostatic equilibrium structures (Vázquez-Semadeni *et al.* 2002). The method of fitting BE profiles to observed cores to derive their physical properties therefore appears unreliable (see also Boss & Hartmann 2002).

The density profile predicted by supersonic turbulence describes the properties of observed prestellar cores very well. However, it could in principle also be reproduced by models where molecular gas clumps are confined by helical magnetic fields (Fiege & Pudritz 2000a,b). But helical field structures would tend to unwind, as magnetic fields have the tendency to “straighten”

themselves out. Therefore these models require external forces to continuously exert strong torques. These forces need to be strong to be able to twist the field lines, thus they would necessarily induce considerable gas motions and make it impossible to achieve the static equilibrium configurations required for the model to work. The hypothesis of static helical magnetic fields being responsible for the observed properties of prestellar cores therefore appears not viable. Other models that have been proposed to describe the properties of protostellar cores are based quasi-static equilibrium conditions (e.g. with composite polytropic equation of state, as discussed by Curry & McKee 2000), or invoke thermal instability (e.g. Yoshii & Sabano 1980, Gilden 1984b, Graziani & Black 1987, Burkert & Lin 2000), gravitational instability through ambipolar diffusion (e.g. Basu & Mouschovias 1994, Nakamura, Hanawa, & Nakano 1995, Indebetouw & Zweibel 2000, Ciolek & Basu 2000), or nonlinear Alfvén waves (e.g. Carlberg & Pudritz 1990, Elmegreen

1990, 1997a, 1999b), or rely on clump collisions (e.g., Gilken 1984a, Murray & Lin 1996, Kimura & Tosa 1996). Altogether models based on supersonic turbulence as discussed here appear to be the ones most consistent with observational data.

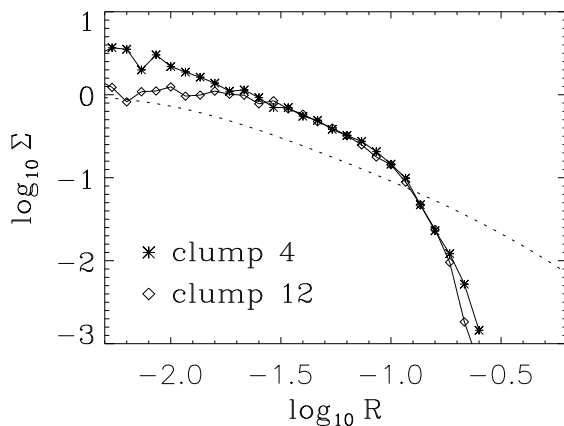


Figure 4.6: Radial surface density profiles for the xz -projection of cores 4 and 12 in Figure 4.5. For the “starless” core 12 the density profile flattens out at small radii, whereas for core 4 it continues as $1/r^2$ all the way towards the center. The density profile of a singular isothermal sphere (with $\rho \propto 1/r^2$) is indicated by the dotted line for comparison. (From Klessen & Burkert 2000.)

Besides the direct comparison of projected surface density maps as discussed in this section, there is ample additional evidence supporting the idea of the turbulent origin of the structure and kinematics of molecular cloud cores and clouds as a whole. It comes for example from comparing numerical models of supersonic turbulence with (1) stellar extinction measurements (Padoan *et al.* 1997), (2) Zeeman splitting measurements (e.g. Padoan & Nordlund 1999), (3) polarization maps (e.g. Padoan *et al.* 2001a), (4) Faraday rotation measurements (e.g. Heitsch *et al.* 2001b, Ostriker, Stone, & Gammie 2001), (5) determination of the velocity structure of dense cores and their immediate environment (e.g. Padoan *et al.* 2001b), or (6) various other statistical measures of structure and dynamics of observed clouds as mentioned in Section 4.1).

4.4 Dynamical Interactions in Clusters

Star forming regions can differ enormously in scale and density as a consequence of supersonic turbulence (as discussed in Section 4.2). Stars almost never form in isolation, but instead in groups and clusters. The number density of protostars and protostellar cores in rich compact clusters can be high enough for mutual dynamical interaction to become important. This has important consequences for the mass growth history of individual stars and the subsequent dynamical evolution of the nascent stellar cluster, because this introduces a further degree of stochasticity to the star formation process in addition to the statistical chaos associated with turbulence and turbulent fragmentation in the first place.

When a molecular cloud region of a few hundred solar masses or more coherently become gravitationally unstable, it will contract and build up a dense cluster of embedded protostars within one or two free-fall timescales. While contracting individually to build up a protostar in their interior, individual protostellar gas clumps still follow the global flow patterns. They stream towards a common center of attraction, may undergo further fragmentation or more likely merge together. The timescales for clump mergers or clump collapse are comparable. Merged clumps therefore may contain multiple protostars now compete with each other for further accretion. They are now embedded in the same limited and rapidly changing reservoir of contracting gas. As the cores are dragged along with the global gas flow, quickly a dense cluster of accreting protostellar cores builds up. Analogous to dense stellar clusters, the dynamical evolution is subject to the complex gravitational interaction between the cluster members, close encounters or even collisions may occur and drastically alter the orbital parameters of protostars. Triple or higher-order systems are likely to form. They are generally unstable and consequently a considerable fraction of protostellar cores becomes expelled from the parental cloud. The expected

complexity of protostellar dynamics already in the deeply embedded phase of evolution is illustrated in Figure 4.7, which shows trajectories of five accreting protostars in a calculation of molecular cloud fragmentation and clustered star formation by Klessen & Burkert (2000).

The effects of mutual dynamical interaction of protostellar cores in the embedded phase of star cluster formation have been investigated by a variety of authors. Here, we list some basic results.

(a) Close encounters in nascent star clusters will influence the accretion disk expected to surround every protostar. These disks may be tidally truncated or even be disrupted. This influences mass accretion through the disk, modify the ability to subfragment and form a binary star, and/or the probability of planet formation (e.g. Clarke & Pringle 1991; Murray & Clarke 1993 ; McDonald & Clarke 1995; Hall *et al.* 1996; Scally & Clarke 2001; Kroupa & Burkert 2001; Smith & Bonnell 2001; Bonnell *et al.* 2001c). In particular, Ida, Larwood, & Burkert (2000) note that an early stellar encounter may explain features of our own solar system, namely the high eccentricities and inclinations observed in the outer part of the Edgeworth-Kuiper Belt at distances larger than 42 AU.

(b) Stellar systems with more than two members are in general are unstable. In a triple system, for example, the lowest-mass member has the highest probability to be expelled. If this happens in the embedded phase, the protostar leaves a region of high-density gas. This terminates further mass growth and sets its final mass. Thus, the dynamical processes have important consequences for the resulting stellar mass spectrum in dense stellar clusters. This will be discussed in Section 4.7. Ejected objects can travel quite far, and indeed this has been suggested to account the so called “run away” T-Tauri stars found in X-ray observation in the vicinities of star-forming molecular clouds (e.g. Sterzik & Durison 1995, 1998, Smith *et al.* 1997; Klessen & Burkert 2000; or for observations e.g. Neuhäuser *et al.* 1995; or Wichmann *et al.* 1997). However, it is not clear whether the observed extended stellar popula-

tion is associated with any currently star forming cloud. These stars may be as old as 100 Myr and may have formed in clouds that long have been dispersed by now. Also, many of these stars could not have traveled to their observed positions if associated with the currently star-forming cloud unless it were extremely long lived.

(c) Dynamical interaction leads to mass segregation. Star clusters evolve towards equipartition. For massive stars this means that they have on average smaller velocities than low-mass stars (in order keep the kinetic energy $K = 1/2 mv^2 \approx \text{constant}$). Thus, massive stars “sink” towards the cluster center, while low-mass stars will predominantly populate large cluster radii. (e.g. Kroupa 1995,a,b,c). This holds already for nascent star clusters in the embedded phase (e.g. Bonnell & Davis 1998).

(d) Dynamical interaction and competition for mass accretion lead to highly time-variable protostellar mass growth rates. This will be discussed in more detail in Section 4.5.

(e) The radii of stars in the pre-main sequence contraction phase are several times larger than stellar radii on the main sequence (for a review on pre-main sequence evolution see, e.g., Palla 2000, 2002). Stellar collisions are therefore more likely to occur during in very early evolution of star clusters. During the embedded phase the encounter probability is further increased by gas drag and dynamical friction. Collisions in dense protostellar clusters have therefore been proposed as mechanism to produce massive stars (Bonnell, Bate, & Zinnecker 1998; Stahler, Palla, & Ho 2000). The formation of massive stars has long been considered a puzzle in theoretical astrophysics, because one-dimensional calculations predict for stars above $\sim 10 M_{\odot}$ the radiation pressure acting on the infalling dust grains to be strong enough to halt or even revert further mass accretion (e.g. Yorke & Krügel 1977; Wolfire & Cassinelli 1987; or Palla 2000, 2001). However, detailed two-dimensional calculations by Yorke & Sonnhalter (2002) demonstrate that in the more realistic scenario of mass growth via an accretion disk the radiation barrier may be overcome. Mass

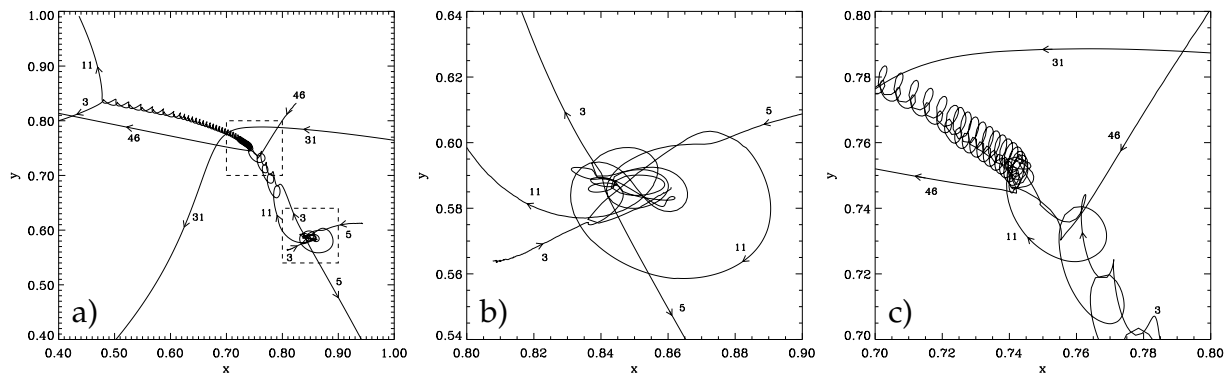


Figure 4.7: Example of protostellar interactions in an embedded nascent star cluster. Figure (a) shows the projected trajectories of five accreting cores in a numerical model of star cluster formation by Klessen & Burkert (2000). For illustration purpose neither the trajectories of other cores in the cluster nor the distribution of gas is depicted. We highlight two events in the evolutionary sequence, (b) the formation of an unstable triple system at the beginning of cluster formation with the lowest mass member being expelled from the cluster, and (c) binary hardening in a close encounter together with subsequent acceleration of the resulting close binary due to another distant encounter during late evolution. The corresponding parts of the orbital paths are enlarged by a factor of six. Numbers next to the trajectory identify the protostellar core. For further detail see Klessen & Burkert (2000).

can accrete from the disk onto the star along the equator while radiation is able to escape along the polar direction. Massive stars, thus, may form via the same processes as ordinary low-mass stars. Collisional processes need not to be invoked.

4.5 Accretion Rates

When a gravitationally unstable gas clump collapses to build up the central star, it follows an observationally well determined sequence. Prior to the formation of a hydrostatic nucleus, an observed pre-stellar condensation exhibits a density structure which has a flat inner part, then decreases outward roughly as $\rho \propto r^{-2}$, and is truncated at some finite radius (e.g. Bacmann *et al.* 2000). Once the central YSO builds up, the class 0 phase is reached and the density follows $\rho \propto r^{-2}$ down to the observational resolution limit. As larger and larger portions of the infalling envelope get accreted the protostar is identified as a class I object, and when accretion fades away it enters the T Tauri phase (e.g. André, Ward-Thompson, & Barsony 2000). In the main accretion phase, the energy budget is dominated

by the release of gravitational energy in the accretion process. Hence, protostars exhibit large IR and sub-mm luminosities and drive powerful outflows. Both phenomena can be used to estimate the protostellar mass accretion rate \dot{M} ; and observations suggest that \dot{M} varies strongly and declines with time. Accretion is largest in the class 0 phase and drops significantly in the subsequent evolution (e.g. André & Montmerle 1994, Bontemps *et al.* 1996, Henriksen, André, & Bontemps 1997). The estimated lifetimes are a few 10^4 years for the class 0 and a few 10^5 years for the class I phase.

These observational findings favor a dynamical description of the star formation process (e.g. Larson 1969, Penston 1969a, Hunter 1977, Henriksen *et al.* 1997, Basu 1997), but raise doubts about the "inside-out" scenario of the collapse of quasi-static isothermal spheres (Shu 1977) which predicts a constant accretion rate (Section 2.3; see Section 2.4 for a critical discussion). As the analytical studies, most numerical work of protostellar core collapse (e.g. Foster & Chevalier 1993, Tomisaka 1996, Ogino, Tomisaka, & Nakamura 1999, Wuchterl & Tscharnuter 2002) concentrates on isolated objects. However, stars predominantly form in groups and clusters. Numerical

studies that investigate the effect of the cluster environment on protostellar mass accretion rates are reported for example by Bonnell *et al.* (1990, 2001a,b), Klessen & Burkert (2000, 2001), Klessen *et al.* (2001), Heitsch *et al.* (2001), Klessen (2001a).

Klessen (2001a) considers the dynamical evolution of a molecular cloud regions with $200 M_{\odot}$ in a volume $(0.32 \text{ pc})^3$ where turbulence is assumed to have decayed and left behind random Gaussian fluctuations in the density structure. As the system contracts gravitationally, a cluster of 56 protostellar cores builds up on a timescale of about two to three free-fall times. These types of numerical models allow for the following predictions on protostellar accretion rates in dense clusters:

(a) Protostellar accretion rates in a dense cluster environment are strongly time variable. This is illustrated in Figure 4.8 for 49 randomly selected cores.

(b) The typical density profiles of gas clumps that give birth to protostars exhibit a flat inner core, followed by a density fall-off $\rho \propto r^{-2}$, and are truncated at some finite radius, which in the dense centers of clusters often is due to tidal interaction with neighboring cores (see Section 4.3 and Section 4.4). As result, a short-lived initial phase of strong accretion occurs when the flat inner part of the pre-stellar clump collapses. This corresponds to the class 0 phase of protostellar evolution. If these cores were to remain isolated and unperturbed, the mass growth rate would gradually decline in time as the outer envelope accretes onto the center. This is the class I phase. Once the truncation radius is reached, accretion fades and the object enters the class II phase. This behavior is expected from analytical models (e.g. Henriksen *et al.* 1997) and agrees with other numerical studies (e.g. Foster & Chevalier 1993). However, collapse does not start from rest for the density fluctuations considered here, and the accretion rates exceed the theoretically predicted values even for the most isolated objects in the simulation.

(c) The mass accretion rates of cores in a dense cluster deviate strongly from the rates of isolated

cores. This is a direct result of the mutual dynamical interaction and competition between protostellar cores. While gas clumps collapse to build up protostars, they may merge as they follow the flow pattern towards the cluster potential minimum. The timescales for both processes are comparable. The density and velocity structure of merged gas clumps generally differs significantly from their progenitor clumps, and the predictions for isolated cores are no longer valid. More importantly, these new larger clumps contain multiple protostars, which subsequently compete with each other for the accretion from a common gas reservoir. The most massive protostar in a clump is hereby able to accrete more matter than its competitors (also Bonnell *et al.* 1997, Klessen & Burkert 2000, Bonnell *et al.* 2001a,b). Its accretion rate is enhanced through the clump merger, whereas the accretion rate of low-mass cores typically decreases. Temporary accretion peaks in the wake of clump mergers are visible in abundance in Figure 4.8. Furthermore, the small aggregates of cores that build up are dynamically unstable and low-mass cores may be ejected. As they leave the high-density environment, accretion terminates and their final mass is reached.

(d) The most massive protostars begin to form first and continue to accrete at high rate throughout the entire cluster evolution. As the most massive gas clumps tend to have the largest density contrast, they are the first to collapse and constitute the center of the nascent cluster. These protostars are fed at high rate and gain mass very quickly. As their parental clumps merge with others, more gas is fed into their 'sphere of influence'. They are able to maintain or even increase the accretion rate when competing with lower-mass objects (e.g. core 1 and 8 in Figure 4.8). Low-mass stars, on average, tend to form somewhat later in the dynamical evolution of the system (as indicated by the absolute formation times in Figure 4.8; also Figure 8 in Klessen & Burkert 2000), and typically have only short periods of high accretion.

(e) As high-mass stars are associated with large core masses, while low-mass stars come from low-mass cores, the stellar population in clusters

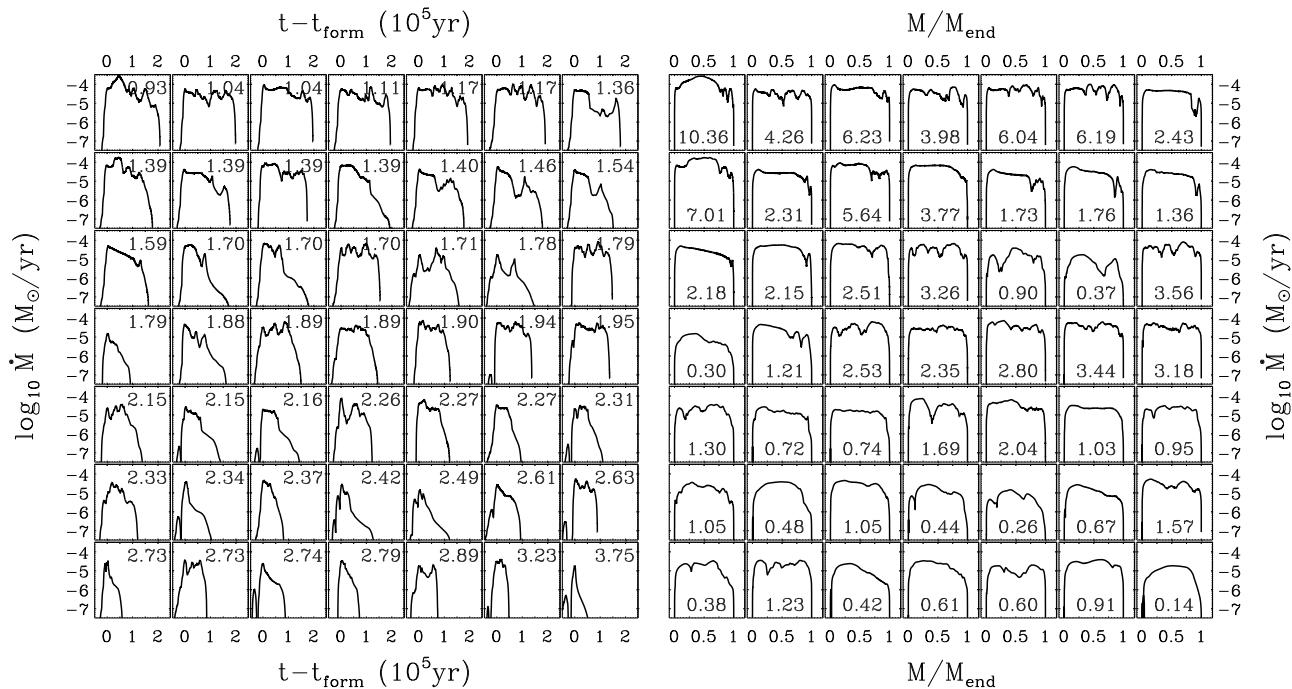


Figure 4.8: Examples of time varying mass accretion rates for protostellar cores forming in a dense cluster environment. The left panel shows accretion rate \dot{M} versus time after formation $t - t_{\text{form}}$ for 49 randomly selected protostellar cores in a numerical model of molecular cloud fragmentation from Klessen & Burkert (2000). Formation time t_{form} is defined by the first occurrence of a hydrostatic protostellar object deeply embedded in the interior of a collapsing gas clump. To link individual accretion histories to the overall cluster evolution, t_{form} is indicated in the upper right corner of each plot and measures the elapsed time since the start of the simulation. The free-fall timescale of the considered molecular region is $\tau_{\text{ff}} \approx 10^5$ years. High-mass stars tend to form early in the dynamical evolution and are able to maintain high accretion rates throughout the entire simulation. On the contrary, low-mass stars tend to form later in the cluster evolution and \dot{M} declines strongly after the short initial peak accretion phase. Altogether, the accretion histories of cores (even of those with similar masses) differ dramatically from each other due to the stochastic influence of the cluster environment, as clumps merge and protostellar cores compete for accretion from a common gaseous environment. The right panel plots for the same cores \dot{M} as function of the accreted mass M with respect to the final mass M_{end} , which is indicated in the center of each plot. Note that the mass range spans two orders of magnitude. (From Klessen 2001a.)

is predicted to be mass segregated right from the beginning. High-mass stars form in the center, lower-mass stars tend to form towards the cluster outskirts. This is in agreement with recent observational findings for the cluster NGC330 in the Small Magellanic Cloud (Sirianni *et al.* 2002). Dynamical effects during the embedded phase of star cluster evolution will enhance this initial segregation even further (see Section 4.4.c).

(f) Individual cores in a cluster environment form and evolve through a sequence of highly probabilistic events, therefore, their accretion histories differ even if they accumulate the same final mass. Accretion rates for protostars of certain mass can only be determined in a statistical sense.

The model predicts that an exponentially declining rate with a peak value of a few $10^5 M_{\odot} \text{ yr}^{-1}$, a time constant in the range 0.5 to $2.5 \times 10^5 \text{ yr}$, and a cut-off related to gas dispersal from the cluster offers a reasonable fit to the typical protostellar mass growth in dense embedded clusters with uncertainties, however, that remain high (see Figure 4.9).

4.6 Protostellar Evolutionary Tracks

In this review, we argue that stars are born in interstellar clouds of molecular hydrogen with

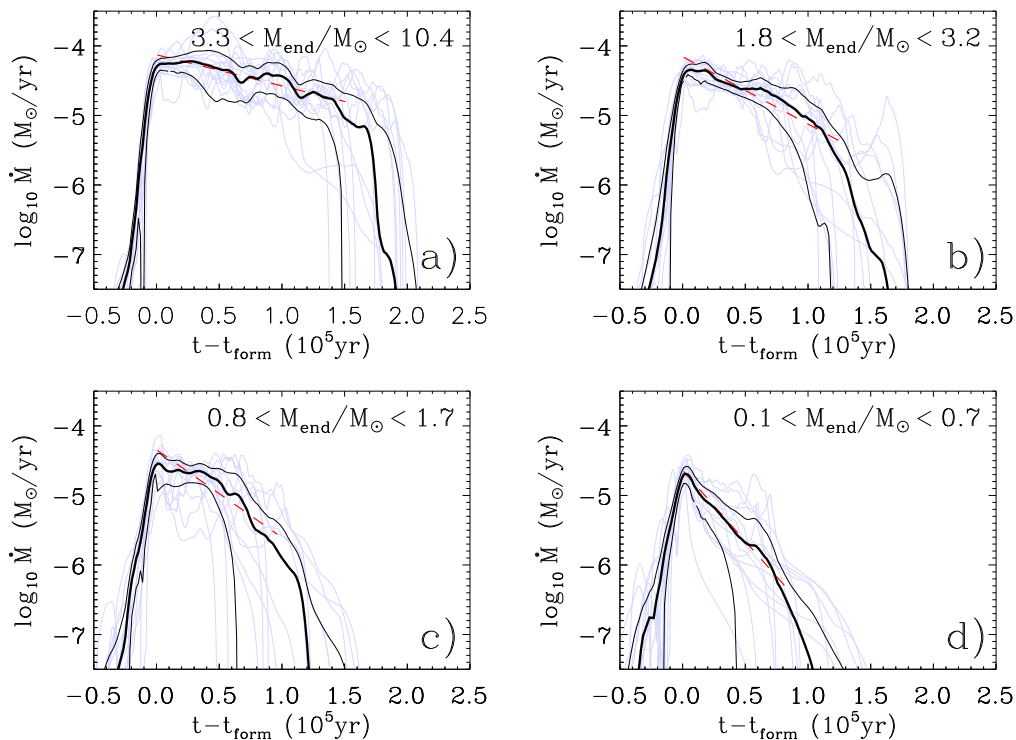


Figure 4.9: Averaged mass accretion rate $\langle \dot{M} \rangle$ (thick line) as function of time relative to core formation $t - t_{\text{form}}$ for four different mass bins (ranging from high to low masses as denoted in the top section of each plot) overlaid on the contributing individual accretion histories. The mean absolute deviation from $\langle \dot{M} \rangle$ is indicated by thin lines. An exponential approximation to $\langle \dot{M} \rangle$ is indicated by the dashed line. (From Klessen 2001a.)

the mass growth rates intimately coupled to the dynamical cloud environment. Once a prestellar core becomes gravitationally unstable, it begins to collapse giving birth to a protostar. While the structure of molecular clouds is well studied observationally (see Section 4.1), our knowledge about intrinsic properties of these youngest stars relies almost entirely on theoretical stellar models. These models give ages, masses and radii when brightness, distance and effective temperature are known (e.g. Palla 2000, 2002). The so determined ages constitute the only practical ‘clock’ for tracing the history of star-formation regions and for studying the evolution of circumstellar disks and planet formation. They constitute the basis of our empirical understanding of the evolution of the young Sun and the origin of solar systems.

Until recently (Wuchterl & Tscharnuter 2003) it was necessary to *assume* a set of initial conditions for the stars at very young ages (typically at a few 10^5 years) in order to calculate the properties at

larger ages. Usually the internal thermal structure of the star is estimated at a moment when the dynamical infall motions from the cloud are thought to have faded and the stellar contraction is sufficiently slow, so that pressure forces balance gravity. Then hydrostatic equilibrium is a good approximation. Young star properties are therefore usually calculated without considering gravitational cloud collapse and protostellar accretion in detail. See, however, Winkler & Newman (1980a,b), but also Hartmann, Cassen & Kenyon (1997) for a discussion of the possible effects of accretion. Altogether, classical PMS calculations typically assume fully convective initial conditions as argued for by Hayashi (1961).

However, it can be shown that the assumption of fully convective stellar structure *does not* result from the collapse of isolated, marginally gravitationally unstable, isothermal, hydrostatic equilibrium, so called ‘Bonnor-Ebert’ spheres (Wuchterl & Tscharnuter 2003). Hence, early stellar evolution theory has to be reconsidered. This has

been done by Wuchterl & Klessen (2001), who presented the first calculation of the properties of the new born star as being a member of a cluster of protostars forming from the fragmentation of a highly-structured molecular cloud, and followed in detail the collapse of a one solar mass fragment until it becomes observable in the visible light. These calculations demonstrated that the newly born star shows the trace of the fragmentation and collapse process during its main accretion phase and the early hydrostatic pre-main sequence (PMS) contraction. At an age of a million years, however, its properties are almost identical for quiet and turbulent cloud conditions.

4.6.1 Dynamical PMS Calculations

Wuchterl & Klessen (2001) considered a molecular cloud region where turbulence is decayed and has left behind density fluctuations characterized by a Gaussian random field which follows a power spectrum $P(k) \propto 1/k^2$ (as discussed in Klessen & Burkert 2000). To describe molecular cloud fragmentation, they solved the equations of hydrodynamics using a particle based method (SPH — smoothed particle hydrodynamics, see Benz 1990, or Monaghan 1992) in combination with the special-purpose hardware device GRAPE (GRAVITY PIPE, see Sugimoto *et al.* 1990, Ebisuzaki *et al.* 1993), focusing on a sub-region of the cloud with mass $196 M_{\odot}$ and size $(0.32 \text{ pc})^3$ and adopting periodic boundary conditions (Klessen 1997). With a mean density of $n(\text{H}_2) = 10^5 \text{ cm}^{-3}$ and temperature $T = 10 \text{ K}$, the simulated volume contained 222 thermal Jeans masses. To be able to continue the calculation beyond the formation of the first collapsing object, compact cores had been replaced by ‘sink’ particles (Bate *et al.* 1995) once they exceed a density of $n(\text{H}_2) = 10^9 \text{ cm}^{-3}$, where we keep track of the mass accretion, and the linear and angular momenta. The ‘sink’ particle size defined the volume of a detailed collapse calculation. The system is gravitationally unstable and begins to form a cluster of 56 protostellar cores (as illustration see Figure 1), corresponding to the ‘clustered’ mode of star formation (Sections 2.5.4 and 4.2).

Besides that specific choice of the initial molecular cloud conditions, the only free parameters that remain in this dynamical star formation model are introduced by the time-dependent convection-model, needed to describe stellar structure in a ‘realistic’ way. These parameters are determined as usual in stellar structure theory by demanding agreement between the model-solution and the actual solar convection zone as measured by helioseismology.

Aiming to describe the birth and the first million years of the Sun, Wuchterl & Klessen (2001) selected from the 3D cloud simulation that protostellar core with final mass closest to $1 M_{\odot}$ and use its mass accretion history (see Section 4.5) to determine the mass flow into a spherical control volume centered on the star. For the stellar mass range considered here feedback effects are not strong enough to halt or delay accretion into this protostellar ‘feeding zone’. Thus, the core accretion rates are good estimates for the actual stellar accretion rates. Deviations may be expected only if the protostellar cores form a binary star, where the infalling mass must be distributed between two stars, or if very high-angular momentum material is accreted, where a certain mass fraction may end up in a circumbinary disk and not accrete onto a star at all. For single stars matter accreting onto a protostellar disk may be temporarily ‘stored’ in the disk before getting transported onto the star. The flow *within* the control volume is calculated by solving the equations of radiation hydrodynamics (RHD) in the grey Eddington approximation and with spherical symmetry (Castor 1972, Mihalas & Mihalas 1984), in their integral form (Winkler & Norman 1986). At any time it is required that the total mass in the volume agrees with the 3D fragmentation calculation. Convective energy transfer and mixing is treated by using a time-dependent convection scheme (Wuchterl & Feuchtinger 1998) derived from the model of Kuhfuß (1987) and including detailed equations of state and opacities. Deuterium burning processes are computed with standard reaction rates (Caughlan & Fowler 1988) including convective mixing. The 1D-RHD calculation covers a spherical volume of radius

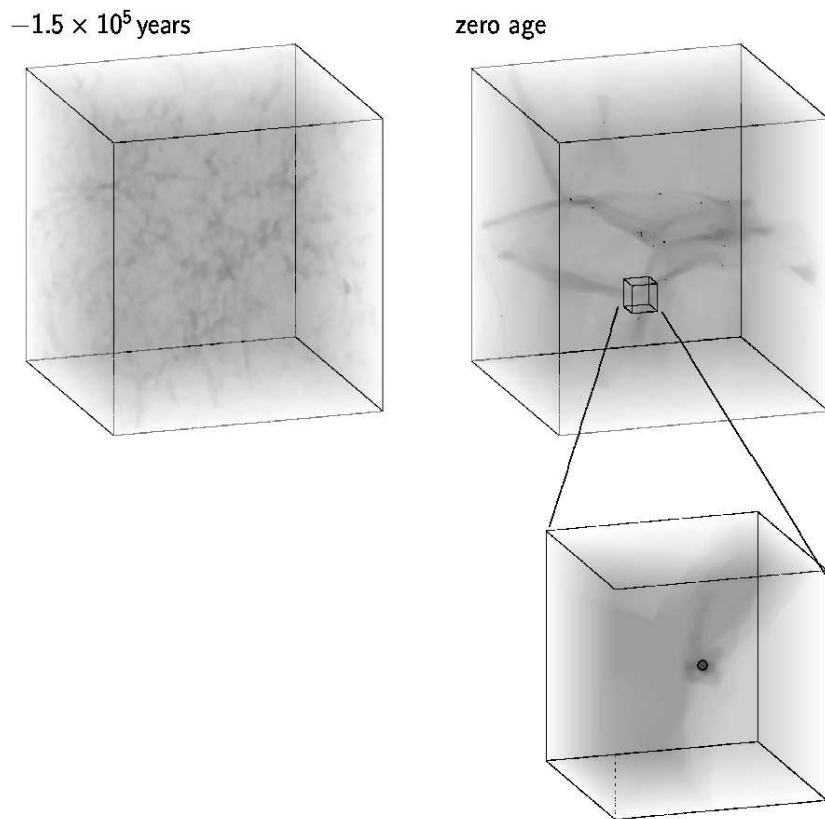


Figure 4.10: The 3D density distribution of the dynamical molecular cloud fragmentation calculation at two different times (model \mathcal{I} of KB00, KB01). As we cannot treat the whole cloud, we focus on a sub-volume of mass $196 M_{\odot}$ and size $(0.32 \text{ pc})^3$. The left image depicts the initial random Gaussian fluctuation field, and the central image shows the system when the young proto-Sun reaches stellar zero age (i.e. when the cloud core for the first time becomes optically thick). During this 1.5×10^5 year period local collapse occurs and a cluster of deeply embedded and heavily accreting pre- and protostellar condensations begins to build up (i.e. objects without and with central hydrostatic core). The region where the proto-solar condensation forms is shown enlarged on the right-hand side. The volume considered in the 1D-RHD simulation is indicated by the circle. — Adopted from Wuchterl & Klessen (2001).

$R = 160 \text{ AU} = 2.46 \times 10^{15} \text{ cm}$ and contains a mass $0.028 M_{\odot}$ at $t = 0$. The calculation started 1.5×10^5 years before the moment of stellar zero age, with a mass $2 \times 10^{-5} M_{\odot}$. The final mass of the star is $0.971 M_{\odot}$.

4.6.2 Formation of a $1 M_{\odot}$ -Star

The fragment we have chosen is highlighted in the 3D cloud structure in Figure 4.10 at the moment when it becomes optically thick and departs from isothermality, as determined by the 1D solution. This defines the stellar zero age (Wuchterl & Tscharnuter 2003). The mass accretion rates obtained for the selected fragment are strongly time varying and peak around $1.5 \times 10^{-5} M_{\odot} \text{ yr}^{-1}$ (Section 4.5).

Before reaching zero age, the temperature is close to the initial cloud value of 10 K and densities are still low enough so that the heat produced by the collapse is easily radiated away from the transparent cloud. Once the envelope becomes optically thick, the temperature increases rapidly as the accretion luminosity rises. We determine the effective temperature at the radius where the optical depth $\tau_{\text{Ross}} = 2/3$ (see Baschek, Scholz, & Wehrse 1991 for a careful discussion). Luminosity and temperature for the non-isothermal phase obtained from the 1D-RHD calculation are shown in Figure 4.11. The zero age is marked by a diamond, close to the beginning of the thick line in the lower right of Figure 4.11. For comparison the results of a Bonnor-Ebert-collapse and a classical hydrostatic stellar evolution calculation

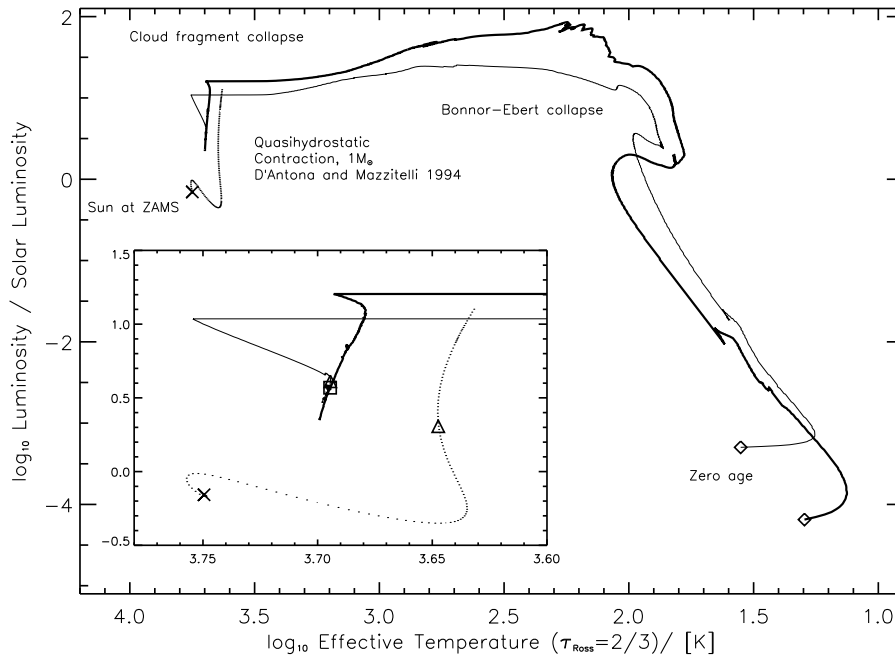


Figure 4.11: Early stellar evolution in the Hertzsprung-Russell diagram. Three evolutionary effective-temperature-luminosity relations (tracks) relevant to the young Sun are compared. The dotted line is a classical stellar structure, hydrostatic-equilibrium PMS track for $1 M_{\odot}$, for an initially fully convective gas sphere (‘MLT Alexander’ model of D’Antona & Mazzitelli 1994). The two other lines are obtained by describing the formation of the star as a result of the collapse of an interstellar cloud. The *thin line* is for a cloud fragment in initial equilibrium (a so called ‘Bonnor-Ebert’ sphere of a solar mass, see Wuchterl & Tscharnuter 2003 for details). The (thick line) is for a cloud fragment that results from the dynamical fragmentation of a molecular cloud (KB00, KB01). The two diamonds, in the lower right, indicate zero age for the two collapse-results. Triangles (Bonnor-Ebert from Wuchterl & Tscharnuter 2003), squares (cluster model from Wuchterl & Klessen 2001) and crosses (D’Antona & Mazzitelli 1994) along the respective evolutionary tracks mark ages of 1, 10, 100, 350 kyr, 0.5 and 1 Myr. The cross at the end of the hydrostatic track denotes the moment when energy generation by nuclear reactions in the stellar interior, for the first time in stellar live *fully* compensates the energy losses due to radiation from the stellar photosphere, i.e. the zero age main sequence (ZAMS). Corresponding age-marks for 0.1, 0.35, 0.5 and 1 Myr are connected by dashed lines in the insert. — Adopted from Wuchterl & Klessen (2001).

(D’Antona & Mazzitelli 1994) are shown as well. The equations used in the latter study correspond to the hydrostatic limit of the current dynamical model, all physical parameters (opacities, etc.) are identical or match closely (see Wuchterl & Tscharnuter 2003).

The non-isothermal phase can be divided into three parts: (1) There is a first luminosity increase up to $20 L_{\odot}$ with the temperature staying below about 100 K. The central density of the fragment rises until a hydrostatic core forms and the accretion flow onto that core is accelerated until quasi-steady state is established. (2) The subsequent main accretion phase leads to an increase in temperature to 2000 K while the luminosity shows a broad maximum at $\sim 100 L_{\odot}$. Com-

pared to the isolated ‘Bonnor-Ebert case’ the violent accretion in the cluster-environment produces a considerably higher luminosity, and the oscillations around maximum reflect the variable rates at which mass is supplied to the accreting protostar as it travels through the dynamical environment of the proto-cluster. (3) Once accretion fades, the star approaches its final mass. The stellar photosphere becomes visible and the luminosity decreases at roughly constant temperature. This is the classical pre-main sequence (PMS) contraction phase, shown as a blow up in Figure 4.11. The luminosity decreases at almost constant temperature and the evolutionary tracks are nearly vertical being approximately parallel to the classical ‘hydrostatic’ track.

4.6.3 Implications

The dynamical model allows us to address the question of whether a trace of the initial fragmentation and collapse process can be found once the young star arrives at its final mass and becomes optically visible. Indeed, the star that forms in a dynamical cloud environment is brighter when it reaches the PMS phase compared to the isolated Bonnor-Ebert case. This is due to the higher accretion in the dynamically evolving cluster environment.

As the mass accretion rates of evolving protostars in dense clusters are influenced by mutual stochastic interactions and differ significantly from isolated ones, the positions of stars in the main accretion phase in the HR diagram are not functions of mass and age alone, but also depend on the statistical properties of the protostellar environment. This affects attempts to infer age and mass at this very early phase using bolometric temperatures and luminosities of protostellar cores (see e.g. Myers & Ladd 1993, Myers *et al.* 1998). It is only possible as the statistical average over many different theoretical accretion histories for different cluster environments or for an observational sample of protostars with similar cloud conditions.

As the accretion flow fades away, however, the evolutionary tracks of protostars *converge*, and the memory of environmental and initial conditions is largely lost in the sense that one (final) mass corresponds to one track. For given mass and elemental composition the stellar properties then depend on age only. For our one solar mass stars this happens at 0.95×10^6 years where the effective temperatures become equal and remain within 20 K until the end of the 1D-RHD calculation at 2×10^6 years. However, substantial *differences* remain compared to the classical hydrostatic calculations. The temperature obtained from collapse models is consistently higher by about 500 K compared to classical hydrostatic computations at corresponding luminosities.³

³To indicate the consequences for stellar mass determinations, we point out that during the second million years the temperature of our one solar mass star corresponds to

This deviation is the result of a *qualitatively* different stellar structure (Wuchterl & Tscharnuter 2003). Most notable, the solar mass stars resulting from collapse are *not* fully convective as is assumed in the hydrostatic calculations, instead they do have a radiative core of similar relative size as the present Sun. Convection is confined to a shell in the outer third of the stellar radius. The star builds up from material with increasing entropy as it passes through the accretion shock. Stellar structure along the new dynamical evolutionary tracks can be viewed as homologous to the present Sun rather than to a fully convective structure. Consequently, the proto-Sun does not evolve along the classical Hayashi track for a solar mass star, but roughly parallel to that. It has a higher effective temperature corresponding to the smaller radius of a partially radiative object of the same luminosity as a fully convective one.

As the dynamical PMS tracks converge for the two most extreme assumptions about the stellar environment (dense stellar clusters vs. isolated stars) we predict that a solar mass star at an age of 10^6 years will have a luminosity of $4 \pm 0.4 L_{\odot}$ and an effective temperature of 4950 ± 20 K. The uncertainties reflect the fading traces of the adopted two highly disparate initial and environmental cloud conditions. For identical assumptions made about convection theory and stellar opacities (D'Antona & Mazzitelli 1994), the classical values are $2.0 L_{\odot}$ and 4440 K, respectively.

These prediction are highly controversial and rely on the correctness of the following assumptions: (1) The structure of young stars can be calculated in spherical symmetry, (2) the prescription of convection used is sufficiently accurate outside the regime where it has been tested, i.e. the present-day Sun, and (3) the radiative transfer treatment and especially the present sources

stars with $2 M_{\odot}$ on the classical hydrostatic tracks. The differences in temperature and luminosity equivalently imply corrections for the inferred ages: the 'classical' luminosity at 10^6 years is $6.2 L_{\odot}$, while the corresponding 'collapse' values are smaller, $3.8 L_{\odot}$ and $4.2 L_{\odot}$, respectively. At 2×10^6 years, the new calculations give luminosities of twice the solar value. The 'classical' age for equivalent luminosities is 0.8×10^6 years.

of stellar opacity are sufficiently complete. However, it needs to be pointed out that *all* those assumptions are also made for the classical calculations that we have used for reference (e.g. D'Antona & Mazzitelli 1994, or Palla 2000, 2002).

4.7 Initial Mass Function

The distribution of stellar masses at birth, described by the initial mass function (IMF), is a necessary ingredient for the understanding of many astrophysical phenomena, but no analytic derivation of the observed IMF has yet stood the test of time. In fact, it appears likely that a fully deterministic formula for the IMF does not exist. Rather, any viable theory must take into account the probabilistic nature of the turbulent process of star formation, which is inevitably highly stochastic and indeterministic. We here give a brief overview of the observational constraints on the IMF, followed by a review of models for it.

4.7.1 The Observed IMF

Hydrogen-burning stars can only exist in a finite mass range

$$0.08 \lesssim m \lesssim 100, \quad (4.4)$$

where the dimensionless mass $m \equiv M/(1 M_{\odot})$ is normalized to solar masses. Objects with masses less than about $0.08 M_{\odot}$ do not have central temperatures hot enough for hydrogen fusion to occur. If they are larger than about ten times the mass of Jupiter, $M_J = 0.001 M_{\odot}$, they are called brown dwarfs, or more generally substellar objects (e.g. Burrows *et al.* 1993, Laughlin & Bodenheimer 1993; or for a review Burrows *et al.* 2001). Stars with masses greater than about $100 M_{\odot}$, on the other hand, blow themselves apart by radiation pressure (e.g. Phillips 1994).

It is complicated and laborious to estimate the IMF in our Galaxy empirically. The first such determination from the solar neighborhood (Salpeter 1955) showed that the number $\xi(m)dm$

of stars with masses in the range m to $m + dm$ can be approximated by a power-law relation

$$\xi(m)dm \propto m^{-\alpha}dm, \quad (4.5)$$

with the index $\alpha \approx 2.35$ for stars in the mass range $0.4 \leq m \leq 10$. However, approximation of the IMF with a single power-law is too simple. Miller & Scalo (1979) introduced a log-normal functional form, again to describe the IMF for Galactic field stars in the vicinity of the Sun,

$$\log_{10} \xi(\log_{10} m) = A - \frac{1}{2(\log_{10} \sigma)^2} \left[\log_{10} \left(\frac{m}{m_0} \right) \right]^2. \quad (4.6)$$

This analysis has been repeated and improved by Kroupa, Tout, & Gilmore (1990), who derive values

$$\begin{aligned} m_0 &= 0.23 \\ \sigma &= 0.42 \\ A &= 0.1 \end{aligned} \quad (4.7)$$

The IMF can also be estimated, probably more directly, by studying individual young star clusters. Typical examples are given in Figure 4.12 (taken from Kroupa 2002), which plots the mass function derived from star counts in the Trapezium Cluster in Orion (Hillenbrand & Carpenter 2000), in the Pleiades (Hambly *et al.* 1999) and in the cluster M35 (Barrado y Navascués *et al.* 2001).

The most popular approach to approximating the IMF empirically is to use a multiple-component power-law of the form (4.5) with the following parameters (Scalo 1998, Kroupa 2002):

$$\xi(m) = \begin{cases} 0.26 m^{-0.3} & \text{for } 0.01 \leq m < 0.08, \\ 0.035 m^{-1.3} & \text{for } 0.08 \leq m < 0.5, \\ 0.019 m^{-2.3} & \text{for } 0.5 \leq m < \infty. \end{cases} \quad (4.8)$$

This representation of the IMF is statistically corrected for unresolved binaries and multiple stellar systems. Binary and higher multiple stars can only be identified as such if their angular separation exceeds the angular resolution of the telescope used to survey the sky, or if they are close

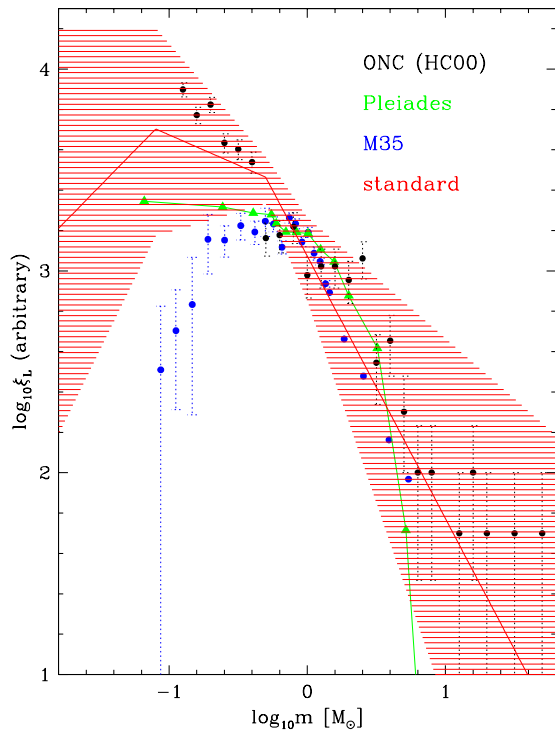


Figure 4.12: The measured stellar mass function ξ as a function of logarithmic mass $\log_{10} m$ in the Orion nebular cluster (solid black circles), the Pleiades (green triangles), and the cluster M35 (blue circles). None of the mass functions is corrected for unresolved multiple stellar systems. The average initial stellar mass function derived from Galactic field stars in the solar neighborhood is shown as red line with the associated uncertainty range indicated by the hatched area. (From Kroupa 2002.)

enough for radial velocity measurements to detect them as spectroscopic binaries. Stars in the middle are falsely counted as single stars. Neglecting this effect overestimates the masses of stars, as well as reducing inferred stellar densities. These mass overestimates influence the derived stellar mass distribution, underestimating the number of low-mass stars. The IMF may steepen further towards high stellar masses and a fourth component could be defined with $\xi(m) = 0.019 m^{-2.7}$ for $m > 1.0$ thus arriving at the IMF proposed by Kroupa, Tout, & Gilmore (1993). In equation (4.8), the exponents for masses $m < 0.5$ are very uncertain due to the difficulty of detecting and determining the masses of very young low-mass stars. The exponent for $0.08 \leq m < 0.5$ could vary between -0.7 and -1.8 , and the value in the substellar regime is even less certain.

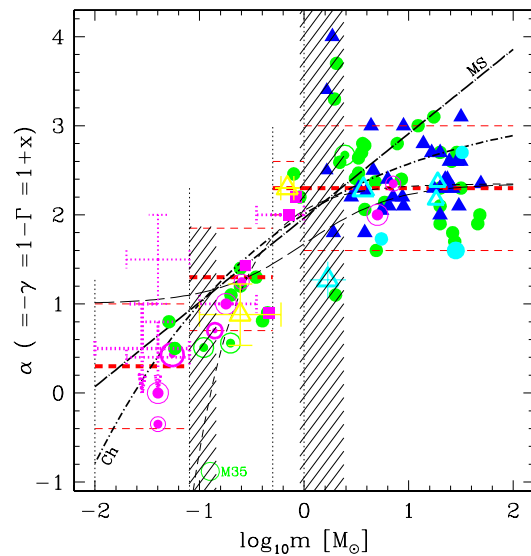


Figure 4.13: A plot of power-law exponents determined for various stellar clusters in the mass range $-2 < \log_{10} m < 2$, to illustrate the observed scatter. The solid green and blue dots and solid triangles are from measurements of Galactic and Large Magellanic Cloud clusters and OB associations, respectively. Globular cluster data are indicated by open yellow triangles. None of these measurements is corrected for unresolved binaries. The mean values of the exponent α derived in the solar neighborhood, equation 4.8, and the associated uncertainties are indicated by horizontal red dashed lines. Note that for low stellar masses the values of α determined from observations in young stellar clusters lie systematically lower due to the inability to resolve close binaries and multiple stellar systems. Black lines indicate alternative functional forms for the IMF, e.g. *MS* gives the Miller-Scalo (1979) IMF or *Ch* the one suggested by Chabrier (2001, 2002). For a more detailed discussion see Kroupa (2002), where the figure is adopted from.

There are some indications that the slope of the mass spectrum obtained from field stars may be slightly shallower than the one obtained from observing stellar clusters (Scalo 1998). The reason for this difference is unknown, and is somehow surprising given the fact most field stars may come from dissolved clusters (Adams & Myer 2001). It is possible that the field star IMF is inaccurate because of incorrect assumptions about past star formation rates and age dependences for the stellar scale height. Both issues are either known or irrelevant for the IMF derived from cluster surveys. On the other hand, the cluster surveys could have failed to include low-mass stars due to extinction or crowding. It has also

been claimed that the IMF may vary between different stellar clusters (Scalo 1998), as the measured exponent α in each mass interval exhibits considerable scatter when comparing different star forming regions. This is illustrated in Figure 4.13, which is again taken from Kroupa (2002). This scatter, however, may be entirely due to effects related to the dynamical evolution of stellar clusters (Kroupa 2001).

Despite these differences in detail, all IMF determinations share the same basic features, and it appears reasonable to say that the basic shape of the IMF is a universal property common to all star forming regions in the present-day Galaxy, perhaps with some intrinsic scatter. There still may be some dependency on the metallicity of the star forming gas, but changes in the IMF do not seem to be gross even in that case. There is no compelling evidence for qualitatively different behavior such as truncation at the low or high-mass end.

4.7.2 Models of the IMF

Existing models to explain the IMF can be divided into five major groups. In the first group feedback from the stars themselves determines their masses. Silk (1995) suggests that stellar masses are limited by the feedback from both ionization and protostellar outflows. Nakano, Hasegawa, & Norman (1995) describe a model in which stellar masses are sometimes limited by the mass scales of the formative medium and sometimes by stellar feedback. The most detailed model in this category stems from Adams & Fatuzzo (1996) and provides a transformation between initial conditions in molecular clouds and final stellar masses. They apply the central limit theorem to the hypothesis that many independent physical variables contribute to the stellar masses to derive a log-normal IMF regulated by protostellar feedback. However, for the overwhelming majority of stars (with masses $M \lesssim 5 M_{\odot}$) protostellar feedback (i.e. winds, radiation and outflows) are unlikely to be strong enough to halt mass accretion, as shown by detailed protostellar collapse calculations (e.g.

Wuchterl & Klessen 2001, Wuchterl & Tscharnuter 2002).

In the second group of models, initial and environmental conditions determine the IMF. In this picture, the structural properties of molecular clouds determine the mass distribution of Jeans-unstable gas clumps, and the clump properties determine the mass of the stars that form within. If one assumes a fixed star formation efficiency for individual clumps, there is a one-to-one correspondence between the molecular cloud structure and the final IMF. The idea that fragmentation of clouds leads directly to the IMF dates back to Hoyle (1953) and later Larson (1973). More recently, this concept has been extended to include the observed fractal and hierarchical structure of molecular clouds Larson (1992, 1995). Indeed random sampling from a fractal cloud seems to be able to reproduce the basic features of the observed IMF (Elmegreen & Mathieu 1983, Elmegreen 1997, 1999, 2000a,c, 2002). A related approach is to see the IMF as a domain packing problem (Richtler 1994).

The hypothesis that stellar masses are determined by clump masses in molecular clouds is supported by observations of the dust continuum emission of protostellar condensations in the Serpens, ρ Ophiuchi, and Orion star forming regions (Testi & Sargent 1998; Motte *et al.* 1998, 2001; Johnstone *et al.* 2000, 2001). These protostellar cores are thought to be in a phase immediately before they build up a star in their interior. Their mass distribution resembles the stellar IMF reasonably well, suggesting a close correspondence between protostellar clump masses and stellar masses, leaving little room for stellar feedback processes, competitive accretion or collisions to act to determine the stellar mass spectrum.

A third group of models relies on competitive coagulation or accretion processes to determine the IMF. This has a long tradition and dates back to investigations by Oort (1954) and Field & Saslaw (1965), but the interest in this concept continues to the present day (e.g. Silk & Takahashi 1979; Lejeune & Bastien 1986; Price & Podsiadlowski 1995; Murray & Lin 1996; Bonnell *et al.* 2001a,b;

Durisen, Sterzik, & Pickett 2001). Stellar collisions require very high stellar densities, however, for which observational evidence and theoretical mechanisms remain scarce.

Fourth, there are models that connect the supersonic turbulent motions in molecular clouds to the IMF. In particular there are a series of attempts to find an analytical relation between the stellar mass spectrum and statistical properties of interstellar turbulence (e.g. Larson 1981, Fleck 1982, Hunter & Fleck 1982, Elmegreen 1993, Padoan 1995, Padoan 1995, Padoan *et al.* 1997, Myers 2000, Padoan & Nordlund 2002). However, properties such as the probability distribution of density in supersonic turbulence in the absence of gravity have never successfully been shown to have a definite relationship to the final results of gravitational collapse (Padoan *et al.* 1997). Even the more sophisticated attempt by Padoan & Nordlund (2002) neglects to take into account that it is likely that not single shock compressions but multiple compressions and rarefactions that determine the density structure of supersonic turbulence (Passot & Vázquez-Semadeni 1998). Furthermore, such models neglect the effects of competitive accretion in dense cluster environments (Section 4.5), which may be important for determining the upper end of the IMF. This makes the attempt to derive stellar mass spectra from the statistical properties difficult.

Finally there is a more statistical approach. Larson (1973) and Zinnecker (1984, 1990) argued that whenever a large set of parameters is involved in determining the masses of stars, invoking the central limit theorem of statistics naturally leads to a log-normal stellar mass spectrum (Adams & Fatuzzo [1996] made similar arguments).

Regardless of the detailed physical processes involved, the common theme in all of these models is the probabilistic nature of star formation. It appears impossible to predict the formation of specific individual objects. Only the fate of an ensemble of stars can be described *ab initio*. The implication is that the star formation process can only be understood within the framework of a probabilistic theory.

4.7.3 Mass Spectra from Turbulent Fragmentation

To illustrate some of the issues discussed above, we examine the mass spectra of gas clumps and collapsed cores from models of self-gravitating, isothermal, supersonic turbulence driven with different wavelengths (Klessen 2001b). In the absence of magnetic fields and more accurate equations of state, these models can only be illustrative, not definitive, but nevertheless they offer insight into the processes acting to form the IMF. Figure 4.14 plots for four different models the mass distribution of gas clumps, of the subset of gravitationally unstable clumps, and of collapsed cores, at four different evolutionary phases. In the initial phase, before local collapse begins to occur, the clump mass spectrum is not well described by a single power law. During subsequent evolution, as clumps merge and grow bigger, the mass spectrum extends towards larger masses, approaching a power law with slope $\alpha \approx -1.5$. Local collapse sets in and results in the formation of dense cores most quickly in the freely collapsing model. The influence of gravity on the clump mass distribution weakens when turbulence dominates over gravitational contraction on the global scale, as in the other three models. The more the turbulent energy dominates over gravity, the more the spectrum resembles the initial case of pure hydrodynamic turbulence. This suggests that the clump mass spectrum in molecular clouds will be shallower in regions where gravity dominates over turbulent energy. This may explain the observed range of slopes for the clump mass spectrum in different molecular cloud regions (Section 4.1.2).

Like the distribution of Jeans-unstable clumps, the mass spectrum of dense protostellar cores resembles a log-normal in the model without turbulent support and in the one with long-wavelength turbulent driving, with a peak at roughly the average thermal Jeans mass $\langle m_J \rangle$ of the system. These models also predict initial mass segregation (Section 4.5.e). However, models supported at shorter wavelength have mass spectra much flatter than observed, suggesting that clump merging and competitive ac-

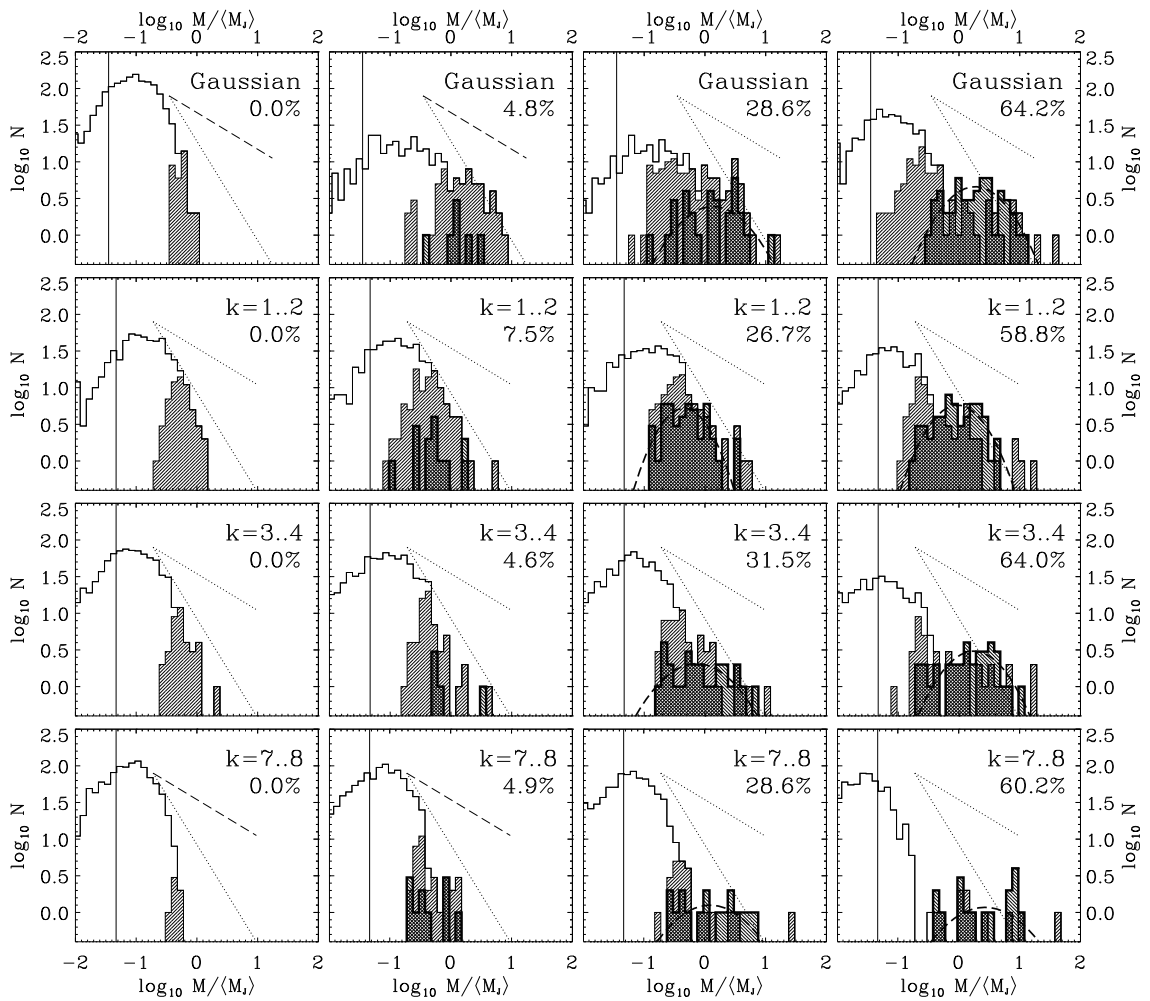


Figure 4.14: Mass spectra of dense collapsed cores (hatched thick-lined histograms), of gas clumps (thin lines), and of the subset of Jeans unstable clumps (thin lines, hatched distribution) for four different models. The decaying model started with Gaussian density perturbations and no turbulence, while the other three models were nominally supported by turbulence driven at long, intermediate or short scales as indicated by the driving wavenumbers k . Masses are binned logarithmically and normalized to the average Jeans mass $\langle m_j \rangle$. The left column gives the initial state of the system when the turbulent flow has reached equilibrium but gravity has not yet been turned on, the second column shows the mass spectra when $m_* \approx 5\%$ of the mass is accreted onto dense cores, the third column shows $m_* \approx 30\%$, and the last one $m_* \approx 60\%$. For comparison with power-law spectra ($dN/dm \propto m^\alpha$), a slope $\alpha = -1.5$ typical for the observed clump mass distribution, and the Salpeter slope $\alpha = -2.33$ for the IMF, are indicated by the dotted lines. The vertical line shows the resolution limit of the numerical model. In columns 3 and 4, the long dashed curve shows the best log-normal fit. (From Klessen 2001b.)

cretion are important factors leading to a log-normal mass spectrum. The protostellar clusters discussed here only contain between 50 and 100 cores. This allows for comparison with the IMF only around the characteristic mass scale, typically about $1 M_\odot$, since the numbers are too small to study the very low- and high-mass end of the distribution. Focusing on low-mass star formation, however, Bate, Bonnell, & Bromm (2002) demonstrate that brown dwarfs are a natural and

frequent outcome of turbulent fragmentation. In this model, brown dwarfs form when dense molecular gas fragments into unstable multiple systems that eject their smallest members from the dense gas before they have been able to accrete to stellar masses. Numerical models with sufficient dynamic range to treat the full range of stellar masses (Equation 4.4) remain yet to be done.

Chapter 5

GALACTIC SCALE STAR FORMATION

How do the mechanisms that control local star formation determine the global rate and distribution of star formation in galaxies? In this section we begin by examining what determines the efficiency of star formation in Section 5.1. We argue that the balance between the density of available gas and its turbulent velocity determines where star formation will occur, and how strongly. Even if the turbulent velocity in a region is relatively high, if the density in that region is also high, the region may still not be supported against gravitational collapse and prompt star formation.

Therefore, any mechanism that increases the local density without simultaneously increasing the turbulent velocity sufficiently can lead to star formation, via molecular cloud formation, as we discuss in Section 5.2. Most mechanisms that increase local density appear to be external to the star formation process, however. Accretion during initial galaxy formation, interactions and collisions between galaxies, spiral gravitational instabilities of galactic disks, and bar formation are major examples. In this review we cannot do justice to the vast literature on galactic dynamics and interactions that determine the density distribution in galaxies. We do, however, examine what physical mechanisms control the velocity dispersion in Section 5.3.

Finally, in Section 5.4 we briefly speculate on how turbulent control of star formation may help explain objects with very different star formation properties, including low surface brightness galaxies, normal galactic disks, globular clusters, galactic nuclei, and primordial dwarf galaxies.

5.1 When is Star Formation Efficient?

5.1.1 Overview

Observers have documented a surprisingly strong connection between the star formation rate and the local velocity dispersion, column density and rotational velocity of disk galaxies (Kennicutt 1998a, Martin & Kennicutt 2001). A global Schmidt (1959) law relating star formation rate surface density to gas surface density as

$$\Sigma_{\text{SFR}} = A \Sigma_{\text{gas}}^N, \quad (5.1)$$

where a value of $N = 1.4 \pm 0.05$ can be derived from the observations (Kennicutt 1989, 1998b). A threshold to star formation is also found (Kennicutt 1989, Martin & Kennicutt 2001) in most galaxies, which also appears related to the gas surface density. The Schmidt law can be interpreted as reflecting star formation on a free-fall timescale, so that (following Wong & Blitz 2001 for example) the star formation rate per unit volume of gas with density ρ is

$$\rho_{\text{SFR}} = \epsilon_{\text{SFR}} \frac{\rho}{\tau_{\text{ff}}} = \epsilon_{\text{SFR}} \frac{\rho}{(G\rho)^{-1/2}} \propto \rho^{1.5}, \quad (5.2)$$

where ϵ_{SFR} is an efficiency factor observed to be substantially less than unity.

The connection between magnetically controlled small-scale star formation and large-scale star formation is not clear in the standard theory. Shu, Adams, & Lizano (1987) did indeed suggest that OB associations were formed by freely collapsing gas that had overwhelmed the local magnetic

field, but that still implied that the star formation rate was controlled by the details of the magnetic field structure, which in turn is presumably controlled by the galactic dynamo. If turbulence, as represented by the velocity dispersion, controls the star formation rate, though, the connection appears clearer. The same physical mechanism controls star formation at all scales. Regions that are globally supported by turbulence still engage in inefficient star formation, but the overall star formation rate will be determined by the frequency of regions of efficient star formation.

The big open question in this area remains the importance of radiative cooling to efficient star formation, either on its own or induced by turbulent compression. Is cooling, and indeed molecule formation, necessary for gravitational collapse to begin, or is it rather a result of already occurring collapse in gravitationally unstable gas? Certainly there are situations where cooling will make the difference between gravitational stability and instability, but are those just marginal cases or the primary driver for star formation in galaxies?

In Figure 5.1 we outline a unified picture that depends on turbulence and cooling to control the star formation rate. After describing the different elements of this picture, we will discuss the steps that we think will be needed to move from this cartoon to a quantitative theory of the star formation rate.

Probably the factor that determines the star formation rate more than any other is whether the gas is sufficiently dense to be gravitationally unstable without additional cooling. Galactic dynamics and interactions with other galaxies and the surrounding intergalactic gas determine the average gas densities in different regions of galaxies. The gravitational instability criterion here includes both turbulent motions and galactic shear, as well as magnetic fields. If gravitational instability sets in at the large scale, collapse will continue so long as sufficient cooling mechanisms exist to prevent the temperature of the gas from rising (effective adiabatic index $\gamma_{\text{eff}} \leq 1$). In this situation, molecular clouds can form in

less than 10^5 yr, as the gas passes through densities of 10^4 cm^{-3} or higher, as an incidental effect of the collapse. A starburst results, with stars forming efficiently in compact clusters. The size of the gravitationally unstable region determines the size of the starburst.

If turbulent support, rather than thermal support, prevents the gas from immediately collapsing, compression-induced cooling can become important. Supersonic turbulence compresses the gas strongly, and most cooling mechanisms depend on the gas density, usually non-linearly. Galactic dynamics will again determine local average density; this mechanism will be more efficient in regions of higher average density. If the cooled regions reach high densities (again, of order 10^4 cm^{-3}), molecule formation will occur quickly, whether or not gravitational instability sets in (see Section 5.2). If the gas cools in compressed regions, they can become gravitationally unstable even if they were not before. Molecule formation will, of course, be more efficient in regions that collapse gravitationally, but it can occur elsewhere as well. The large-scale star formation efficiency will already be much reduced in this case, as much of the gas will not be compressed sufficiently to cool.

If the turbulence in the cooled regions does support the gas against general gravitational collapse, isolated, low-rate star formation can still occur in regions further compressed by the turbulence. This may describe regions of low-mass star formation like the Taurus clouds. On the other hand, if the cooled gas does begin to collapse gravitationally, locally efficient star formation can occur. The size of the gravitationally unstable region then really determines whether a group, OB association, or bound cluster eventually forms. Star formation in regions like Orion may result from this branch.

5.1.2 Gravitational Instabilities in Galactic Disks

Now let us consider the conditions under which gravitational instability will set in. On galactic scales, the Jeans instability criterion for gravitational instability must be modified to include

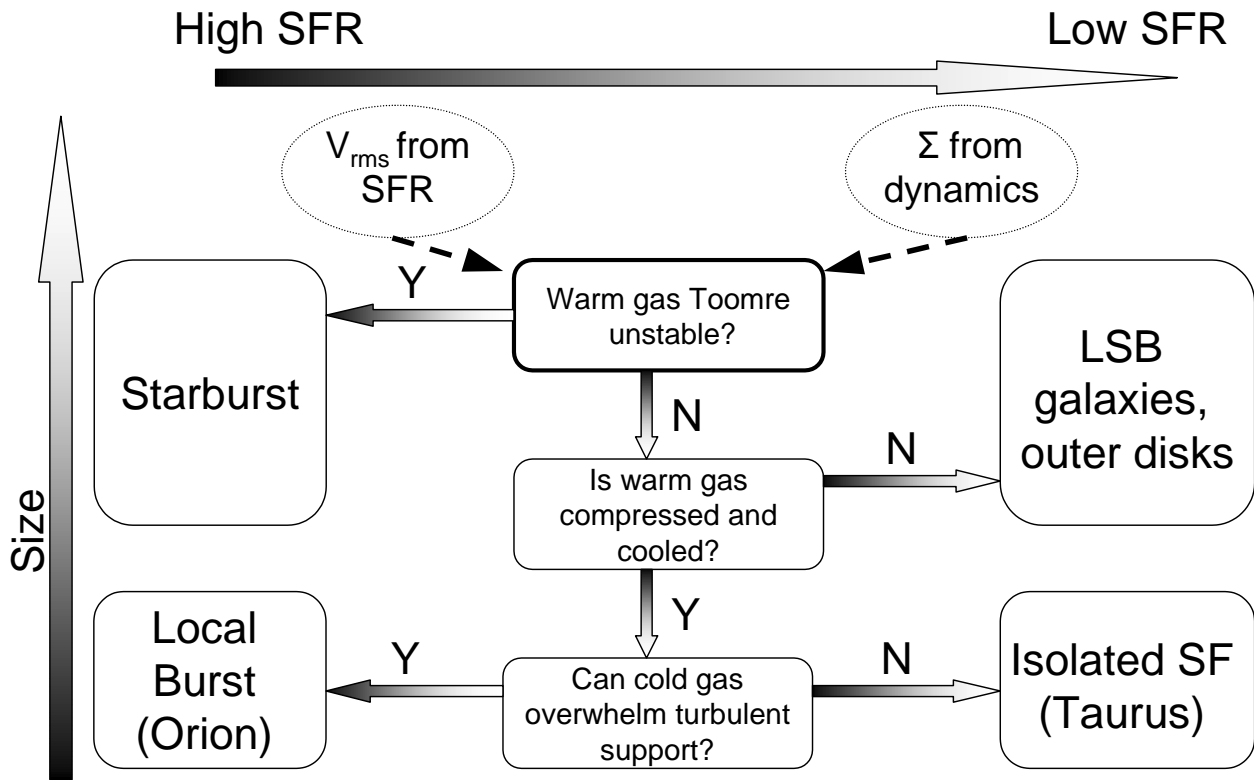


Figure 5.1: Illustration of physics determining star formation in galaxies.

the additional support offered by the shear coming from differential rotation, as well as the effects of magnetic fields. The gravitational potential of the stars can also contribute to gravitational instability on large scales. Which factor determines the onset of gravitational instability remains unknown. Five that have been proposed are the temperature of the cold phase, the surface density, the local shear, the presence of magnetic fields, and the velocity dispersion, in different combinations.

We can heuristically derive the Toomre (1964) criterion for stability of a rotating, thin disk with uniform velocity dispersion σ and surface density Σ using time scale arguments (Schaye 2002). First consider the Jeans criterion for instability in a thin disk, which requires that the time scale for collapse of a perturbation of size λ

$$t_{\text{coll}} = \sqrt{\lambda/G\Sigma} \quad (5.3)$$

be shorter than the time required for the gas to respond to the collapse, the sound crossing time

$$t_{\text{sc}} = \lambda/c_s. \quad (5.4)$$

This implies that gravitational stability requires perturbations with size

$$\lambda < c_s^2/G\Sigma. \quad (5.5)$$

Similarly, in a disk rotating differentially, a perturbation will rotate around itself, generating centrifugal motions that can also support against gravitational collapse. This will be effective if the collapse time scale t_{coll} exceeds the rotational period $t_{\text{rot}} = 2\pi/\kappa$, where κ is the epicyclic frequency, so that stable perturbations have

$$\lambda > 4\pi^2 G\Sigma\kappa^2. \quad (5.6)$$

A regime of gravitational instability occurs if there are wavelengths that lie between the regimes of pressure and rotational support, with

$$\frac{c_s^2}{G\Sigma} < \lambda < \frac{4\pi^2 G\Sigma}{\kappa^2}. \quad (5.7)$$

This will occur if

$$c_s\kappa/2\pi G\Sigma < 1, \quad (5.8)$$

which is the Toomre criterion for gravitational instability to within a factor of two. The full criterion from a linear analysis of the equations of motion of gas in a shearing disk gives a factor of π in the denominator (Safronov 1960, Goldreich & Lynden-Bell 1965), while a kinetic theory approach appropriate for a collisionless stellar system gives a factor of 3.36 (Toomre 1964).

Kennicutt (1989) and Martin & Kennicutt (2001) have demonstrated that the Toomre criterion generally can explain the location of the edge of the star-forming disk in galaxies, although they must introduce a correction factor $\alpha = 0.69 \pm 0.2$ into the left-hand-side of equation (5.8). Schaye (2002) notes that this factor should be corrected to $\alpha = 0.53$ to correct for the use of both the velocity dispersion rather than sound velocity, and the exact Toomre criterion for a stellar rather than a gas disk.

The Toomre criterion given in Equation (5.8) was derived for a pure gas disk with uniform temperature and velocity dispersion, and no magnetic field. Relaxation of each of these assumptions modifies the criterion, and indeed each has been argued to be the controlling factor in determining star formation thresholds by different authors.

Stars in a gas disk will respond as a collisionless fluid to density perturbations large compared to their mean separation. Jog & Solomon (1984a) computed the Toomre instability in a disk composed of gas and stars, and found it to always be more unstable than either component considered individually. Both components contribute to the growth of density perturbations, allowing gravitational collapse to occur more easily. Taking into account both gas (subscript g) and stars (subscript r), instability occurs when

$$2\pi Gk \left(\frac{\Sigma_r}{\kappa^2 + k^2 c_s r^2} + \frac{\Sigma_g}{\kappa^2 + k^2 c_s g^2} \right) > 1, \quad (5.9)$$

where $k = 2\pi/\lambda$ is the wavenumber of the perturbation considered. Taking into account the effects of the stars always makes a disk more unstable than it is due to its gas content alone. Jog & Solomon (1984a) and Romeo (1992) extended this model to include the effect of the finite thickness of the disk. Elmegreen (1995) was able with

some effort to derive an effective Toomre parameter that includes the effects of both stars and gas, but that can only be analytically computed in the thin disk limit. To compute it, independent measures of the velocity dispersion of the stars and of the gas are, of course, needed. Jog (1996) numerically computed the effective stability parameter for a wide range of values of stellar and gas disk parameters. The contribution of the stellar disk may alone be sufficient to explain the correction factors found by Kennicutt (1989) and Martin & Kennicutt (2001).

Magnetic fields offer direct support against collapse through their magnetic pressure and tension. However, Chandrasekhar (1954) and Lynden-Bell (1966) were the first to note that they can also have the less expected effect of destabilization of a rotating system. The magnetic field in this case acts to brake the shear that would otherwise prevent collapse, redistributing angular momentum and allowing collapse to occur down field lines. Elmegreen (1987) performed a linear analysis of the growth rate of gravitational instability in a rotating, magnetized disk, which was extended by Fan & Lou (1997) to follow the excitation of the different modes.

Kim & Ostriker (2001) were able to identify the regimes in which the magnetic field acts to either stabilize against collapse or promote it. When shear is strong, as it is in the parts of galactic disks with flat rotation curves, and the field is moderate or weak, with plasma $\beta \leq 1$, swing amplification stabilized by magnetic pressure dominates. Sufficiently unstable disks, with Toomre $Q \leq 1.0$ – 1.1 (depending on field strength), collapse due to nonlinear secondary instabilities despite magnetic stabilization. On the other hand, if shear is weak, and fields are stronger ($\beta > 1$), magnetic tension forces act against epicyclic motions, reducing their stabilizing effect, and producing magneto-Jeans instabilities along the field lines.

Numerical models by Kim & Ostriker (2001) showed these mechanisms in operation, generating large regions of gravitational collapse, although in the outer parts of disks, the collapse rate from swing amplification is so slow that additional effects such as spiral arm amplification

may be important to drive the formation of observed regions of star formation. Kim & Ostriker (2002) show that the introduction of spiral arms indeed produce feathers similar to those observed, with masses comparable to the largest star forming regions. These results suggest that the presence of magnetic fields may actually enhance the star formation rate in disks.

The temperature and the velocity of the coldest gas in a multi-phase interstellar medium at any point in the disk may be the determining factor for gravitational instability, rather than some average temperature. Schaye (2002) suggests that the sharp rise in temperature associated with the lack of molecular gas causes the sharp drop in the star formation rate at the edges of disk galaxies. He derives the disk surface density required to allow molecule formation in the presence of the intergalactic ultraviolet background field and suggests that this is consistent with the observed threshold column densities. However, Martin & Kennicutt (2001) show a wide variation in the atomic gas fraction at the critical radius (see their Figure 9a), calling this idea into question.

The balance between gravitation and local shear is argued by Hunter, Elmegreen, & Baker (1998) to be a better criterion than the Toomre (1964) criterion, which balances gravitation against Coriolis forces. Effectively this substitutes the Oort A constant (Binney & Tremaine 1997) for the epicyclic frequency κ in Equation (5.8). The difference is small (of order 10%) in galaxies with flat rotation curves, but can lower the critical density substantially in galaxies with rising rotation curves, such as dwarf galaxies.

5.1.3 Thermal Instability

Thermal instability has been the organizing principle behind the most influential models of the ISM (Pikel'ner 1968; Field, Goldsmith, & Habing 1969; McKee & Ostriker 1977; Wolfire *et al.* 1995). Under the assumption of approximate pressure and thermal equilibrium, thermal instability can explain the widely varying densities observed in the ISM. It can not explain the order of magnitude higher pressures observed in molecular

clouds, though, so it was thought that most molecular clouds must be confined by their own self-gravity. Turbulent pressure fluctuations in a medium with effective adiabatic index less than unity (that is, one that cools when compressed, like the ISM) can provide an alternative explanation for both pressure and density fluctuations. Although thermal instability exists, it does not necessarily act as the primary structuring agent, nor, therefore, as the determining factor for the star formation rate.

Thermal instability occurs when small perturbations from thermal equilibrium grow. The dependence on density ρ and temperature T of the heat-loss function $\mathcal{L} = \Lambda - \Gamma$, the sum of energy losses minus gains per gram per second, determines whether instability occurs. Parker (1953) derived the isochoric instability condition, while Field (1965) pointed out that cooling inevitably causes density changes, either due to dynamical flows if the region is not isobaric, or due to pressure changes if it is. He then derived the isobaric instability condition. The alternative of dynamical compression in a region large enough to be unable to maintain isobaric conditions has received renewed attention as described below.

The isobaric instability condition derived by Field (1965) is

$$\left(\frac{\partial \mathcal{L}}{\partial T}\right)_p = \left(\frac{\partial \mathcal{L}}{\partial T}\right)_\rho - \frac{\rho_0}{T_0} \left(\frac{\partial \mathcal{L}}{\partial \rho}\right)_T < 0, \quad (5.10)$$

where ρ_0 and T_0 are the equilibrium values. Optically thin radiative cooling in the interstellar medium gives a cooling function that can be expressed as a piecewise power law $\Lambda \propto \rho^2 T^{\beta_i}$, where β_i gives the value for a temperature range $T_{i-1} < T < T_i$, while photoelectric heating is independent of temperature. Isobaric instability occurs when $\beta_i < 1$, while isochoric instability only occurs with $\beta_i < 0$ (e.g. Field 1965).

In interstellar gas cooling with equilibrium ionization, there are two temperature ranges subject to thermal instability. In the standard picture of the three-phase interstellar medium governed by thermal instability (McKee & Ostriker 1977), the higher of these, with temperatures $10^{4.5} \text{ K} < T <$

10^7 K (Raymond, Cox, & Smith 1977), separates hot gas from the warm ionized medium. The lower range of $10^{1.7}$ K $< T < 10^{3.7}$ K (Figure 3a of Wolfire *et al.* 1995) separates the warm neutral medium from the cold neutral medium. Cooling of gas out of ionization equilibrium has been studied in a series of papers by Spaans (1996, Spaans & Norman 1997, Spaans & Van Dishoeck 1997, Spaans & Carollo 1998) as described by Spaans & Silk (2000). The effective adiabatic index depends quite strongly on the details of the local chemical, dynamical and radiation environment, in addition to the pressure and temperature of the gas. Although regions of thermal instability occur, the pressures and temperatures may depend strongly on the details of the radiative transfer in a turbulent medium, the local chemical abundances, and other factors.

When thermal instability occurs, it can drive strong motions that dynamically compress the gas nonlinearly. Thereafter, neither the isobaric nor the isochoric instability conditions hold, and the structure of the gas is determined by the combination of dynamics and thermodynamics (Meerson 1996, Burkert & Lin 2000, Lynden-Bell & Tout 2001, Kritsuk & Norman 2002).

Vázquez-Semadeni, Gazol, & Scalo (2000) examined the behavior of thermal instability in the presence of driven turbulence, magnetic fields, and Coriolis forces and concluded that the structuring effect of the turbulence overwhelmed that of thermal instability in a realistic environment. Gazol *et al.* (2001) found that about half of the gas in such a turbulent environment will actually have temperatures falling in the thermally unstable region, and emphasize that a bimodal temperature distribution may simply be a reflection of the gas cooling function, not a signature of a discontinuous phase transition. Mac Low *et al.* (2002) examined supernova-driven turbulence and found a broad distribution of pressures, which were more important than thermal instability in producing a broad range of densities in the interstellar gas.

The discovery of substantial amounts of gas out of thermal equilibrium by Heiles (1999) has

provided observational support for a picture in which turbulent flows rather than thermal instability dominates structure formation prior to gravitational collapse. Heiles (1999) measured the temperature of gas along lines of sight through the warm and cold neutral medium by comparing absorption and emission profiles of the HI 21 cm fine structure line. He found that nearly half of the warm neutral clouds measured showed temperatures that are unstable according to the application of the isobaric instability condition, Equation (5.10), to the Wolfire *et al.* (1995) equilibrium ionization phase diagram.

Although the heating and cooling of the gas clearly plays an important role in the star formation process, the presence or absence of an isobaric instability may be less important than the effective adiabatic index, or similar measures of the behavior of the gas on compression, in determining its ultimate ability to form stars. However, Schaye (2002) has made the argument that it is exactly the ability of the gas to cool above some critical column density that determines the edge of the star-forming region in disks.

5.2 Formation and Lifetime of Molecular Clouds

How do molecular clouds form? Any explanation must account for the low star-formation efficiencies observed in nearby molecular clouds, as well as the broad linewidths observed at scales larger than about 0.1 pc in such clouds. At the same time, the efficient star formation seen in regions of massive star formation must still be permitted.

Molecular gas forms on dust grains at a rate calculated by Hollenbach, Werner, & Salpeter (1971) to be

$$t_{\text{form}} = (1.5 \times 10^9 \text{ yr}) \left(\frac{n}{1 \text{ cm}^{-3}} \right)^{-1}, \quad (5.11)$$

where n is the number density of gas particles. Experimental work by Piranello *et al.* (1997a, 1997b, 1999) on molecular hydrogen formation on graphite and olivine suggests that rates may

be strongly temperature dependent and that the Hollenbach *et al.* (1971) result may be a lower limit to the formation time. However, the same group reports that molecule formation is rather more efficient on amorphous ices (Manicó *et al.* 2001) such as would be expected on grain surfaces deep within dark clouds, so that the rates computed by Hollenbach *et al.* (1971) may be reached after all. Further experimental investigation of molecule formation appears necessary.

The linear density dependence of the formation rate implies that molecular gas either forms very slowly, over tens of millions of years at the average densities of order 10^2 cm^{-3} in molecular regions, or else it forms at very high densities, $\gtrsim 10^4 \text{ cm}^{-3}$ in a few hundred thousand years. The latter idea becomes increasingly attractive.

When molecular clouds were first discovered, they were thought to have lifetimes of over 100 Myr (e.g. Scoville & Hersh 1979) because of their apparent predominance in the inner galaxy. These estimates were shown to depend upon too high a conversion factor between CO and H₂ masses by Blitz & Shu (1980). They revised the estimated lifetime down to roughly 30 Myr based on the association with spiral arms, apparent ages of associated stars, and overall star formation rate in the Galaxy.

Chemical equilibrium models of dense cores in molecular clouds (as reviewed, for example, by Irvine, Goldsmith, & Hjalmarsen 1986) showed disagreements with observed abundances in a number of molecules. These cores would take as much as 10 Myr to reach equilibrium, which could still occur in the standard model. However, Prasad, Heere, & Tarafdar (1991) demonstrated that the abundances of the different species agreed much better with the results at times of less than 1 Myr from time-dependent models of the chemical evolution of collapsing cores. Bergin *et al.* (1997) came to a similar conclusion from a careful study of several giant cores in comparison to an extensive chemical model network, while Saito *et al.* (2002) studied deuterium fractionation, also finding short lifetimes.

Ballesteros-Paredes, Hartmann, & Vázquez-

Semadeni (1999) have argued for a lifetime of less than 10 Myr for molecular clouds as a whole. They base their argument on the notable lack of a population of 5 – 20 Myr old stars in molecular clouds. Stars in the clouds typically have ages under 3 – 5 Myr, judging from their position on pre-main-sequence evolutionary tracks in a Hertzsprung-Russell diagram (D’Antona & Mazzitelli 1994; Swenson *et al.* 1994; with discrepancies resolved by Stauffer, Hartmann, & Barro y Navascues 1995). Older weak-line T Tauri stars identified by X-ray surveys with *Einstein* (Walter *et al.* 1988) and *ROSAT* (Neuhäuser *et al.* 1995) are dispersed over a region as much as 70 pc away from molecular gas, suggesting that they were not formed in the currently observed gas (Feigelson 1996). Leisawitz, Bash, & Thaddeus (1989), Fukui *et al.* (1999) and Elmegreen (2000) have made similar arguments based on the observation that only stellar clusters with ages under about 10 Myr are associated with substantial amounts of molecular gas in the Milky Way and the LMC.

For these short lifetimes to be plausible, either molecule formation must proceed quickly, and therefore at high densities, or observed molecular clouds must be formed from preexisting molecular gas, as suggested by Pringle, Allen, & Lubow (2001). A plausible place for fast formation of H₂ at high density is the shock compressed layers naturally produced in a SN-driven ISM, as shown in Figure 5.2 from Mac Low *et al.* (2001)¹. They showed that pressures in the ISM are broadly distributed, with peak pressures in cool gas ($T \sim 10^3$ K) as much as an order of magnitude above the average because of shock compressions. This gas is swept up from ionized 10^4 K gas, so between cooling and compression its density has already been raised up to two orders of magnitude from $n \approx 1 \text{ cm}^{-3}$ to $n \approx 100 \text{ cm}^{-3}$. These simulations did not include a correct cooling curve below 10^4 K, so further cooling could not occur even if

¹Similar morphologies have been seen in many other global simulations of the ISM, including Rosen, Bregman, & Norman (1993), Rosen & Bregman (1995), Rosen, Bregman, & Kelson (1996), Korpi *et al.* (1999), Avillez (2000), and Wada & Norman (1999, 2001). Mac Low (2000) reviews such simulations.

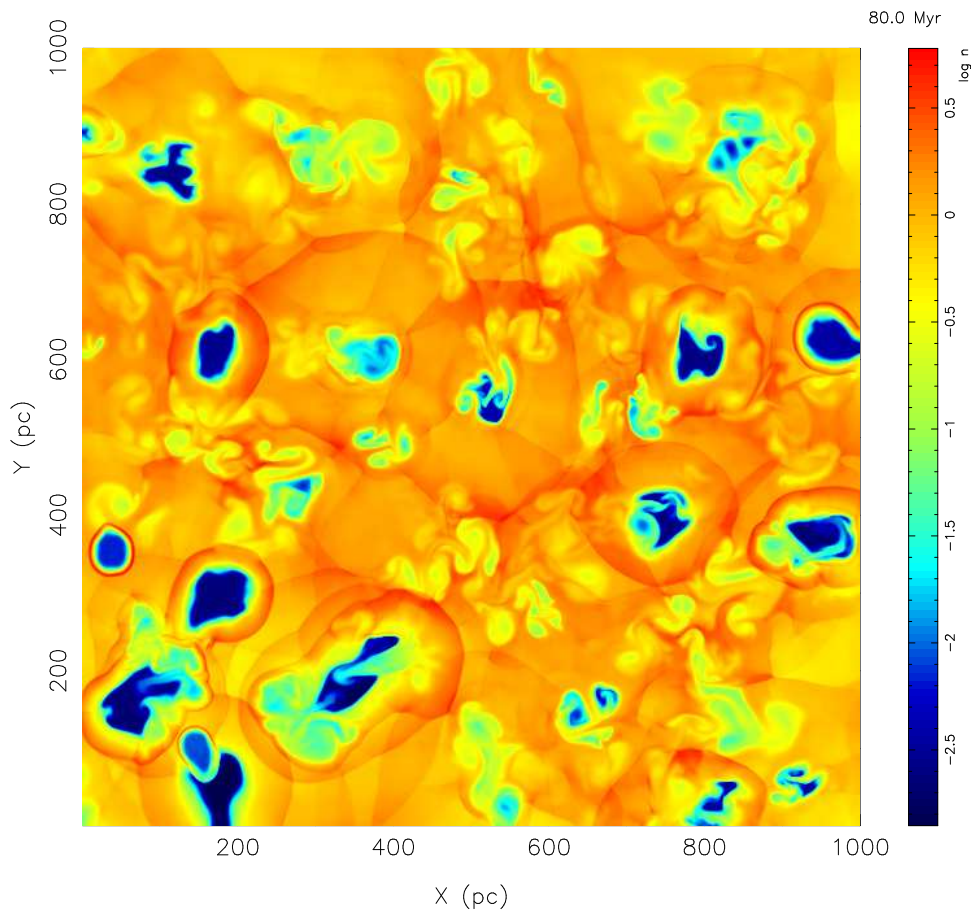


Figure 5.2: Log of number density from a three-dimensional SN-driven model of the ISM with resolution of 1.25 pc, including radiative cooling and the gravitational field of the stellar disk, as described by Mac Low *et al.* (2001). High-density, shock-confined regions are naturally produced by intersecting SN-shocks from field SNe.

physically appropriate, but it would be expected.

We can understand this compression quantitatively. The sound speed in the warm gas is $(8.1 \text{ km s}^{-1})(T/10^4 \text{ K})^{1/2}$, taking into account the mean mass per particle $\mu = 2.11 \times 10^{-24} \text{ g}$ for gas 90% H and 10% He by number. The typical velocity dispersion for this gas is $10 - 12 \text{ km s}^{-1}$ (e.g. Dickey & Lockman 1990, Dickey, Hanson, & Helou 1990), so that shocks with Mach numbers $\mathcal{M} = 2-3$ are moderately frequent. Temperatures in these shocks reach values $T \leq 10^5 \text{ K}$, which is close to the peak of the interstellar cooling curve (e.g. Dalgarno & McCray 1972; Raymond, Cox, & Smith 1976), so the gas cools quickly back to 10^4 K . The density behind an isothermal shock is $\rho_1 = \mathcal{M}^2 \rho_0$, where ρ_0 is the pre-shock density, so order of magnitude density enhancements occur easily. The optically-thin radiative cool-

ing rate $\Lambda(T)$ drops off at 10^4 K as H atoms no longer radiate efficiently (Dalgarno & McCray 1972; Spaans & Norman 1997), but the radiative cooling $L \sim n^2 \Lambda(T)$. The quadratic sensitivity to density means that density enhancements strongly enhance cooling. Hennebelle & Péroult (1999) show that such shock compressions can trigger the isobaric thermal instability (Field, Goldsmith, & Habing 1969; Wolfire *et al.* 1995), reducing temperatures to of order 100 K or less. Heiles (2000) observes a broad range of temperatures for neutral hydrogen from below 100 K to a few thousand K. The reduction in temperature by two orders of magnitude from 10^4 K to 100 K raises the density correspondingly, for a total of as much as three orders of magnitude of compression. Gas that started at densities somewhat higher than average of say 10 cm^{-3} can be compressed to densities of 10^4 cm^{-3} , enough

to reduce H_2 formation times to a few hundred thousand years.

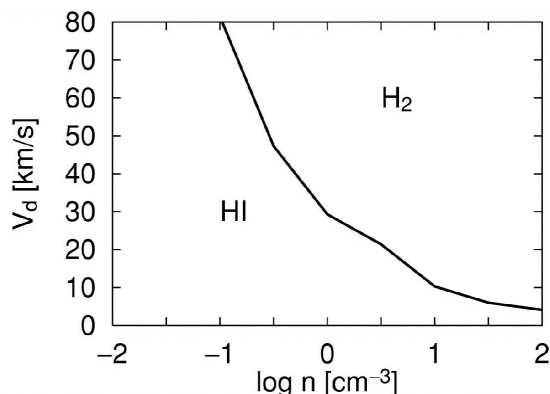


Figure 5.3: Shock velocities V_d and pre-shock number densities n at which the cold post-shock layer is more than 8% molecular, taken from one-dimensional simulations by Koyama & Inutsuka (2000) that include H_2 formation and dissociation, and realistic heating and cooling functions from Wolfire *et al.* (1995).

Koyama & Inutsuka (2000) have demonstrated numerically that shock-confined layers do indeed quickly develop high enough densities to form H_2 in under a million years, using one-dimensional computations including heating and cooling rates from Wolfire *et al.* (1995) and H_2 formation and dissociation. In Figure 5.3 we show the parameter space in which they find H_2 formation is efficient. Hartmann, Ballesteros-Paredes, and Bergin (2001) make a more general argument for rapid H_2 formation, based in part on lower-resolution, two-dimensional simulations described by Passot, Vázquez-Semadeni, & Pouquet (1995) that could not fully resolve realistic densities like those of Koyama & Inutsuka (2000), but do include larger-scale flows showing that the initial conditions for the one-dimensional models are not unreasonable. Hartmann *et al.* (2001) further argue that the self-shielding against the background UV field also required for H_2 formation will become important at approximately the same column densities required to become gravitationally unstable.

As was already noted by Ballesteros-Paredes *et al.* (1999b), shock-confined layers were shown numerically to be unstable by Hunter *et al.* (1986) in the context of colliding spherical density en-

hancements, and by Stevens, Blondin, & Pollack (1992) in the context of colliding stellar winds. Vishniac (1994) demonstrated analytically that isothermal, shock-confined layers are subject to a nonlinear thin shell instability (NTSI). The physical mechanism can be seen by considering a shocked layer perturbed sinusoidally. The ram pressure on either side of the layer acts parallel to the incoming flow, and thus at an angle to the surface of the perturbed layer. Momentum is deposited in the layer with a component parallel to the surface, which drives material towards extrema in the layer, causing the perturbation to grow. A careful numerical study by Blondin & Mark (1996) in two dimensions demonstrated that the NTSI saturates in a thick layer of transsonic turbulence when the flows become sufficiently chaotic that the surface no longer rests at a substantial angle to the normal of the incoming flow.

Thermal instability will act in conjunction with shock confinement (see Section 5.1.3). Burkert & Lin (2000) computed the nonlinear development of the thermal instability, demonstrating that shock waves form during the dynamical collapse of nonlinear regions. Hennebelle & Pérault (1999) demonstrated that shock compression can trigger thermal instability in otherwise stable regions in the diffuse ISM, even in the presence of magnetic fields (Hennebelle & Pérault 2000), so that compressions much greater than the isothermal factor of \mathcal{M}^2 can occur.

These cold, dense layers are themselves subject to dynamical instabilities, as has been shown in two-dimensional computations by Koyama & Inutsuka (2002). The instabilities they found are caused by some combination of thermal instability and mechanisms very similar to the NTSI studied by Vishniac (1994) for the isothermal case. Figure 5.4 shows another example of these instabilities from a numerical study by Walder & Folini (2000). These dynamical instabilities can drive strongly supersonic motions in the cold, dense layer. If that layer is dense enough for molecule formation to proceed quickly, those molecules will show strongly supersonic linewidths on all but the very small-

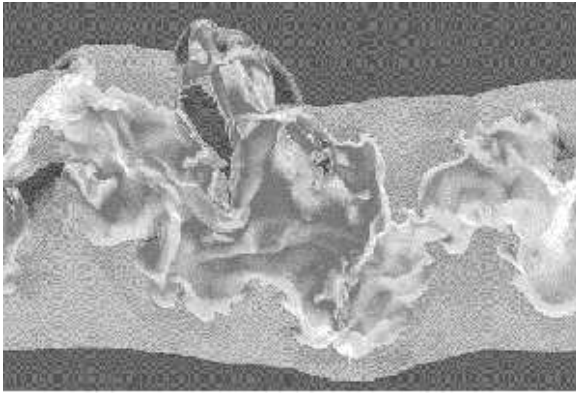


Figure 5.4: Instability of cooled layer confined by strong radiative shocks (from above and below, Mach number $M \sim 20$), computed in two dimensions with an adaptive mesh refinement technique by Walder & Folini (2000). Darkest regions have densities of 14 cm^{-3} , while white represents a density of $2 \times 10^4 \text{ cm}^{-3}$.

est scales, as seen in the models of Koyama & Inutsuka (2002), in agreement with the observations of molecular clouds. It remains to be shown whether this scenario can quantitatively explain the full ensemble of molecular clouds observed in the solar neighborhood, or elsewhere in our own and external galaxies.

5.3 Driving Mechanisms

Both support against gravity and maintenance of observed motions appear to depend on continued driving of the turbulence, which has kinetic energy density $e = (1/2)\rho v_{\text{rms}}^2$. Mac Low (1999, 2002) estimates that the dissipation rate for isothermal, supersonic turbulence is

$$\begin{aligned} \dot{e} &\simeq -(1/2)\rho v_{\text{rms}}^3/L_d & (5.12) \\ &= -(3 \times 10^{-27} \text{ erg cm}^{-3} \text{ s}^{-1}) \\ &\times \left(\frac{n}{1 \text{ cm}^{-3}}\right) \left(\frac{v_{\text{rms}}}{10 \text{ km s}^{-1}}\right)^3 \left(\frac{L_d}{100 \text{ pc}}\right)^{-1}, \end{aligned}$$

where L_d is the driving scale, which we have somewhat arbitrarily taken to be 100 pc (though it could well be smaller), and we have assumed a mean mass per particle $\mu = 2.11 \times 10^{-24} \text{ g}$. The dissipation time for turbulent kinetic energy

$$\begin{aligned} \tau_d &= e/\dot{e} \simeq L/v_{\text{rms}} = & (5.13) \\ &= (9.8 \text{ Myr}) \left(\frac{L_d}{100 \text{ pc}}\right) \left(\frac{v_{\text{rms}}}{10 \text{ km s}^{-1}}\right)^{-1}, \end{aligned}$$

which is just the crossing time for the turbulent flow across the driving scale (Elmegreen 2000b). What then is the energy source for this driving? We here review the energy input rates for a number of possible mechanisms.

5.3.1 Magnetorotational Instabilities

One energy source for interstellar turbulence that has long been considered is shear from galactic rotation (Fleck 1981). However, the question of how to couple from the large scales of galactic rotation to smaller scales remained open. Work by Sellwood & Balbus (1999) has shown that the magnetorotational instability (Balbus & Hawley 1991, 1998) could couple the large-scale motions to small scales efficiently. The instability generates Maxwell stresses (a positive correlation between radial B_R and azimuthal B_ϕ magnetic field components) that transfer energy from shear into turbulent motions at a rate $\dot{e} = T_{R\phi}\Omega$ (Sellwood & Balbus 1999). Numerical models suggest that the Maxwell stress tensor $T_{R\phi} \simeq 0.6B^2/(8\pi)$ (Hawley, Gammie & Balbus 1995). For the Milky Way, the value of the rotation rate recommended by the IAU is $\Omega = (220 \text{ Myr})^{-1} = 1.4 \times 10^{-16} \text{ rad s}^{-1}$, though this may be as much as 15% below the true value (Olling & Merrifield 1998, 2000). The magnetorotational instability may thus contribute energy at a rate

$$\begin{aligned} \dot{e} &= (3 \times 10^{-29} \text{ erg cm}^{-3} \text{ s}^{-1}) \\ &\times \left(\frac{B}{3 \mu\text{G}}\right)^2 \left(\frac{\Omega}{(220 \text{ Myr})^{-1}}\right). \end{aligned} \quad (5.14)$$

For parameters appropriate to the HI disk of a sample small galaxy, NGC 1058, including $\rho = 10^{-24} \text{ g cm}^{-3}$, Sellwood & Balbus (1999) find that the magnetic field required to produce the observed velocity dispersion of 6 km s^{-1} is roughly $3 \mu\text{G}$, a reasonable value for such a galaxy. Similar arguments would hold for the outer disk of the Milky Way. This instability may provide a base value for the velocity dispersion below which no galaxy will fall. If that is sufficient to prevent collapse, little or no star formation will occur, producing something like a low surface brightness galaxy with large amounts of HI and few stars. This may also apply to the outer disk of our own Galaxy.

5.3.2 Gravitational Instabilities

Motions coming from gravitational collapse have often been suggested as a local driving mechanism in molecular clouds, but fail due to the quick decay of the turbulence (Section 2.5.4). If the turbulence decays in less than a free-fall time, as suggested by Equation (2.13), then it cannot delay collapse for substantially longer than a free-fall time.

On the galactic scale, spiral structure can drive turbulence in gas disks. Roberts (1969) first demonstrated that shocks would form in gas flowing through spiral arms formed by gravitational instabilities in the stellar disk (Lin & Shu 1964, Lin, Yuan, & Shu 1969). These shocks were studied in thin disks by Tubbs (1980) and Soukup & Yuan (1981), who found few vertical motions. It has been realized that in a more realistic thick disk, the spiral shock will take on some properties of a hydraulic bore, with gas passing through a sudden vertical jump at the position of the shock (Martos & Cox 1998, Gómez & Cox 2002). Behind the shock, downward flows of as much as 20 km s^{-1} appear (Gómez & Cox 2002). Some portion of this flow will contribute to interstellar turbulence. However, the observed presence of interstellar turbulence in irregular galaxies without spiral arms, as well as in the outer regions of spiral galaxies beyond the regions where the arms extend suggest that this cannot be the only mechanism driving turbulence. A more quantitative estimate of the energy density contributed by spiral arm driving has not yet been done.

The interaction between rotational shear and gravitation can, at least briefly, drive turbulence in a galactic disk, even in the absence of spiral arms. This process has been numerically modeled at high resolution (sub-parsec zones) in two dimensions in a series of papers by Wada & Norman (1999, 2001), Wada, Spaans, & Kim (2000), and Wada, Meurer & Norman (2002). However, these models all share two limitations: they do not include the dominant stellar component, and gravitational collapse cannot occur beneath the grid scale. The computed filaments of dense gas

are thus artificially supported, and would actually continue to collapse to form stars, rather than driving turbulence in dense disks, see Sánchez-Salcedo (2001) for a detailed critique. In very low density disks, where even the dense filaments remained Toomre stable, this mechanism might operate, however.

Wada *et al.* (2002) estimated the energy input from this mechanism following the lead of Sellwood & Balbus (1999), but substituting Newton stresses (Lynden-Bell & Kalnajs 1972) for Maxwell stresses. The Newton stresses will only add energy if a positive correlation between radial and azimuthal gravitational forces exists, however, which is not demonstrated by Wada *et al.* (2002). Nevertheless, they estimate the order of magnitude of the energy input from Newton stresses as

$$\begin{aligned} \dot{\epsilon} &\simeq G(\Sigma_g/H)\lambda^2\Omega & (5.15) \\ &\simeq (4 \times 10^{-29} \text{ erg cm}^{-3} \text{ s}^{-1}) \\ &\quad \times \left(\frac{\Sigma_g}{10 \text{ M}_\odot \text{ pc}^{-2}}\right)^2 \left(\frac{H}{100 \text{ pc}}\right)^{-2} \\ &\quad \times \left(\frac{\lambda}{100 \text{ pc}}\right)^2 \left(\frac{\Omega}{(220 \text{ Myr})^{-1}}\right), \end{aligned}$$

where G is the gravitational constant, Σ_g the density of gas, H , the scale height of the gas, λ a length scale of turbulence, and Ω the angular velocity of the disk. Values chosen are appropriate for the Milky Way. This is two orders of magnitude below the value required to maintain interstellar turbulence, see Equation (5.12).

5.3.3 Protostellar Outflows

Protostellar jets and outflows are a popular suspect for the energy source of the observed turbulence. We can estimate their average energy input rate, following McKee (1989), by assuming that some fraction f_w of the mass accreted onto a star during its formation is expelled in a wind traveling at roughly the escape velocity. Shu *et al.* (1988) argue that $f_w \approx 0.4$, and that most of the mass is ejected from close to the stellar surface, where the

escape velocity

$$v_{\text{esc}} = \left(\frac{2GM}{R} \right)^{1/2} = (200 \text{ km s}^{-1}) \times \left(\frac{M}{1 M_{\odot}} \right)^{1/2} \left(\frac{R}{10 R_{\odot}} \right)^{-1/2}, \quad (5.16)$$

where the scaling is appropriate for a solar-type protostar with radius $R = 10 R_{\odot}$. Observations of neutral atomic winds from protostars suggest outflow velocities of roughly this value (Lizano *et al.* 1988, Giovanardi *et al.* 2000).

The total energy input from protostellar winds will substantially exceed the amount that can be transferred to the turbulence due to radiative cooling at the wind termination shock. We represent the fraction of energy lost there by η_w . A reasonable upper limit to the energy loss is offered by assuming fully effective radiation and momentum conservation, so that

$$\eta_w < \frac{v_{\text{rms}}}{v_w} = 0.05 \left(\frac{v_{\text{rms}}}{10 \text{ km s}^{-1}} \right) \left(\frac{200 \text{ km s}^{-1}}{v_w} \right) \quad (5.17)$$

where v_{rms} is the rms velocity of the turbulence, and we have assumed that the flow is coupled to the turbulence at typical velocities for the diffuse ISM. If we assumed that most of the energy went into driving dense gas, the efficiency would be lower, as typical rms velocities for CO outflows are 1–2 km s⁻¹. The energy injection rate

$$\begin{aligned} \dot{e} &= \frac{1}{2} f_w \eta_w \frac{\dot{\Sigma}_*}{H} v_w^2 \quad (5.18) \\ &\simeq (2 \times 10^{-28} \text{ erg cm}^{-3} \text{ s}^{-1}) \left(\frac{H}{200 \text{ pc}} \right)^{-1} \\ &\quad \times \left(\frac{f_w}{0.4} \right) \times \left(\frac{v_w}{200 \text{ km s}^{-1}} \right) \left(\frac{v_{\text{rms}}}{10 \text{ km s}^{-1}} \right) \\ &\quad \times \left(\frac{\dot{\Sigma}_*}{4.5 \times 10^{-9} M_{\odot} \text{ pc}^{-2} \text{ yr}^{-1}} \right), \end{aligned}$$

where $\dot{\Sigma}_*$ is the surface density of star formation, and H is the scale height of the star-forming disk. The scaling value used for $\dot{\Sigma}_*$ is the solar neighborhood value (McKee 1989).

Although protostellar jets and winds are indeed quite energetic, they deposit most of their energy into low density gas (Henning 1989), as is

shown by the observation of multi-parsec long jets extending completely out of molecular clouds (Bally & Devine 1994). Furthermore, observed motions of molecular gas show increasing power on scales all the way up to and perhaps beyond the largest scale of molecular cloud complexes (Ossenkopf & Mac Low 2002). It is hard to see how such large scales could be driven by protostars embedded in the clouds.

5.3.4 Massive Stars

In active star-forming galaxies, however, massive stars appear likely to dominate the driving. They do so through ionizing radiation and stellar winds from O stars, and clustered and field supernova explosions, predominantly from B stars no longer associated with their parent gas. The supernovae appear likely to dominate, as we now show.

Stellar Winds

First, we consider stellar winds. The total energy input from a line-driven stellar wind over the main-sequence lifetime of an early O star can equal the energy from its supernova explosion, and the Wolf-Rayet wind can be even more powerful. However, the mass-loss rate from stellar winds drops as roughly the sixth power of the star's luminosity if we take into account that stellar luminosity varies as the fourth power of stellar mass (Vink, de Koter & Lamers 2000), and the powerful Wolf-Rayet winds (Nugis & Lamers 2000) last only 10⁵ years or so, so only the very most massive stars contribute substantial energy from stellar winds. The energy from supernova explosions, on the other hand, remains nearly constant down to the least massive star that can explode. As there are far more lower-mass stars than massive stars, with a Salpeter IMF giving a power-law in mass of $\alpha = -2.35$ (Equation 4.5), supernova explosions will inevitably dominate over stellar winds after the first few million years of the lifetime of an OB association.

HII Region Expansion

Next, we consider ionizing radiation from OB stars. The total amount of energy contained in ionizing radiation is vast. Abbott (1982) estimates the total luminosity of ionizing radiation in the disk to be

$$\dot{e} = 1.5 \times 10^{-24} \text{ erg s}^{-1} \text{ cm}^{-3}. \quad (5.19)$$

However, only a very small fraction of this total energy goes to driving interstellar motions.

Ionizing radiation primarily contributes to interstellar turbulence by ionizing HII regions, heating them to 7000–10,000 K, and raising their pressures above that of surrounding neutral gas, so that they expand supersonically. Matzner (2002) computes the momentum input from the expansion of an individual HII region into a surrounding molecular cloud, as a function of the cloud mass and the ionizing luminosity of the central OB association. By integrating over the HII region luminosity function derived by McKee & Williams (1997), he finds that the average momentum input from a Galactic region is

$$\begin{aligned} \langle \delta p \rangle &\simeq (260 \text{ km s}^{-1}) \left(\frac{N_{\text{H}}}{1.5 \times 10^{22} \text{ cm}^{-2}} \right)^{-3/14} \\ &\times \left(\frac{M_{\text{cl}}}{10^6 M_{\odot}} \right)^{1/14} \langle M_{*} \rangle. \end{aligned} \quad (5.20)$$

The column density N_{H} is scaled to the mean value for Galactic molecular clouds (Solomon *et al.* 1987), which varies little as cloud mass M_{cl} varies. The mean stellar mass per cluster in the Galaxy $\langle M_{*} \rangle = 440 M_{\odot}$ (Matzner 2002).

The number of OB associations contributing substantial amounts of energy can be drawn from the McKee & Williams (1997) cluster luminosity function

$$\mathcal{N}(> S_{49}) = 6.1 \left(\frac{108}{S_{49}} - 1 \right), \quad (5.21)$$

where \mathcal{N} is the number of associations with ionizing photon luminosity exceeding $S_{49} = S/(10^{49} \text{ s}^{-1})$. The luminosity function is rather flat below $S_{49} = 2.4$, the luminosity of a single star of $120 M_{\odot}$, which was the highest mass star

considered, so taking its value at $S_{49} = 1$ is about right, giving $\mathcal{N}(> 1) = 650$ clusters.

To derive an energy input rate per unit volume \dot{e} from the mean momentum input per cluster $\langle \delta p \rangle$, we need to estimate the average velocity of momentum input v_i , the time over which it occurs t_i , and the volume V under consideration. Typically expansion will not occur supersonically with respect to the interior, so $v_i < c_{s,i}$, where $c_{s,i} \simeq 10 \text{ km s}^{-1}$ is the sound speed of the ionized gas. McKee & Williams (1997) argue that clusters typically last for about five generations of massive star formation, where each generation lasts $\langle t_{*} \rangle = 3.7 \text{ Myr}$. The scale height for massive clusters is $H_c \sim 100 \text{ pc}$ (e.g. Bronfman *et al.* 2000), and the radius of the star-forming disk is roughly $R_{sf} \sim 15 \text{ kpc}$, so the relevant volume $V = 2\pi R_{sf}^2 H_c$. The energy input rate from HII regions is then

$$\begin{aligned} \dot{e} &= \frac{\langle \delta p \rangle \mathcal{N}(> 1) v_i}{V t_i} \quad (5.22) \\ &= (3 \times 10^{-30} \text{ erg s}^{-1} \text{ cm}^{-3}) \\ &\times \left(\frac{N_{\text{H}}}{1.5 \times 10^{22} \text{ cm}^{-2}} \right)^{-3/14} \left(\frac{M_{\text{cl}}}{10^6 M_{\odot}} \right)^{1/14} \\ &\times \left(\frac{\langle M_{*} \rangle}{440 M_{\odot}} \right) \left(\frac{\mathcal{N}(> 1)}{650} \right) \left(\frac{v_i}{10 \text{ km s}^{-1}} \right) \\ &\times \left(\frac{H_c}{100 \text{ pc}} \right)^{-1} \left(\frac{R_{sf}}{15 \text{ kpc}} \right)^{-2} \left(\frac{t_i}{18.5 \text{ Myr}} \right)^{-1}, \end{aligned}$$

where all the scalings are appropriate for the Milky Way as discussed above. Nearly all of the energy in ionizing radiation goes towards maintaining the ionization degree of the diffuse medium, and hardly any towards driving turbulence. Flows of ionized gas may be important very close to young clusters and may terminate star formation locally (Section 2.5.11), but do not appear to contribute significantly on a global scale.

Supernovae

The largest contribution from massive stars to interstellar turbulence comes from supernova explosions. To estimate their energy input rate, we begin by finding the supernova rate in the

Galaxy σ_{SN} . Cappellaro *et al.* (1999) estimate the total supernova rate in supernova units to be 0.72 ± 0.21 SNU for galaxies of type S0a-b and 1.21 ± 0.37 SNU for galaxies of type Sbc-d, where $1 \text{ SNU} = 1 \text{ SN} (100 \text{ yr})^{-1} (10^{10} L_B / L_\odot)^{-1}$, and L_B is the blue luminosity of the galaxy. Taking the Milky Way as lying between Sb and Sbc, we estimate $\sigma_{SN} = 1 \text{ SNU}$. Using a Galactic luminosity of $L_B = 2 \times 10^{10} L_\odot$, we find a supernova rate of $(50 \text{ yr})^{-1}$, which agrees well with the estimate in equation (A4) of McKee (1989). If we use the same scale height H_c and star-forming radius R_{sf} as above, we can compute the energy input rate from supernova explosions with energy $E_{SN} = 10^{51} \text{ erg}$ to be

$$\begin{aligned} \dot{e} &= \frac{\sigma_{SN} \eta_{SN} E_{SN}}{\pi R_{sf}^2 H_c} \\ &= (3 \times 10^{-26} \text{ erg s}^{-1} \text{ cm}^{-3}) \\ &\quad \times \left(\frac{\eta_{SN}}{0.1} \right) \left(\frac{\sigma_{SN}}{1 \text{ SNU}} \right) \left(\frac{H_c}{100 \text{ pc}} \right)^{-1} \\ &\quad \times \left(\frac{R_{sf}}{15 \text{ kpc}} \right)^{-2} \left(\frac{E_{SN}}{10^{51} \text{ erg}} \right). \end{aligned} \quad (5.23)$$

The efficiency of energy transfer from supernova blast waves to the interstellar gas η_{SN} depends on the strength of radiative cooling in the initial shock, which will be much stronger in the absence of a surrounding superbubble (e.g. Heiles 1990). Substantial amounts of energy can escape in the vertical direction in superbubbles as well, however. Norman & Ferrara (1996) make an analytic estimate of the effectiveness of driving by SN remnants and superbubbles. The scaling factor $\eta_{SN} \simeq 0.1$ used here was derived by Thornton *et al.* (1998) from one-dimensional numerical simulations of SNe expanding in a uniform ISM, or can alternatively be drawn from momentum conservation arguments comparing a typical expansion velocity of 100 km s^{-1} to typical interstellar turbulence velocity of 10 km s^{-1} . Detailed multi-dimensional modeling of the interactions of multiple SN remnants (e.g. Avillez 2000) will be required to better determine it.

Supernova driving appears to be powerful enough to maintain the turbulence even with the dissipation rates estimated in equation (5.12). It

provides a large-scale self-regulation mechanism for star formation in disks with sufficient gas density to collapse despite the velocity dispersion produced by the magnetorotational instability. As star formation increases in such galaxies, the number of OB stars increases, ultimately increasing the supernova rate and thus the velocity dispersion, which restrains further star formation.

Supernova driving not only determines the velocity dispersion, but may actually form molecular clouds by sweeping gas up in a turbulent flow. Clouds that are turbulently supported will experience inefficient, low-rate star formation, while clouds that are too massive to be supported will collapse (e.g. Kim & Ostriker 2001), undergoing efficient star formation to form OB associations or even starburst knots.

5.4 Applications

Different types of objects with different star formation properties can be qualitatively explained by the combination of density determined by galactic dynamics and turbulence driven by different mechanisms. We here present illustrative scenarios for different objects, moving from low to high star formation efficiency.

5.4.1 Low Surface Brightness Galaxies

Low surface brightness galaxies have large fractions of their baryonic mass in gas, whether they have masses typical of massive (Schombert *et al.* 1992, McGaugh & de Blok 1997) or dwarf galaxies (Schombert, McGaugh, & Eder 2001). Nevertheless, their star formation rates lie well below typical values for high surface brightness galaxies (van der Hulst *et al.* 1993; McGaugh & de Blok 1997). Their rotation curves have been derived from both HI measurements (van der Hulst *et al.* 1993, de Blok, McGaugh, & van der Hulst, 1996), and higher resolution H α measurements (Swaters, Madore, & Trewthall, 2000; McGaugh, Rubin, & de Blok, 2001, Matthews & Gallagher 2002) which may sometimes disagree with the HI in the

innermost regions (Swaters *et al.* 2000), but are in generally good agreement (McGaugh *et al.* 2001). They have lower gas and stellar surface densities than high surface brightness galaxies (van der Hulst *et al.* 1987; de Blok & McGaugh 1996).

The question of whether their disks have surface densities lying below the Kennicutt (1989) threshold for star formation has been studied using rotation curves derived from HI measurements for both massive (van der Hulst *et al.* 1993) and dwarf (van Zee *et al.* 1997) galaxies. In the case of massive galaxies, surface densities beneath the Kennicutt (1989) threshold do indeed appear to explain the lack of star formation (van der Hulst 1993). The moderate levels of turbulence required to maintain the observed velocity dispersions may be produced by magnetorotational instabilities (Sellwood & Balbus 1999). Other explanations for the lack of star formation, such as an inability to form molecular hydrogen (Gerritsen & de Blok 1999) or to cool it (Mihos, Spaans, & McGaugh 1999), were derived from numerical models that did not include magnetic effects, and thus had no source of support other than thermal pressure to counteract gravitational collapse and star formation. If magnetorotational instability is the dominant support mechanism, then star formation will not be suppressed in the center where the rotational shear drops. This is in fact where star formation is found in low surface brightness galaxies.

In the case of dwarf galaxies (Hunter 1997), the situation appears to be slightly more complex. Van Zee *et al.* (1997) demonstrate that the surface density in a sample of low surface brightness dwarf galaxies falls systematically below the Kennicutt threshold, with star formation observed in regions that approach the threshold, while van Zee, Skillman, & Salzer (1998) show that blue compact dwarf galaxies have surface densities exceeding the threshold in their centers. Hunter, Elmegreen, & Baker (1998), on the other hand, argue that a criterion based on local shear correlates better with the observations, especially in galaxies with rising rotation curves. Another factor that may be contributing to the star formation histories of dwarf galaxies is that star-

bursts in the smaller ones (under $10^8 M_{\odot}$) can actually push all the gas well out into the halo, from where it will take some hundreds of millions of years to collect back in the center (Mac Low & Ferrara 1999). This scenario may be consistent with observations in some galaxies, as summarized by Simpson & Gottesman (2000).

5.4.2 Galactic Disks

In normal galactic disks, where SNe appear to dominate the driving of the turbulence, most regions will have a star formation rate just sufficient to produce turbulence that can balance the local surface density in a self-regulating fashion. However, as spiral arms or other dynamical features increase the local density, this balance fails, leading to higher local star formation rates. Because the increase in star formation rate as turbulence is overwhelmed is continuous, the enhanced star formation in spiral arms and similar structures does not globally approach starburst rates except when the densities are greatly enhanced. Locally, however, even relatively small regions can reach starburst-like star formation efficiencies if they exceed the local threshold for turbulent support and begin to collapse freely. A classic example of this is the massive star formation region NGC 3603, which locally resembles a starburst knot, even though the Milky Way globally does not have a large star formation rate. Also the Trapezium cluster in Orion is thought to be formed with efficiency of $\lesssim 50\%$ (Hillenbrand & Hartmann 1998).

5.4.3 Globular Clusters

Globular clusters may simply be the upper end of range of normal cluster formation. Whitmore (2000) reviews evidence showing that young clusters have a power-law distribution reaching up to globular cluster mass ranges. The luminosity function for old globular clusters is log normal, which Fall & Zhang (2001) attribute to the evaporation of the smaller clusters by two-body relaxation, and the destruction of largest clusters by dynamical interactions with the background

galaxy. They suggest that the power-law distribution of young clusters is related to the power-law distribution of molecular cloud masses found by Harris & Pudritz (1995). However, numerical models of gravitational collapse tend to produce mass distributions that appear more log-normal, and are not closely related in shape to the underlying mass distributions of density peaks (Klessen 2001, Klessen *et al.* 2000). It remains unknown whether cluster masses are determined by the same processes as the masses of individual collapsing objects, but the simulations do not include any physics that would limit them to one scale and not the other. Further investigation of this question will be interesting.

5.4.4 Galactic Nuclei

In galaxies with low star formation rates, the galactic nucleus is often the only region with substantial star formation occurring. As rotation curves approach solid body in the centers of galaxies, magnetorotational instabilities will die away, leaving less turbulent support and perhaps greater opportunity for star formation. In more massive galaxies, gas is often funneled towards the center by bars and other disk instabilities, again increasing the local density sufficiently to overwhelm local turbulence and drive star formation.

Hunter *et al.* (1998) and Schaye (2002) note that central regions of galaxies appear to have normal star formation despite having surface densities that appear to be stable according to the Toomre criterion. This could be due to reduced turbulence in these regions reducing the surface density required. This has classically been difficult to measure because H I observations with sufficient velocity resolution to measure typical turbulent linewidths of 6–12 km s⁻¹ have generally had rather low spatial resolution, with just a few beams across the galaxy. Most calculations of the critical surface density just assume a constant value of the turbulent velocity dispersion, which may well be incorrect (Wong & Blitz 2002).

As an alternative, or perhaps additional explanation, Kim & Ostriker (2001) point out that

the magneto-Jeans instability acts strongly in the centers of galaxies. The magnetic tension from strong magnetic fields can reduce or eliminate the stabilizing effects from Coriolis forces in these low shear regions, effectively reducing the problem to a two-dimensional Jeans stability problem along the field lines.

5.4.5 Primordial Dwarfs

In the complete absence of metals, cooling becomes much more difficult. Thermal pressure supports gas that accumulates in dark matter haloes until the local Jeans mass is exceeded. The first objects that can collapse are the ones that can cool from H₂ formation through gas phase reactions. Abel, Bryan, & Norman (2000, 2002) and Bromm, Coppi, & Larson (1999) have computed models of the collapse of these first objects. Abel *et al.* (2000, 2002) used realistic cosmological initial conditions, and found that inevitably a single star formed at the highest density peak before substantial collapse had occurred elsewhere in the galaxy. Bromm *et al.* (1999) used a flat-top density perturbation that was able to fragment in many places simultaneously, due to its artificial symmetry.

Work by Li, Klessen, & Mac Low (2003) suggests that the lack of fragmentation seen by Abel *et al.* (2000, 2002) may be due to the relatively stiff equation of state of metal-free gas. Li *et al.* found that fragmentation of gravitationally collapsing gas is strongly influenced by the polytropic index γ of the gas, with fragmentation continuously decreasing from $\gamma \sim 0.2$ to $\gamma \sim 1.3$. The limited cooling available to primordial gas even with significant molecular fraction may raise its polytropic index sufficiently to suppress fragmentation. Abel and coworkers argue that the resulting stars are likely to have masses exceeding 100 M_⊙, leading to prompt supernova explosions with accompanying metal pollution and radiative dissociation of H₂.

5.4.6 Starburst Galaxies

Star burst galaxies convert gas into stars at such enormous rates, that the timescale to exhaust the

available material becomes short compared to the age of the universe (see the review by Sanders & Mirabel 1996). Starbursts are therefore short-lived phenomena typically lasting for a few tens of Myr, however, may occur several times during the lifespan of a galaxy. The star formation rates in starburst galaxies can be as high as $1000 M_{\odot} \text{ yr}^{-1}$ (Kennicutt 1998) which is three orders of magnitude above the current rate of the Milky Way. Starbursting galaxies are rare in the local universe, but rapidly increase in frequency at larger lookback times suggesting that the starburst phenomenon was a dominant phase of early galaxy evolution at high redshifts. The strongest star bursts are observed towards galactic nuclei or in circumnuclear regions. However, in interacting galaxies, star formation is also triggered far away from the nucleus in the overlapping regions or in spiral arms or sometimes even in tidal tails. In such an interaction a significant number of super-star clusters are formed, which may be the progenitors of present-day globular clusters. The Antennae galaxy, the product of a major merger of two spiral galaxies (NGC 4038 and 4039), is a famous example where star formation is most intense in the overlap region between the two galaxies (Whitmore & Schweizer 1995). Merging events seem always associated with the most massive and most luminous starburst galaxies, the ‘ultraluminous IR galaxies’ – ULIRG’s – (Sanders & Mirabel 1996). However, the starburst phenomenon can also be triggered in a more gentle, minor merger. Such an event disturbs but does not disrupt the primary galaxy. It will recover from the interaction without dramatic changes in its overall morphology. In particular, this may apply to the lower-mass ‘luminous blue compact galaxies’ which often show very little or no sign of interaction (e.g. van Zee, Salzer, & Skillman 2001). Alternative triggers of the starburst phenomenon that have been suggested for these galaxies including bar instabilities in the galactic disk (Shlosman, Begelman, & Frank 1990), or also the compressional effects of multiple supernovae and winds from massive stars (e.g. Heckman, Armus, & Miley 1990) which then would lead to very localized burst of star formation. Regardless of the specific nature of the

triggering mechanism, the relevant property is a fast and efficient flow of gas into a concentrated region on timescales short enough to beat stellar feedback processes. This can only be provided by gravitational torques (Combes 2001). We conclude that starburst galaxies are extreme examples of a continuum of star formation phenomena, with gravity overwhelming any resistive effects of turbulent gas motions on kpc scales.

Chapter 6

CONCLUSIONS

6.1 Summary

The formation of stars represents the triumph of gravity over a succession of opponents. These include thermal pressure, turbulent flows, magnetic flux, and angular momentum. For several decades, magnetic fields were thought to dominate the resistance against gravity, with star formation occurring quasistatically. A growing body of observational evidence suggests that when star formation actually occurs it does so quickly and dynamically, with a rate controlled by driven supersonic turbulence. Such turbulence is required to explain the broad linewidths observed in star-forming clouds, as magnetic fields cannot explain them. The varying balance between turbulence and gravity then provides a natural explanation for the widely varying star formation rates seen both locally and globally. Scattered, inefficient star formation is a signpost of turbulent support, while clustered, efficient star formation occur in regions lacking support. In this picture, gravity has already won in all or nearly all observed dense protostellar cores: dynamical collapse seems to explain their observed properties better than the alternatives. The mass distribution of stars then depends at least partly on the density and velocity structure resulting from the turbulence, perhaps explaining the apparent local variations of the stellar initial mass function (IMF) despite its broad universality.

In Section 2 we summarize and critically discuss the physical phenomena that regulate stellar birth. We begin with a historical overview of the classical dynamical theory of star formation (Section 2.1), which already included turbu-

lent flows, but only in the microturbulent approximation, treating them as an addition to the thermal pressure. We then turn to the development of the standard theory of star formation (Section 2.3) which was motivated by growing understanding of the importance of the interstellar magnetic field in the 1960's and 1970's.

The standard theory relies on ion-neutral drift, also known as ambipolar diffusion, to solve the magnetic flux problem for protostellar cores, which were thought to be initially magnetohydrostatically supported. At the same time magnetic tension resulted in braking of rotating protostellar cores, thus solving the angular momentum problem as well. The timescale for ambipolar diffusion to remove enough magnetic flux from the cores for gravitational collapse to set in can exceed the free-fall time by as much as an order of magnitude, suggesting that magnetic support could also explain low observed star formation rates. Finally, magnetic fields were also invoked to explain observed supersonic motions.

However, both observational and theoretical results have begun to cast doubt on the standard theory. In Section 2.4 we summarize theoretical limitations of the standard isothermal sphere model that forms the basis for many of the practical applications of the standard theory. We discuss several observational findings that put the fundamental assumptions of that theory into question. The observed magnetic field strengths in molecular cloud cores appear too weak to support against gravitational collapse. At the same time, the infall motions measured around star forming cores extend too broadly, while the central density profiles of cores are flatter than ex-

pected for isothermal spheres. Furthermore, the chemically derived ages of cloud cores are comparable to the free-fall time instead of the much longer ambipolar diffusion timescale. Observations of young stellar objects also appear discordant. Accretion rates appear to decrease rather than remaining constant, far more embedded objects have been detected in cloud cores than predicted, and the spread of stellar ages in young clusters does not approach the ambipolar diffusion time.

New theoretical and numerical studies of turbulence that point beyond the standard theory while looking back to the classical dynamical theory for inspiration have now emerged (Section 2.5). Numerical studies demonstrated that supersonic turbulence decays rapidly, in roughly a crossing time of the region under consideration, regardless of magnetic field strength. Under molecular cloud conditions, it decays in less than a free-fall time. This implies that the turbulence in star-forming clouds needs to be continuously driven in order to maintain the observed motions. Driven turbulence has long been thought capable of supporting gas against gravitational collapse. Numerical models were used to test this, showing that turbulence indeed can offer global support, while at the same time leading to local collapse on small scales. In strongly compressible turbulence, gravitational collapse occurs localized in the density enhancements produced by shocks. The rate of local collapse depends strongly on the strength and driving scale of the turbulence. This gives a natural explanation for widely varying star formation rates. Magnetic fields not strong enough to provide static support make a quantitative but not a qualitative difference, reducing the collapse rate somewhat, but not preventing local collapse. They may still act to transfer angular momentum so long as they are coupled to the gas, however.

We outline the shape of the new theory in Section 2.6. Rather than relying on quasistatic evolution of magnetostatically supported objects, it suggests that supersonic turbulent support controls star formation. Inefficient, isolated star formation is a hallmark of turbulent support, while

efficient, clustered star formation occurs in its absence. When stars form, they do so dynamically, collapsing on the local free-fall time. The initial conditions of clusters appear largely determined by the properties of the turbulent gas, as is the rate of mass accretion onto these objects. The balance between turbulent support and local density then determines the star formation rate. Turbulent support is provided by some combination of supernovae and galactic rotation, along with possible contributions from other processes. Local density is determined by galactic dynamics and interactions, along with the balance between heating and cooling in a region. The initial mass function is at least partly determined by the initial distribution of density resulting from turbulent flows, although a contribution from stellar feedback and interactions with nearby stars cannot be ruled out. The initial conditions for stellar clusters in this theory come from the turbulent flow from which they formed.

We explore the implications of the control of star formation by supersonic turbulence at the scale of individual stars and stellar clusters in Section 4. We begin by looking more closely at the structure of turbulent molecular clouds (Section 4.1), noting that some well known descriptions like Larson's (1981) laws may be natural consequences of a turbulent flow observed in projection. Observations indicate that interstellar turbulence is driven on large scales, quite likely on scales substantially larger than the clouds themselves (see also Section 5.3). We examine how turbulent fragmentation determines the star forming properties of molecular clouds (Section 4.2), and then turn to discuss protostellar cores (Section 4.3) and stellar clusters (Section 4.4) in particular. Strongly time-varying protostellar mass growth rates may result as a natural consequence of competitive accretion in nascent embedded clusters (Section 4.5). Turbulent models predict protostellar mass distributions that appear roughly consistent with the observed stellar mass spectrum (Section 4.7), although more work needs to be done to arrive at a full understanding of the origin of stellar masses.

The same balance between turbulence and grav-

ity that seems to determine the efficiency of star formation in molecular clouds may also work at galactic scales, as we discuss in Section 5. We begin by describing the effects of differential rotation and thermal instability competing and cooperating with turbulence to determine the overall star formation efficiency in Section 5.1. The transient nature of molecular clouds suggests that they form from gas compressed by large-scale turbulent flows in galactic disks. This very same flow may also drive the turbulent motions observed within the clouds, and furthermore, may also be responsible for their destruction on a short timescale (Section 5.2). We then examine the physical mechanisms that could drive the interstellar turbulence, focusing our discussion on the energy available from each mechanism in Section 5.3. In star-forming regions of disks, supernovae appear to overwhelm all other possibilities. In outer disks and low surface brightness galaxies, on the other hand, the situation is not so clear: magnetorotational or gravitational instabilities look most likely to drive the observed flows. Finally, in Section 5.4, we give examples of how this picture may apply to different types of objects, including low surface brightness, normal, and starburst galaxies, as well as galactic nuclei and globular clusters.

6.2 Future Research Problems

Although the outline of a new theory of star formation has emerged, it is by no means complete. The ultimate goal of a predictive, quantitative theory of the star formation rate and initial mass function remains elusive. It may be that the problem is intrinsically so complex, like terrestrial climate, that no single solution exists, but only a series of temporary, quasi-steady states. Certainly our understanding of the details of the star formation process can be improved, though. Ultimately, coupled models capturing different scales are likely necessary to capture the interaction of the turbulent cascade with the varying thermodynamics, chemistry, and opacity of gas at different densities. We can identify several major questions that capture the outstanding problems. As

we merely want to summarize these open issues in star formation, we refrain from giving an in-depth discussion and the associated references, which may largely be found in the body of the review.

How can we describe turbulence driven by astrophysical processes? It is not uniform at the driving scale, both because of its magnetization, and because of the non-uniformity of explosions and other drivers. The scalefree nature of the turbulent cascade is further perturbed by the drastic changes in the equation of state that occur as densities increase, leading to stronger radiative cooling and the reduction of heating by the exclusion of cosmic rays. At small scales, diffusion and dissipation mechanisms determine the structure. Although ambipolar diffusion probably limits the production of small-scale magnetic field structures, there is increasing theoretical support for additional density and velocity structure at scales below the ambipolar diffusion cutoff, whose interaction with self-gravity needs to be investigated. Ultimately, the dense regions produced by this imperfect cascade play one of the major roles in determining the initial mass function of stars.

What determines the masses of individual stars? The size of the initial reservoir of collapsing gas, determined by turbulent flow, must be one element. Subsequent accretion from the turbulent gas, perhaps in competition with other stars, or even by collisions between either protostellar cores or stars, could also be important, but must be shown to occur, in particular in a magnetized medium. The properties of protostellar objects depend on the time history of this accretion. Feedback from the newly formed star itself, or from its neighbors, in the form of radiation pressure, ionizing radiation, or stellar winds and jets, may yet prove to be another bounding term on stellar mass.

At what scales does the conservation of angular momentum and magnetic flux fail? That they must fail is clear from the vast discrepancy between galactic and stellar values. Protostellar jets almost certainly form when magnetic fields redistribute angular momentum away from accreting gas. This demonstrates that the conservation of

flux and angular momentum must be coupled at least at small scales. However, the observational hint that molecular cloud cores may be lacking substantial magnetic flux from the galactic value suggests that magnetic flux may already be lost at rather large scales. Sweeping gas along field lines during the formation of molecular clouds, magnetic reconnection processes, and ambipolar diffusion in combination with turbulent transport offer possible solutions that require further investigation. These processes allow for the necessary compression of gas to higher densities while at the same time increase the mass-to-flux ratio. However, on scales of individual stellar systems, the observed high fraction of binary stars suggests that magnetic braking cannot be completely efficient at draining angular momentum from collapsing protostars, and indicates that ambipolar diffusion may limit the effectiveness of braking.

What determines the initial conditions of stellar clusters? The spatial distribution of stars of different masses in a stellar cluster or association, the initial velocity dispersion of its stars, and its binary distribution probably all depend largely on the properties of the turbulent flow from which it formed. How much depends on the details of the turbulence, and how much depends on the properties of dynamically collapsing gas must still be determined. The influence of magnetic fields on these properties remains an almost unexplored field, although their ability to redistribute angular momentum suggests that they must play at least some role.

What controls the distribution and metallicity of gas in star-forming galaxies? At the largest scale, gas follows the potential of a galaxy just as do all its other constituents. The dissipative nature of gas can allow it to quickly shed angular momentum in disturbed potentials and fall to the centers of galaxies, triggering starbursts. Even in normal galaxies, gravitational instability may determine the location of the largest concentrations of gas available for star formation. How important is turbulence in determining the location and properties of molecular clouds formed from that gas? Are the molecular clouds destroyed again by the

same turbulent flow that created them, or do they decouple from the flow, only to be destroyed by star formation within them? How slowly do turbulent flows mix chemical inhomogeneities, and can the scatter of metallicities apparent in stars of apparently equal age be explained by the process?

Where and how fast do stars form in galaxies? The existence of the empirical Schmidt Law relating gas column density to star formation rate, probably with a threshold at low column density, still needs to be definitively explained. Can the threshold be caused by a universal minimum level of turbulence, or by a minimum column density below which it is difficult for gas to cool? In either case, examination of low-metallicity and dwarf galaxies may well provide examples of objects sufficiently different from massive disk galaxies in both cooling and rotation to demonstrate one or the other of these possibilities.

What determines the star formation efficiency of galaxies? The relative importance of turbulence, rotation, gravitational instability, and thermal instability remains unresolved. At this scale, turbulence can only play an instrumental role, transmitting the influence of whatever drives it to the interstellar gas. One possibility is that galaxies are essentially self-regulated, with Type II supernovae from recent star formation determining the level of turbulence, and thus the ongoing star formation rate. Another possibility is that a thermal or rotational bottleneck to star formation exists, and that galaxies actually form stars just as fast as they are able, more or less regardless of the strength of the turbulence in most reasonable regimes. Finding observational and theoretical means to distinguish these scenarios represents the great challenge of understanding the large-scale behavior of star formation in galaxies.

BIBLIOGRAPHY

- Abbott, D. C., 1982, *Astrophys. J.*, **263**, 723
- Adams, F. C., and M. Fatuzzo, 1996, *Astrophys. J.*, **464**, 256
- Adams, F. C., and P. C. Myers, 2001, *Astrophys. J.*, **553**, 744
- Adams, F. C., and J. J. Wiseman, 1994, *Astrophys. J.*, **435**, 693
- Aikawa, Y., N. Ohashi, S. Inutsuka, E. Herbst, and S. Takakuwa, 2001, *Astrophys. J.*, **552**, 639
- Alves, J. F., C. J. Lada, and E. A. Lada, 1999, *Astrophys. J.*, **515**, 265
- Alves, J. F., C. J. Lada, and E. A. Lada, 2001, *Nature*, **409**, 159
- André, P., and T. Montmerle, 1994, *Astrophys. J.*, **420**, 837
- André, P., D. Ward-Thompson, and M. Barsony, 2000, in *Protostars and Planets IV*, edited by V. Mannings, A. P. Boss, and S. S. Russell (University of Arizona Press, Tucson), p. 59
- André, P., D. Ward-Thompson, and F. Motte, 1996, *Astron. Astrophys.*, **314**, 625
- Avillez, M. A., 2000, *Mon. Not. R. Astron. Soc.*, **315**, 479
- Arons, J., and C. E. Max, 1975, *Astrophys. J. (Letters)*, **196**, L77
- Bacmann, A., P. André, J. -L Puget, A. Abergel, S. Bontemps, and D. Ward-Thompson, 2000, *Astron. Astrophys.*, **361**, 555
- Balbus, S. A., and J. F. Hawley, 1991, *Astrophys. J.*, **376**, 214
- Balbus, S. A., and J. F. Hawley, 1998, *Rev. Mod. Phys.*, **70**, 1
- Baldry, I. K. et al. 2002, *Astrophys. J.*, **569**, 582
- Balk, A. M., 2001, *Phys. Lett. A*, **279**, 370
- Balkovsky, E., and G. Falkovich, 1998, *Phys. Rev. E*, **57**, R1231
- Balkovsky, E., G. Falkovich, I. Kolokolov, V. Lebedev, 1997, *Phys. Rev. Lett.*, **78**, 1452
- Ballesteros-Paredes, J., and M.-M. Mac Low, 2002, *Astrophys. J.*, **570**, 734
- Ballesteros-Paredes, J., L. Hartmann, and E. Vázquez-Semadeni, 1999a, *Astrophys. J.*, **527**, 285
- Ballesteros-Paredes, J., R. S. Klessen, and E. Vázquez-Semadeni, 2003, *Astrophys. J.*, in press (astro-ph/0301546)
- Ballesteros-Paredes, J., E. Vázquez-Semadeni, and A. A. Goodman, 2002, *Astrophys. J.* **571**, 334
- Ballesteros-Paredes, J., E. Vázquez-Semadeni, and J. Scalo, 1999b, *Astrophys. J.*, **515**, 286
- Bally, J., and D. Devine, 1994, *Astrophys. J.*, **428**, L65
- Bally, J., D. Devine, and B. Reipurth, 1996, *Astrophys. J.*, **473**, L49
- Balsara, D. S., 1996, *Astrophys. J.*, **465**, 775
- Balsara, D., and A. Pouquet, 1999, *Phys. Plasmas*, **6**, 89
- Balsara, D. S., D. Ward-Thompson, and R. M. Crutcher, 2001, *Mon. Not. R. Astron. Soc.*, **327**, 715
- Balsara, D. S., R. M. Crutcher, and A. Pouquet, 2001, *Astrophys. J.*, **557**, 451
- Barrado y Navascués, D., J. R. Stauffer, J. Bouvier, and E. L. Martín, 2001, *Astrophys. J.*, **546**, 1006
- Baschek, B., M. Scholz, and R. Wehrse, 1991, *Astron. Astrophys.*, **246**, 374
- Bastien, P., J. Arcoragi, W. Benz, I. A. Bonnell, and H. Martel, 1991, *Astrophys. J.*, **378**, 255
- Basu, S., 1997, *Astrophys. J.*, **485**, 240
- Basu, S. and T. C. Mouschovias, 1994, *Astrophys. J.*, **432**, 720
- Basu, S. and T. C. Mouschovias, 1995a, *Astrophys. J.*, **452**, 386
- Basu, S. and T. C. Mouschovias, 1995b, *Astrophys. J.*, **453**, 271
- Batchelor, G. K., 1949, *Austral. J. Sci. Res.*, **2**, 437
- Bate, M. R., 2000, *Mon. Not. R. Astron. Soc.*, **314**, 33
- Bate, M. R., and A. Burkert, 1997, *Mon. Not. R. Astron. Soc.*, **288**, 1060
- Bate, M. R., C. J. Clarke, and M. J. McCaughrean, 1998, *Mon. Not. R. Astron. Soc.*, **297**, 1163
- Bate, M. R., I. A. Bonnell, and V. Bromm, 2002, *Mon. Not. R. Astron. Soc.*, **332**, L65
- Bate, M. R., I. A. Bonnell, and N. M. Price, 1995, *Mon. Not. R. Astron. Soc.*, **277**, 362
- Baureis, P., R. Ebert, and F. Schmitz, 1989, *Astron. Astrophys.*, **225**, 405
- Beckwith, S. V. W., 1999, in *NATO ASIC Proc. 540: The Origin of Stars and Planetary Systems*, edited by C. J. Lada and N. D. Kylafis (Kluwer Academic Publishers), p. 579
- Beichman, C. A., P. C. Myers, J. P. Emerson, S. Harris, R. Mathieu, P. J. Benson, and R. E. Jennings, 1986, *Astrophys. J.*, **307**, 337
- Bensch F., J. Stutzki, and V. Ossenkopf, 2001, *Astron. Astrophys.* **336**, 636
- Benson, P. J., and P. C. Myers, 1989, *Astrophys. J. Suppl. Ser.*, **71**, 89
- Benz, W., 1990, in *The Numerical Modelling of Nonlinear Stellar Pulsations*, edited by J. R. Buchler (Kluwer, Dordrecht), 269
- Bergin, E. A., and W. D. Langer, 1997, *Astrophys. J.*, **486**, 316

- Bergin, E. A., P. F. Goldsmith, R. L. Snell, and W. D. Langer, 1997a, *Astrophys. J.*, **428**, 285
- Bergin, E. A., H. Ungerechts, P. F. Goldsmith, R. L. Snell, W. M. Irvine, and F. P. Schloerb, 1997b, *Astrophys. J.*, **482**, 267
- Bertoldi, F., and C. C. McKee, 1996, in *Amazing Light: A Volume Dedicated to C. H. Townes on his 80th Birthday*, edited by R. Chiao (Springer, New York), p. 41
- Bertout, C., 1989, *Ann. Rev. Astron. Astrophys.*, **27**, 351
- Bertschinger, E., 1998, *Ann. Rev. Astron. Astrophys.*, **36**, 599
- Binney, J., and S. Tremaine, 1987, *Galactic Dynamics* (Princeton University Press, Princeton)
- Biskamp, D., W. C. Müller, 1999, *Phys. Rev. Lett.*, **83**, 2195
- Biskamp, D., and W.-C. Müller, 2000, *Phys. Plasmas*, **7**, 4889
- Black, D. C., and P. Bodenheimer, 1976, *Astrophys. J.*, **206**, 138
- Blitz, L., 1993, in *Protostars and Planets III*, edited by E. H. Levy and J. I. Lunine (University of Arizona Press, Tucson), p. 125
- Blitz, L., and F. H. Shu, 1980, *Astrophys. J.*, **238**, 148
- Bodenheimer, P., 1995, *Ann. Rev. Astron. Astrophys.*, **33**, 199
- Bodenheimer, P., and A. Sweigart, 1969, *Astrophys. J.*, **152**, 515
- Bodenheimer, P., and W. Tscharnuter, 1979, *Astron. Astrophys.*, **74**, 288
- Bodenheimer, P., A. Burkert, R. I. Klein, and A. P. Boss, 2000, in *Protostars and Planets IV*, edited by V. Mannings, A. P. Boss, and S. S. Russell (University of Arizona Press, Tucson), p. 327
- Boldyrev, S., 2002, *Astrophys. J.*, **569**, 841
- Boldyrev, S., Å. Nordlund, and P. Padoan, 2002a, *Astrophys. J.*, **573**, 678
- Boldyrev, S., Å. Nordlund, and P. Padoan, 2002b, *Phys. Rev. Lett.*, submitted (astro-ph/0203452)
- Bonazzola, S., E. Falgarone, J. Heyvaerts, M. Perault, and J. L. Puget, 1987, *Astron. Astrophys.*, **172**, 293
- Bonazzola, S., M. Perault, J. L. Puget, J. Heyvaerts, E. Falgarone, J. F. Panis, 1992, *J. Fluid Mech.*, **245**, 1
- Bonnell, I. A., and M. R. Bate, 2002, *Mon. Not. R. Astron. Soc.*, in press
- Bonnell, I. A., and M. B. Davies, 1998, *Mon. Not. R. Astron. Soc.*, **295**, 691.
- Bonnell, I. A., M. R. Bate, and H. Zinnecker, 1998, *Mon. Not. R. Astron. Soc.*, **298**, 93
- Bonnell, I. A., M. R. Bate, C. J. Clarke, and J. E. Pringle, 1997, *Mon. Not. R. Astron. Soc.*, **285**, 201
- Bonnell, I. A., M. R. Bate, C. J. Clarke, and J. E. Pringle, 2001a, *Mon. Not. R. Astron. Soc.*, **323**, 785
- Bonnell, I. A., C. J. Clarke, M. R. Bate, and J. E. Pringle, 2001b, *Mon. Not. R. Astron. Soc.*, **324**, 573
- Bonnell, I. A., K. W. Smith, M. B. Davies, and K. Horne, 2001c, *Mon. Not. R. Astron. Soc.*, **322**, 859
- Bonnor, W. B., 1956, *Mon. Not. R. Astron. Soc.*, **116**, 351
- Bontemps, S., P. André, S. Terebey, and S. Cabrit, 1996, *Astron. Astrophys.*, **311**, 858
- Bontemps, S. and 21 colleagues, 2001, *Astron. Astrophys.*, **372**, 173
- Boratav, O., A. Eden, A., and A. Erzan (eds.), 1997, *Turbulence Modeling and Vortex Dynamics* (Springer Verlag, Heidelberg)
- Boss, A. P., 1980a, *Astrophys. J.*, **237**, 563
- Boss, A. P., 1980b, *Astrophys. J.*, **237**, 866
- Boss, A. P., 1996, *Astrophys. J.*, **468**, 231
- Boss, A. P., 2000, *Astrophys. J. (Letters)*, **545**, 61
- Boss, A. P., 2002, *Astrophys. J.*, **568**, 743
- Boss, A. P. and P. Bodenheimer, 1979, *Astrophys. J.*, **234**, 289
- Boss, A. P., and L. Hartmann, 2002, *Astrophys. J.*, **562**, 842
- Boss, A. P., and E. A. Myhill, 1995, *Astrophys. J.*, **451**, 218
- Boss, A. P., R. T. Fisher, R. I. Klein, and C. F. McKee, 2000, *Astrophys. J.*, **528**, 325
- Bourke, T. L., P. C. Myers, G. Robinson, and A. R. Hyland, 2001, *Astrophys. J.*, **554**, 916
- Brandl, B., W. Brandner, F. Eisenhauer, A. F. J. Moffat, F. Palla, and H. Zinnecker, 1999, *Astron. Astrophys.*, **352**, L69
- Bronfman, L., S. Casassus, J. May, and L.-Å. Nyman, 2000, *Astron. Astrophys.*, **358**, 521
- Bronstein, I. N., and K. A. Semendjajew, 1979, *Taschenbuch der Mathematik* (Teubner Verlagsgesellschaft, Leipzig)
- Burkert, A., M. R. Bate, and P. Bodenheimer, 1997, *Mon. Not. R. Astron. Soc.*, **289**, 497
- Burkert, A., and P. Bodenheimer, 1993, *Mon. Not. R. Astron. Soc.*, **264**, 798
- Burkert, A., and P. Bodenheimer, 1996, *Mon. Not. R. Astron. Soc.*, **280**, 1190
- Burkert, A. and D. N. C. Lin, 2000, *Astrophys. J.*, **537**, 270
- Burkert, A., M. R. Bate, and P. Bodenheimer, 1997, *Mon. Not. R. Astron. Soc.*, **289**, 497
- Burrows, A., W. B. Hubbard, J. I. Lunine, and J. Liebert, 2001, *Rev. Mod. Phys.*, **73**, 719
- Burrows, A., W. B. Hubbard, D. Saumon, and J. I. Lunine, 1993, *Astrophys. J.*, **406**, 158
- Butner, H. M., E. A. Lada, and R. B. Loren, 1995, *Astrophys. J.*, **448**, 207
- Cabrit, S., and C. Bertout, 1992, *Astron. Astrophys.*, **261**, 274
- Cao, N., S. Chen, and Z.-S. She, 1996, *Phys. Rev. Lett.*, **76**, 3711
- Cambrésy, L., C. A. Beichman, T. H. Jarrett, and R. M. Cutri, 2002, *Astron. J.*, **123**, 2559
- Cappellaro, E., R. Evans, and M. Turatto, 1999, *Astron. Astrophys.*, **351**, 459
- Carlberg, R. G., and R. E. Pudritz, 1990, *Astrophys. J.*, **247**, 353

- Carpenter, J. M., M. R. Meyer, C. Dougados, S. E. Strom, and L. A. Hillenbrand, 1997, *Astron. J.*, **114**, 198
- Carr, J. S., 1987, *Astrophys. J.*, **323**, 170
- Caselli, P. and P. C. Myers, 1995, *Astrophys. J.*, **446**, 665
- Castiglione, P., A. Mazzino, P. Muratore-Ginanneschi, and A. Vulpiani, 1999, *Physica D*, **134**, 75
- Castor, J. I., 1972, *Astrophys. J.*, **178**, 779
- Caughlan, G. R., and W. A. Fowler, 1988, *Atomic Data and Nuclear Data Tables*, **40**, 283
- Cernicharo, J., 1991, in *The Physics of StarFormation and Early Stellar Evolution*, edited by C. J. Lada and N. Kylafis (Kluwer Academic Publishers, Dordrecht), p. 287
- Chabrier, G., 2001, *Astrophys. J.*, **554**, 1274
- Chabrier, G., 2002, *Astrophys. J.*, **567**, 304
- Chandrasekhar, S., 1949, *Astrophys. J.*, **110**, 329
- Chandrasekhar, S., 1951a, *Proc. R. Soc. London A*, **210**, 18
- Chandrasekhar, S., 1951b, *Proc. R. Soc. London A*, **210**, 26
- Chandrasekhar, S., 1953, *Astrophys. J.*, **118**, 116
- Chandrasekhar, S., 1954, *Astrophys. J.*, **119**, 7
- Chandrasekhar, S., and E. Fermi, 1953a, *Astrophys. J.*, **118**, 113
- Chandrasekhar, S., and E. Fermi, 1953b, *Astrophys. J.*, **118**, 116
- Chapman, S., H. Pongracic, M. Disney, A. Nelson, J. Turner, and A. Whitworth, 1992, *Nature*, **359**, 207
- Chen, H., P. C. Myers, E. F. Ladd, and D. O. S. Wood, 1995, *Astrophys. J.*, **445**, 377
- Chertkov, M., I. Kolokolov, and M. Vergassola, 1997, *Phys. Rev. E*, **56**, 5483
- Cho, J., and A. Lazarian, 2002, in *Acoustic emission and scattering by turbulent flows*, edited by M. Rast (Springer Verlag, Heidelberg) (astro-ph/0301462)
- Cho, J., A. Lazarian, and E. T. Vishniac, 2002, *Astrophys. J.*, **566**, L49
- Chu, Y.-H., N. B. Suntzeff, J. E. Hesser, and D. A. Bohlender, 1999, *New Views of the Magellanic Clouds* (Proceedings of IAU Symposium 190, ASP Conference Series, Vol. 190)
- Ciolek, G. E., and S. Basu, 2000, *Astrophys. J.*, **529**, 925
- Ciolek, G. E., and S. Basu, 2001, *Astrophys. J.*, **547**, 272
- Ciolek, G. E. and T. C. Mouschovias, 1993, *Astrophys. J.*, **418**, 774
- Ciolek, G. E. and T. C. Mouschovias, 1994, *Astrophys. J.*, **425**, 142
- Ciolek, G. E. and T. C. Mouschovias, 1995, *Astrophys. J.*, **454**, 194
- Ciolek, G. E. and T. C. Mouschovias, 1996, *Astrophys. J.*, **468**, 749
- Ciolek, G. E. and T. C. Mouschovias, 1998, *Astrophys. J.*, **504**, 280
- Clarke, C. J., and J. E. Pringle, 1991, *Mon. Not. R. Astron. Soc.*, **249**, 584
- Clarke, C. J., I. A. Bonnell, and L. A. Hillenbrand, 2000, in *Protostars and Planets IV*, edited by V. Mannings, A. P. Boss, and S. S. Russell (University of Arizona Press, Tucson), p. 151
- Clarke, D. 1994, National Center for Supercomputing Applications Technical Report
- Clemens, D. P., 1985, *Astrophys. J.*, **295**, 422
- Coleman, G., J. Kim, and R. D. Moser, 1995, *J. Fluid Mech.*, **305**, 159
- Combes, F., 2001, in *The Central Kiloparsec of Starbursts and AGN*, edited by J. H. Knapen, J. E. Beckman, I. Shlosman, and T. J. Mahoney (ASP Conference Series 249), p. 475.
- Cook, T. L., and F. H. Harlow, 1978, *Astrophys. J.*, **225**, 1005
- Crutcher, R. M., 1999, *Astrophys. J.*, **520**, 706
- Crutcher, R. M. and T. H. Troland, 2000, *Astrophys. J.*, **537**, L139
- Curry, C. L., 2002, *Astrophys. J.*, **576**, 849
- Curry C. L., and C. F. McKee, 2000, *Astrophys. J.*, **528**, 734
- Dalgarno, A. and R. A. McCray, 1972, *Ann. Rev. Astron. Astrophys.*, **10**, 375
- Dame, T. M., B. G. Elmegreen, R. S. Cohen, and P. Thaddeus, 1986, *Astrophys. J.*, **305**, 892
- D'Antona, F., and I. Mazzitelli, 1994, *Astrophys. J. Suppl. Ser.*, **90**, 467
- Davies, R. D. and W. L. H. Shuter, 1963, *Mon. Not. R. Astron. Soc.*, **126**, 369
- de Blok, W. J. G., and S. S. McGaugh, 1996, *Astrophys. J. (Letters)*, **469**, L89
- Dehnen, W., and J. J. Binney, 1998, *Mon. Not. R. Astron. Soc.*, **294**, 429
- Deiss, B. M., A. Just, and W. H. Kegel, 1990, *Astron. Astrophys.*, **240**, 123
- Desch, S. J. and T. C. Mouschovias, 2001, *Astrophys. J.*, **550**, 314
- de Vega, H. J., and N. Sánchez, 2000, *Phys. Lett. B*, **490**, 180
- de Vega, H. J., and N. Sánchez, 2001a, (astro-ph/0101568)
- de Vega, H. J., and N. Sánchez, 2001a, (astro-ph/0101568)
- de Vega, H. J., N. Sánchez, and F. Combes, 1996a, *Nature*, **383**, 56
- de Vega, H. J., N. Sánchez, and F. Combes, 1996b, *Phys. Rev. D*, **54**, 6008
- Dewar, R. L., 1970, *Phys. Fluids*, **13**, 2710
- Diaz-Miller, R. I., J. Franco, and S. N. Shore, 1998, *Astrophys. J.*, **501**, 192.
- Dickey, J. M., M. M. Hanson, and G. Helou, 1990, *Astrophys. J.*, **352**, 522
- Dickey, J. M., and F. J. Lockman, 1990, *Ann. Rev. Astron. Astrophys.*, **28**, 215

- Dickman, R. L., R. L. Snell, and F. P. Schloerb, 1986, *Astrophys. J.*, **309**, 326
- Domolevo, K., and L. Sainsaulieu, 1997, *J. Comput. Phys.*, **133**, 256
- Draine, B. T., 1980, *Astrophys. J.*, **241**, 1021
- Dubinski, J., R. Narayan, and T. G. Phillips, 1995, *Astrophys. J.*, **448**, 226
- Duquennoy, A., and M. Mayor, 1991, *Astron. Astrophys.*, **248**, 485
- Durisen, R. H., M. F. Sterzik, and B. K. Pickett, 2001, *Astron. Astrophys.*, **371**, 952
- Ebert, R., 1955, *Z. Astrophys.*, **36**, 222
- Ebert, R., 1957, *Z. Astrophys.*, **42**, 263
- Ebert, R., S. von Hoerner, and St. Temesváry, 1960, in *Die Entstehung von Sternen durch Kondensation diffuser Materie*, authored by G. R. Burbidge, F. D. Kahn, R. Ebert, S. von Hoerner, and St. Temesváry (Springer Verlag, Berlin), 184
- Ebisuzaki T., Makino J., Fukushige T., Taiji M., Sugimoto D., Ito T., Okumura S.K. 1993, *Pub. Astron. Soc. Japan* **45**, 269
- Efremov, Y. N., and B. G. Elmegreen, 1998, *Mon. Not. R. Astron. Soc.*, **299**, 588
- Elmegreen, B. G., 1979, *Astrophys. J.*, **232**, 729
- Elmegreen, B. G., 1985, *Astrophys. J.*, **299**, 196
- Elmegreen, B. G., 1991, in *NATO ASIC Proc. 342: The Physics of Star Formation and Early Stellar Evolution*, edited by C. J. Lada and N. D. Kylafis (Kluwer Academic Publishers), p. 35
- Elmegreen, B. G., 1990, *Astrophys. J.*, **361**, L77
- Elmegreen, B. G., 1993, *Astrophys. J.*, **419**, L29
- Elmegreen, B. G., 1995, *Mon. Not. R. Astron. Soc.*, **275**, 944
- Elmegreen, B. G., 1997a, *Astrophys. J.*, **480**, 674.
- Elmegreen, B. G., 1997b, *Astrophys. J.*, **486**, 944
- Elmegreen, B. G., 1999a, *Astrophys. J.*, **515**, 323
- Elmegreen, B. G., 1999b, *Astrophys. J.*, **527**, 266
- Elmegreen, B. G., 2000a, *Mon. Not. R. Astron. Soc.*, **311**, L5
- Elmegreen, B. G., 2000b, *Astrophys. J.*, **530**, 277
- Elmegreen, B. G., 2000c, *Astrophys. J.*, **539**, 342
- Elmegreen, B. G., 2002a, *Astrophys. J.*, **564**, 773
- Elmegreen, B. G., 2002b, *Astrophys. J.*, **577**, in press (astro-ph/02027114)
- Elmegreen, B. G., and E. Falgarone, 1996, *Astrophys. J.*, **471**, 816
- Elmegreen, B. G., and R. D. Mathieu, 1983, *Mon. Not. R. Astron. Soc.*, **203**, 305
- Elmegreen, B. G., and F. Combes, 1992, *Astron. Astrophys.*, **259**, 232
- Elmegreen, B. G., C. J. Lada, and D. F. Dickinson, 1979 *Astrophys. J.*, **230**, 415
- Elmegreen, B. G., Y. Efremov, R. E. Pudritz, and H. Zinnecker, 2000, in *Protostars and Planets IV*, edited by V. Mannings, A. P. Boss, and S. S. Russell (University of Arizona Press, Tucson), p. 179
- Falgarone, E., and T. G. Phillips, 1996, *Astrophys. J.*, **472**, 191
- Falgarone, E., J. L. Puget, and M. Perault, 1992, *Astron. Astrophys.*, **257**, 715
- Falgarone, E., D. C. Lis, T. G. Phillips, A. Pouquet, D. H. Porter, and P. R. Woodward, 1994, *Astrophys. J.*, **436**, 728
- Falgarone, E., J.-F. Panis, A. Heithausen, M. Pérault, J. Stutzki, J.-L. Puget, and F. Bensch, 1998, *Astron. Astrophys.*, **331**, 669
- Falkovich, G., and V. Lebedev, 1997, *Phys. Rev. Lett.*, **79**, 4159
- Feigelson, E. D., 1996, *Astrophys. J.*, **468**, 306
- Fiedler, R. A. and T. C. Mouschovias, 1992, *Astrophys. J.*, **391**, 199
- Fiedler, R. A. and T. C. Mouschovias, 1993, *Astrophys. J.*, **415**, 680
- Fiege, J. D., and R. E. Pudritz, 1999, in *New Perspectives on the Interstellar Medium*, edited by A. R. Taylor, T. L. Landecker, and G. Joncas (ASP Conference Series 168), p. 248
- Fiege, J. D., and R. E. Pudritz, 2000a, *Mon. Not. R. Astron. Soc.*, **311**, 85
- Fiege, J. D., and R. E. Pudritz, 2000b, *Mon. Not. R. Astron. Soc.*, **311**, 105
- Field, G. B., 1965, *Astrophys. J.*, **142**, 531
- Field, G. B., 1978, in *Protostars and Planets*, edited by T. Gehrels (University of Arizona Press, Tucson), p. 243
- Field, G. B., D. W. Goldsmith, and H. J. Habing, 1969, *Astrophys. J.*, **155**, L49
- Fischer, D. A., and G. W. Marcy, 1992, *Astrophys. J.*, **396**, 178
- Fleck, R. C., 1981, *Astrophys. J.*, **246**, L151
- Fleck, R. C., 1982, *Mon. Not. R. Astron. Soc.*, **201**, 551
- Forbes, D., 1996, *Astron. J.*, **112**, 1073
- Franco, J., and A. Carraminana (eds.), 1999, *Interstellar Turbulence* (Cambridge University Press)
- Foster, P. N., and R. A. Chevalier, 1993, *Astrophys. J.*, **416**, 303
- Franco, J., S. N. Shore, and G. Tenorio-Tagle, 1994, *Astrophys. J.*, **436**, 795
- Fricke, K. J., C. Moellenhoff, and W. Tscharnuter, 1976, *Astron. Astrophys.*, **47**, 407
- Frisch, U., 1995, *Turbulence – The Legacy of A. N. Kolmogorov* (Cambridge University Press)
- Fukui, Y. et al., 1999, *Pub. Astron. Soc. Japan*, **51**, 745
- Fuller, G. A., and P. C. Myers, 1992, *Astrophys. J.*, **384**, 523
- Galli, D., F. H. Shu, G. Laughlin, and S. Lizano, 2001, *Astrophys. J.*, **551**, 367
- Galli, D., S. Lizano, Z. Y. Li, F. C. Adams, and F. H. Shu, 1999, *Astrophys. J.*, **521**, 630

- Galli, D. and F. H. Shu, 1993a, *Astrophys. J.*, **417**, 220
- Galli, D. and F. H. Shu, 1993b, *Astrophys. J.*, **417**, 243
- Gammie, C. F., and E. C. Ostriker, 1996, *Astrophys. J.*, **466**, 814
- Gazol, A., E. Vázquez-Semadeni, F. J. Sánchez-Salcedo, and J. Scalo, 2001, *Astrophys. J.*, **557**, L121
- Genzel, R., 1991, in *The Physics of Star Formation and Early Stellar Evolution*, edited by C. J. Lada and N. D. Kylafis (Kluwer Academic Publishers, Dordrecht), p. 155
- Gilden, D. L., 1984a, *Astrophys. J.*, **279**, 335
- Gilden, D. L., 1984b, *Astrophys. J.*, **283**, 679
- Gill, A. G., and R. N. Henriksen, 1990, *Astrophys. J.*, **365**, L27
- Giovanardi, C., L. F. Rodríguez, S. Lizano, and J. Cantó, 2000, *Astrophys. J.*, **538**, 728
- Gladwin, P. P., S. Kitsionas, H. M. J. Boffin, and A. P. Whitworth, 1999, *Mon. Not. R. Astron. Soc.*, **302**, 305
- Goldreich, P. and S. Sridhar, 1995, *Astrophys. J.*, **438**, 763
- Goldreich, P. and S. Sridhar, 1997, *Astrophys. J.*, **485**, 680
- Goldsmith, P., 2001, *Astrophys. J.*, **557**, 736
- Goldsmith, P. F., and W. D. Langer, 1978, *Astrophys. J.*, **222**, 881
- Gómez, G. C., and D. P. Cox, 2002, *Astrophys. J.*, **580**, 235
- Gómez, M., B. F. Jones, L. Hartmann, S. J. Kenyon, J. R. Stauffer, R. Hewett, and I. N. Reid, 1992, *Astron. J.*, **104**, 762
- Gomez, T., Politano, H., Pouquet, A., Larchevêque, M., 2001, *Phys. Fluids*, **13**, 2065
- Graziani, F., and D. C. Black, 1981, *Astrophys. J.*, **251**, 337
- Greene, T. P., and M. R. Meyer, 1995, *Astrophys. J.*, **450**, 233
- Gueth, F., S. Guilloteau, A. Dutrey, R. Bachiller, 1997, *Astron. Astrophys.*, **323**, 943
- Hall, S. M., C. J. Clarke, and J. E. Pringle, 1996, *Mon. Not. R. Astron. Soc.*, **278**, 303
- Hambly, N. C., S. T. Hodgkin, M. R. Cossburn, and R. F. Jameson, 1999, *Mon. Not. R. Astron. Soc.*, **303**, 835
- Hanawa, T., and K. Nakayama, 1997, *Astrophys. J.*, **484**, 238
- Hartigan, P., S. Edwards, and L. Ghandour, 1995, *Astrophys. J.*, **452**, 736
- Hartmann, L., 1998, *Accretion processes in star formation*, Cambridge astrophysics series, Vol. 32, (Cambridge University Press)
- Hartmann, L., 2001, *Astron. J.*, **121**, 1030
- Hartmann, L., 2002, *Astrophys. J.*, submitted (astro-ph/0207216)
- Hartmann, L., J. Ballesteros-Paredes, and E. A. Bergin, 2001, *Astrophys. J.*, **562**, 852
- Hartmann, L., P. Cassen, and S. J. Kenyon, 1997, *Astrophys. J.*, **475**, 770
- Hawley, J. F., and J. M. Stone, 1995, *Computer Phys. Comm.*, **89**, 127
- Hawley, J. F., C. F. Gammie, and S. A. Balbus, 1996, */apj*, **464**, 690
- Hayashi, C., 1961, *Pub. Astron. Soc. Japan*, **13**, 450
- Hayashi, C., 1966, *Ann. Rev. Astron. Astrophys.*, **4**, 171
- Heckman, T. M., L. Armus, and G. K. Miley, 1990, *Astrophys. J. Suppl. Ser.*, **74**, 833
- Heiles, C., 1990, *Astrophys. J.*, **354**, 483
- Heiles, C., A. A. Goodman, C. F. McKee, and E. G. Zweibel, 1993, in *Protostars and Planets III*, edited by E. H. Levy and J. I. Lunine (University of Arizona Press, Tucson), p. 279
- Heisenberg, W., 1948a, *Z. Phys.*, **124**, 628
- Heisenberg, W., 1948b, *Proc. R. Soc. London A*, **195**, 402
- Heithausen, A., F. Bensch, J. Stutzki, E. Falgarone, and J. F. Panis, 1998, *Astron. Astrophys.*, **331**, L68
- Heitsch, F., M. Mac Low, and R. S. Klessen, 2001a, *Astrophys. J.*, **547**, 280
- Heitsch, F., E. G. Zweibel, M.-M. Mac Low, P. Li, and M. L. Norman, 2001b, *Astrophys. J.*, **561**, 800
- Hendriksen, R. N., 1989, *Mon. Not. R. Astron. Soc.*, **240**, 917
- Hendriksen, R. N., P. André, and S. Bontemps, 1997, *Astron. Astrophys.*, **323**, 549
- Hennebelle, P. and M. Pérault, 1999, *Astron. Astrophys.*, **351**, 309
- Hennebelle, P. and M. Pérault, 2000, *Astron. Astrophys.*, **359**, 1124
- Henning, T., 1989, *Astron. Nach.*, **310**, 363
- Henning, T., and R. Launhardt, 1998, *Astron. Astrophys.*, **338**, 223
- Henriksen, R., P. André, and S. Bontemps, 1997, *Astron. Astrophys.*, **323**, 549
- Heyer, M. H., and F. P. Schloerb, 1997, *Astrophys. J.*, **475**, 173
- Hillenbrand, L. A., 1997, *Astron. J.*, **113**, 1733
- Hillenbrand, L. A., and J. M. Carpenter, 2000, *Astrophys. J.*, **540**, 236
- Hillenbrand, L. A., and L. W. Hartmann, 1998, *Astrophys. J.*, **492**, 540
- Hiltner, W. A., 1949, *Astrophys. J.*, **109**, 471
- Hiltner, W. A., 1951, *Astrophys. J.*, **114**, 241
- Hockney, R. W., and J. W. Eastwood, 1988, *Computer Simulation using Particles* (IOP Publishing Ltd., Bristol and Philadelphia)
- Hodapp, K. and J. Deane, 1993, *Astrophys. J. Suppl. Ser.*, **88**, 119
- Hogerheijde, M. R., E. F. van Dishoeck, G. A. Blake, and H. J. van Langevelde, 1998, *Astrophys. J.*, **502**, 315
- Hollenbach, D. J., M. W. Werner, and E. E. Salpeter, 1971, *Astrophys. J.*, **163**, 165
- Hoyle, F., 1953, *Astrophys. J.*, **118**, 513

- Huang, P. G., G. N. Coleman, and P. Bradshaw, 1995, *J. Fluid Mech.*, **305**, 185
- Hubbard, W. B., A. Burrows, and J. I. Lunine, 2002, *Ann. Rev. Astron. Astrophys.*, **40**, 103
- Hunter, C., 1977, *Astrophys. J.*, **218**, 834
- Hunter, C., 1986, *Mon. Not. R. Astron. Soc.*, **223**, 391
- Hunter, D. A., 1997, *Pub. Astron. Soc. Pacific*, **109**, 937
- Hunter, D. A., B. G. Elmegreen, and A. L. Baker, 1998, *Astrophys. J.*, **493**, 595
- Hunter, D. A., E. J. Shaya, P. Scowen, J. J. Hester, E. J. Groth, R. Lynds, and E. J. O'Neil, 1995, *Astrophys. J.*, **444**, 758
- Hunter, J. H., and R. C. Fleck, 1982, *Astrophys. J.*, **256**, 505
- Ida, S., J. Larwood, and A. Burkert, 2000, *Astrophys. J.*, **528**, 351
- Inutsuka, S., and S. M. Miyama, 1992, *Astrophys. J.*, **388**, 392
- Inutsuka, S., and S. M. Miyama, 1997, *Astrophys. J.*, **480**, 681
- Indebetouw, R., and E. G. Zweibel, 2000, *Astrophys. J.*, **532**, 361
- Irvine, W. M., P. F. Goldsmith, and A. Hjalmarson, 1986, in *Interstellar Processes*, edited by D. J. Hollenbach and H. A. Thronson, Jr. (Reidel, Dordrecht), 561
- Isichenko, M. B., 1992, *Rev. Mod. Phys.*, **64**, 961
- Jahyesh, and Z. Warhaft, 1991, *Phys. Rev. Lett.*, **67**, 3503
- Jayawardhana, R., L. Hartmann, and N. Calvet, 2001, *Astrophys. J.*, **548**, 310
- Jeans, J. H., 1902, *Phil. Trans. A.*, **199**, 1
- Johnstone, D. and J. Bally, 1999, *Astrophys. J.*, **510**, L49
- Johnstone, D., C. D. Wilson, G. Moriarty-Schieven, G. Joncas, G. Smith, E. Gregersen, and M. Fich, 2000, *Astrophys. J.*, **545**, 327
- Johnstone, D., M. Fich, G. F. Mitchell, and G. Moriarty-Schieven, 2001, *Astrophys. J.*, **559**, 307
- Jones, C. E., S. Basu, and J. Dubinski, 2001, *Astrophys. J.*, **551**, 387
- A. Kawamura, A., T. Onishi, Y. Yonekura, K. Dobashi, A. Mizuno, H. Ogawa, Y. Fukui, 1998, *Astrophys. J. Suppl. Ser.*, **117**, 387
- Kegel, W. H., 1989, *Astron. Astrophys.*, **225**, 517
- Kennicutt, R. C., Jr., 1998a, *Ann. Rev. Astron. Astrophys.*, **36**, 189
- Kennicutt, R. C., Jr., 1998b, *Astrophys. J.*, **498**, 541
- Keto, E. R., J. C. Lattanzio, and J. J. Monaghan, 1991, *Astrophys. J.*, **383**, 639
- Kida, S., and Y. Murakami, 1989, *Fluid Dyn. Res.*, **4**, 347
- Kim, W.-T., and E. C. Ostriker, 2001, *Astrophys. J.*, **559**, 70
- Kim, W.-T., and E. C. Ostriker, 2002, *Astrophys. J.*, **570**, 132
- Kimura, T., and M. Tosa, 1996, *Astron. Astrophys.*, **308**, 979
- Kippenhahn, R., and A. Weigert, 1990, *Stellar Structure and Evolution* (Springer Verlag, Berlin, Heidelberg)
- Kitamura, Y., K. Sunada, M. Hayashi, T. Hasegawa, 1993, *Astrophys. J.*, **413**, 221
- Klapp, J., L. D. G. Sigalotti, and F. de Felice, 1993, *Astron. Astrophys.*, **273**, 175
- Klein, R. I., 1999, *J. Comput. Appl. Math.*, **109**, 123
- Klein, R. I., C. F. McKee, and P. Colella, 1994, *Astrophys. J.*, **420**, 213
- Kleiner, S. C., and R. L. Dickman, 1987, *Astrophys. J.*, **312**, 837
- Klessen, R. S., 1997, *Mon. Not. R. Astron. Soc.*, **292**, 11
- Klessen, R. S., 2000, *Astrophys. J.*, **535**, 869
- Klessen, R. S., 2001a, *Astrophys. J.*, **550**, L77
- Klessen, R. S., 2001b, *Astrophys. J.*, **556**, 837
- Klessen, R. S., and A. Burkert, 2000, *Astrophys. J. Suppl. Ser.*, **128**, 287
- Klessen, R. S., and A. Burkert, 2001, *Astrophys. J.*, **549**, 386
- Klessen, R. S., and P. Kroupa, 2001, *Astron. Astrophys.*, **372**, 105
- Klessen, R. S., A. Burkert, and M. R. Bate, 1998, *Astrophys. J.*, **501**, L205
- Klessen, R. S., F. Heitsch, and M.-M. Mac Low, 2000, *Astrophys. J.*, **535**, 887
- Kolmogorov, A. N., 1941a, *Dokl. Akad. Nauk SSSR*, **30**, 301 — translated and reprinted 1991 in *Proc. R. Soc. London A*, **343**, 9
- Kolmogorov, A. N., 1941b, *Dokl. Akad. Nauk SSSR*, **31**, 538
- Königl, A., and R. E. Pudritz, in *Protostars and Planets IV*, edited by V. Manning, A. P. Boss, and S. S. Russell (U. of Arizona Press, Tucson), 759
- Korpi, M. J., A. Brandenburg, A. Shukorov, I. Tuominen, and Å. Nordlund, 1999, *Astrophys. J. (Letters)*, **514**, L99
- Koyama, H., and S. Inutsuka, 2000, *Astrophys. J.*, **532**, 980
- Koyama, H., and S. Inutsuka, 2002, *Astrophys. J. (Letters)*, **564**, L97
- Kramer, C., J. Stutzki, R. Rohrig, U. Corneliussen, 1998, *Astron. Astrophys.*, **329**, 249
- Kramer C., J. Alves, C. J. Lada, E. A. Lada, A. Sievers, H. Ungerechts, and C. M. Walmsley, 1999, *Astron. Astrophys.*, **342**, 257
- Krebs, J., and W. Hillebrandt, 1983, *Astron. Astrophys.*, **128**, 411
- Kroupa, P., 1995a, *Mon. Not. R. Astron. Soc.*, **277**, 1491
- Kroupa, P., 1995b, *Mon. Not. R. Astron. Soc.*, **277**, 1507
- Kroupa, P., 1995c, *Mon. Not. R. Astron. Soc.*, **277**, 1522
- Kroupa, P., 2001, *Mon. Not. R. Astron. Soc.*, **322**, 231
- Kroupa, P., 2002, *Science* **295**, 82
- Kroupa, P., and A. Burkert, 2001, *Astrophys. J.*, **555**, 945
- Kroupa, P., C. A. Tout, G. Gilmore, 1990, *Mon. Not. R. Astron. Soc.*, **244**, 76
- Kroupa, P., C. A. Tout, G. Gilmore, 1993, *Mon. Not. R. Astron. Soc.*, **262**, 545

- Kuhfuß, R., 1987, PhD-Thesis, TU München
- Kulsrud, R. M., and W. P. Pearce, 1969, *Astrophys. J.*, **156**, 445
- Kutner, M. L., K. D. Tucker, G. Chin, and P. Thaddeus, 1977, *Astrophys. J.*, **215**, 521
- Leisawitz, D., F. N. Bash, and P. Thaddeus, 1989, *Astrophys. J. Suppl. Ser.*, **70**, 731
- Léorat, J., T. Passot, and A. Pouquet, 1990, *Mon. Not. R. Astron. Soc.*, **243**, 293
- LaRosa, T. N., S. N. Shore, and L. Magnani, 1999, *Astrophys. J.*, **512**, 761
- Lada, C. J., J. Alves, and E. A. Lada, 1996, *Astron. J.*, **111**, 1964
- Lada, C. J., E. A. Lada, D. P. Clemens, and J. Bally, 1994, *Astrophys. J.*, **429**, 694
- Lada, E. A., 1992, *Astrophys. J.*, **393**, L25
- Lada, C. J., J. Alves, and E. A. Lada, 1999, *Astrophys. J.*, **515**, 265
- Lada, E. A., J. Bally, and A. A. Stark, 1991, *Astrophys. J.*, **368**, 432
- Lamballais, E., M. Lesieur, and O. Métais, 1997, *Phys. Rev. E*, **56**, 761
- Langer, W., R. Wilson, and C. Anderson, 1993, *Astrophys. J.*, **408**, L25
- Langer, W. D., T. Velusamy, T. B. H. Kuiper, W. Levin, E. Olsen, V. Migenes, 1995, *Astrophys. J.*, **453**, 293
- Langer, W. D., E. F. van Dishoeck, E. A. Bergin, G. A. Blake, A. G. G. M. Tielens, T. Velusamy, and D. C. B. Whittet, 2000, in *Protostars and Planets IV*, edited by V. Mannings, A. P. Boss, and S. S. Russell (University of Arizona Press, Tucson), p. 29
- Lanzetta, K. M., A. Yahil, and A. Fernández-Soto, 1996, *Nature*, **381**, 759
- Lanzetta, K. M., N. Yahata, S. Pascarelle, H. Chen, and A. Fernández-Soto, 2002, *Astrophys. J.*, **570**, 492
- LaRosa, T. N., S. N. Shore, and L. Magnani, 1999, *Astrophys. J.*, **512**, 761
- Larson, R. B., 1969, *Mon. Not. R. Astron. Soc.*, **145**, 271
- Larson, R. B., 1972, *Mon. Not. R. Astron. Soc.*, **156**, 437
- Larson, R. B., 1973, *Mon. Not. R. Astron. Soc.*, **161**, 133
- Larson, R. B., 1981, *Mon. Not. R. Astron. Soc.*, **194**, 809
- Larson, R. B., 1992, *Mon. Not. R. Astron. Soc.*, **256**, 641
- Larson, R. B., 1995, *Mon. Not. R. Astron. Soc.*, **272**, 213
- Laughlin, G., and P. Bodenheimer, 1993, *Astrophys. J.*, **403**, 303
- Lechner, R., J. Sesterhenn, and R. Friedrich, 2001, *J. Turbulence*, **2**, 001
- Lee, C. W., P. C. Myers, and M. Tafalla, 1999, *Astrophys. J.*, **526**, 788
- Lee, C. W., P. C. Myers, and M. Tafalla, 2001, *Astrophys. J. Suppl. Ser.*, **136**, 703
- Lee, Y., R. L. Snell, & R. L. Dickman, 1996, *Astrophys. J.*, **472**, 275
- Leinert, C., T. Henry, A. Glindemann, and D. W. McCarthy, 1997, *Astron. Astrophys.*, **325**, 159
- Leisawitz, D., F. N. Bash, and P. Thaddeus, 1989, *Astrophys. J. Suppl. Ser.*, **70**, 731
- Lejeune, C., and P. Bastien, 1986, *Astrophys. J.*, **309**, 167
- Lesieur, M., 1997, *Turbulence in Fluids*, 3rd ed. (Kluwer, Dordrecht), p. 245
- Li, P., M. L. Norman, F. Heitsch, and M.-M. Mac Low, 2000, *Bull. Amer. Astron. Soc.*, **197**, 05.02
- Li, Y., R. S. Klessen, and M.-M. Mac Low, 2003, in *Extragalactic Globular Cluster Systems*, edited by M. Kissler-Patig (Springer, Heidelberg), in press (astro-ph/0210479)
- Li, Z., and F. H. Shu, 1996, *Astrophys. J.*, **472**, 211
- Li, Z., and F. H. Shu, 1997, *Astrophys. J.*, **475**, 237
- Lillo, F. and R. N. Mantegna, 2000, *Phys. Rev. E*, **61**, R4675
- Lilly, S. J., O. Le Fevre, F. Hammer, and D. Crampton, 1996, *Astrophys. J. (Letters)*, **460**, L1
- Lin, C. C., and F. H. Shu, 1964, *Astrophys. J.*, **140**, 646
- Lin, C. C., C. Yuan, and F. H. Shu, 1969, *Astrophys. J.*, **155**, 721
- Lis, D. C., J. Keene, T. G. Phillips, and J. Pety, 1998, *Astrophys. J.*, **504**, 889
- Lis, D. C., J. Pety, T. G. Phillips, and E. Falgarone, 1996, *Astrophys. J.*, **463**, 623
- Lissauer, J. J., 1993, *Ann. Rev. Astron. Astrophys.*, **31**, 129
- Lithwick, Y., and P. Goldreich, 2001, *Astrophys. J.*, **562**, 279
- Lizano, S., and F. H. Shu, 1989, *Astrophys. J.*, **342**, 834
- Lizano, S., C. Heiles, L. F. Rodríguez, B.-C. Koo, F. H. Shu, T. Hasegawa, S. Hayashi, I. F. Mirabel, 1988, *Astrophys. J.*, **328**, 763
- Lombardi, M., and G. Bertin, 2001, *Astron. Astrophys.*, submitted (astro-ph/0106336)
- Lombardi, J. C., A. Sills, F. A. Rasio, and S. L. Shapiro, 1999, *J. Comput. Phys.*, **152**, 687
- Loren, R. B., 1989, *Astrophys. J.*, **338**, 902
- Lynden-Bell, D., and A. J. Kalnajs, 1972, *Mon. Not. R. Astron. Soc.*, **157**, 1
- Müller, W.-C., and D. Biskamp, 2000, *Phys. Rev. Lett.*, **84**, 475
- Machiels, L., and M. O. Deville, 1998, *J. Comput. Phys.*, **145**, 256
- Mac Low, M.-M., 1999, *Astrophys. J.*, **524**, 169
- Mac Low, M.-M., 2000, in *Stars, Gas and Dust in Galaxies: Exploring the Links*, edited by D. Alloin, K. Olson, and G. Galaz, ASP Conf. Ser. No. 221 (ASP, San Francisco) 55
- Mac Low, M.-M., 2002, in *Simulations of magnetohydrodynamic turbulence in astrophysics*, edited by T. Passot and E. Falgarone (Springer, Heidelberg) in press (astro-ph/0201157)

- Mac Low, M.-M., D. S. Balsara, M. A. de Avillez, and J. Kim, 2001, *Astrophys. J.*, submitted (astro-ph/0106509)
- Mac Low, M.-M., and A. Ferrara, 1999, *Astrophys. J.*, **513**, 142
- Mac Low, M.-M., R. S. Klessen, A. Burkert, and M. D. Smith, 1998, *Phys. Rev. Lett.*, **80**, 2754
- Mac Low, M.-M., C. F. McKee, R. I. Klein, J. M. Stone, and M. L. Norman, 1994, *Astrophys. J.*, **433**, 757
- Mac Low M.-M. and V. Ossenkopf, 2000, *Astron. Astrophys.*, **353**, 339
- Madau, P., H. C. Ferguson, M. E. Dickinson, M. Giavalisco, C. C. Steidel, and A. Fruchter, 1996, *Mon. Not. R. Astron. Soc.*, **283**, 1388
- Maddalena, R. J., and P. Thaddeus, 1985, *Astrophys. J.*, **294**, 231
- Magnani, L., L. Blitz, L., and L. Mundy, 1985, *Astrophys. J.*, **295**, 402
- Manicó, G., G. Raguñi, V. Pirronello, J. E. Roser, and G. Vidali, 2001, *Astrophys. J. (Letters)*, **548**, L253
- Maron, J., and P. Goldreich, 2001, *Astrophys. J.*, **554**, 1175
- Martin, C. L., and R. C. Kennicutt, Jr., 2001, *Astrophys. J.*, **555**, 301
- Martos, M. A., and D. P. Cox, 1998, *Astrophys. J.*, **509**, 703
- Masunaga, H., S. M. Miyama, and S. Inutsuka, 1998, *Astrophys. J.*, **495**, 346
- Masunaga, H., and S. Inutsuka, 2000a, *Astrophys. J.*, **531**, 350
- Masunaga, H., and S. Inutsuka, 2000b, *Astrophys. J.*, **536**, 406
- Mathieu, R. D., A. M. Ghez, E. L. N. Jensen, and M. Simon, 2000, in *Protostars and Planets IV*, edited by V. Mannings, A. P. Boss, and S. S. Russell (University of Arizona Press, Tucson), p. 703
- Matthews, L. D., and J. S. Gallagher, III, 2002, *Astrophys. J. Suppl. Ser.*, **141**, 429
- Matzner, C. D., 2002, *Astrophys. J.*, **566**, 302
- McDonald, J. M., and C. J. Clarke, 1995, *Mon. Not. R. Astron. Soc.*, **275**, 671
- McGaugh, S. S., and W. J. G. de Blok, 1997, *Astrophys. J.*, **481**, 689
- McGaugh, S. S., V. C. Rubin, and W. J. G. de Blok, 2001, *Astrophys. J.*, **122**, 2381
- McKee, C. F., 1989, *Astrophys. J.*, **345**, 782
- McKee, C. F., 1999, in *NATO ASIC Proc. 540: The Origin of Stars and Planetary Systems*, edited by C. J. Lada and N. D. Kylafis (Kluwer Academic Publishers), p. 29
- McKee, C. F., and J. P. Ostriker, 1977, *Astrophys. J.*, **218**, 148
- McKee, C. F., and J. P. Williams, 1997, *Astrophys. J.*, **476**, 144
- McKee, C. F., and E. G. Zweibel, 1992, *Astrophys. J.*, **399**, 551
- McKee, C. F., and E. G. Zweibel, 1995, *Astrophys. J.*, **440**, 686
- McKee, C. F., E. G. Zweibel, A. A. Goodman, and C. Heiles, 1993, in *Protostars and Planets III*, edited by E. H. Levy and J. I. Lunine (University of Arizona Press, Tucson), p. 327
- Mestel, L., and L. Spitzer, Jr., 1956, *Mon. Not. R. Astron. Soc.*, **116**, 503
- Metzler, R., and J. Klafter, 2000, *Phys. Report*, **339**, 1
- Miesch, M.S., and J. M. Bally, 1994, *Astrophys. J.*, **429**, 645
- Miesch, M.S., and J. M. Scalo, 1995, *Astrophys. J.*, **450**, L27
- Miesch, M.S., J. M. Scalo, and J. Bally, 1999, *Astrophys. J.*, **524**, 895
- Mihalas, D., and B. W. Mihalas, 1984, *Foundations of Radiation Hydrodynamics* (Oxford University Press, New York)
- Mihos, J. C., M. Spaans, and S. S. McGaugh, 1999, *Astrophys. J.*, **515**, 89
- Miller, G. E., and J. M. Scalo, 1979, *Astrophys. J. Suppl. Ser.*, **41**, 513
- Mitchell, G. F., D. Johnstone, G. Moriarty-Schieven, M. Fich, and N. F. H. Tothill, 2001, *Astrophys. J.*, **556**, 215
- Mizuno, A., T. Onishi, Y. Yonekura, T. Nagahama, H. Ogawa, and Y. Fukui, 1995, *Astrophys. J.*, **445**, L161
- Moffat, A. F. J., M. F. Corcoran, I. R. Stevens, G. Skalkowski, S. V. Marchenko, A. Mücke, A. Ptak, B. S. Koribalski, L. Brenneman, R. Mushotzky, J. M. Pittard, A. M. T. Pollock, and W. Brandner, 2002, *Astrophys. J.*, 573, 191
- Monaghan, J. J., 1992, *Ann. Rev. Astron. Astrophys.*, **30**, 543
- Mooney, T. J., and P. M. Solomon, 1988, *Astrophys. J.*, **334**, L51
- Morton, S. A., T. C. Mouschovias, and G. E. Ciolek, 1994, *Astrophys. J.*, **421**, 561
- Moser, R. D., J. Kim, and N. N. Mansour, 1999, *Phys. Fluids*, **11**, 943
- Motte, F., and P. André, 2001, *Astron. Astrophys.*, **365**, 440
- Motte, F., P. André, and R. Neri, 1998, *Astron. Astrophys.*, **336**, 150
- Motte, F., P. André, D. Ward-Thompson, and S. Bontemps, 2001, *Astron. Astrophys.*, **372**, L41
- Mouschovias, T. C., 1991a, *Astrophys. J.*, **373**, 169
- Mouschovias, T. Ch., 1991b, in *The Physics of Star Formation and Early Stellar Evolution*, edited by C. J. Lada and N. D. Kylafis (Kluwer, Dordrecht), p. 61
- Mouschovias, T. Ch., 1991c, in *Physics of Star Formation and Early Stellar Evolution*, edited by C. J. Lada and N. D. Kylafis (Kluwer, Dordrecht), p. 449
- Mouschovias, T. C., and S. A. Morton, 1991, *Astrophys. J.*, **371**, 296
- Mouschovias, T. C., and S. A. Morton, 1992a, *Astrophys. J.*, **390**, 144
- Mouschovias, T. C., and S. A. Morton, 1992b, *Astrophys. J.*, **390**, 166
- Mouschovias, T. C., and E. V. Paleologou, 1979, *Astrophys. J.*, **230**, 204
- Mouschovias, T. C., and E. V. Paleologou, 1980, *Astrophys. J.*, **237**, 877
- Mouschovias, T. Ch., and L. Spitzer, Jr., 1976, *Astrophys. J.*, **210**, 326

- Müller, W. C., and D. Biskamp, 2000, *Phys. Rev. Lett.*, **84**, 475
- Murray, S. D., and C. J. Clarke, 1993, *Mon. Not. R. Astron. Soc.*, **265**, 169
- Murray, S. D., and D. N. C. Lin, 1996, *Astrophys. J.*, **467**, 728
- Myers, P. C., 1983, *Astrophys. J.*, **270**, 105
- Myers, P. C., 2000, *Astrophys. J.*, **530**, L119
- Myers, P. C., and A. A. Goodman, 1988 *Astrophys. J.*, **326**, L27
- Myers, P. C., and V. K. Khersonsky, 1995, *Astrophys. J.*, **442**, 186
- Myers, P. C., and E. E. Ladd, 1993, *Astrophys. J.*, **413**, L47
- Myers, P. C., N. J. Evans, and N. Ohashi, 2000, in *Protostars and Planets IV*, edited by V. Mannings, A. P. Boss, and S. S. Russell (University of Arizona Press, Tucson), p. 217
- Myers, P. C., F. C. Adams, H. Chen, and E. Schaff, 1998, *Astrophys. J.*, **492**, 703
- Myers, P. C., G. A. Fuller, A. A. Goodman, and P. J. Benson, 1991, *Astrophys. J.*, **376**, 561
- Myers, P. C., D. Mardones, M. Tafalla, J. P. Williams, and D. J. Wilner, 1996, *Astrophys. J.*, **465**, L133
- Nakajima, Y., K. Tachihara, T. Hanawa, and M. Nakano, 1998, *Astrophys. J.*, **497**, 721
- Nakamura, F., T. Hanawa, and T. Nakano, 1995, *Astrophys. J.*, **444**, 770
- Nakano, T., 1976, *Pub. Astron. Soc. Japan*, **28**, 355
- Nakano, T., 1979, *Pub. Astron. Soc. Japan*, **31**, 697
- Nakano, T., 1982, *Pub. Astron. Soc. Japan*, **34**, 337
- Nakano, T., 1983, *Pub. Astron. Soc. Japan*, **35**, 209
- Nakano, T., 1998, *Astrophys. J.*, **494**, 587
- Nakano, T., and T. Nakamura, 1978, *Pub. Astron. Soc. Japan*, **30**, 681
- Nakano, T., T. Hasegawa, and C. Norman, 1995, *Astrophys. Space Science*, **224**, 523
- Nakazawa, K., C. Hayashi, and M. Takahara, 1976, *Prog. Theo. Phys.*, **56**, 515
- Narlikar, J. V., and T. Padmanabhan, 2001, *Ann. Rev. Astron. Astrophys.*, **39**, 211
- Neuhäuser, R., M. F. Sterzik, G. Torres, E. L. Martín, 1995, *Astron. Astrophys.*, **299**, L13
- Ng, C. S., and A. Bhattacharjee, 1996, *Astrophys. J.*, **465**, 845
- Norman, C. A., and A. Ferrara, 1996, *Astrophys. J.*, **467**, 280
- Norman, C. A., and J. Silk, 1980, *Astrophys. J.*, **239**, 968
- Norman, M. L., J. R. Wilson, and R. T. Barton, 1980, *Astrophys. J.*, **239**, 968
- Nugis, T., and H. J. G. L. M. Lamers, 2000, *Astron. Astrophys.*, **360**, 227
- Obukhov, A. M., 1941, *Dokl. Akad. Nauk SSSR*, **32**, 22
- Ogino, S., K. Tomisaka, and F. Nakamura, 1999, *Pub. Astron. Soc. Japan*, **51**, 637
- Olling, R. P., and M. R. Merrifield, 1998, *Mon. Not. R. Astron. Soc.*, **297**, 943
- Olling, R. P., and M. R. Merrifield, 2000, *Mon. Not. R. Astron. Soc.*, **311**, 361
- Olmi, L., and L. Testi, 2002, *Astron. Astrophys.*, **392**, 1053
- Onishi, T., A. Mizuno, A. Kawamura, H. Ogawa, Y. Fukui, 1996, *Astrophys. J.*, **465**, 815
- Oort, J. H., 1954, *Bull. Astron. Inst. Netherlands*, **12**, 177
- Oort, J. H., & L. Spitzer, Jr., 1955, *Astrophys. J.*, **121**, 6
- Ossenkopf, V. 2002, *Astron. Astrophys.*, **391**, 295
- Ossenkopf V., and M.-M. Mac Low, 2002, *Astron. Astrophys.*, **390**, 307
- Ossenkopf V., R. S. Klessen, and F. Heitsch, 2001, *Astron. Astrophys.*, **379**, 1005
- Ossenkopf V., Bensch F., Stutzki J. 2000, in *The Chaotic Universe*, edited by V. G. Gurzadyan and R. Ruffini (World Sci.), p. 394
- Ossia, S., and M. Lesieur, *J. Turbulence*, **2**, 013
- Osterbrock, D. E., 1961, *Astrophys. J.*, **134**, 270
- Ostriker, E. C., C. F. Gammie, and J. M. Stone, 1999, *Astrophys. J.*, **513**, 259
- Ostriker, E. C., J. M. Stone, and C. F. Gammie, 2001, *Astrophys. J.*, **546**, 980
- Padoan, P., 1995, *Mon. Not. R. Astron. Soc.*, **277**, 377
- Padoan, P., and Å. Nordlund, 1999, *Astrophys. J.*, **526**, 279
- Padoan, P., and Å. Nordlund, 2002, *Astrophys. J.*, **576**, 870
- Padoan, P., L. Cambrésy, and W. Langer, 2002, *Astrophys. J.* submitted (astro-ph/0208217)
- Padoan, P., A. A. Goodman, B. T. Draine, M. Juvela, Å. Nordlund, and Ö. E. Rögnvaldsson, 2001a, *Astrophys. J.*, **559**, 1005
- Padoan, P., M. Juvela, J. Bally, and Å. Nordlund, 2000, *Astrophys. J.*, **529**, 259
- Padoan, P., M. Juvela, A. A. Goodman, and Å. Nordlund, 2001b, **553**, 227
- Padoan, P., Å. Nordlund, and B. J. T. Jones, 1997, *Mon. Not. R. Astron. Soc.*, **288**, 145
- Padoan, P., E. Zweibel, and Å. Nordlund, 2000, *Astrophys. J.*, **540**, 332
- Padoan, P., Å. Nordlund, Ö. E. Rögnvaldsson, and A. Goodman, 2002, *Astrophys. J.*, submitted (astro-ph/0011229)
- Palla, F., 2000, in *The Origin of Stars and Planetary Systems* edited by C. J. Lada and N. D. Kylafis (Kluwer Academic Publisher, Dordrecht), p. 375
- Palla, F., 2002, in *Physics on Star Formation in Galaxies, Saas-Fee Advanced Course 29*, edited by A. Maeder and G. Meynet (Springer-Verlag, Heiderberg), p. 9
- Palla, F., and S. W. Stahler, 1999, *Astrophys. J.*, **525**, 77
- Palla, F., and S. W. Stahler, 2000, *Astrophys. J.*, **540**, 255
- Palmer, P., and B. Zuckerman, 1967, *Astrophys. J.*, **148**, 727

- Passot, T., and E. Vázquez-Semadeni, 1998, *Phys. Rev. E*, **58**, 4501
- Passot, T., A. Pouquet, and P. R. Woodward, 1988, *Astron. Astrophys.*, **197**, 392
- Passot, T., E. Vázquez-Semadeni, and A. Pouquet, 1995, *Astrophys. J.*, **455**, 536
- Penston, M. V., 1969a, *Mon. Not. R. Astron. Soc.*, **144**, 425
- Penston, M. V., 1969b, *Mon. Not. R. Astron. Soc.*, **145**, 457
- Persi, P., and 20 colleagues, 2000, *Astron. Astrophys.*, **357**, 219
- Phillips, A. C., 1994, *The Physics of Stars* (Wiley, Chichester, New York)
- Pikel'ner, S. B. 1968, *Sov. Astron.*, **11**, 737.
- Pirronello, V., O. Biham, C. Liu, L. Shen, and G. Vidali, 1997a, *Astrophys. J. (Letters)*, **483**, L131
- Pirronello, V., C. Liu, J. E. Roser, and G. Vidali, 1999, *Astron. Astrophys.*, **344**, 681
- Pirronello, V., C. Liu, L. Shen, and G. Vidali, 1997b, *Astrophys. J. (Letters)*, **475**, L69
- Plume, R., D. T. Jaffe, N. J. Evans, I., J. Martín-Pintado, and J. Gómez-González, 1997, *Astrophys. J.*, **476**, 730
- Porter, D. H., and P. R. Woodward, 1992, *Astrophys. J. Suppl. Ser.*, **93**, 309
- Porter D. H., and P. R. Woodward, 2000, *Astrophys. J.*, **127**, 159
- Porter, D. H., A. Pouquet, and P. R. Woodward, 1992, *Phys. Rev. Lett.*, **68**, 3156
- Porter, D. H., A. Pouquet, and P. R. Woodward, 1994, *Phys. Fluids*, **6**, 2133
- Porter, D. H., A. Pouquet, I. V. Sytine, and P. R. Woodward, 1999, *Phys. A*, **263**, 263
- Potter, D., 1977, *Computational Physics* (Wiley, New York)
- Prasad, S. S., K. R. Heere, and S. P. Tarafdar, 1991, **373**, 123
- Pratap, P., J. E. Dickens, R. L. Snell, M. P. Miralles, E. A. Bergin, W. M. Irvine, and F. P. Schloerb, 1997, *Astrophys. J.*, **486**, 862
- Price, N. M., and P. Podsiadlowski, 1995, *Mon. Not. R. Astron. Soc.*, **273**, 1041
- Pringle, J. E., R. J. Allen, and S. H. Lubow, 2001, *Mon. Not. R. Astron. Soc.*, **327**, 663
- Prosser, C. F., J. R. Stauffer, L. Hartmann, D. R. Soderblom, B. F. Jones, M. W. Werner, and M. J. McCaughrean, 1994, *Astrophys. J.*, **421**, 517
- Pöppel, W. G. L., *Fund. Cosm. Phys.*, **18**, 1
- Rana, N. C., 1991, *Ann. Rev. Astron. Astrophys.*, **29**, 129
- Rand, R. J., and S. R. Kulkarni, 1989, *Astrophys. J.*, **343**, 760
- Rand, R. J., and A. G. Lyne, 1994, *Mon. Not. R. Astron. Soc.*, **268**, 497
- Raymond, J. C., D. P. Cox, and B. W. Smith, 1976, *Astrophys. J.*, **204**, 290
- Reipurth, B., and C. Clarke, 2001, *Astron. J.*, **122**, 432
- Richardson, L. F., 1922, *Weather Prediction by Numerical Process* (Cambridge University Press, Cambridge)
- Richer, J. S., D. S. Shepherd, S. Cabrit, R. Bachiller, and E. Churchwell, 2000, in *Protostars and Planets IV*, edited by V. Mannings, A. P. Boss, and S. S. Russell (University of Arizona Press, Tucson), p. 867
- Richtler, T., 1994, *Astron. Astrophys.*, **287**, 517
- Roberts, W. W., 1969, *Astrophys. J.*, **158**, 123
- Rodriguez-Gaspar, J. A., G. Tenorio-Tagle, and J. Franco, 1995, *Astrophys. J.*, **451**, 210
- Romeo, A. B., 1992, *Mon. Not. R. Astron. Soc.*, **256**, 307
- Rosen, A. and J. N. Bregman, 1995, *Astrophys. J.*, **440**, 634
- Rosen, A., J. N. Bregman, and D. D. Kelson, 1996, *Astrophys. J.*, **470**, 839
- Rosen, A., J. N. Bregman, and M. L. Norman, 1993, *Astrophys. J.*, **413**, 137
- Rosolowsky, E. W., A. A. Goodman, D. J. Wilner, and J. P. Williams, 1999, *Astrophys. J.*, **524**, 887
- Rozyczka, M., W. M. Tscharnuter, K. -H. Winkler, and H. W. Yorke, 1980, *Astron. Astrophys.*, **83**, 118
- Ruden, S. P., 1999, in *NATO ASIC Proc. 540: The Origin of Stars and Planetary Systems*, edited by C. J. Lada and N. D. Kylafis (Kluwer Academic Publishers), p. 643
- Ryden, B. S., 1996, *Astrophys. J.*, **471**, 822
- Saito, S., Y. Aikawa, E. Herbst, M. Ohishi, T. Hirota, S. Yamamoto, and N. Kaifu, 2002, *Astrophys. J.*, **569**, 836
- Sánchez-Salcedo, F. J., 2001, *Astrophys. J.*, **563**, 867
- Safier, P. N., C. F. McKee, and S. W. Stahler, 1997, *Astrophys. J.*, **485**, 660
- Safronov, V. S., 1960, *Ann. Astrophys.*, **23**, 979
- Salpeter, E. E., 1955, *Astrophys. J.*, **121**, 161
- Sanders, D. B., and I. F. Mirabel, 1996, *Ann. Rev. Astron. Astrophys.*, **34**, 749
- Saraceno, P., P. André, C. Ceccarelli, M. Griffin, and S. Molinari, 1996, *Astron. Astrophys.*, **309**, 827
- Sarma, A. P., T. H. Troland, D. A. Roberts, and R. M. Crutcher, 2000, *Astrophys. J.*, **533**, 271
- Scally, A., and C. Clarke, 2001, *Mon. Not. R. Astron. Soc.*, **325**, 449
- Scalo, J. M., 1984, *Astrophys. J.*, **277**, 556
- Scalo, J. M., 1986, *Fund. Cos. Phys.*, **11**, 1
- Scalo, J. M., 1990, in *Physical Processes in Fragmentation and Star Formation* edited by R. Capuzzo-Dolcetta and C. Chiosi (Kluwer Academic Publishers, Dordrecht), p. 151
- Scalo, J. M., 1998, in *The Stellar Initial Mass Function (38th Herstmonceux Conference)*, edited by G. Gilmore, I. Parry, and S. Ryan (ASP Conf. Ser. Vol. 142), p. 201
- Scalo, J. M., E. ázquez-Semadeni, D. Chappell, T. Passot, 1998, *Astrophys. J.*, **504**, 835
- Schombert, J. M., G. D. Bothun, S. E. Schneider, and S. S. McCaugh, 1992, *Astrophys. J.*, **103**, 1107

- Schombert, J. M., S. S. McGaugh, and J. A. Eder, 2001, *Astrophys. J.*, **121**, 2420
- Schmitz, F., 1983, *Astron. Astrophys.*, **120**, 234
- Schmitz, F., 1984, *Astron. Astrophys.*, **131**, 309
- Schmitz, F., 1986, *Astron. Astrophys.*, **169**, 171
- Schmitz, F., 1987, *Astron. Astrophys.*, **179**, 167
- Schmitz, F., 1988, *Astron. Astrophys.*, **200**, 127
- Schmitz, F., and R. Ebert, 1986, *Astron. Astrophys.*, **154**, 214
- Schmitz, F., and R. Ebert, 1987, *Astron. Astrophys.*, **181**, 41
- Scoville, N. Z. and K. Hersh, 1979, *Astrophys. J.*, **229**, 578
- Sellwood, J. A., and S. A. Balbus, 1999, *Astrophys. J.*, **511**, 660
- She, Z.-S., 1991, *Fluid Dyn. Res.*, **8**, 143
- She, Z.-S., and E. Leveque, 1994, *Phys. Rev. Lett.*, **72**, 336
- She, Z.-S., E. Jackson, and S. A. Orszag, 1991, *Proc. R. Soc. London A*, **434**, 101
- Shlosman, I., M. C. Begelman, and J. Frank, 1990, *Nature*, **345**, 679
- Shu, F. H., 1977, *Astrophys. J.*, **214**, 488
- Shu, F. H., 1991, in *Physics of Star Formation and Early Stellar Evolution*, edited by C. J. Lada and N. D. Kylafis (Kluwer, Dordrecht), p. 365
- Shu, F. H., and Z. Li, 1997, *Astrophys. J.*, **475**, 251
- Shu, F. H., S. Lizano, S. P. Ruden, and J. Najita, 1998, *Astrophys. J. (Letters)*, **328**, L19
- Shu, F. H., J. Najita, D. Galli, E. Ostriker, and S. Lizano, 1993, in *Protostars and Planets III*, edited by E. H. Levy and J. I. Lunine (University of Arizona Press, Tucson), p. 3
- Shu, F. H., F. C. Adams, and S. Lizano, 1987, *Ann. Rev. Astron. Astrophys.*, **25**, 23
- Shu, F. H., A. Allen, H. Shang, E. C. Ostriker, and Z. Li, 1999, in *NATO ASIC Proc. 540: The Origin of Stars and Planetary Systems*, edited by C. J. Lada and N. D. Kylafis (Kluwer Academic Publishers), p. 193
- Shu, F. H., G. Laughlin, S. Lizano, and D. Galli, 2000, *Astrophys. J.*, **535**, 190
- Silk, J., 1995, *Astrophys. J.*, **438**, L41
- Silk, J., and T. Takahashi, 1979, *Astrophys. J.*, **229**, 242
- Silk, J., and Y. Suto, 1988, *Astrophys. J.*, **335**, 295
- Simon, M., 1997, *Astrophys. J.*, **482**, L81
- Simon, R., J. M. Jackson, D. P. Clemens, T. M. Bania, M. H. Heyer, 2001, *Astrophys. J.*, **551**, 747
- Simpson, C. E., and S. T. Gottesman, 2000, *Astron. J.*, **120**, 2975
- Sirianni, M., A. Nota, G. De Marchi, C. Leitherer, and M. Clampin, 2002, *Astrophys. J.*, **579**, 275
- Smith, K. W., I. A. Bonnell, and M. R. Bate, 1997, *Mon. Not. R. Astron. Soc.*, **288**, 1041
- Smith, K. W. and I. A. Bonnell, 2001, *Mon. Not. R. Astron. Soc.*, **322**, L1
- Smith, M. D., and M.-M. Mac Low, 1997, *Astron. Astrophys.*, **326**, 801
- Smith, M. D., M.-M. Mac Low, and F. Heitsch, 2000, *Astron. Astrophys.*, **362**, 333
- Snell, R. L., R. B. Loren, and R. L. Plambeck, 1980, *Astrophys. J. (Letters)*, **239**, L17
- Solomon, P. M., A. R. Rivolo, J. Barrett, and A. Yahil, 1987, *Astrophys. J.*, **319**, 730
- Soukup, J. E., and C. Yuan, *Astrophys. J.*, **246**, 376
- Spaans, M., 1996, *Astron. Astrophys.*, **307**, 271
- Spaans, M., and C. M. Carollo, 1998, *Astrophys. J.*, **502**, 640
- Spaans, M., and C. A. Norman, 1997, *Astrophys. J.*, **488**, 27
- Spaans, M., and J., Silk, 2000, *Astrophys. J.*, **538**, 115
- Spaans, M., and E. F. van Dishoeck, 1997, *Astrophys. J.*, **323**, 953
- Spitzer, L., Jr., 1968, *Diffuse Matter in Space*, (Wiley Interscience, New York)
- Stahler, S. W., 1988, *Astrophys. J.*, **332**, 804
- Stahler, S. W., F. Palla, and P. T. P. Ho, 2000, in *Protostars and Planets IV*, edited by V. Mannings, A. P. Boss, & S. S. Russell (University of Arizona Press, Tucson), p. 327
- Stauffer, J. R., L. W., Hartmann, and D. Barrado y Navascues, 1995, *Astrophys. J.*, **454**, 910
- Steinmetz, M., 1996, *Mon. Not. R. Astron. Soc.*, **278**, 1005
- Sterzik, M. F., and R. H. Durisen, 1995, *Astron. Astrophys.*, **304** L9.
- Sterzik, M. F., and R. H. Durisen, 1998, *Astron. Astrophys.*, **339**, 95
- Stone, J. M., and M. L. Norman, 1992a, *Astrophys. J. Suppl. Ser.*, **80**, 753
- Stone, J. M., and M. L. Norman, 1992b, *Astrophys. J. Suppl. Ser.*, **80**, 791
- Stone, J. M., E. C. Ostriker, and C. F. Gammie, 1998, *Astrophys. J.*, **508**, L99
- Strittmatter, P. A., 1966, *Mon. Not. R. Astron. Soc.*, **132**, 359
- Strom, K. M., S. E. Strom, and K. M. Merrill, 1993, *Astrophys. J.*, **412**, 233
- Stutzki, J., and R. Güsten, 1990, *Astrophys. J.*, **356**, 513
- Stutzki J., F. Bensch, A. Heithausen, V. Ossenkopf, and M. Zielinsky, 1998, *Astron. Astrophys.*, **336**, 697
- Sugimoto, D., Y. Chikada, J. Makino, T. Ito, T. Ebisuzaki, and M. Umemura, 1990, *Nature*, **345**, 33
- Suto, Y., and J. Silk, 1988, *Astrophys. J.*, **326**, 527
- Swaters, R. A., B. F. Madore, & M. Trewhella, 2000, *Astrophys. J. (Letters)*, **531**, L107
- Swenson, F. J., J. Faulkner, F. J. Rogers, and C. A. Iglesias, 1994, *Astrophys. J.*, **425**, 286
- Sytine, I. V., D. H. Porter, P. R. Woodward, S. W. Hodson, and K.-H. Winkler, 2000, *J. Comput. Phys.*, **158**, 225

- Tafalla, M., D. Mardones, P. C. Myers, P. Caselli, R. Bachiller, and P. J. Benson, 1998, *Astrophys. J.*, **504**, 900
- Tatematsu, K., and 15 colleagues, 1993, *Astrophys. J.*, **404**, 643
- Taylor, G. I., 1921, *Proc. London Math. Soc.*, **20**, 126
- Testi, L., and A. I. Sargent, 1998, *Astrophys. J. (Letters)*, **508**, L91
- Testi, L., and A. I. Sargent, 2000, in *Imaging at Radio through Sub-millimeter wavelengths*, edited by J. Magnum and S. Radford (ASP Conf. Series 217), p. 283
- Testi, L., F. Palla, and A. Natta, 1999, *Astron. Astrophys.*, **342**, 515
- Terebey, S., F. H. Shu, and P. Cassen, 1984, *Astrophys. J.*, **286**, 529
- Thornton, K., M. Gaudlitz, H.-Th. Janka, and M. Steinmetz, 1998, *Astrophys. J.*, **500**, 95
- Tohline, J. E., 1980, *Astrophys. J.*, **235**, 866
- Tohline, J. E., 1982, *Fund. Cosmic Phys.*, **8**, 1
- Tomisaka, K., 1991, *Astrophys. J.*, **376**, 190
- Tomisaka, K., 1995, *Astrophys. J.*, **438**, 226
- Tomisaka, K., 1996a, *Pub. Astron. Soc. Japan*, **48**, 701
- Tomisaka, K., 1996b, *Pub. Astron. Soc. Japan*, **48**, L97
- Tomisaka, K., S. Ikeuchi, and T. Nakamura, 1988a, *Astrophys. J.*, **326**, 208
- Tomisaka, K., S. Ikeuchi, and T. Nakamura, 1988b, *Astrophys. J.*, **335**, 239
- Tomisaka, K., S. Ikeuchi, and T. Nakamura, 1989a, *Astrophys. J.*, **341**, 220
- Tomisaka, K., S. Ikeuchi, and T. Nakamura, 1989b, *Astrophys. J.*, **346**, 1061
- Tomisaka, K., S. Ikeuchi, and T. Nakamura, 1990, *Astrophys. J.*, **362**, 202
- Toomre, A., 1964, *Astrophys. J.*, **139**, 1217
- Troland, T. H., R. M. Crutcher, A. A. Goodman, C. Heiles, I. Kazes, P. C. Myers, 1996, *Astrophys. J.*, **471**, 302
- Troland, T. H., and C. Heiles, 1986, *Astrophys. J.*, **301**, 339
- Truelove, J. K., R. I. Klein, C. F. McKee, J. H. Holliman, L. H. Howell, and J. A. Greenough, 1997, *Astrophys. J.*, **489**, L179
- Truelove, J. K., R. I. Klein, C. F. McKee, J. H. Holliman, L. H. Howell, J. A. Greenough, and D. T. Woods, 1998, *Astrophys. J.*, **495**, 821
- Tsai, J. C., and J. J. L. Hsu, 1995, *Astrophys. J.*, **448**, 774
- Tscharnuter, W., 1975, *Astron. Astrophys.*, **39**, 207
- Tsuribe, T. and S. Inutsuka, 1999a, *Astrophys. J.*, **523**, L155
- Tsuribe, T. and S. Inutsuka, 1999b, *Astrophys. J.*, **526**, 307
- Tubbs, A. D., 1980, *Astrophys. J.*, **239**, 882
- Turner, J. A., S. J. Chapman, A. S. Bhattal, M. J. Disney, H. Pongracic, and A. P. Whitworth, 1995, *Mon. Not. R. Astron. Soc.*, **277**, 705
- Umemura, M., T. Fukushige, J. Makino, T. Ebisuzaki, D. Sugimoto, E. L. Turner, and A. Loeb, 1993, *Pub. Astron. Soc. Japan*, **45**, 311
- Vainshtein, S. I., 1997, *Phys. Rev. E*, **56**, 6787
- van der Hulst, J. M., E. D. Skillman, T. R. Smith, G. D. Bothun, S. S. McGaugh, and W. J. G. de Blok, 1993, *Astrophys. J.*, **106**, 548
- van der Hulst, J. M., E. D. Skillman, R. C. Kennicutt, & G. D. Bothun, 1987, *Astron. Astrophys.*, **177**, 63
- van der Marel, R. P., and M. Franx, 1993, *Astrophys. J.*, **407**, 525
- van Dishoeck, E. F. and G. A. Blake, 1998, *Ann. Rev. Astron. Astrophys.*, **36**, 317
- van Dishoeck, E. F., and M. R. Hogerheijde, 2000, in *The Origin of Stars and Planetary Systems* edited by C. J. Lada and N. D. Kylafis (Kluwer Academic Publisher, Dordrecht), p. 97
- van Dishoeck, E. F., G. A. Blake, B. T. Draine, and J. I. Lunine, 1993, in *Protostars and Planets III*, edited by E. H. Levy and J. I. Lunine (University of Arizona Press, Tucson), p. 163
- van Leer, B., 1977, *J. Comput. Phys.*, **23**, 276
- van Zee, L., M. P. Haynes, J. J. Salzer, and A. H. Broeils, 1997, *Astron. J.*, **113**, 1618
- van Zee, L., J. J. Salzer, and E. D. Skillman, 2001, *Astron. J.*, **122**, 121
- van Zee, L., E. D. Skillman, and J. J. Salzer, 1998, *Astron. J.*, **116**, 1186
- Vázquez-Semadeni, E. 1994, *Astrophys. J.*, **423**, 681
- Vázquez-Semadeni, E., 2000, in *The Chaotic Universe*, edited by V. G. Gurzadyan and R. Ruffini (World Sci.), p. 379
- Vázquez-Semadeni, E., and A. Gazol, 1995, *Astron. Astrophys.*, **303**, 204
- Vázquez-Semadeni, E., and J. Scalo, 1992, *Phys. Rev. Lett.*, **68**, 2921
- Vázquez-Semadeni, E., J. Ballesteros-Paredes, and L. F. Rodríguez, 1997, *Astrophys. J.*, **474**, 292
- Vázquez-Semadeni, E., J. Ballesteros-Paredes, and R. S. Klessen, 2003, *Astrophys. J.*, submitted
- Vázquez-Semadeni, E., T. Passot, and A. Pouquet, 1995, *Astrophys. J.*, **441**, 702
- Vázquez-Semadeni, E., T. Passot, and A. Pouquet, 1996 *Astrophys. J.*, **473**, 881
- Vázquez-Semadeni, E., M. Shadmehri, J. Ballesteros-Paredes, 2002, *Astrophys. J.*, submitted (astro-ph/0208245)
- Vázquez-Semadeni, E., E. C. Ostriker, T. Passot, C. F. Gammie, and J. M. Stone, 2000, in *Protostars and Planets IV*, edited by V. Mannings, A. P. Boss, and S. S. Russell (University of Arizona Press, Tucson), p. 3
- Verschuur, G. L., 1995a, *Astrophys. J.*, **451**, 624

- Verschuur, G. L., 1995b, *Astrophys. J.*, **451**, 645
- Vincent, A., and M. Meneguzzi, 1991, *J. Fluid Mech.*, **225**, 1
- Vink, J. S., A. de Koter, and H. J. G. L. M. Lamers, 2000, *Astron. Astrophys.*, **362**, 295
- Vio, R., G. Fasano, M. Lazzarin, and O. Lessi, 1994, *Astron. Astrophys.*, **289**, 640
- von Weizsäcker, C. F., 1943, *Z. Astrophys.*, **22**, 319
- von Weizsäcker, C. F., 1951, *Astrophys. J.*, **114**, 165
- Wada, K., G. Meurer, and C. A. Norman, 2002, *Astrophys. J.*, **577**, 197
- Wada, K., and C. A. Norman, 1999, *Astrophys. J. (Letters)*, **516**, L13
- Wada, K., and C. A. Norman, 2001, *Astrophys. J.*, **547**, 172
- Wada, K., M. Spaans, and S. Kim, 2000, *Astrophys. J.*, **540**, 797
- Walborn, N. R., R. H. Barbá, W. Brandner, M. ; Rubio, E. K. Grebel, and R. G. Probst, 1999, *Astron. J.*, **117**, 225
- Walder, R. and D. Folini, 2000, *Astrophys. Space Science*, **274**, 343
- Walker, T. P., G. Steigman, H.-S. Kang, D. M. Schramm, and K. A. Olive, 1991, *Astrophys. J.*, **376**, 51
- Walter, F. M., A. Brown, R. D. Mathieu, P. C. Myers, and F. V. Vrba, 1988, *Astron. J.*, **96**, 297
- Ward-Thompson, D., F. Motte, and P. André, 1999, *Mon. Not. R. Astron. Soc.*, **305**, 143
- Ward-Thompson, D., J. M. Kirk, R. M. Crutcher, J. S. Greaves, W. S. Holland, and P. André, 2000, *Astrophys. J.*, **537**, L135
- Ward-Thompson, D., P. F. Scott, R. E. Hills, and P. André, 1994, *Mon. Not. R. Astron. Soc.*, **268**, 276
- Wardle, M., 1990, *Mon. Not. R. Astron. Soc.*, **246**, 98
- Whitmore, B. C., and F. Schweizer, 1995, *Astron. J.*, **109**, 960
- Whitmore, B. C., 2000, in *Space Telescope Symposium Series, No. 14*, edited by M. Livio (Cambridge U. Press, Cambridge) in press (astro-ph/0012546)
- Whitworth, A. P., 1979, *Mon. Not. R. Astron. Soc.*, **186**, 59
- Whitworth, A. P., and D. Summers, 1985, *Mon. Not. R. Astron. Soc.*, **214**, 1
- Whitworth, A. P., and D. Ward-Thompson, 2001, *Astrophys. J.*, **547**, 317
- Whitworth, A. P., A. S. Bhattal, N. Francis, and S. J. Watkins, 1996, *Mon. Not. R. Astron. Soc.*, **283**, 1061
- Whitworth, A. P., S. J. Chapman, A. S. Bhattal, M. J. Disney, H. Pongracic, and J. A. Turner, 1995, *Mon. Not. R. Astron. Soc.*, **277**, 727
- Wichmann, R., J. Krautter, E. Covino, J. M. Alcalá, R. Neuhauser, J. H. M. M. Schmitt, 1997, *Astron. Astrophys.*, **320**, 185
- Wiesemeyer, H., R. Guesten, J. E. Wink, H. W. Yorke, 1997, *Astron. Astrophys.*, **320**, 287
- Wilden, B. S., B. F. Jones, D. N. C. Lin, and D. R. Soderblom, 2002, *Astron. J.*, **124**, 2799
- Williams, J. P., and L. Blitz, 1995, *Astrophys. J.*, **451**, 252
- Williams, J. P., L. Blitz, and C. F. McKee, 2000, in *Protostars and Planets IV*, edited by V. Mannings, A. P. Boss, and S. S. Russell (University of Arizona Press, Tucson), p. 97
- Williams, J. P., L. Blitz, and A. A. Stark, 1995, *Astrophys. J.*, **494**, 657
- Williams, J. P., E. J. de Geus, L. Blitz, 1994, *Astrophys. J.*, **428**, 693
- Williams, J. P., P. C. Myers, D. J. Wilner, and J. di Francesco, 1999, *Astrophys. J.*, **513**, L61
- Wilner, D. J., P. C. Myers, D. Mardones, and M. Tafalla, 2000, *Astrophys. J.*, **544**, L69
- Winkler, K.-H. A., and M. J. Newman, 1980a, *Astrophys. J.*, **236**, 201
- Winkler, K.-H. A., and M. J. Newman, 1980b, *Astrophys. J.*, **238**, 311
- Winkler, K.-H. A., and M. L. Norman, 1986, in *Astrophysical Radiation Hydrodynamics*, editors K.-H. A. Winkler and M. L. Norman (Reidel Publishing, Dordrecht)
- Wiseman, J. J., and F. C. Adams, 1994, *Astrophys. J.*, **435**, 708
- Wolfire, M. G., and J. P. Cassinelli, 1987, *Astrophys. J.*, **319**, 850
- Wolfire, M. G., D. Hollenbach, C. F. McKee, A. G. G. M. Tielens, and E. L. O. Bakes, 1995, *Astrophys. J.*, **443**, 152
- Wong, T., and L. Blitz, 2002, *Astrophys. J.*, **569**, 157
- Wood, D. O. S., P. C. Myers, and D. A. Daugherty, 1994, *Astrophys. J. Suppl. Ser.*, **95**, 457
- Wuchterl, G., and M. U. Feuchtinger, 1998, *Astron. Astrophys.*, **340**, 419
- Wuchterl, G., and R. S. Klessen, 2001, *Astrophys. J.*, **560**, L185
- Wuchterl, G., and W. Tscharnuter, 2003, *Astron. Astrophys.*, **398**, 1081
- Yonekura, Y., K. Dobashi, A. Mizuno, H. Ogawa, Y. Fukui, 1997, *Astrophys. J. Suppl. Ser.*, **110**, 21
- Yorke, H. W., and E. Krügel, 1977, *Astron. Astrophys.*, **54**, 183
- Yorke, H. W., and C. Sonnhalter, 2002, *Astrophys. J.*, **569**, 846
- Yorke, H. W., Tenorio-Tagle, G., Bodenheimer, P., and M. Różyczka, 1989, *Astron. Astrophys.*, **216**, 207
- Yoshii, Y., and Y. Sabano, 1980, *Pub. Astron. Soc. Japan*, **32**, 229
- Zhang, Q., S. M. Fall, and B. C. Whitmore, 2001, *Astrophys. J.*, **561**, 727
- Zhou, S., N. J. Evans, C. Koempe, and C. M. Walmsley, 1993, *Astrophys. J.*, **404**, 232
- Zielinsky M., and J. Stutzki, 1999, *Astron. Astrophys.*, **347**, 633
- Zinnecker, H., 1984, *Mon. Not. R. Astron. Soc.*, **210**, 43
- Zinnecker, H., 1990, in *Physical Processes in Fragmentation and Star Formation*, edited by R. Capuzzo-Dolcetta and C. Chiosi (Kluwer Academic Publisher, Dordrecht), p. 201
- Zuckerman, B., 2001, *Ann. Rev. Astron. Astrophys.*, **39**, 459
- Zuckerman, B., and P. Palmer, 1974, *Ann. Rev. Astron. Astrophys.*, **12**, 279

Zweibel, E. G., and A. Brandenburg, 1997, *Astrophys. J.*, **478**,
563

Zweibel, E. G., and K. Josafatsson, 1983, *Astrophys. J.*, **270**,
511

Thanks...

... to all those people whose help and friendship made this work possible!

Special thanks to Mordecai-Mark Mac Low, and to Javier Ballesteros-Paredes, Peter Bodenheimer, Andreas Burkert, Fabian Heitsch, Pavel Kroupa, Douglas N. C. Lin, Enrique Vázquez-Semadeni, and Hans Zinnecker. They have accompanied my scientific career with long-term collaborations, discussions, and exchange of ideas and results.

I acknowledge support by the Emmy Noether Program of the Deutsche Forschungsgemeinschaft (DFG: KL1358/1) and funding by the NASA Astrophysics Theory Program through the Center for Star Formation Studies at NASA's Ames Research Center, UC Berkeley, and UC Santa Cruz. Preparation of this work made furthermore extensive use of the NASA Astrophysical Data System Abstract Service.

Beyond all others, I thank Sibylle, Johanna, Jonathan and my mother for love and faith and everything.

